DOE Grant No: DE-FE0009168

Development of Improved Caprock Integrity and Risk Assessment Techniques

Final Report

For Period
Oct. 1, 2012 to Sept. 30, 2014

Dr. Michael S. Bruno (PI)
GeoMechanics Technologies
103 E. Lemon Ave., Suite 200
Monrovia, CA 91016
Phone: 626 305-8460
Fax: 626 305-8462

December 15, 2014

Disclaimer:

1 Abstract

GeoMechanics Technologies has completed a geomechanical caprock integrity analysis and risk assessment study funded through the US Department of Energy. The project included: a detailed review of historical caprock integrity problems experienced in the natural gas storage industry; a theoretical description and documentation of caprock integrity issues; advanced coupled transport flow modelling and geomechanical simulation of three large-scale potential geologic sequestration sites to estimate geomechanical effects from CO_2 injection; development of a quantitative risk and decision analysis tool to assess caprock integrity risks; and, ultimately the development of recommendations and guidelines for caprock characterization and CO_2 injection operating practices. Historical data from gas storage operations and CO_2 sequestration projects suggest that leakage and containment incident risks are on the order of 10^{-1} to 10^{-2}, which is higher risk than some previous studies have suggested for CO_2. Geomechanical analysis, as described herein, can be applied to quantify risks and to provide operating guidelines to reduce risks. The risk assessment tool developed for this project has been applied to five areas: The Wilmington Graben offshore Southern California, Kevin Dome in Montana, the Louden Field in Illinois, the Sleipner CO_2 sequestration operation in the North Sea, and the In Salah CO_2 sequestration operation in North Africa. Of these five, the Wilmington Graben area represents the highest relative risk while the Kevin Dome area represents the lowest relative risk.

Table of Contents

List of Figures

List of Tables

2 Executive Summary

A primary factor influencing long-term geologic storage of CO_2 is caprock integrity. Large-scale CO_2 injection projects require improved and advanced simulation tools and risk assessment techniques to better predict and manage system failures. GeoMechanics Technologies has completed a multi-phase geomechanical caprock integrity study to advance understanding of caprock integrity issues.

First, we completed a detailed review, description, and analysis of historical leakage events related to caprock integrity within the natural gas storage industry. The majority of underground natural gas storage (UNGS) occurs in depleted oil and gas reservoirs (85%). Although accounting for only 10% of storage facilities overall, most *geologically controlled* leakage has occurred from aquifers converted to gas storage (65%). In these cases, conduits in the caprock are present due to fracturing or faulting associated with reservoir-creating anticlinal structures. Leaks occur as a result of the more challenging nature of aquifer gas storage: less geologic data, higher required pressures, and unconfirmed sealing. To estimate failure rates and risk, several researchers have documented incidents of leakage at UNGS facilities. Based on our survey of these studies, the rate of failure can be estimated: of 485 operational and abandoned UNGS facilities in the U.S., Europe and Central Asia available for study, 22 of these reservoirs have leaked because of some form of caprock failure, representing a 4.5% failure rate. Although leakage events involving well failure are much more common (about 200 such cases, or 41% incident rate), leaks occurring from caprock failure are more difficult to detect and control in-situ and, therefore, have demanded particular pre-operational attention and, as a result, been largely avoided in the past 35 years. The review of these incidents provides new and critical information for the CO_2 sequestration industry that can significantly improve project design and operating practices. From our detailed review, analysis, and description of historical leakage events related to caprock integrity within the natural gas storage industry, we conclude that risks for gas leakage events are generally higher than previously estimated and published, and are in the range of 10^{-2} to 10^{-1}.

Second, we developed and described analytical equations and numerical models that can be applied for first order estimates of induced stresses and strains due to pressure and temperature changes related to CO_2 injection.

Third, a process for one-way coupled fluid and heat flow simulation and geomechanical simulation to estimate induced stresses and failure risks was applied to three large-scale potential geologic sequestration sites to ascertain their risk of caprock failure due to geomechanical damage: the offshore Los Angeles Wilmington Graben; the northern Montana Kevin Dome structure; and the Louden natural gas storage field in central Illinois. Detailed geologic models of each site were created from stratigraphic and lithologic information collected from maps and wells located throughout the fields. The completed geologic models of each of these three sites were used as input for CO_2 injection and fluid migration modelling. To manage areas with uncertain geology, several geologic scenarios were simulated to determine the horizontal and vertical extent of the CO_2 plume after 30 or more years of injection. Geomechanical models were used to evaluate induced deformations and stresses within the reservoirs and overlying caprocks and to analyze potential fault activation. This report includes detailed results from our fluid flow and geomechanical modelling for these three potential geologic sequestration sites in the US.

Fourth, a quantitative risk and decision analysis tool (QRDAT) to assess caprock integrity was also developed and applied. Loss of caprock integrity was assumed to occur via tensile fracturing, fault activation and wellbore failure. The likelihood of loss events can be assessed with a spreadsheet model for these leakage pathways based on a set of general gas-storage and CCS-specific risk factors. For each factor, a range of parameter values associated with high, moderate and low leakage potential was made available and assigned a score. This leads to a total score of each set of site-specific parameter values, which can be translated into a loss event probability. The tool has been applied to the three modeled potential sequestration sites, as well as two operating large-scale sequestration sites, resulting in relative risk estimates.

Last, we have developed recommendations and guidelines for caprock characterization and CO_2 injection operating practices which will reduce caprock integrity damage risks.

3 Historical Data Review and Documentation of Caprock Integrity Observations in the Gas Storage Industry and in the Oil and Gas Waste Injection Industry

We have reviewed historical data and documented caprock integrity problems in the gas storage industry. Reviewing and analyzing many of these incidents provide new and critical information to the CO_2 sequestration industry, which should significantly improve project design and operating practices to help ensure permanent geologic storage. This effort has consisted in collecting and analyzing gas storage data associated with caprock integrity problems, and examining maximum pressure limits and analyzing past failure incidents that have occurred during gas storage operations.

Some of this information was gathered by contacting State Oil and Gas Boards. This information is public but not commonly known to be available. Several examples include migration of storage gas from the Mt. Simon formation, the St. Peters formation and others into overlying formations at several storage fields throughout the Illinois Basin.

The primary source of information has come from a review of publicly available literature, as well as from incident reports, petitions, affidavits, and root cause analysis reports submitted to State Oil and Gas Boards. Additional information has come from legal court filings. We have searched records for all states with historical gas storage operations in depleted reservoirs and saline aquifers.

3.1 Underground Storage of Natural Gas

Natural gas is stored underground primarily in depleted gas and oil reservoirs, aquifers, and mined salt caverns to help meet cyclic seasonal and/or daily demands for gas. It is a practice that reduces price volatility and balances the flow in pipeline systems (Benson, 2002; DNV, 2010).

In seasonal (or base-load) storage, natural gas is injected during the summer, when demand for heating is low, and is withdrawn during the winter season. Depleted gas reservoirs and aquifers are used for this type of storage. Salt caverns are used for short-term storage, because they can quickly switch from injection to withdrawal and operate at large injection and extraction rates. Salt caverns are more expensive to construct, but have the flexibility to react immediately to unexpected changes in gas demand and/or price (Benson, 2002).

Natural gas can be stored for an indefinite period of time. The exploration, production, and transportation of natural gas all take time, and the natural gas that reaches its destination is not always needed right away, so it is often injected into these underground storage facilities. These storage facilities can be located near market centers that do not have a ready supply of locally produced natural gas (NaturalGas.org, 2011).

The necessary conditions for underground natural gas storage are (Figure 1):

- A geologic structure under which fluid can accumulate (e.g., an anticline with sufficient closure). Closure is the vertical distance from the top of the anticline to the highest adjoining syncline (or possible spill point).
- A reservoir (i.e., porous and permeable layers of rock).
- A caprock (i.e., impermeable or low-permeable, water-wet rock layers that prevent the stored fluid from rising or moving laterally to rise elsewhere).
- Water present to confine the stored fluid in all directions.
- Adequate overburden (depth) to allow the storage of fluids under sufficiently high pressures.

The most common form of underground storage consists of depleted gas/oil reservoirs (about 80% of all storage fields in North America). The presence of hydrocarbons indicates the existence of a reservoir and an effective caprock to hold fluids below it (Katz and Coats, 1968). Depleted reservoirs are those formations from which most recoverable hydrocarbons have already been produced. This leaves a naturally occurring, underground formation already proven to be geologically capable of securely holding natural gas for millennia in the past. Furthermore, using an already developed reservoir for storage purposes allows the use of the extraction and distribution equipment (existing wells, gathering systems, pipeline connections, etc.) left over from when the field was productive. Having this network in place reduces the cost of converting a depleted reservoir into a storage facility.

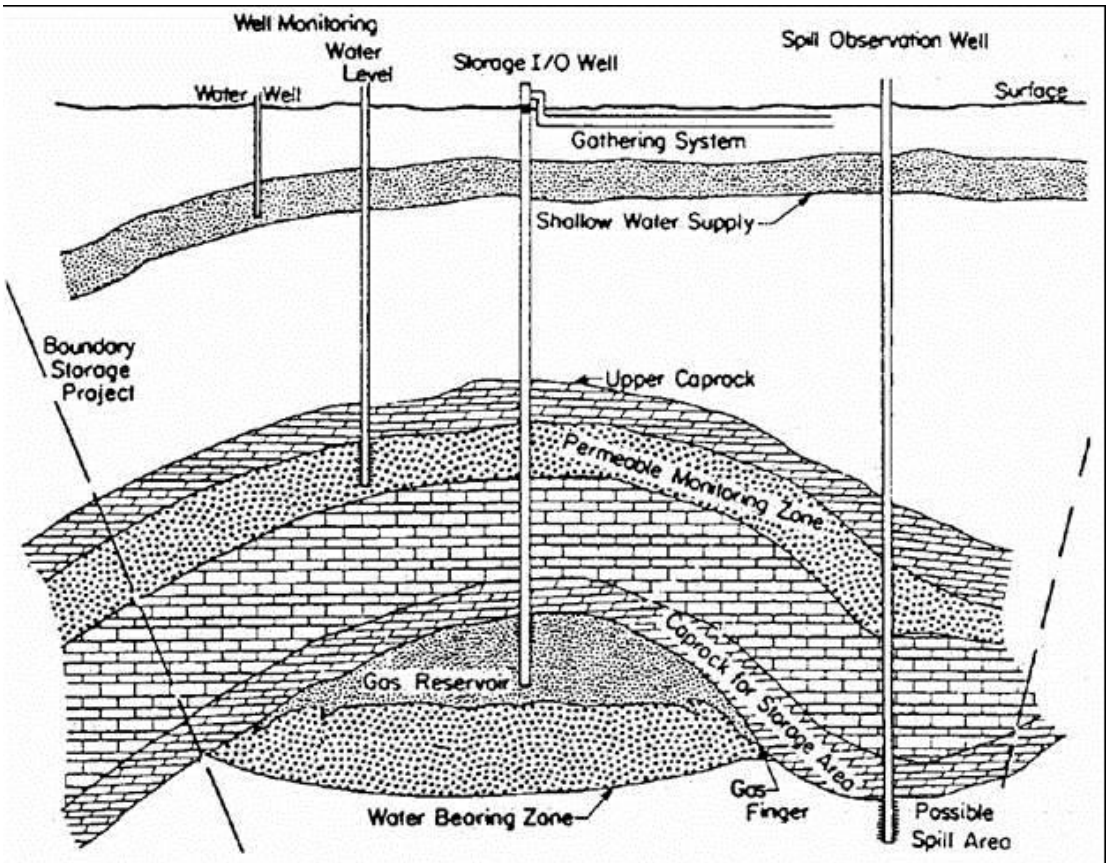

Figure 1. Definition of a Storage System (section of an anticlinal reservoir; Katz, 1978)

Aquifers are more expensive to develop for gas storage than depleted O&G fields and generally less desirable for a number of reasons. First, the geological characteristics of aquifer formations are not as thoroughly known, as with depleted reservoirs. A significant amount of time and money goes into evaluating the geological characteristics of an aquifer, and determining its suitability as a natural gas storage facility. Second, in order to develop a natural aquifer into an effective natural gas storage facility, all of the associated infrastructure must be developed. Third, aquifer formations often require a great deal more 'cushion gas' than depleted reservoirs. Finally, aquifer storage creates pressure gradients that the storage and caprock formations have not previously experienced. This could result in failure of the caprock due to the displacement of the static water column, forcing water out of the caprock and permitting gas to leak from the storage formation. This process is known as exceeding the threshold displacement pressure or threshold pressure (Evans & West, 2008).

The final primary gas storage environment is within solution mined salt caverns. These have the advantage of high deliverability and relative simplicity (generally requiring only a single well per cavern). They have the disadvantage of relatively small volume, and the further disadvantage of long-term salt creep (on the order of 1% to 5% closure rate per year in some instances). Salt caverns were initially assumed to be more secure than depleted reservoirs because of the relatively impermeable nature of the surrounding salt. In practice, however, the rate of failure and loss events in salt caverns has been similar to, if not more frequent, than depleted reservoir storage. And because the high pressure gas can release so quickly, loss events at salt caverns have been more catastrophic and damaging with several fires and blowouts occurring over the past 10 years.

3.2 Leakage from Gas Storage Operations

Gas storage fields are operated around the world, and the majority of these operate without problems. In some instances, however, gas has migrated from the storage zone to overlying formations, to shallow groundwater, and even to the surface. Some of the primary leakage mechanisms are illustrated in Figure 2, and include but are not limited to:

- Pore space/capillary pressure/permeation (caprock matrix)
- Fault plane/fracture transmission (structural; Figure 3)
- Induced fracturing, faulting and bedding slip (geomechanical; Figure 4)
- Dissolution channels/shrinkage cracks (geochemical); and,
- Leakage along poorly cemented wells.

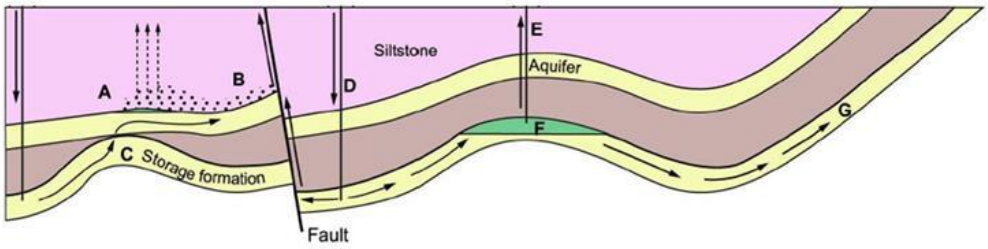

Matrix

- Capillary entry pressure
- Seal permeability
- Pressure seals
- High permeability zones

Structural

- Flow on faults
- Flow on fractures
- Flow on hydraulic fractures
- Flow between permeable zones due to juxtapositions
- Fractured shales

Geomechanics

- Hydraulic fracturing
- Creation of shear fractures
- Earth quake release

Figure 2. Some Gas Storage Reservoir Leakage Mechanisms (Nygaard, 2010)

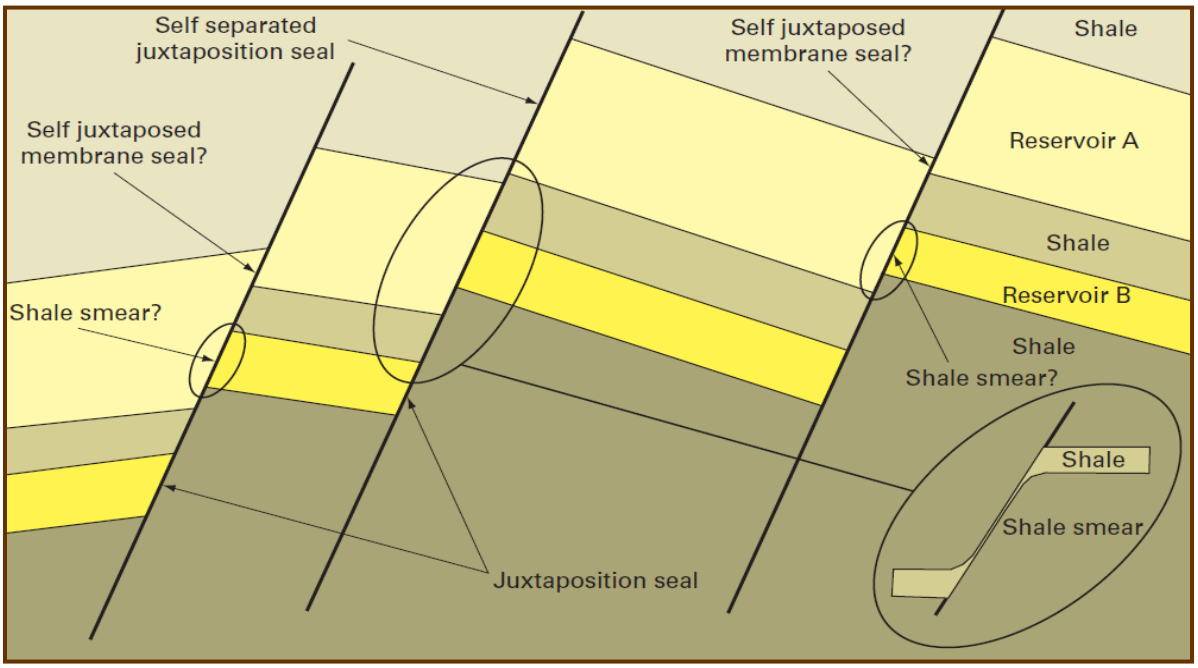

Figure 3: Schematic illustration of faulted sand-shale sequence (after Færseth, 2006)

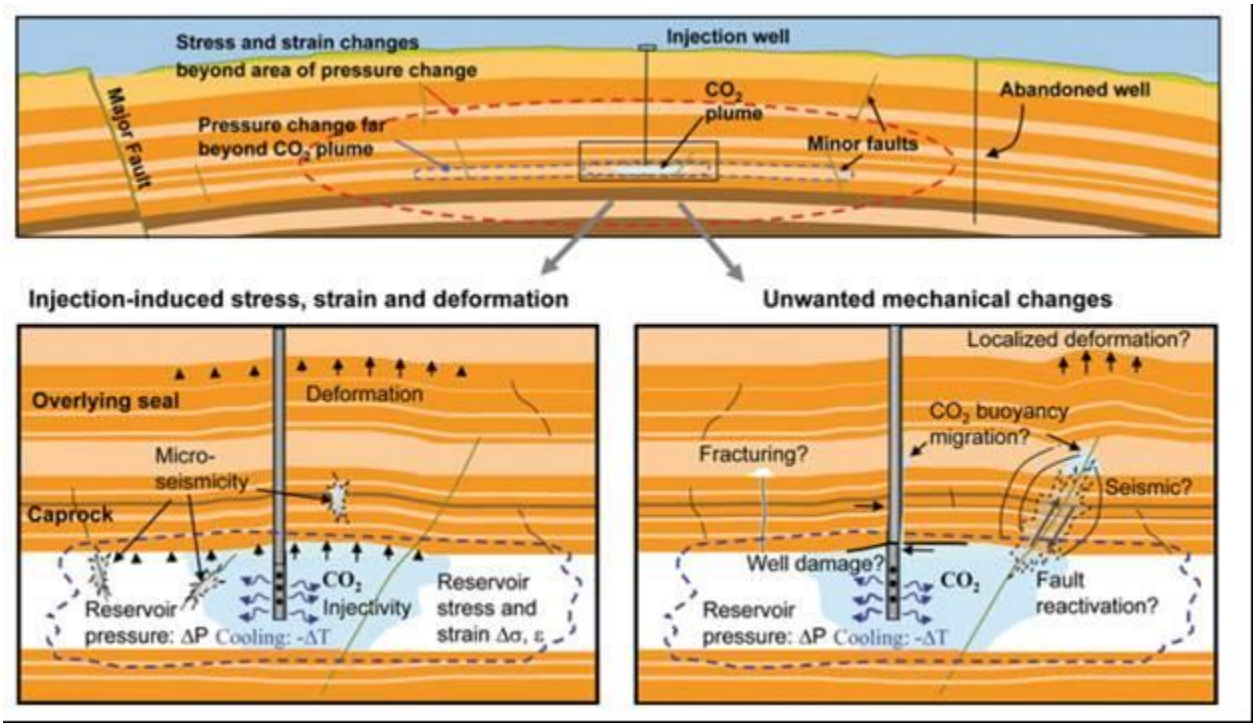

Figure 4. Geomechanical processes associated with geologic sequestration of CO_2

Though created to demonstrate CO_2 injection geomechanical processes, natural gas injection in geomechanically analogous in this context. *Top:* different regions of plume, pressure and geomechanical changes; *bottom left:* injection-induced stress, strain, deformations, and microseismicity resulting from temperature and pressure changes; *bottom right:* unwanted inelastic changes compromising sequestration efficiency (Rutqvist, 2012).

Most instances of *geologically controlled* gas migration problems have occurred in aquifer gas storage operations. In some cases the flaws in the caprock were associated with previously unrecognized fracturing or faulting associated with the anticlinal structure of the gas storage field. With depleted oil and gas operations, the initial seal is relatively secure, but can sometimes become degraded over time with repeated pressure and stress cycling. This is particularly true if the caprock is relatively thin and brittle. Finally, gas storage in salt caverns presents the added problem of long term salt creep and large scale deformations, which can lead to significant well damage.

In the vast majority of cases overall, gas leakage has been caused by defective wells (poorly completed or improperly plugged abandoned wells) or by wells which became damaged due to deformations. Over time, as engineering practices have improved and regulatory oversight has grown more stringent, wells have become better designed and more secure. But leaks that occur due to caprock integrity issues are more difficult to detect and control (Benson, 2002).

The gas storage industry has successfully applied several caprock integrity testing techniques, individually or combined to assess safe storage conditions (Perry, 2005). These include:

- Geologic assessment
- Threshold pressure

- Production/injection tests (pump test)
- Flow/shut-in pressure tests
- Air/CO_2 injection

3.3 US Gas Storage Overview

The first instance of natural gas successfully being stored underground occurred in Weland County, Ontario, Canada, in 1915. This storage facility used a depleted natural gas well that had been reconditioned into a storage field. The Zoar field, also a depleted gas reservoir located south of Buffalo, New York, is the oldest U.S. storage project. It has been in use since 1916 and is still in commercial operation today. By 1930, there were nine storage facilities in six different states. Until the first aquifer storage project in 1946, essentially all subsurface natural gas storage was in partially or fully depleted gas reservoirs. Storage in mined cavities came later. Depleted reservoirs remain the most commonly used underground storage sites because of their wide availability and proven ability to store hydrocarbons (Benson, 2002).

According to Evans (2009), as of 2005 there were 410 UNGS facilities operting in in the United States (Evans, 2009), clustered mainly in Illinois, Michigan, Ohio, Pennsylvania, West Virginia, Louisiana, Texas, and California (see Figure 5 and Figure 6), and distributed thusly among the three principal types of storage (EIA, 2013 a&b):

- depleted natural gas or oil fields (330);
- aquifers (43); and,
- salt caverns (37).

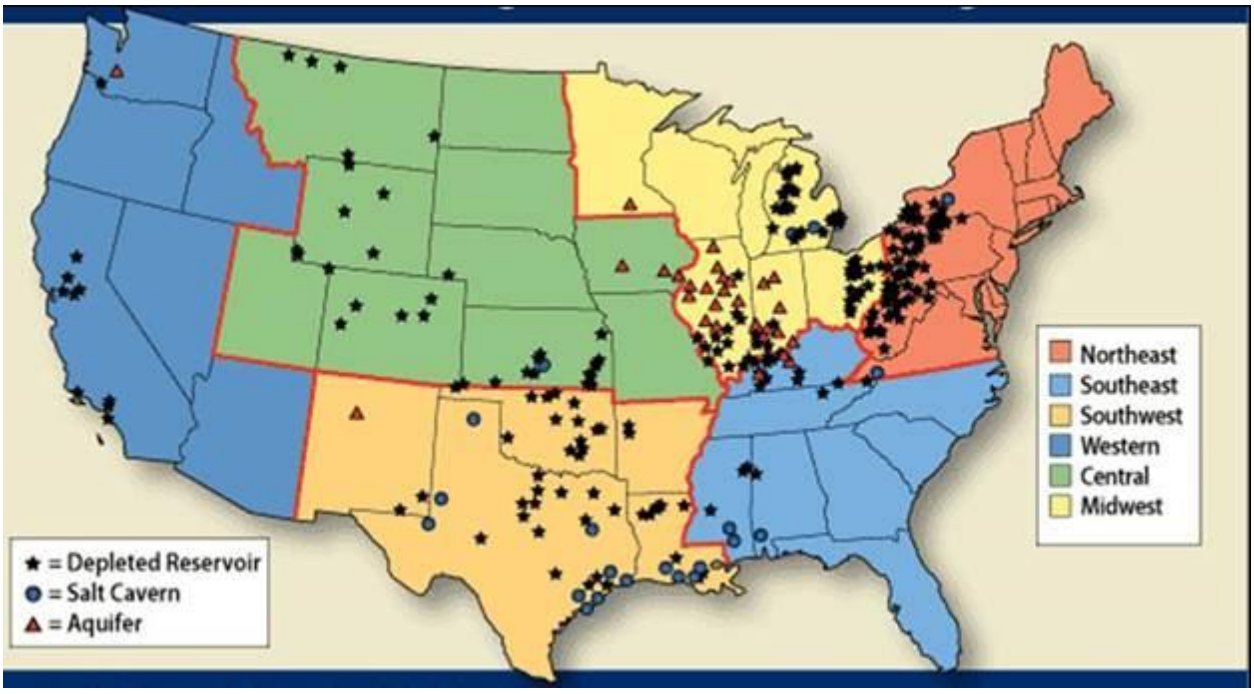

Figure 5. U.S. Underground Natural Gas Storage Facilities (EIA)

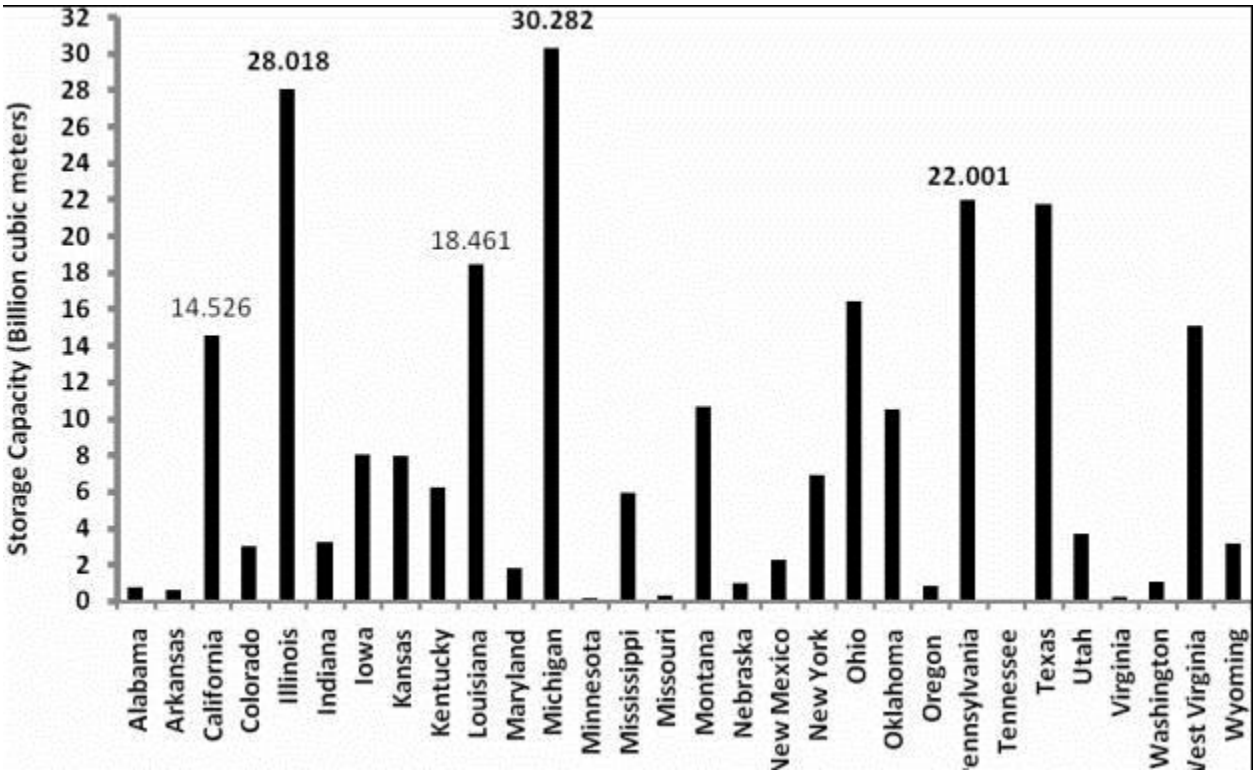

Figure 6: Underground gas storage states in the U.S. (EIA, 2006)

In 2012, the largest monthly total amount of natural gas stored in subsurface formations in the U.S. was about 8.3 Tcf (169 million metric tonnes (Mt)) in early November; 3.9 Tcf (79 Mt) as working or active gas and 4.4 Tcf (90 Mt) as base or cushion gas. Base gas is the volume of gas that must be left underground to provide pressure and volume to cycle the normal working storage volume and to avoid water intrusion. Working gas is the maximum developed volume of gas in the storage reservoir above the designed level of base gas (EIA, 2013a & 2013b).

3.4 US Storage Leak Risks and Incidents

A number of researchers have attempted to document incidents of leakage at gas storage facilities in the US, with the aim to estimate failure rates and risk (Evans & West, 2008; Evans, 2009; Benson, 2002; Perry, 2005; Keeley, 2008; Miyazaki, 2009). Evans (2009) identifies 228 reported events of widely varying cause, nature, and severity at underground storage facilities. We present in Table 1 a summary of reported incidents (modified from Evans, 2009). Based on these incidents alone, the approximate risk for leakage at any facility can be estimated as follows:

- ~373 US UNGS facilities operational and abandoned in O&G fields and aquifers
- 28 of these reservoirs have leaked

- 28/373 = 7.5% leakage risk

It is important to note, however, that not all instances of leakage are reported and published. GeoMechanics Technologies has been contracted to provide forensic analysis and testimony on several fields that have not been documented and published. These fields have gas migration out of the storage interval and into a higher interval being produced by another operator, leading to legal dispute. After settlement, these cases are generally sealed under confidentiality agreements. It is our belief that the number of actual leak incidents is significantly larger that the number of reported incidents, and that the estimate shown above is low.

The majority of the incidents presented in Table 1and Table 2 (about 65%) have occurred in aquifers storage facilities, even though they are fewer in number than depleted reservoir storage facilities. This is not surprising, given the more challenging aspects of storing gas in aquifers (due to less geologic data, higher pressures required, and unconfirmed sealing).

Table 1 Reported gas loss events at US UNGS facilities
(modified from Evans, 2009)

Contributory processes/mechanisms attributed to leakage/failure	Storage Facility Type		
	O&G Fields	Aquifers	Totals
Migration from Injection Footprint/Cavern (not Due Entirely to Well Problems)	11	13	24
Caprock - Not Gas Tight/Salt Thick Enough	**3**	**12**	**15**
Caprock - Fractured/Faulted, Not Gas-Tight	**4**	**5**	**9**
Seismic Activity	1	0	1
Not Available	4	1	5

Table 2 Reported Leak/Migration Incidents from UNGS Reservoirs Attributed to Caprock Integrity Issues
Roughly chronological order, depleted O&G fields in peach, aquifers in green; US & European incidents (after Evans, 2009)

Facility	State/Prov	Country	Operator	Date	Leakage (Bcf)	Storage Type	Description	Mechanism
Herscher	IL	USA	Natural Gas Storage Company of Illinois	April-July 1953	2.947	Aquifer	Gas found in shallow water wells w/in 5 weeks of operation	Caprock leakage, injection ceased, relief wells drilled - withdraw water from periphery & injected into overlying formations to increase hydrostatic pressure
Troy Grove	IL	USA	Northern Illinois Gas Company	1957-59	0	Aquifer	Gas migration from reservoir known since early development	Caprock leakage, gas withdrawn from higher levels and re-injected at depth. Facility still operational
Manlove	IL	USA	Peoples Gas Light and Coke Company	1961-63	0	Aquifer	Gas migrated from 2 upper reservoirs into glacial drift deposits	Caprock leakage, reservoirs abandoned but 3rd, deeper one later developed
Brookville	IL	USA	Natural Gas Pipeline Company	1963-66	0.894	Aquifer	Water pump and injection tests indicated leak from reservoir	Faulting, caprock leakage, facility abandoned
Waverly	IL	USA	Panhandle Eastern Pipeline Company	1960s	0	Aquifer	Gas migration to shallower levels	Caprock leakage, gas either recycled into reservoir or produced
Leaf River	IL	USA	Northern Illinois Gas Company	1968-71	0	Aquifer	Water pump and injection tests reveal leak	Faulting, caprock leakage, facility abandoned
Pontiac	IL	USA	Northern Illinois Gas Company	1963-74	0	Aquifer	Testing & injection with inert combustion gas	Ineffective seal provided by caprock, facility was inactive in 1974
Sdota	IL	USA	Central Illinois Public Service Company	1971-74	0.02	Aquifer	Testing & injection 1971-72	Ineffective seal provided by caprock, facility abandoned in 1974
El Segundo	CA	USA	N/A	Early 70's	?	Depleted O&G	Gas migration threatened housing development	Gas migration from reservoir to surface along fault planes. Facility initially shut-in (pre 1993) but now abandoned
Pleasant Creek	CA	USA	N/A	1972-76	?	Aquifer	Soil gas surveys detect gas over storage area.	Soil gas surveys detect gas over storage area.
Chalk Creek & Coalville	UT	USA	Questar, still operational	1970s	?	Aquifer	Soil gas surveys detect gas over storage area.	Gas migrating up out of reservoirs via faults?
Northern Indiana	IN	USA	N/A	60's-70's	?	Aquifer	Gas escape	Reservoir selected too shallow, number of water wells were affected by the intrusion of natural gas
East Whittier	CA	USA	SoCal	1970's	?	Depleted O&G	Gas migrated away from injection site	Injected gas produced by other company, facility closed 2003
Leroy *	WY	USA	Mountain Fuel Supply Company	1973-1982	0.6	Aquifer	Numerious incidents of gas escaping. Found bubbling up in streams and ponds.	Corroded well casing and overpressuring of aquifer
Montbello	CA	USA	SoCal	1950-80's	?	Depleted O&G	Storage gas lost over extended period	Fractures/Faulst in Caprock, among other problems
Kalle	Lower Saxony	Germany	RWE	1999	2.7	Aquifer	Loss of stored product - pressure differences noted	Leakage from reservoir, probably via two wells & over an extended period at maximum of 60,000cm/day
Ketzin * (Knobluch)	Berlin	Germany	UGS Mittenwalde	1960's-2000	?	Aquifer	1960's migration from reservoir to surface.	Caprock not gas tight - migration along faults in caprock also likely. One death from CO migrating up old well into house.
Loudon *	IL	USA	Natural Gas Pipeline Company	2000	?	Depleted O&G	Storage gas produced by exploration company in strata overlaying caprock	Exploration company drilling & fracturing above caprock induced fracturing or opened sealed fractures in caprock, creating vertical pathways for stored gas in reservoir below.
Playa del Rey *	CA	USA	SoCal	1940's-present	7	Depleted O&G	Migration of large amounts of stored gas	Stored gas has migrated from PDR structure to Venice structure from earliest days, connection b/n structures, faults & well related
SW Kinsale gasfield	Offshore	Ireland	Marathon	1971-present	?	Depleted O&G	Leakage of original reserve to seafloor	Converted to storage in 2001, leaking through caprock before and after conversion
Castaic Hills & Honor Rancho	CA	USA	SoCal	1975-present	?	Depleted O&G	Migration from Castaic laterally and vertically	Migration from Castaic laterally and vertically
Huntsman, Cheyenne Co	NE	USA	Kinder Morgen	present	10	Depleted O&G	Gas migrated laterally from injection footprint out of structure and into adjoining field.	Gas migrated across leaking fault previously thought to be sealing fault.

The amount of leakage for the incidents listed in Table 2 is given where known, but this is for only about half of the cases. For those which have a leakage of "0 Bcf" this is the result of either the leaked gas being produced at a higher stratigraphic level than the target reservoir, before it is able to reach the surface (e.g., Troy Grove & Waverly), or the abandonment of the operation before any natural gas was injected, but after failed injection tests (e.g., Leaf River & Pontiac). For most with a "?" value, simply no record of a leaked volume was found (almost all CA leaks), but for some it is difficult to evaluate because they are leaking into adjacent producing areas (e.g., Castaic Hills & SW Kinsale), though this has been measured in the case of Huntsman. The total leaked gas for the five incidents for which it has been reported is about 14.5 Bcf. Extending an average of 3 Bcf/incident to the 12 unknown cases, ~50 Bcf of total leaked natural gas due to caprock integrity issues is a reasonable estimate for all depleted O&G and aquifer storage operations, over the past 60 years of UNGS history. This amounts to less than half of the most recent estimated yearly methane emissions from the natural gas transmission and underground storage segment in the U.S. (~106 Bcf in 2011), less than 12% of methane emissions for the same period for the entire oil & natural gas industry in the U.S. (~424 Bcf), and only a half a percent for all U.S. methane emissions in 2011 (~986 Bcf; EPA, 2013a & 2013b).

3.4.1 Loudon

As of 2009, Illinois ranked second only to Michigan, with total underground natural gas storage capacity at 28.01×10^9 m^3 (Figure 6). In past years, some of the aquifer storage facilities experienced leak problems, and some were shut down. The leaks were generally the result of inadequately sealing caprocks and problems associated with faulting (Agyarko & Mansoori, 2013). We have analyzed nine such geologically controlled leakage incidents in Illinois (Table 2 & Figure 7), and have chosen to present here our in-depth examination one such relatively recent incident, at the Loudon Field.

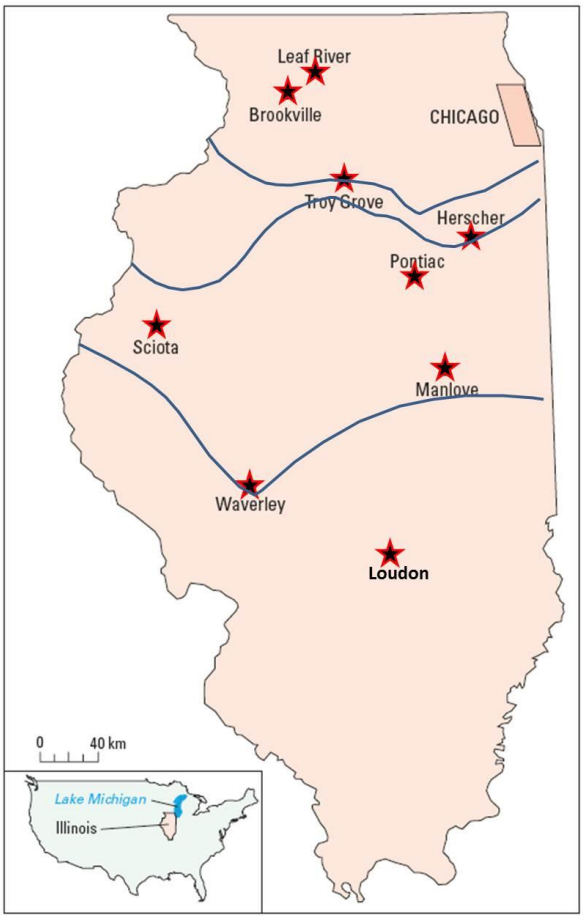

Figure 7. Locations of main gas storage sites in Illinois having experienced difficulties with caprock integrity
blue lines indicate southern limits of the Mt. Simon, Galesville, and St. Peter Sandstones, respectively, as USDWs (after Evans & West, 2008)

The Loudon Field is located in Fayette County, Illinois within the Illinois Basin (Figure 8). Loudon Field was discovered in 1937 by Carter Oil Company. It is an asymmetrical NE-SW anticline 14 miles long by 4 miles wide (Figure 9), with 146 feet of closure on top of the storage formation, the Devonian Grand Tower. Over 350 million barrels of oil have been produced from strata of Mississippian, Devonian and Ordovician age, making it the only former oil reservoir used for gas storage in Illinois. The Grand Tower dolomitic reservoir produced 19.5 million barrels of oil before, its 100 wells were recompleted with new casing and storage operation began in 1969 (Buschbach & Bond, 1974; *PETCO/BPC v NGPL*, 2004).

Figure 8. Loudon & Illinois Basin

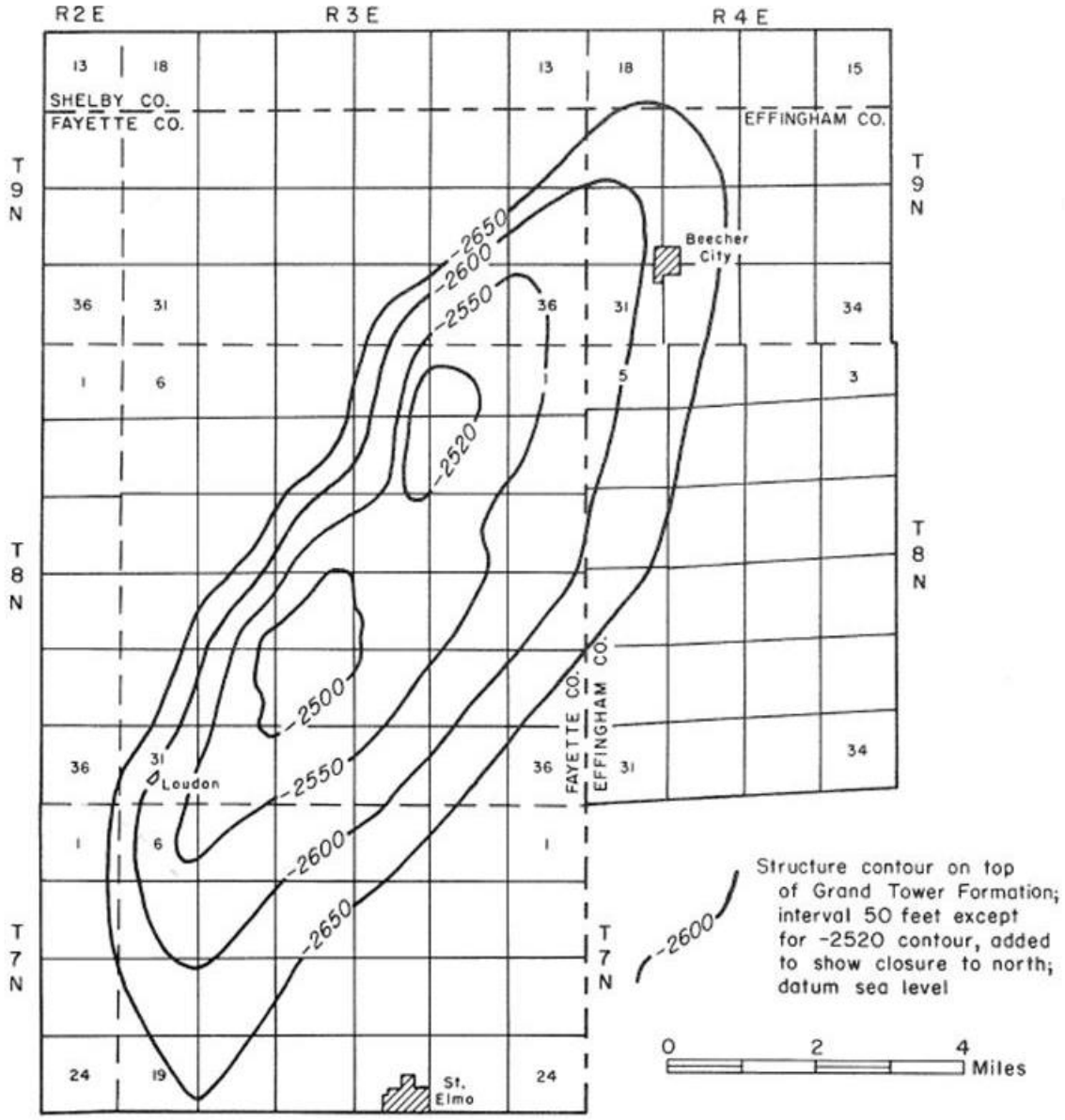

Figure 9. Structure Map of Grand Tower formation
(Buschbach & Bond, 1974)

In 1964, Humble Oil and Refining Company, Carter Oil company's successor, entered into an agreement with The Natural Gas Pipeline Company of America (NGPL) to utilize the depleted Devonian Grand Tower dolomite reservoir for underground gas storage, using the 85 feet thick Cedar Valley dense limestone as the primary caprock and the 100+ foot thick New Albany shale as secondary, and ultimate, caprock (Figure 10). NPGL began injection in 1967, testing in 1968 and injection operation in 1969 (Buschbach & Bond, 1974). In 1992, Bergman Petroleum Corp. (BPC) acquired the Loudon Field rights to the stata immediately overlying the New Albany Shale from Humble and contracted with PETCO Petroleum Corporation for operation activities. Original reservoir pressure of the Grand Tower reservoir was 1,350 psi. Peak bottom hole pressure during gas storage operation reached 1,675 psi during the onset of the winter heating season (*PETCO/BPC v NGPL*, 2004).

Figure 10 is a schematic stratigraphic column for Loudon Field in the vicinity of Lydia Weaber #8 (LW#8) well. Paleozoic sediments lie over the basement rock. The predominant lithology is dolomites followed by limestones, shales and sandstones. Erosion dominated post Paleozoic history. The area was then covered by Pleistocene glacial drift.

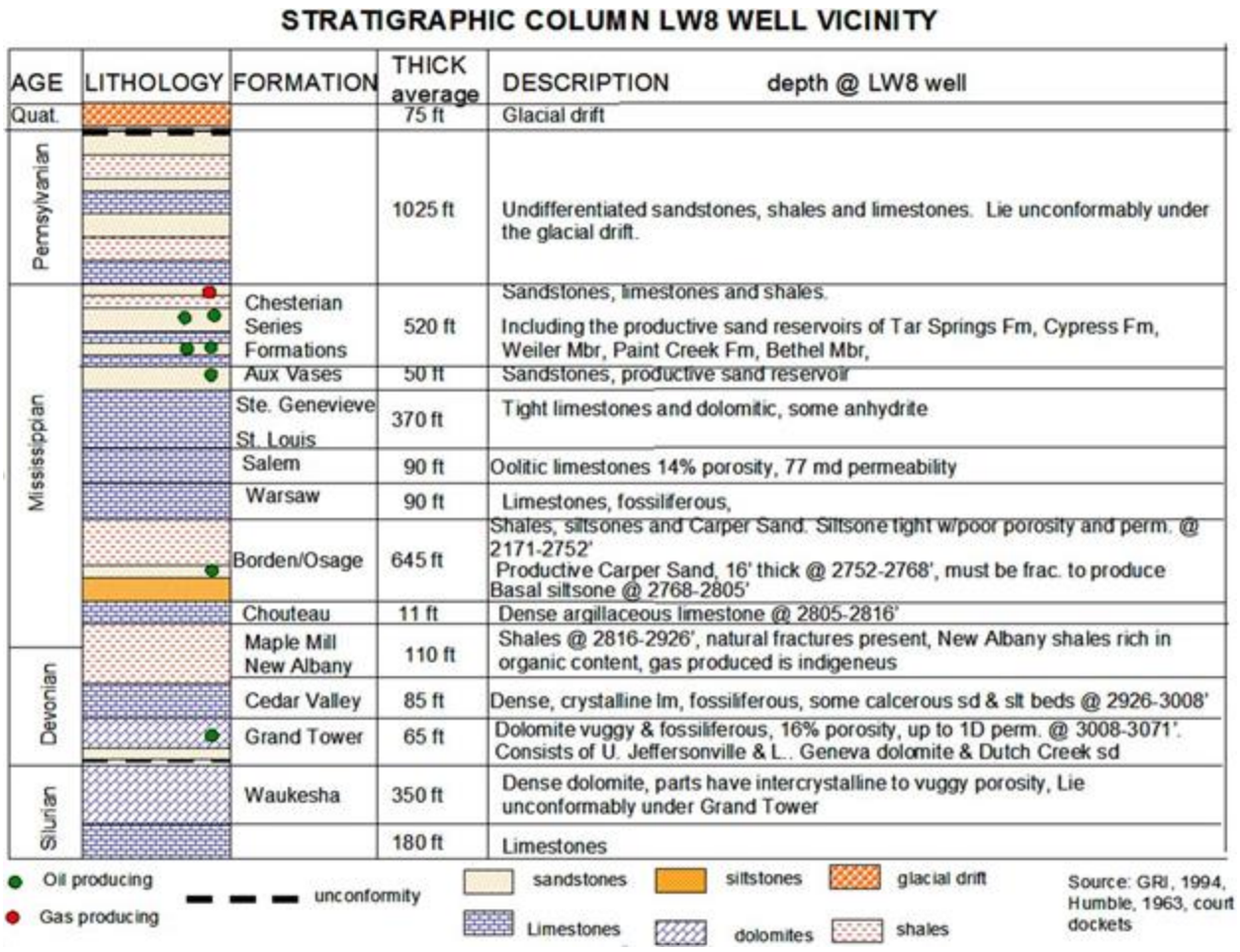

Figure 10. Stratigraphic Column of Loudon Field near LW#8 well vicinity

The Devonian age Grand Tower Formation is 3050 feet below surface, and a 65 feet thick vuggy and fossiliferous dolomite with an average porosity of 16% and up to 1 Darcy calculated permeability from performance data (Buschbach & Bond, 1973). New Albany shales are rich in organic content (Total Organic Content 1 to 2.5%), have indigenous gas, and cover the Cedar Valley Formation. Within the Illinois Basin, New Albany shales have been an effective cap rock in confining Devonian production. A thin Mississippian age limestone bed, the Chouteau Formation rests on top of the New Albany shales. Above the Chouteau, the Carper

Sand is a member of the Borden/Osage Formation. This productive sand is 16 feet thick and must be fractured to produce (*PETCO/BPC v NGPL*, 2004).

Two small normal faults with approximately 40 feet displacement are recognized on the western flank of the Loudon Field structure. These faults are confined to rocks of the Mississippian age; therefore should not affect caprock integrity, which is of Devonian age (PETCO/BPC v NGPL, 2004).

After June 16, 2000 stored gas from the Grand Tower formation was found in the gas produced by PETCO/BPC from the Carper Sand. PETCO/BPC suspected, or at least contended, that this was trespass caused by NGPL either overpressurizing their reservoir in the Grand Tower during injection, and thus either fracturing or reopening fractures in the New Albany Shale underlaying the former, overlying the latter, or allowing one of their wells to leak into the Carper. This specific date is important, however, as tests of gas samples before that date indicate no shows of the stored Grand Tower gas, though they do afterwards. And this is the date on which PETCO/BPC conducted a fracturing treatment in the thin Carper Sand above the New Albany Shale. Subsequent hearings (*PETCO/BPC v NGPL*, 2004, 2011a & 2011b) determined that it was these fracturing treatments above the ultimate caprock which led to the breech of the ultimate caprock, and communication between the two reservoirs

3.4.2 Southern California

There are nine natural gas storage fields in northern and southern California, owned and operated either by PG&E or Southern California Gas. These storage facilities, designed to help meet seasonal gas demand and improve the efficiency of securing gas supplies, are regulated by the California Public Utilities Commission (Burton et al, 2007). Five gas storage fields that have operated in the Los Angeles area and experienced migration problems due in part, perhaps, to caprock integrity issues include Castaic & Honor Rancho, Playa Del Rey, El Segundo, Whittier, and Montebello (the latter three have been abandoned, Figure 11 & Figure 12).

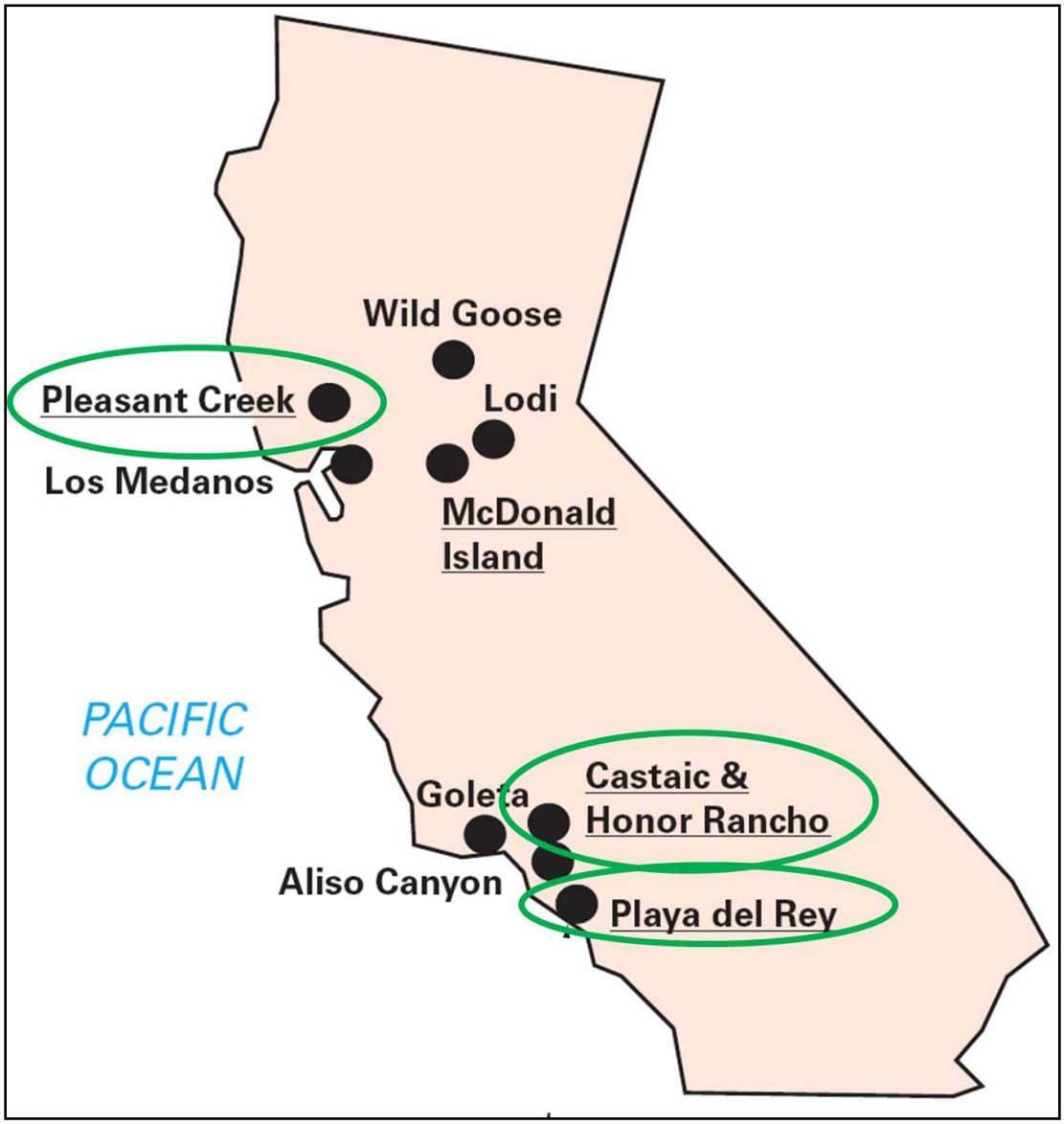

Figure 11. California, showing 3 UNGS storage sites discussed
Castaic & Honor Rancho and Playa del Rey are in this section, Pleasant Creek following (after Evans, 2008)

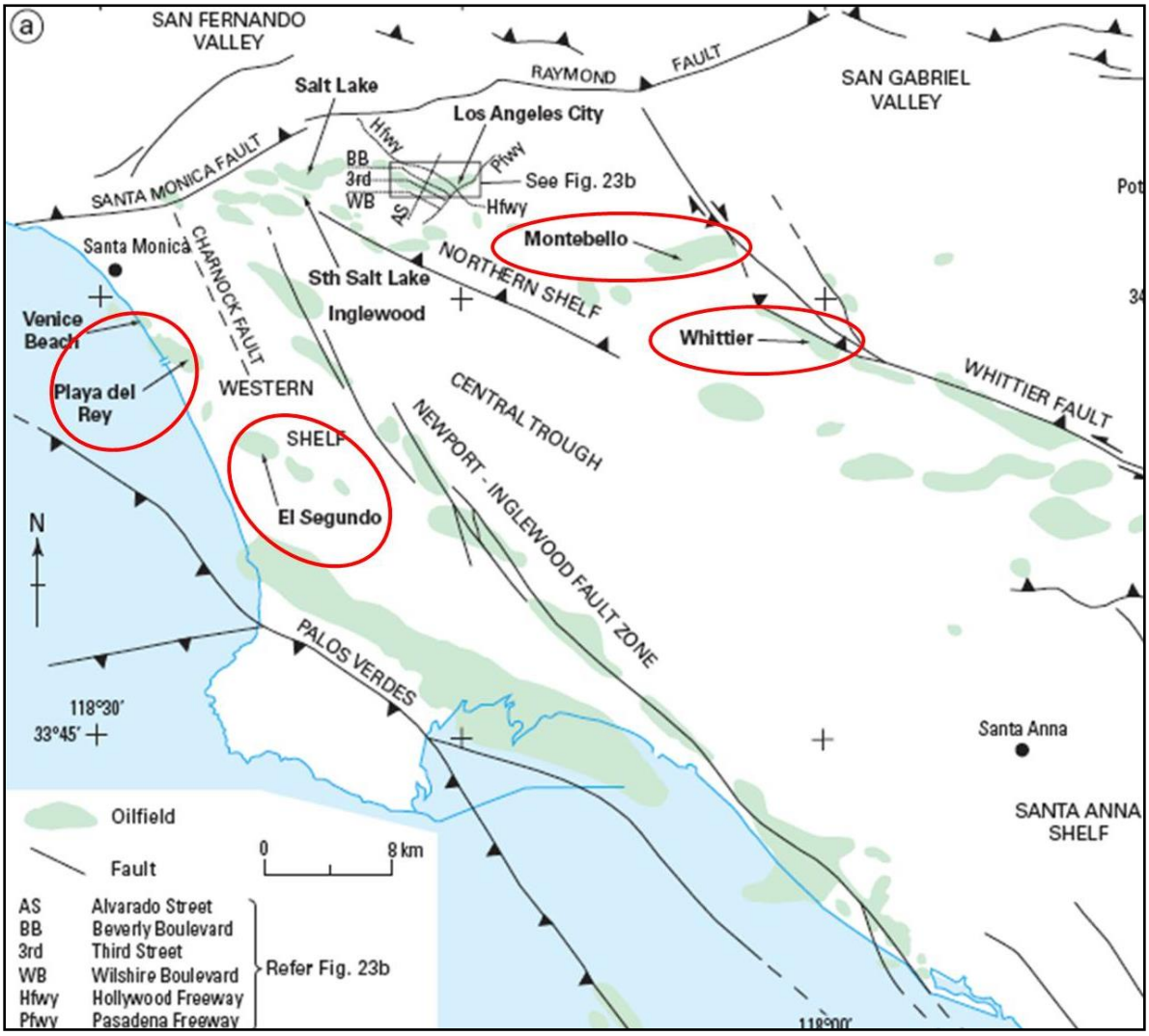

Figure 12. Map of oilfields and main tectonic features of the Los Angeles Basin
4 of 5 Southern California UNGS sites experiencing caprock integrity issues circled in red, see Figure 11 above for Castaic & Honor Rancho (After Evans, 2008)

Underground fuel storage facilities in California account for the majority of the documented problems in depleted oil and gas fields (69%), and 18.5% of all problems (Keeley, 2008), but Southern California in particular provides a very different environment to that of other UGS storage regions in a number of significant respects. First, there are many more poorly located wells stemming from a long history of relatively unregulated oil exploration. Second, it is a tectonically very active area, with present day seismic activity and major faults causing surface ground ruptures. Many of the oilfields are compressional features formed during the Cenozoic (late Miocene to present) with associated faulting of the reservoir and caprock units causing ongoing leakage from the reservoirs and in one case, fracturing of a well (Evans, 2008 & 2009).

The Los Angeles region has been an area of intense hydrocarbon exploration and production since the latter part of the 19th Century. Over 70 oilfields have been discovered, most of them in the early part of the 20th Century, with hundreds of oil wells having been drilled from derricks that once blanketed the landscape (Figure 13). The majority of these oilfields are now abandoned, but the area has been left with a legacy of old wells, the locations of which are often poorly known, but which now lie beneath densely populated urban areas (Evans, 2008).

Figure 13. Oil Derricks along Ocean Front at Playa del Rey
(Evans, 2008)

The Los Angeles basin is a deep, sediment filled structural depression with recent alluvial deposits overlying older Miocene and Pliocene sedimentary rocks (Figure 14), with major through-going fault zones (Figure 12). It was formed during rifting that commenced in early Miocene times, forming a series of basins and basement highs, the latter comprising the Catalina Schists and granites (Figure 14). These basement rocks were a source

of the Puente and Repetto Formations, which form a thick sequence of coarse, clastic sediments unconformably overlying the basement rocks and deposited by late Miocene and early Pliocene subaqueous fan systems. The sedimentary rocks have been uplifted, tilted, and folded by compressive movements between the North American and Pacific plates to produce structures that have trapped and accumulated oil and gas, resulting in numerous oil and gas fields within the basin (Figure 12).

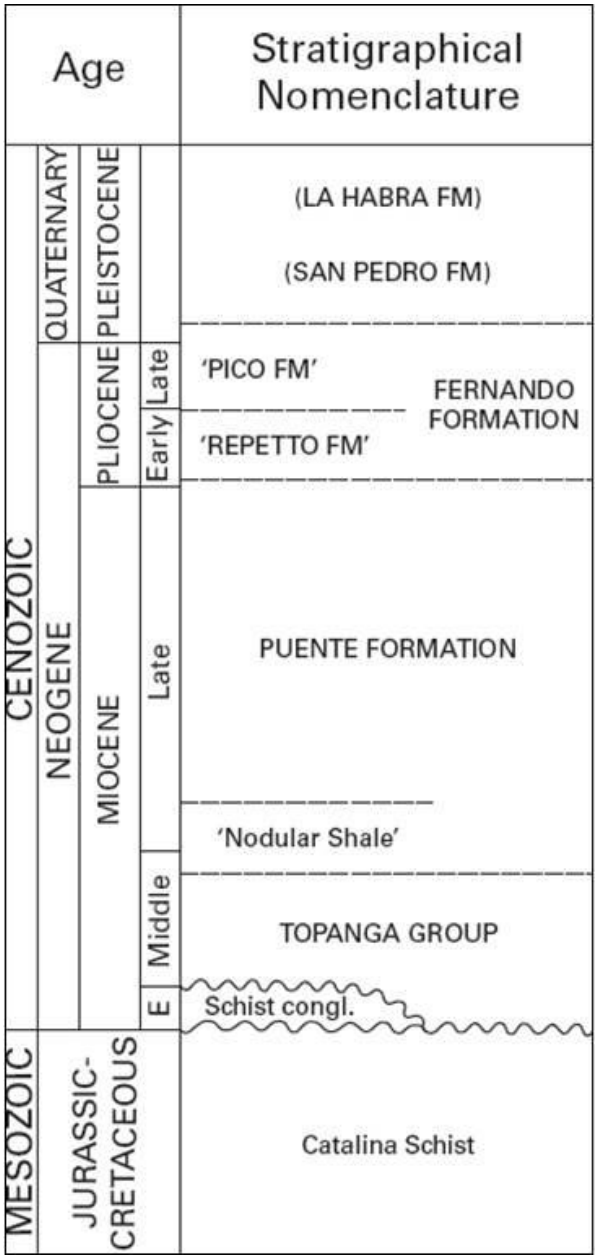

Figure 14. Stratigraphy of the Los Angeles area
(After Evans, 2008)

Clearly, there is plenty to beware of in the Southern California subsurface, in terms of storing fluids securely. However, to illustrate that the integrity of such reservoirs, their caprocks, and even their wells, are not universally vulnerable, even in the event of a major and proximal seismic event, the following case is offered. The magnitude 6.7 Northridge Earthquake of 1994 occurred almost directly beneath (within 5 miles of) the Aliso Canyon Gas Storage Field, which stores more than 100 billion cubic feet of gas for the metropolitan Los Angeles area (Figure 11 & Figure 15). The main quake occurred at a depth of almost 12 miles, aftershocks up to magnitude 3 were scattered within the field itself at typical well depths, and caused no significant problems (only one out of 400 wells was deformed slightly, without any gas release).

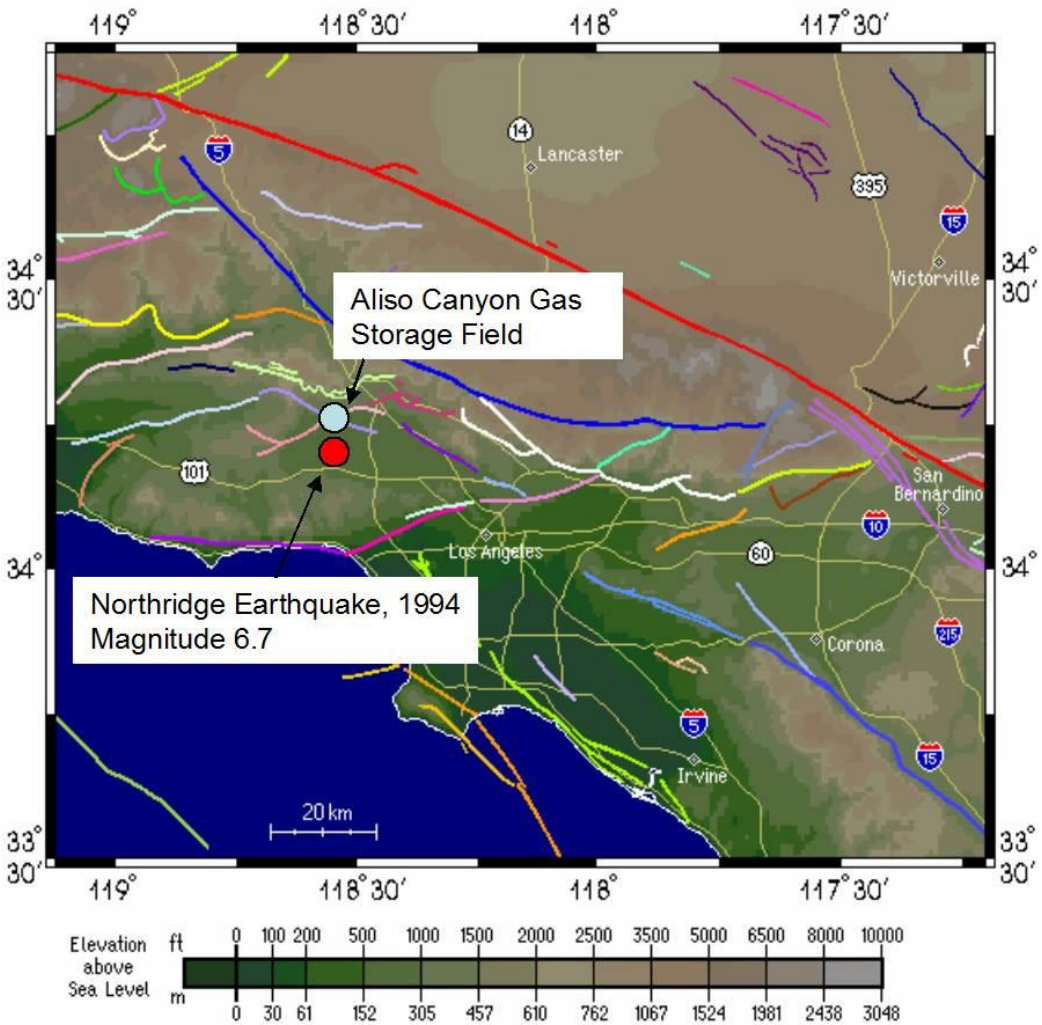

Figure 15. Approximate Location of the Aliso Canyon Gas Storage Field and the Epicenter of Northridge Earthquake
(After SCEC, 2013)

3.4.2.1 Montebello

We have analyzed all five potentially geologically controlled leakage incidents in Southern California (Figure 11 & Figure 12), and have chosen to present here our in-depth examination of leakage at the Montebello oilfield storage location.

At the depleted Montebello oilfield in Los Angeles (Figure 12 & Figure 16), gas had been injected by Southern California Gas at a depth of 7500ft (2286m) from the early 1960's, ceasing in 1986 after significant gas seepages were discovered at the surface within a large housing development above the gas storage facility (Khilyuk et al, 2000).

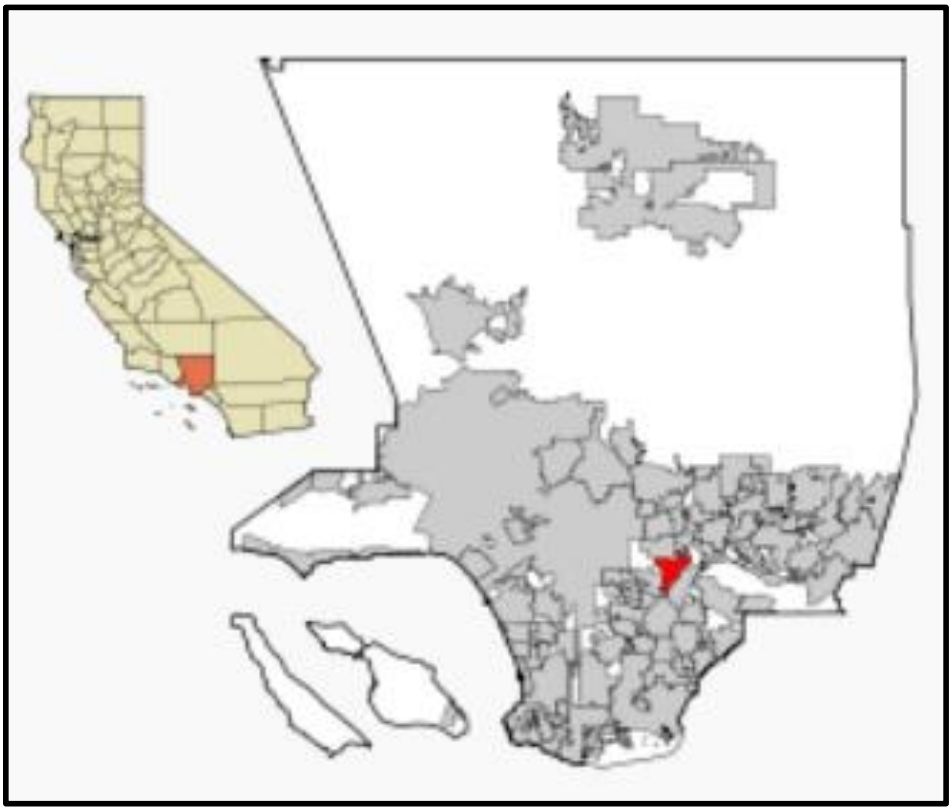

Figure 16. Location map for Los Angeles County & the Montebello field

The oilfield produced from multiple zones in the Puente and Repetto Formations. Gas storage began in the 1950's in the depleted 8th zone (Figure 17). During the 1970's, soil-gas was detected in a residential area overlying the NE part of the Montebello Gas Storage Field. Analytic test results indicated the presence of imported and processed storage gas. Several homes were purchased and demolished. Seven shallow extraction wells were installed in the early 1980's, along with a collection system and blower to extract soil-gas. This system successfully reduced soil gas concentrations to undetectable levels for 20 years, during which time the cushion gas was extracted, leading to the decommissioning of the storage facility in 2003 (Miyazaki, 2009).

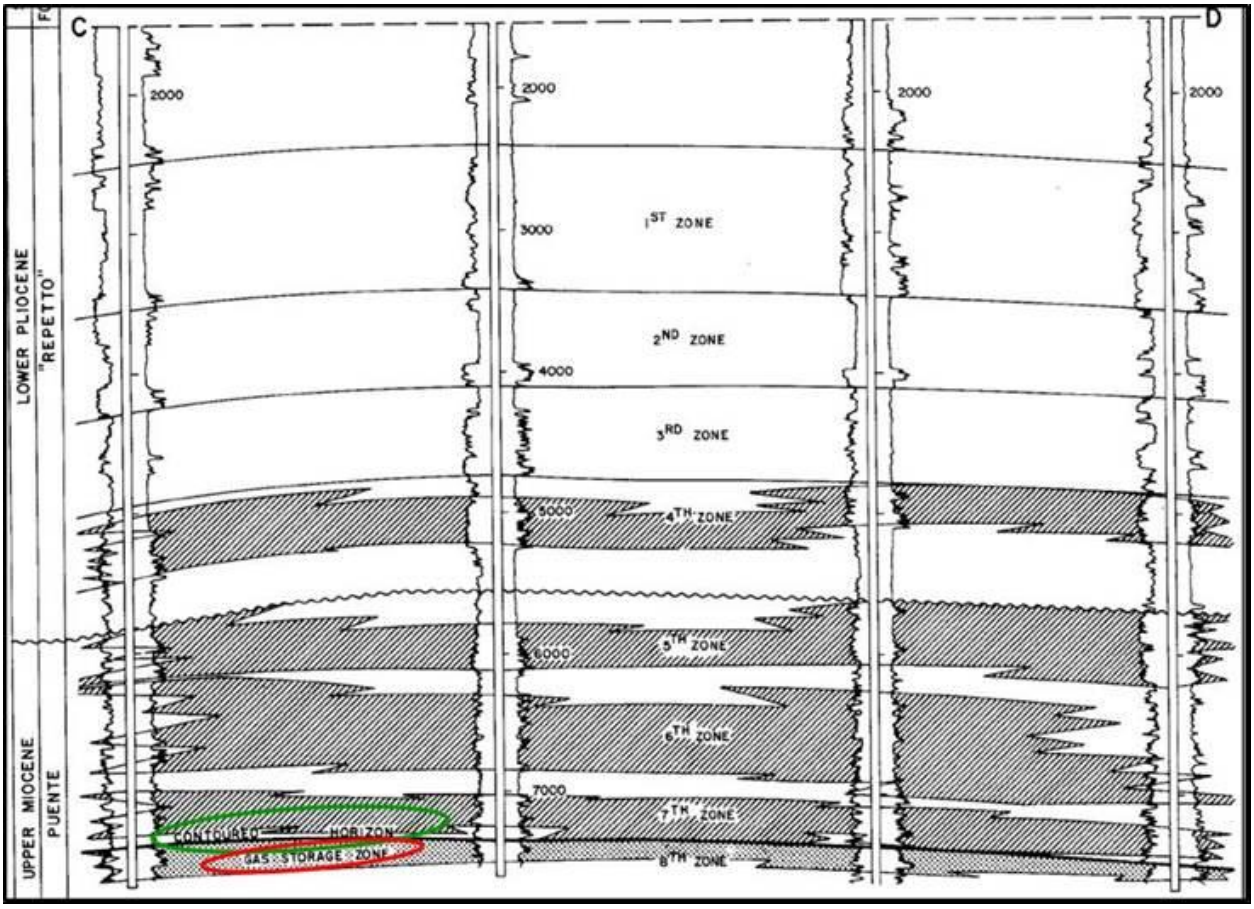

Figure 17. Montebello Cross Section
(See for Figure 18 location, DOGGR, 1992)

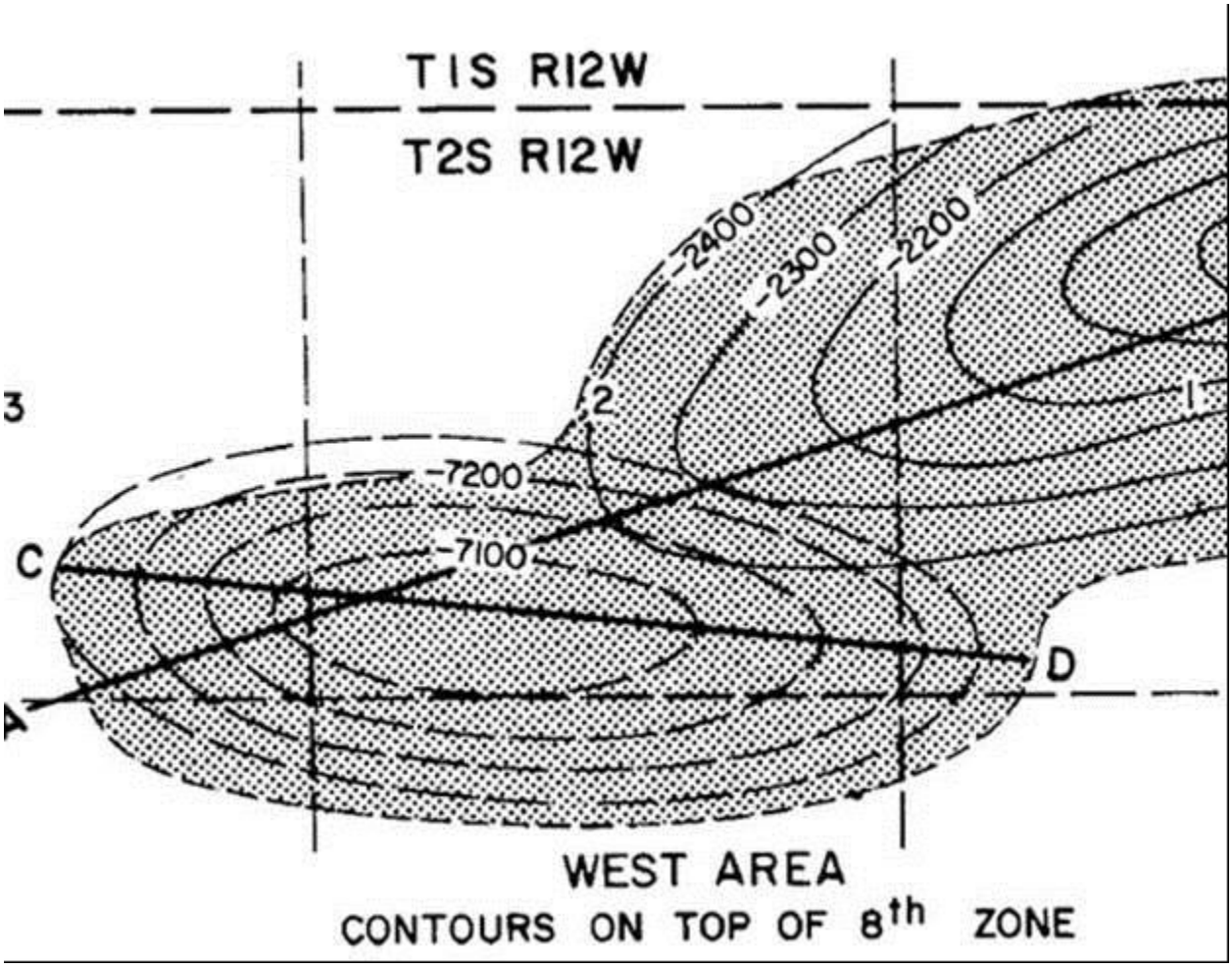

Figure 18. Montebello Structure Map of gas storage reservoir
Cross section CD in Figure 17 (DOGGR, 1992)

It has been determined that gas was found to be leaking to the surface along old wells, many of which were drilled in the 1930's, before today's rigorous drilling and completion standards were implemented and applied (Evans, 2008). Investigations revealed that the old well casings and cements were unable to cope with the increased pressures (injection pressures exceeded 105.6 kg/cm^2 (1502 psi)), allowing high-pressure gas to enter the old wells and migrate to shallower depths (Benson & Hepple, 2005).

In addition to leaky wells, leakage also occurred along fractures and faults in the caprock, some pre-existing, some the result of high injection pressures, exceeding prior oil field pressures (Gurevich et al, 1993).

3.5 European Gas Storage Overview

According to Gas Storage Europe (GSE, 2012, a subdivision of Gas Infrastructe Europe), there are 111 underground gas storage (UGS) facilities operating in depleted oil and/or gas fields and aquifers in Europe

(including Turkey, Belarus and Ukraine; (Figure 19 & Table 3), with Ukraine, Germany and France leading the way (Figure 20).

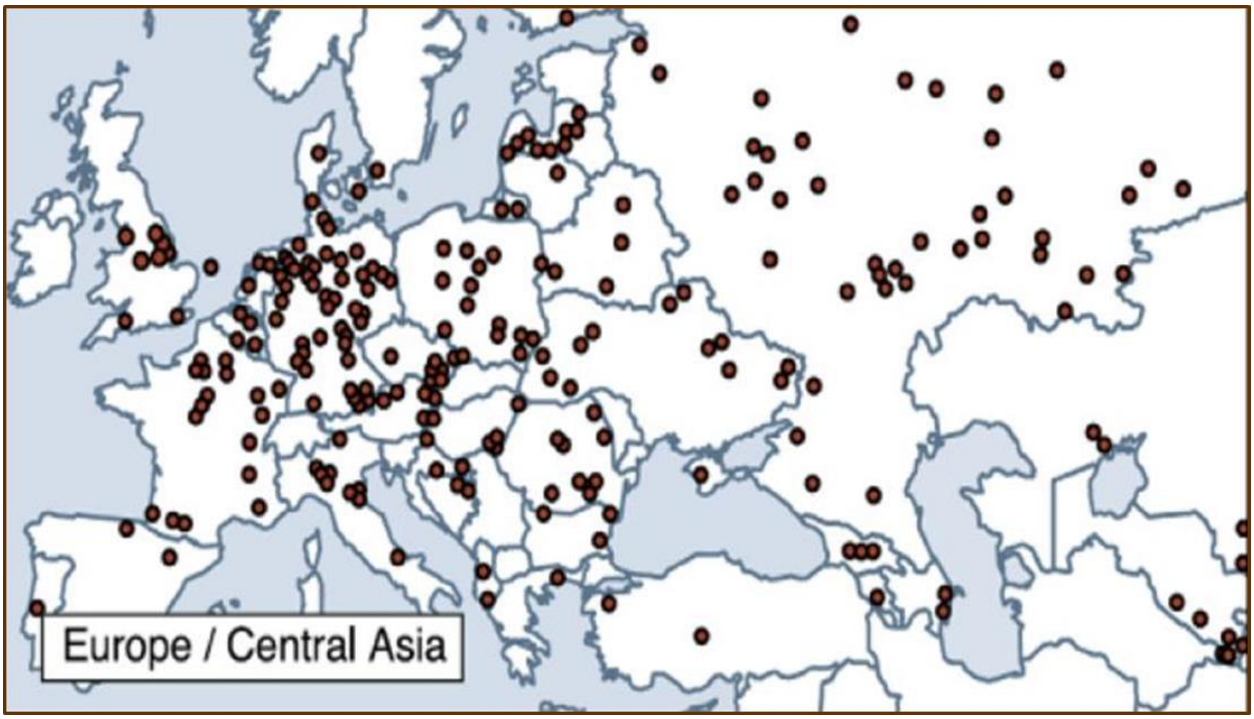

Figure 19. UGS sites in the Europe and Central Asia
(IEAGHG, 2009)

Table 3 155 Operational European Underground Natural Gas Storage Facilities
(Gas Infrastructure Europe: GSE Storage Map May 2012)

Country	Depleted field	Aquifer	Salt Cavern	Mine/ Rock Cavern	Sum
Austria	8				8
Belarus	2				2
Belgium		1			1
Bulgaria	1				1
Croatia	1				1
Czech Republic	6	1		1	8
Denmark		1	1		2
France	2	14	6		22
Germany	11	11	25		47
Hungary	5				5
Ireland	1				1
Italy	9				9
Latvia	1				1
Netherlands	1		1		2
Poland	7		1		8
Portugal			2		2
Romania	8				8
Slovakia	2				2
Spain	3				3
Sweden				1	1
Turkey					2
UK	3		3		6
Ukraine	11	2			13
Sum	82	30	39	2	155

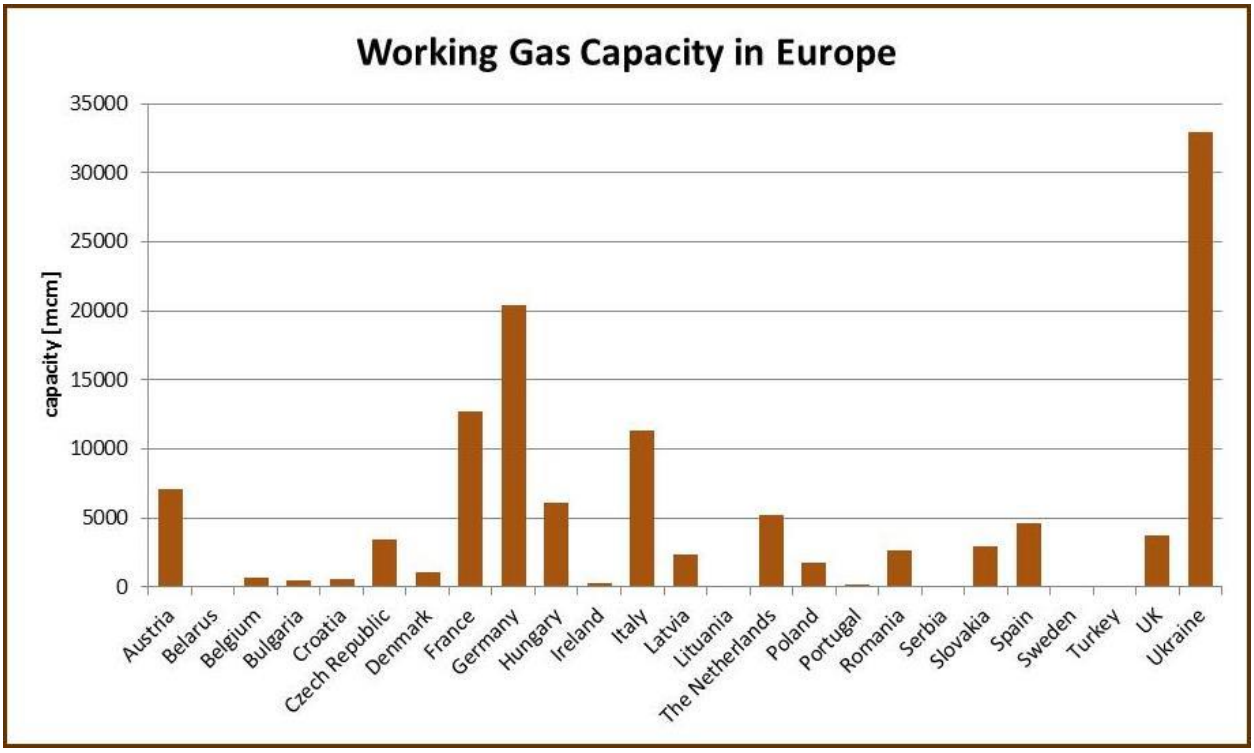

Figure 20. Working Gas Capacity by Country in Europe
(Gas Infrastructure Europe: GSE Storage Map May 2012)

3.6 European Storage Leak Risks and Incidents

- ~112 European UGS facilities operational and abandoned in O&G fields and aquifers (Table 3)
- 11 of these reservoirs have leaked (Table 4)
- 11/112 = 9.8% leakage risk

Table 4 European UGS Leakage Events (Evans, 2009)

Storage Facility Type					
Country	**Depleted field**	**Aquifer**	**Salt Cavern**	**Mine/ Rock Cavern**	**Total**
Russia			6		**6**
France		1	3		**4**
Germany	1	4	2		**7**
Poland		1			**1**
Hungary		1			**1**
Belgium				1	**1**
Denmark		1			**1**
Finlang				1	**1**
GB&Ireland	2		1		**3**
Sum	**3**	**8**	**12**	**2**	**25**

Evans (2009) reports that only two of these facilities have experienced leakage due to caprock integrity issues (see Table 5 and Table 6), but geologic data suggests a faulted caprock may have played a significant role in another european gas storage leak as well. We have analyzed all three of these incidents, but have selected our in-depth study of Ketzin to present here.

Table 5 European UGS Leakage Events for Depleted O&G Fields (Evans, 2009)

Depleted Oil/Gasfield Storage					
Facility	Operator	Product	Date	Description of efent/fatalities/injuries	Reported cause/comment
Rough Gasfield, Southern North Sea, UK sector	Centrica	Gas	Feb-06	Explosion and fire, 2 injured, 31 airlifted from platform	Catastrophic failure of a cooler unit in one of the four glycol dehydration units, leading to explosion in vicinity
Breitbrunn/Eggstatt, Gasfield in Bavaria, Germany	not available	Gas	2003	Pressure increase in the first annulus of the borehole	Failure of the well completion
SW Kinsale gasfield, offshore SE Ireland	Marathon	Gas	?1971-present	Leakage of original gas reserves to seabed, Field discovered in 1971	Geochemical studies indicate original gas leaking through caprock prior to conversion & operation as gas storage in 2001

Table 6 European UGS Leakage Events for Aquifers (Evans, 2009)

Aquifer Storage					
Facility	Operator	Product	Date	Description of efent/fatalities/injuries	Reported cause/comment
Spandau, Germany	GASAG	Gas	Apr-04	Explosion, 9 injured, 3 serviously, 500 evacuated in 1 km radius of incident	Explosion, perhaps linked to mainenance work, a defective seal, or work on the facilities contents gauges, destroyed the wellhead
Ketzin (Knoblauch), Berlin, Germany	1960s - not available, laterally UGS Mittenwalde	Town gas (1960s), natural gas (1970s - 2000)	1960s - 2000	1960s - gas migration from reservoir to surface, twon of Knoblauch evacuated (permanently ?), 1 fatality in house	Cap rock not gas tight - migration along faults in cap rock also thought likely. The 1 fatality linked to CO migration up old well into house
Kalle, Germany	RWE	Gas	1999	Loss of stored product - pressure differences noted	Leakage from reservoir, probably via two wells & over an extended perod at maximum of 60 000 m³/d
Stenlille, Denmark	Danish Oil and Gas company	Gas	1995	Gas in shallow aquifer and bubbled to surface	Casing leak, quickly corrected
Chémery, France	Gaz de France	Gas	Sept. 1989	Major gas leak, no explosion. Flights diverted around gas cloud	During routine maintenance of well completion and replacement of a filter
Frankenthal, Germany	Saar-Ferngas	Gas	Sept. 1980	Gas escape, no explosion, no casualities	Drilling into existing pipework
Poland	not available	Gas	not available	Well blowout leading to fire	Well blowout during drilling of horizontal well to increase reservoir capacity. Large volumes of gas lost, which was ignited by an electrical unit
Hungary	not available	Gas	not available	Well blowout during workover	Control of a swab kick lost during workover, resulting in blowout & fire, well killed & plugged

3.6.1 Ketzin, Germany

The Ketzin gas storage facility (Table 6) is a former aquifer storage site ~25 km (15.5 miles) west of Berlin operated by UGS Mittenwalde (Evans, 2009). It was developed in the Northeast German Basin (NEGB), part of a Permian basin system that extends from the east of England and the North Sea across Denmark, the Netherlands and northern Germany to Poland (Figure 21; Förster et al, 2006). Thick sequences of salt were deposited during the Permian, followed by a thick series of sandstones and mudstones deposited during Triassic and Jurassic times. Consequent vertical and lateral salt flow resulted in a series of pillows, walls and diapirs, further resulting in deformation of the overlying Mesozoic sedimentary overburden, and forming a system of anticlines and synclines (Figure 22; Förster et al., 2006; Juhlin et al., 2006).

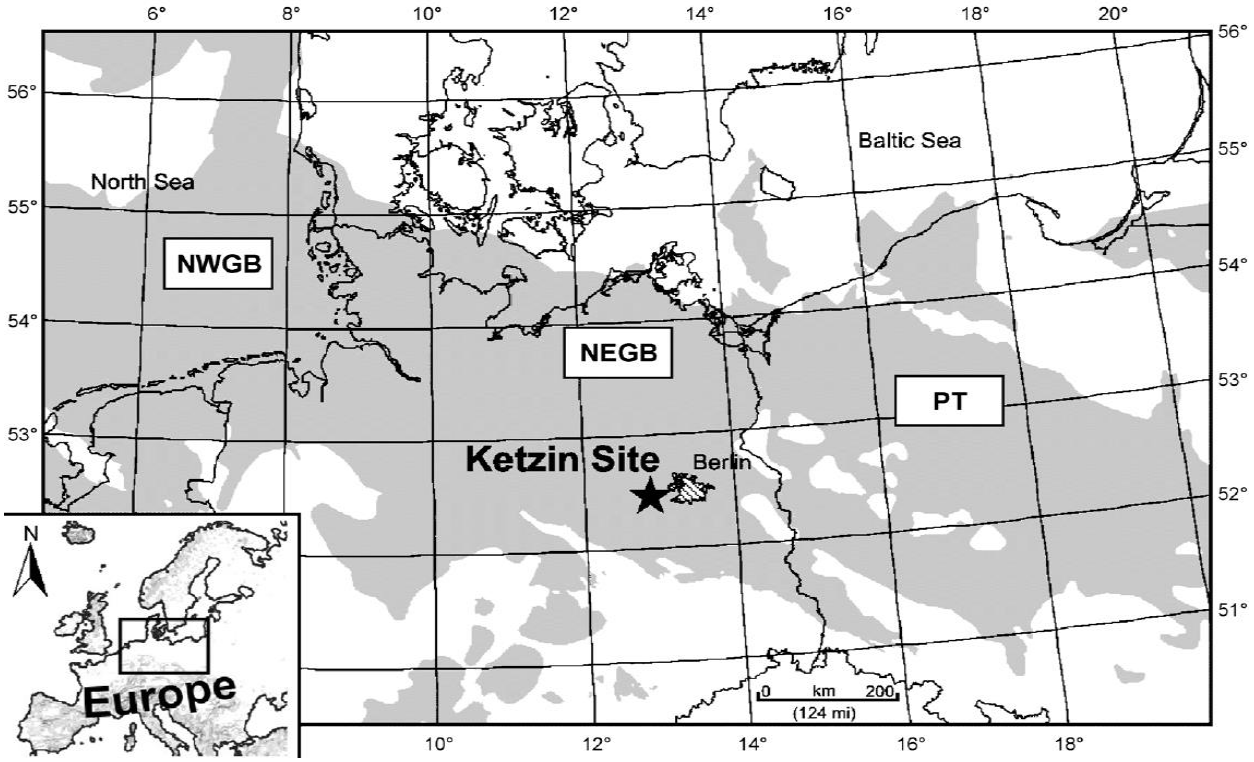

Figure 21. Permian Basin (grey), with Northeast German Basin (NEGB)
(Förster et al, 2006)

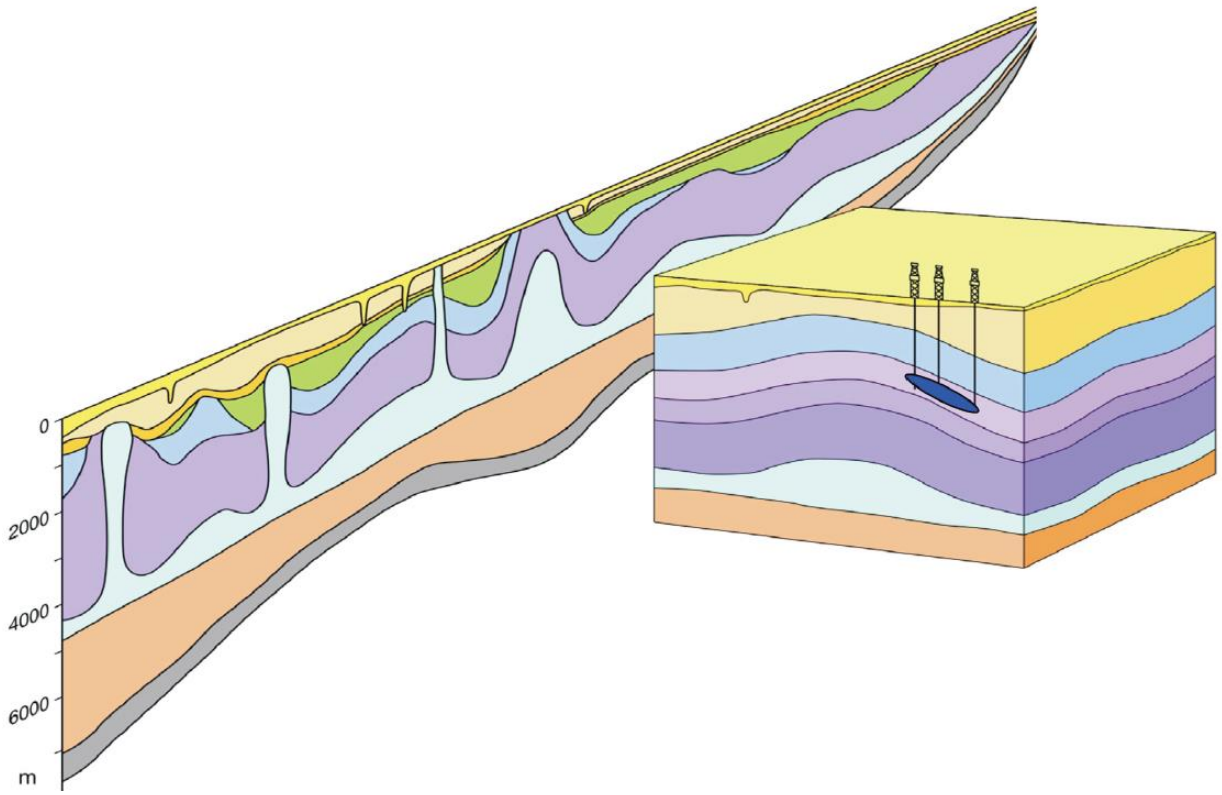

Figure 22. Schematic cross section and block diagram of regional and local, respectively, deformation of Paleozoic salt sequences (light blue) and overlying Mesozoic sedimentary series (purple, blue and green) at Ketzin
Ketzin is represented in the block diagram, also note Quaternary glacial troughs (uppermost yellow), which in some cases reach down into the Upper Mesozoic (CO_2sink.org)

The Ketzin site lies on the eastern part of a double anticline, the Roskow-Ketzin Anticline (Figure 23), which is formed above an elongated NNE-SSW trending salt pillow that developed at a depth of 1500-2000 m (4925-6550 ft). The anticline developed during several phases of salt movement during the Mesozoic (Juhlin et al., 2006). The axis of the anticline similarly strikes NNE-SSW; the flanks gently dip about 15° (Yordkayhun et al, 2009). Lower Cretaceous rocks were eroded around 106 Ma, or perhaps never deposited on this local structural high, but Jurassic rocks clearly were deposited then eroded at this later time, about 500 m (1600 ft) thereof (Figure 24 & Figure 25; Förster et al, 2006). Sediments of the Oligocene (Rupelian) form the first formation unaffected by anticlinal uplift resting above Jurassic sediments. These transgressive sediments are the first indicators of regional downwarping of the central parts of the NEGB that lasts until present (Förster et al, 2006).

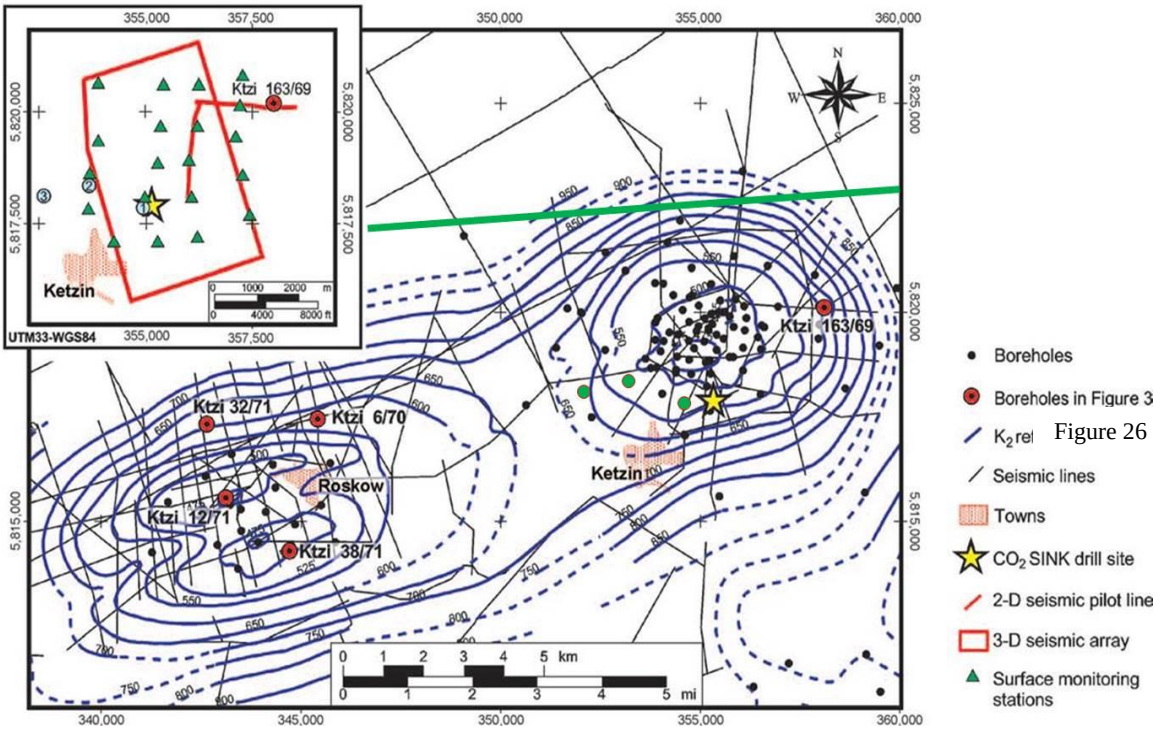

Figure 23. Roskow-Ketzin double anticline

Isolines (m) indicate K2 (gypsum/anhydrite) seismic reflector (for stratigraphic relation see Figure 26; for shallow cross section along green line of section see Figure 29; encircled numbers on inset map denote locations of shallow boreholes, also on main map in green, used for structure map in Figure 30: after Förster et al, 2006)

Faulting affects the crest of the anticlinal structure, with a 600-800 m (1970-2625 ft) wide E-W striking central graben fault zone (CGFZ) (Figure 24). Faulting in the CGFZ extends down to Triassic levels and the bounding faults have about 30 m (100 ft) of downthrow, but faulting appears to die out quickly in the overlying Rupelian clay/mudstones (Figure 24 & Figure 25; Juhlin et al., 2006).

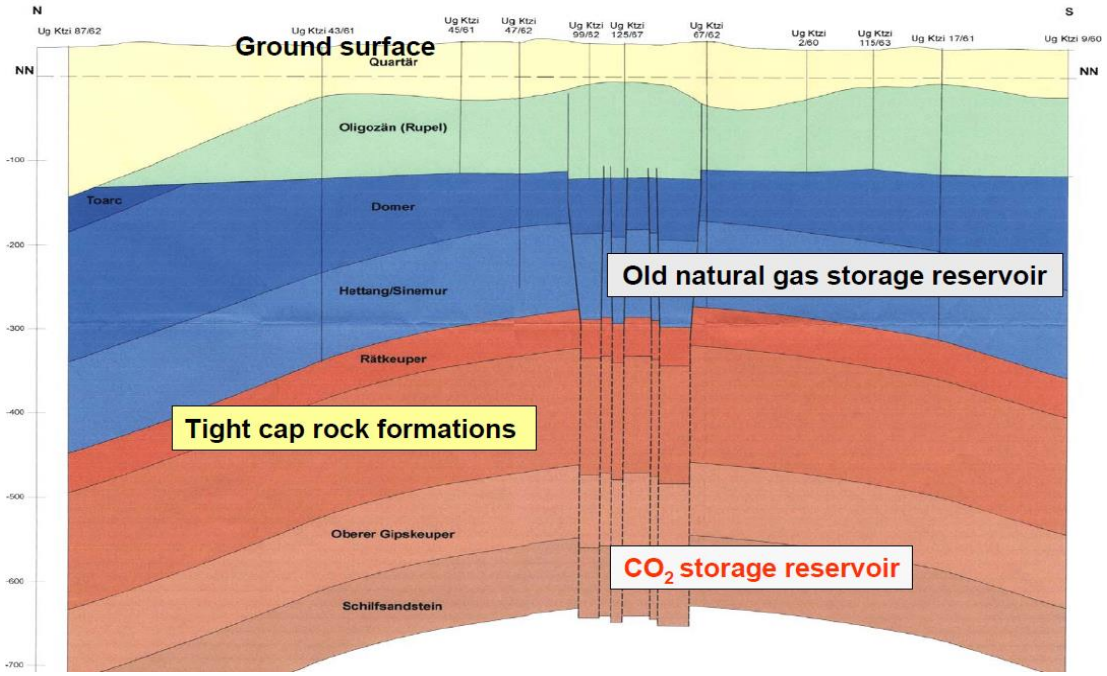

Figure 24. Geologic cross section through Ketzin Anticline, showing normal faulting in anticline crest
(Christensen, 2004)

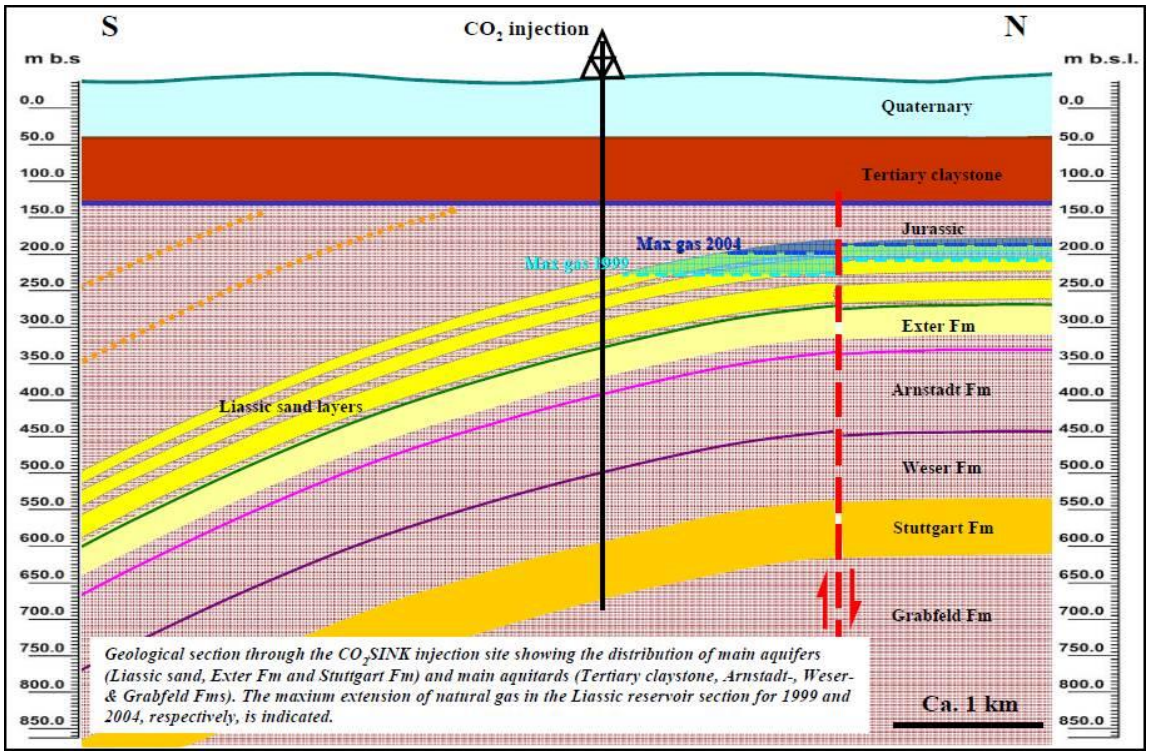

Figure 25. UGS cross section of maximum gas distribution in 1999 and 2004
Note that the shown fault would be the furthest south normal fault in the CGFZ (Schilling, 2007)

Saline aquifers of Lower Jurassic age (Hettangian stage Lias sands) at between 250 and 400 m (820-1310 ft) below sea level are present in the Ketzin anticline and were used for storage of natural gas between the 1960s and 2000 (Juhlin et al., 2006). The thick (80-90 m (260-295 ft)) overlying Tertiary (Oligocene) Rupelian clay/mudstones form the caprock for the aquifer system (Figure 24 - Figure 26; Yordkayhun et al, 2009). This Tertiary clay acts as a major aquitard separating the saline waters (brines) in the deeper aquifers from the non-saline groundwater in shallow Quaternary aquifers (Yordkayhun et al, 2009). The facility was largely imported from Siberia originally but was modernized in the 1990's (Schilling, 2007). In 2000 injection ceased, and in 2004 the site was abandoned (Yordkayhun et al, 2009) after the (aquifer) reservoir pressure had been lowered to approximately 17 bar (247 psi) below hydrostatic pressure (Juhlin et al., 2006). The maximum extents of the stored gas plume just before injection ceased and at the time of abandonment five years later are shown in Figure 27.

Although abandoned in 2004, some infrastructure from the facility remained and deeper aquifers in the lithologically heterogeneous Stuttgart Formation of Upper Triassic age have been tested for CO_2 storage purposes since (Figure 22 - Figure 27; Juhlin et al., 2006). Establishment of the EU-funded CO_2SINK, the first European research and development project related to the in-situ testing of geologic sequestration (Förster et al, 2006), and, consequently, the characterization of the Stuttgart Formation and its overlying thick mudstone formations for CO_2 sequestration, began as soon as the site was abandoned, in April 2004, and trial injection of CO_2 commenced in June 2008 (Bergmann et al, 2011). Whereas the gas storage reservoir was largely within the CGFZ, the CO_2 sequestration trial is being carried out outside of the fault zone (Figure 25 & Figure 27 & Figure 28).

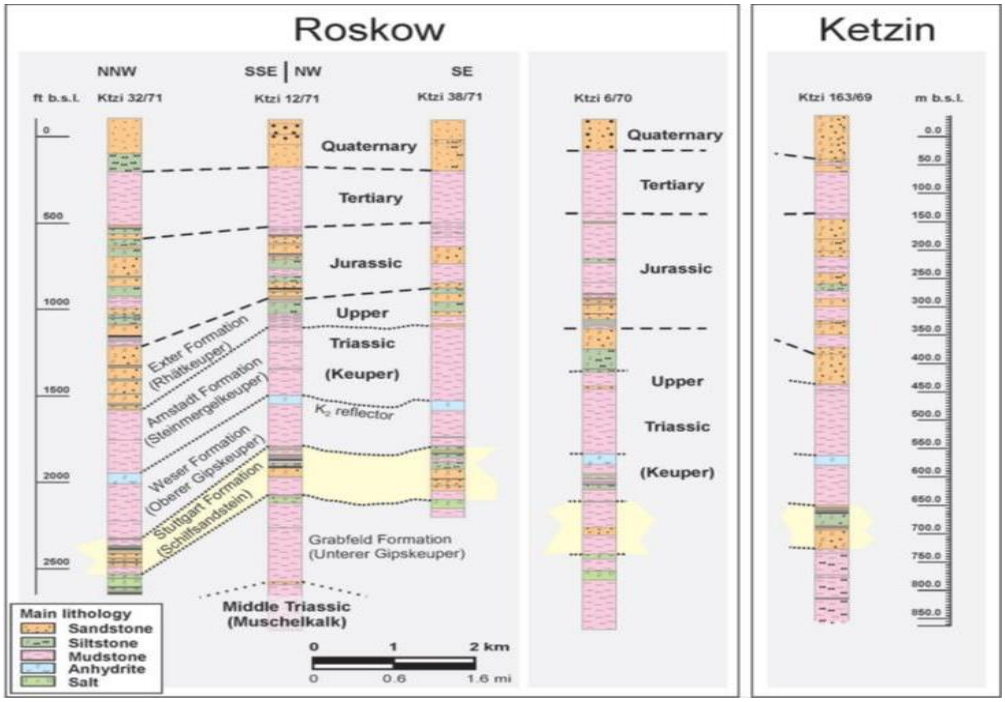

Figure 26. Well-correlated stratigraphic column for Roskow-Ketzin Anticline
(for borehole locations see Figure 23; Förster et al, 2006)

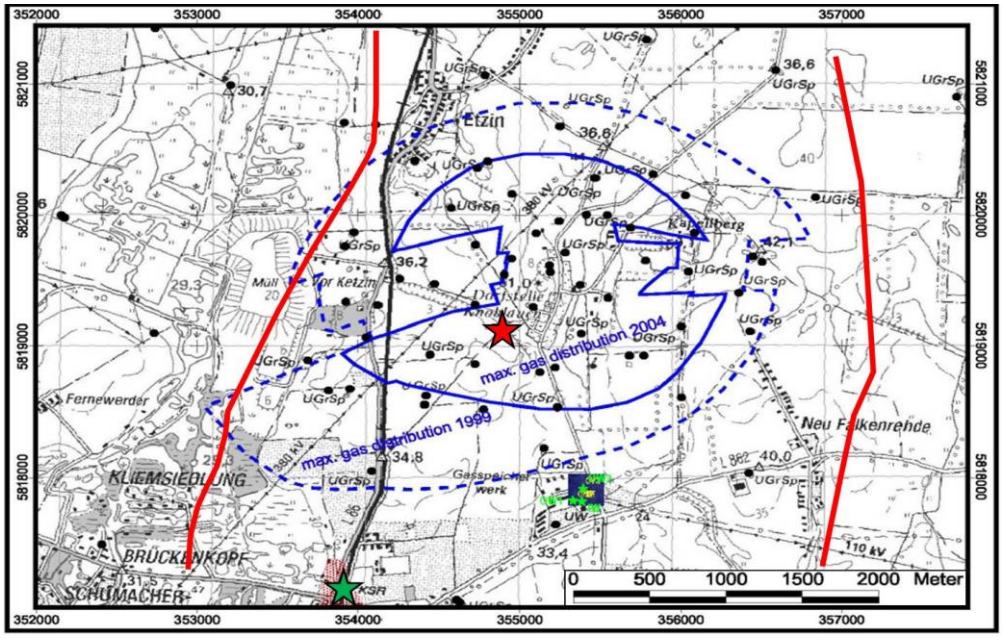

Figure 27. UGS map of maximum gas distribution in 1999 and 2004
CO_2 injection site denoted by blue square, just south of 1999 max gas extent; red lines indicate near sides of glacially eroded troughs depicted in Figure 29 & Figure 30; red star indicates location of Knoblauch, the green star the location of the town, Ketzin (after Schilling, 2007)

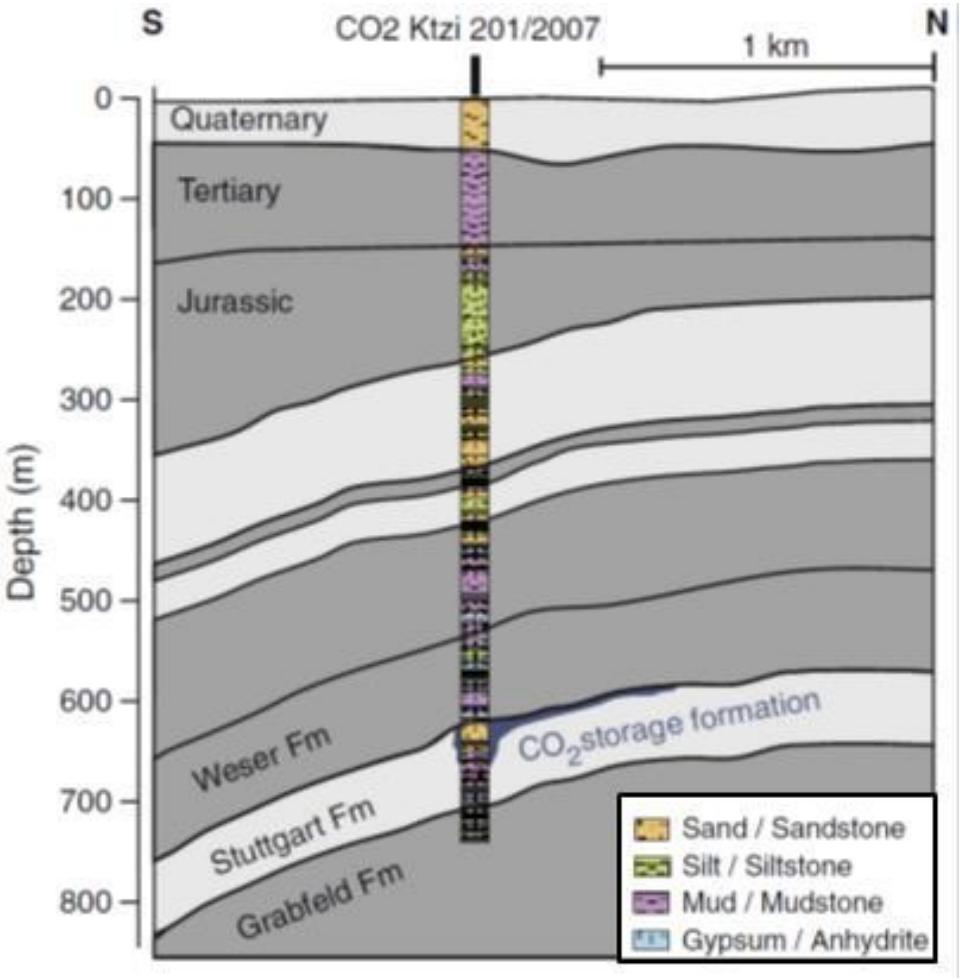

Figure 28. Simplified geology of Ketzin anticline with lithology
Aquifers in light gray, auqitards in dark gray (Bergmann et al, 2011)

Though information is incomplete during the 1960's when this area was in the GDR (DDR), reports indicate that stored gas migrated out of the reservoir and found its way to the surface, causing the permanent evacuation of the nearby village of Knoblauch (see Figure 27 for location; Kanter, 2007).

One source (not independently verified; Augustiniak) indicates that wells were originally drilled in 1963 and that gas was injected for the first time in September 1964. CO was detected in Knoblauch houses in the winter of 1965. A wellhead blowout occurred in the summer of 1966, followed by a larger blowout in October 1966 resulting in evacuations. Consequently, GDR (DDR) officials decided to completely and permanently evacuate the town in December 1966. This was carried out in early 1967, with most of the residents being relocated about 2.5 km (1.5 miles) SSW to the town of Ketzin.

The mechanism by which this migration occurred has been attributed to an insufficient caprock (not gas tight) or leaky faults in the caprock, or both (Evans, 2008). A third possibility is that the caprock seems to be nonexistent in some places due to deep Quaternary glacial erosion (Förster et al, 2006; Yordkayhun et al, 2009).

Seismic reflection studies about 2005 revealed amplitude anomalies in the aquifer units, indicating that remnant (cushion or residual) gas remained in some aquifer units near the crest of the Central Graben Fault Zone (CGFZ; Figure 24 & Figure 25). Amplitude anomalies and a gas chimney about 1 km (3281 ft) long and 100 m (328 ft) wide was observed on seismic reflection data acquired over the southwestern, east-west striking main fault of the CGFZ. This indicated that the stored or remnant gas either had been or was at that time migrating out of the reservoir formations, circumstantially implicating the faults as conduits (Juhlin et al., 2006).

While characterizing the deeper aquifers for CO_2 sequestration, special attention in the scrutiny of previous exploration data was directed toward fault zones that may cross the Ketzin anticline and may become crucial in evaluating Triassic caprock integrity as part of the risk assessment. Several seismic sections in the NEGB show that the Mesozoic and younger overburden in anticlinal structures are intersected by faults of the CGFZ. The fault zone is about 600 m (1968 feet) wide, with subtle throws from 0 to 20 m (66 feet). The identification and mapping of fault zones has not been without controversy in the Ketzin structure, especially with regard to extent at depth, but there does seem to be convergence of opinion with regard to the faulted nature of the Jurassic section, in which the natural gas was stored (Förster et al, 2006).

Concerning the possibility that the caprock is "insufficiently gas tight," this is explained further in the literature. Given that the Rupelian caprock of clay/mudstones is 80-90 m (260-295 ft) thick and has proven to be an effective aquitard separating brines in the deeper aquifers from non-saline groundwater in the shallow Quaternary aquifers (Figure 24 - Figure 26 & Figure 28; Yordkayhun et al, 2009), perhaps any non-faulted migrations of storage gas are attributable to glacially eroded 'gaps' in the caprock. There is evidence that local erosion of the Rupelian aquitard at some locations does in fact allow saline waters to ascend and mix with fresh water in the shallower aquifers (Förster et al, 2006).

A typical feature of the subhorizontal base of the Quaternary is a glacial erosional trough incised down to the Upper Jurassic and filled with Quaternary sediments (Figure 29). At the western and eastern flanks of the Ketzin anticline, two glacial, NNE-SSW oriented erosional troughs are incised into the Tertiary clay aquitard and into the Jurassic (Figure 30). These troughs are filled with Quaternary sediments. The local erosion of the Rupelian aquitard may allow saline waters to ascend and mix with fresh water in shallow aquifers. The lower part of the Quaternary sedimentary infill consists of two sand aquifers which are hydraulically connected with the Jurassic aquifer system and are separated from each other by clayey and silty units (Förster et al, 2006; Yordkayhun et al, 2009).

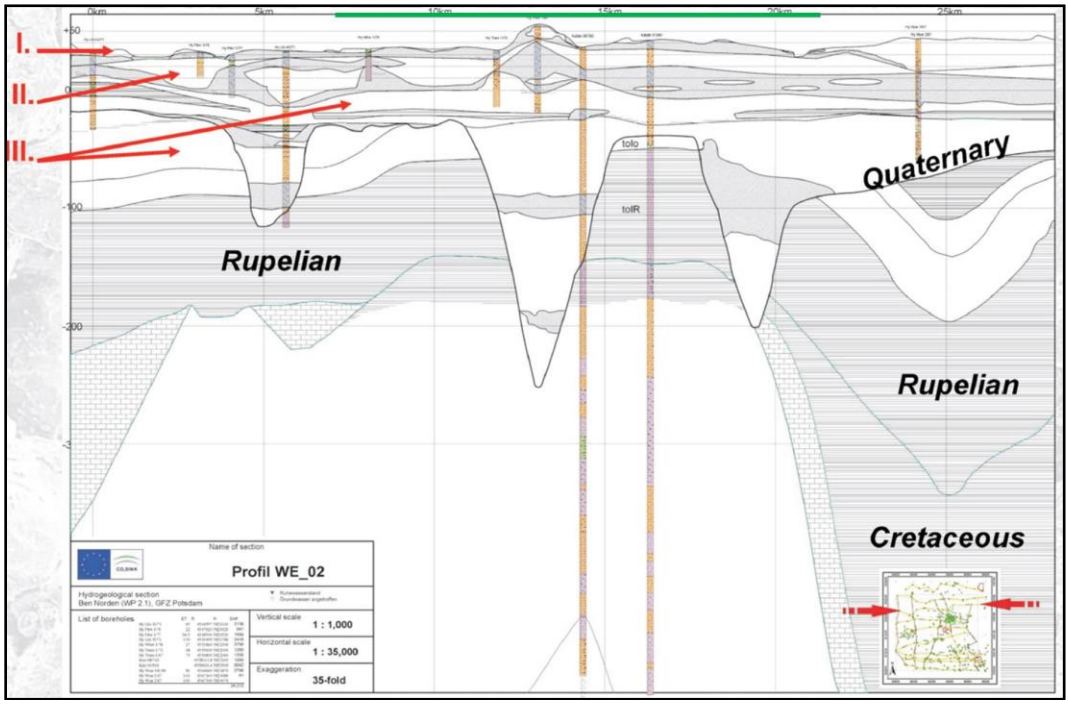

Figure 29. Schematic cross section of the Quaternary groundwater system at Ketzin. Below the Rupelian clay saline groundwater is present, freshwater above; glacially eroded and filled surface also shown

Location of green line of section indicated on Figure 23 (after CO_2sink.org)

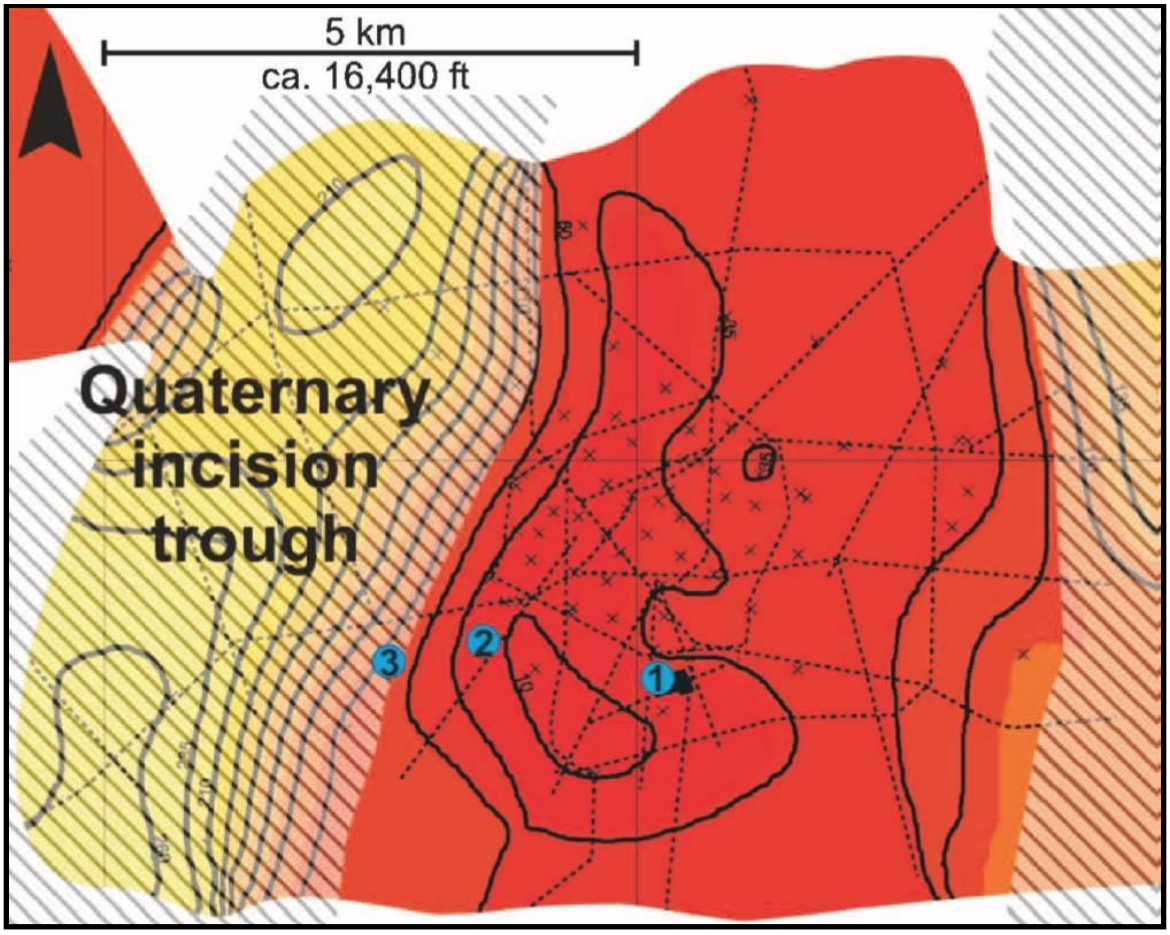

Figure 30. Structural map of the base of Quaternary (CI: 25 m [82 ft]) derived from a numerical geological model. Dotted lines denote seismic lines, and crosses denote boreholes incorporated in this spatial model. Areas of glacial troughs incised into the Upper Jurassic are hachured. Blue numbered dots designate shallow boreholes also found on Figure 23 (after Förster et al, 2006)

Although the upper part of the trough fill predominantly comprises silty and clayey sediments mostly prohibiting an upward migration of saline water, by geographically coordinating and overlaying different maps, it also seems possible that stored natural gas in the 1960's could have found a path to the surface via these erosional troughs (Figure 27 & Figure 30). In fact, given these Figures (Figure 23 & Figure 29 as well), it's surprising that more gas wasn't reported to have migrated out of the Jurassic reservoir after the 1960's.

3.7 Gas Leakage Incident Rates

We have reviewed historical data and documented caprock integrity problems of the gas storage industry. Reviewing and analyzing many of these incidents provides useful information to the CO_2 sequestration industry, helping to recognize and identify risk conditions and improve project design and operating practices to help ensure permanent geologic storage. This effort consisted in collecting and analyzing gas storage data associated with caprock integrity problems, and examining maximum pressure limits and analyzing past failure incidents that have occurred during gas storage operations.

Relying principally on two previous studies (Perry 2005 & Evans 2009), we identified 22 incidents of gas leakage due to caprock integrity issues worldwide, about 10% of all reported leakage incidents. Of these, half were due solely to an insufficiently gas-tight caprock, whether too thin, too permeable, or made of dissoluble constituents. Another quarter of these incidents were due solely to undetected or incorrectly characterized faults and/or fractures through the caprock, allowing fluid communication between the reservoir and formations unintended for storage. Finally, the remaining quarter were cases in which both of these factors are believed to have played a role in leakage.

It should come as no surprise that most instances of these *geologically related* gas migration problems have occurred in aquifer gas storage operations. While comprising only about 10% of natural gas storage reservoirs overall, aquifer storage operations account for about 65% of these 22 incidents. In these cases, conduits in the caprock are present because of previously unrecognized fracturing or faulting of the gas storage field. Leaks occur as a result of the more challenging nature of aquifer gas storage: less geologic data, higher required pressures and unconfirmed sealing.

Typically, a large anticlinal structure with as many feet of closure as possible is an important criteria for an aquifer gas storage field (see Fig. 2). Large structural deformation, however, introduces a greater possibility of caprock flaws and potential leakage (Perry 2005), since the same forces that create folded structures also create faulted structures.

Thus the two root causes for failures for many of these, and likely for all of these 22, cases are because the geology of the site was not properly characterized and/or the pressure in the storage reservoir was too high (Benson 2002).

Creating pressure gradients that the storage formations have not experienced before can result in the displacement of the static water column, forcing water out of the caprock and causing gas to leak from the storage formation (Katz 1999), thus exceeding the threshold displacement pressure or threshold pressure (i.e., the gas pressure is high enough to displace water-gas menisci in the rock pores) (Benson 2002).

It is also important to recognize that the pressure required to fracture a reservoir is not constant, but changes with average reservoir pressure. It is easier to fracture a formation that is in a pressure depleted state as compared to the reservoir at original pressure conditions.

We estimated failure rates and risk based on our survey of the studies mentioned above. The rate of failure for O&G and aquifer gas storage fields can be estimated thusly: of 485 operational and abandoned such UNGS facilities in the U.S., Europe and Central Asia studied, 22 have experienced leakage due to caprock insufficiencies, representing a 4.5% rate of caprock failure.

It is very important to recognize, however, that reported and documented leakage incidents are not at all comprehensive. Most leakage incidents are not documented. During the past five years GeoMechanics Technologies has been involved in half a dozen legal disputes involving storage gas migration which are not documented or mentioned in literature. The natural gas storage industry has a strong economic incentive not to lose gas. Yet it does not achieve anything close to 99% containment over decades, the stated goal of some organizations such as the US Department of Energy Geologic Storage Program. In our opinion 99% containment over 100 years is a worthy goal, but not a likely outcome.

Based on historical data from the gas storage industry, and even based on recent experience with large scale CO_2 sequestration projects to date (consider In Salah for example), a one in ten (10^{-1}) probability of out-of-zone leakage incidents is a reasonable order of magnitude estimate for leakage risk with CO_2 sequestration projects. That is, of every 10 large scale CO_2 sequestration projects, expect that one or more will experience out of zone leakage incidents. But it is also important to note that leakage out of zone does not generally result in leakage to surface. Reservoir and overburden geologic and geomechanical characterization is a critical requirement for risk assessment.

3.8 Summary: UNGS Caprock Lessons for CCS

No reservoir caprock or trap has ever been shown to be a perfect seal to hydrocarbon migration (Keeley, 2008), especially not over a geologic timescale, but a review of all 22 cases in our final report (Table 1) indicate that on a human timescale such migration can be avoided by proper geologic characterization, using modern tools and protocols, and keeping reservoir pressures below threshold displacement pressures (Benson, 2002). A detailed list of critical factors requiring consideration for avoiding all incidents at UNGS facilities is offered by Evans & West (2008), offered as an appendix in our final report.

If a unit already traps hydrocarbons at depth, especially natural gas, then it is highly likely that it will also trap CO_2 for millennia. For aquifer storage projects, however, extensive site characterization is required. The quality of the caprock needs to be determined by examining cores and testing them in the laboratory. Well testing methods have been developed specifically for evaluating the permeability of the caprock. In addition, capillary pressure measurements on core samples can quantify the amount of buoyant force a caprock can maintain before failing. Conventional well-logging tools and techniques, field measurements, and stratigraphic mapping and analysis are particularly useful for determining the large-scale features of the caprock that could not be tested on laboratory samples, such as thickness and lateral continuity, an appropriate structure with sufficient closure, and the presence of faults or fractures (Benson, 2002 & Burton et al, 2007). And, of course, if a structure with sufficient closure is identified, the presence of faults and fractures is all the more likely, and in need of close scrutiny (Perry, 2005).

Evaluating safe operating conditions for CO_2 injection in reservoirs, which would guarantee the absence of CO_2 leakage from overpressuring, is a challenge being met at UNGS facilities with the development of both geomechanical and fluid flow models. Such simulations can determine when, upon fluid injection, the joint action of pressure buildup and thermal expansion will lead to the development of tensile stresses in the caprock. When these stresses overcome the tensile strength of the rock, the caprock fractures. Whether such fractures can cause CO_2 leakage depends on their ability to propagate, which is driven by fluid outflow from the reservoir (Gor et al, 2012).

As has been pointed out, most leaks are because of wellbore issues (Evans & West, 2008; Evans, 2009; Perry, 2005), but we don't know how to fix caprock integrity problems. The gas storage and oil and gas industries have been successful in repairing wellbore leaks but there is no known case where a geologic leak through a confining layer or caprock has been sealed (Perry, 2005). This has been due, at least in part, to the two industries which mainly rely on caprock integrity not having had sufficient economic reason to develop such an

ex post facto fix. First, in the case of the oil and gas industry, the need is usually not present, as any caprock flaw would have precluded the trapping of commercial volumes of hydrocarbons in the first place. Without the commercial potential the oil and gas industry has neither interest in these features nor any incentive to investigate caprock seals. Second, the gas storage industry clearly does have interest in caprock seals, especially in the aquifer storage area, and has performed some, but limited, research (Perry, 2005). But a review of the 22 cases in our final report (Table 2) indicates that caprock leakage has been largely avoided in the past 35 years, most likely through the application of geologic characterization and geomechanical and fluid flow simulations, as recommended here, both more economical and practical than *in situ*, underground remediation.

The loss of gas from UNGS facilities should not be overstated, however. The release rates of gas from non-point leaks in depleted O&G fields are relatively slow (Table 7). And Evans & West (2008) estimate that for all leakage events in the U.S., not just caprock integrity breaches, data covering more than 10,000 facility years demonstrate that "operational engineered storage systems can contain methane with release rates of 10^{-4} to 10^{-6} per year." (Evans & West, 2008) Unfortunately they don't include units here, but those are relatively small release rates, no matter the units. And this is a rough estimation, as Evans opines, "a lack of information relating to many of the 65 problems described above means that at this stage, information on the number of wells at any one site, the years of operation/downtime or exact opening/closure date is not available. It is, therefore, difficult to determine the incident rates relative to 'storage experience', either as the total operational hours of gas storage against number of incidents, or the total operational well hours against the number of incidents." (ibid.)

Table 7 Summary of CH_4 leakage rates for different pathways from a depleted O&G field
For a reservoir area of 1km^2, thickness of 100m, and temperature of 288K, the amount of reservoir gas is 2.67e9 to 1.00e10 kg (Watson et al, 2008).

Storage scenario	*Release pathway*	*Mass discharge (kg/s)*	*Area of discharge (m^2)*	*Mass flux (kg/s/m^2)*	*Time to exhaust source*	*Probability of occurrence*
Depleted oil/gas fields – mixed permeability	Rapid advective	240	0.05	N/A	1.4 years	Low
	Viscous dominated – 400 m deep	9.89E-5	200	4.95E-7	9.9E+12 years	Intermediate
	Viscous dominated – 1500 m deep	2.73E-4	200	1.37E-6	3.7E+13 years	Intermediate
	Diffusive	1.12E-7	2.5E+5	4.5E-13	1.2E+18 years	High
	Near-surface exsolution	5.9E-7	1200	4.9E-10	N/A	Intermediate

Nonetheless, Perry suggests there have been significant advances in recent years in many areas that may allow for the successful sealing of a caprock leaks in the future. While not successful to date, significant potential has been indicated through application of newer seismic and well steering for locating and accessing the leak zone. And new fluids such as foams and other materials to control fluid flow in the storage zone and the overlying caprock could then be applied. Thus, this is an area where the CO_2 storage industry may wish to perform additional research (Perry, 2005).

4 Theoretical Description and Documentation of Caprock Integrity Issues

4.1 Numerical Development

Injection of large quantities of CO_2 into a porous media necessarily requires elevation of the pore pressure in order to displace the existing fluids. Large scale CO_2 injection also modifies temperature, as injected material is generally lower temperature than the formation. These pressure and temperature changes in the storage zone cause formation expansion and induce stresses in the overlying caprock. The geomechanical integrity of the caprock can be compromised by three basic mechanisms. These are:

1. Potential tensile fracturing;
2. Potential fault activation;
3. Potential bedding plane slip.

In general the stresses induced in the caprock and resulting damage risk must be determined through 3D geomechanical modelling and numerical simulation. It is important, however, to consider the underlying physics and fundamental analytical solutions upon which such analyses are based, in order to gain insight into the important mechanisms and parameters which influence caprock integrity.

If we consider a small volume element V within the storage zone, the change in volume ΔV induced by pressure and temperature changes may be expressed as:

$$\Delta V/V = Cb\Delta P + 3\alpha\Delta T \qquad (1)$$

where Cb is the material bulk compressibility and α is the linear coefficient of thermal expansion. Note that both pressure increase and temperature increase induce expansion. Conversely, a pressure decrease and a temperature decrease induce contraction.

If the storage formation was completely free to expand or contract in all directions, there would be no stresses induced. The surrounding formations, however, constrain this deformation. The result is that stresses are induced both within the storage reservoir and within the surrounding material (including the caprock). Considering only pore pressure increase, for example, compressive stresses are induced within the storage zone and tensile and shear stresses are induced in the caprock. These can lead to one or several of the caprock failure mechanisms listed above.

To further illustrate and discuss this fundamental mechanism inducing stresses in the caprock, we consider the displacements that are induced in the surrounding formation due to a center of dilation or contraction within the storage zone. As a first approximation, we describe and consider the fundamental equations for displacements, strains, and stresses in a continuum. Using index notation, strains ε_{ij} are related to displacement gradients $u_{i,j}$ through the equations:

$$\varepsilon_{ij} = \frac{1}{2}\left(u_{i,j} + u_{j,i}\right) \quad (2)$$

For general elasticity, the stresses in a body σ_{ij} are related to the strains through a general stiffness matrix C_{ijkl} and tensor relationship as follows:

$$\sigma_{ij} = C_{ijkl}\varepsilon_{kl} \quad (3)$$

The number of independent material properties contained in the stiffness relations of equation (3) depends on the type of material behavior. For completely "isotropic" materials (in which stiffness properties do not vary in any direction), there are only two independent material properties. Sedimentary formations are typically "transversely isotropic". That is, stiffness properties are constant in both directions parallel to bedding, but different in a direction perpendicular to bedding. For such materials, there are five independent material properties. But sedimentary layers with vertical fracture will have different stiffness properties even in the two directions parallel to bedding. Such materials are called "orthotropic", and contain nine independent material properties. Considering the simplest case of isotropic materials, the stress-strain and stress-displacement relations can be expressed as follows:

$$\sigma_{ij} = \lambda\delta_{ij}\varepsilon_{kk} + 2G\varepsilon_{ij} = \lambda\delta_{ij}u_{i,j} + G\left(u_{i,j} + u_{j,i}\right) \quad (4)$$

where λ and G are two independent material properties and δ_{ij} is the Kronecker delta which takes a value of unity when i=j and a value of zero otherwise. The material properties λ and G are can be expressed in terms of the more commonly used Young's Modulus, E, and Poisson's Ratio, ν, through:

$$\lambda = \frac{\nu E}{(1+\nu)(1-2\nu)} \text{ and } G = \frac{E}{2(1+\nu)} \quad (5)$$

Equation (4) can be applied to estimate the stresses induced in the caprock if the strains or displacement field is known. Solutions for the displacements and stresses induced in a half-space due to a center of dilation (or contraction) have been presented by Sen (1950) and Geertsma (1973) and applied by a number of researchers to evaluate subsidence and casing deformations induced by compacting reservoirs (see for example Bruno et al. 1998 & 2002). The displacement field produced by a center of dilation located at position (x_o, y_o, z_o) with pressure and temperature change, as given in Equation (1), is provided by the set of equations below:

$$u_x = P\left[\frac{\partial V_1}{\partial x} + 2z\frac{\partial^2 V_2}{\partial x\,\partial z} + (3-4\nu)\frac{\partial V_2}{\partial x}\right] \quad (6)$$

$$u_y = P\left[\frac{\partial V_1}{\partial y} + 2z\frac{\partial^2 V_2}{\partial y\,\partial z} + (3-4\nu)\frac{\partial V_2}{\partial y}\right] \quad (7)$$

$$u_z = P\left[\frac{\partial V_1}{\partial z} + 2z\frac{\partial^2 V_2}{\partial z^2} - (3-4\nu)\frac{\partial V_2}{\partial z}\right] \quad (8)$$

Where,

$$P = \frac{(1+\nu)}{12\pi(1-\nu)}\left[C_b\,\Delta P + 3\alpha\Delta T\right] \quad (9)$$

$$V_1 = \left[(x-x_0)^2 + (y-y_0)^2 + (z-z_0)^2\right]^{-\frac{1}{2}} \quad (10)$$

$$V_2 = [(x - x_0)^2 + (y - y_0)^2 + (z + z_0)^2]^{-\frac{1}{2}} \quad (11)$$

Equation (4) may now be combined with equations (6) through (11) to determine the stresses induced in the caprock due to pressure and temperature changes occurring within the storage zone. This is valid for elastic behavior of isotropic materials. For example, the horizontal shear stresses induced in the caprock, which might lead towards bedding plane slip and well damage, can be expressed as:

$$\sigma_{xz} = G\left[\partial u_x/\partial z + \partial u_z/\partial x\right] = \frac{EP}{(1+\nu)}\left[\frac{\partial^2 V_1}{\partial x\,\partial z} + 2z\frac{\partial^3 V_2}{\partial x\,\partial z^2} + \frac{\partial^2 V_2}{\partial x\,\partial z}\right] \quad (12)$$

and,

$$\sigma_{yz} = G\left[\partial u_y/\partial z + \partial u_z/\partial y\right] = \frac{EP}{(1+\nu)}\left[\frac{\partial^2 V_1}{\partial y\,\partial z} + 2z\frac{\partial^3 V_2}{\partial y\,\partial z^2} + \frac{\partial^2 V_2}{\partial y\,\partial z}\right] \quad (13)$$

Similar equations can be developed for any of the stress components at any location within the caprock. The change in pressure and temperature is measured from some reference state (typically the initial reservoir conditions) from which induced stresses are to be determined. The total induced stresses caused by varying temperature and pressure fields within an arbitrarily shaped reservoir can be obtained by integrating the contribution of all the center of dilation points over the entire reservoir volume. The equations above may be integrated analytically if the pressure and temperature distribution and reservoir shapes are simple functions, or numerically if they are more complex.

To illustrate a typical distribution of shear stresses within the caprock at the top of a reservoir, we present parametric results from numerical integration of equations (12) and (13) for an axisymmetric reservoir volume of radius R and height H, located at depth d below the surface, in which pressure change varies linearly from a maximum of ΔP at r=0 to zero at r=R. Shear stresses in
Figure 31. Nare normalized with respect to reservoir radius, height, pressure change, and material properties.

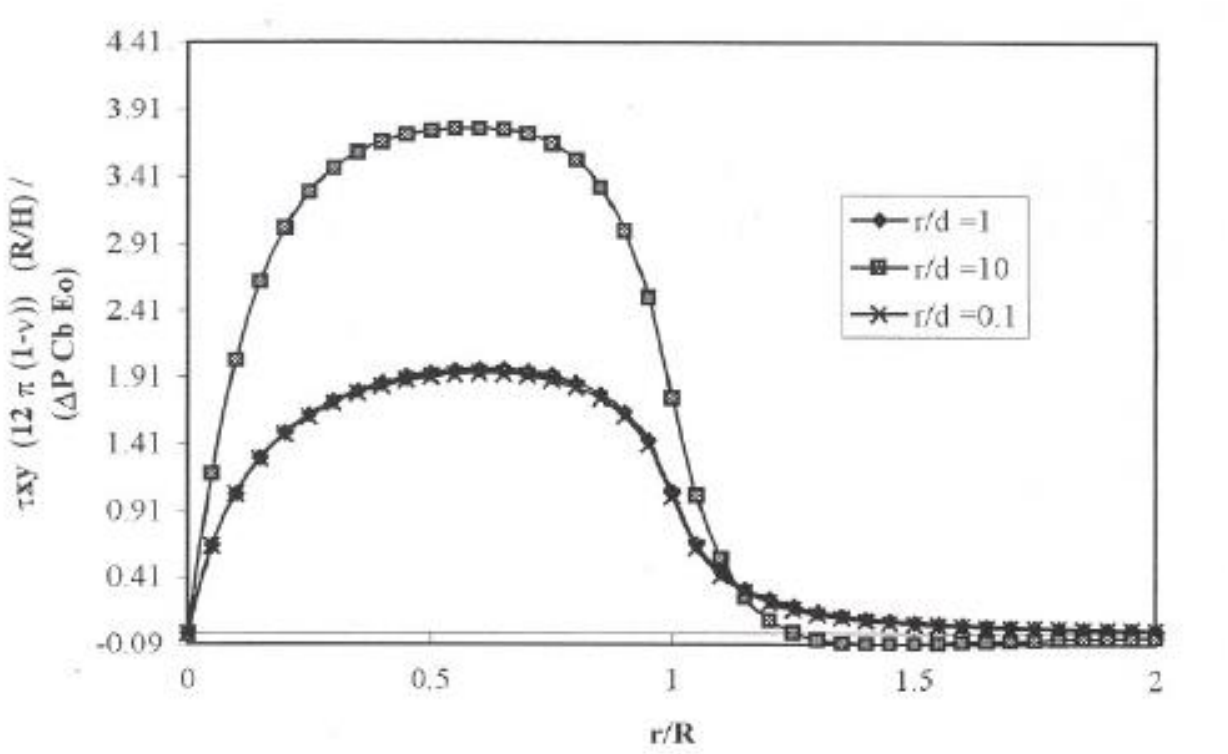

Figure 31. Normalized shear stress at the top of an axisymmetric reservoir with linear pressure change distribution

Although only a very few simple reservoir configurations can be solved analytically, the theoretical description nevertheless provides insight and guidance on relative risk factors. For example, it can be seen that induced shear stress magnitude increases with larger radius to depth ratio. But once a reservoir is deeper than about the distance of its radius, shear stress magnitude is relatively insensitive to depth and is instead controlled primarily by the ratio of reservoir thickness to reservoir radius. That is, pressure changes over a thicker reservoir interval will induce proportionately large shear stresses in the caprock than the same pressure change generated over a thinner reservoir interval. Analytical solutions can also be used for comparison and validation of numerical modelling approaches.

4.2 Theoretical Geomechanical Model Study

A 3D geomechanical model was created using FLAC 3D (Figure 32) to illustrate a typical distribution of induced shear stresses, caused by uniform pressure and linear pressure changes in the reservoir, within the caprock at the top of a radial shaped reservoir. For the first case, the pressure change is uniform over the entire reservoir, for the second case, the pressure change varies linearly from the center of the reservoir to its boundary.

The reservoir is near the center of the model (Figure 33). We have done a sensitivity study by varying the reservoir thickness (100m, 200m, and 400m) and radius (500m, 1000m, and 2000m). Additionally, we also vary

reservoir depth. For the initial model, the depth from the surface to the center of reservoir is 1000m, the caprock bottom is at the top of reservoir, and the formation surrounding the reservoir extends down to 4000m. The distance from the boundary to the center of the model in x, y directions is about six times the reservoir radius. For example, if the reservoir radius is 1000m, the model dimension will range from -6000m to 6000m in both x, y directions, and range from 0 to -4000m in z direction (Figure 32). About 216,000 total elements compose the model.

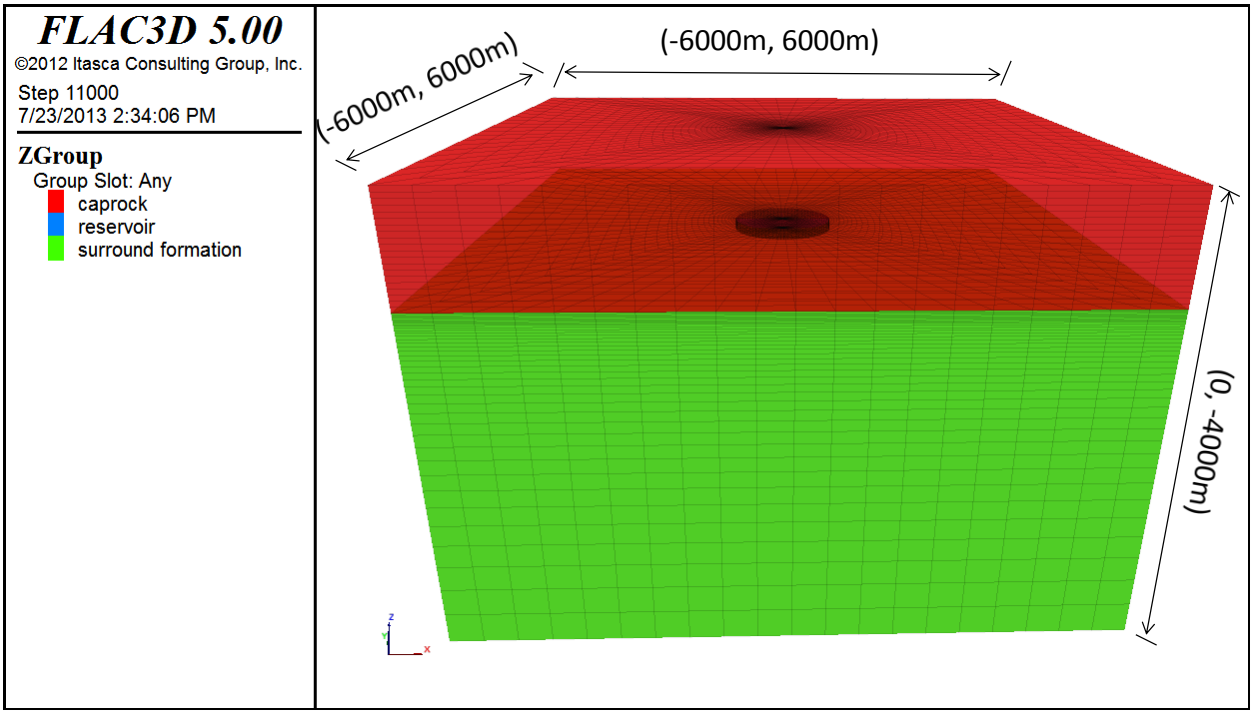

Figure 32. 3D geomechanical model used to illustrate induced shear stress in caprock

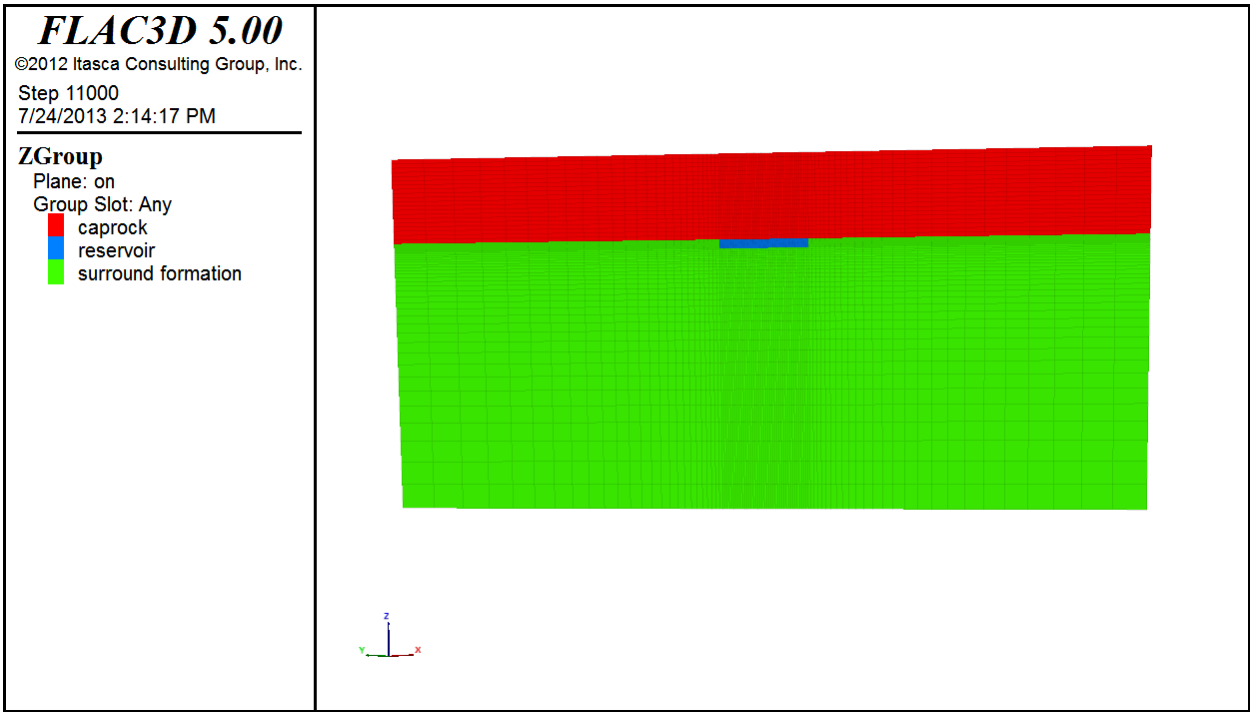

Figure 33. Cross section view of the geomechanical model through the model center

To illustrate the influence of pressure distribution shape on shear stress pattern and magnitude, we present in Figure 34 a comparison of uniform and linear pressure change in the field. In the example, the maximum pressure change is 8.25 MPa, the reservoir radius is 325m, the thickness is 50m, and the reservoir depth is 475m. The Young's Modulus for the caprock, reservoir and 'surround formation' is assumed to be 1 GPa, and the Poisson ratio is 0.25. Note that for a linearly varying pressure distribution, the shear stress is relatively uniformly distributed over the top of the reservoir. However, for the constant pressure distribution, the shear stress is asymptotic at the outer radius where there is severe discontinuity in the reservoir pressure and volume strain.

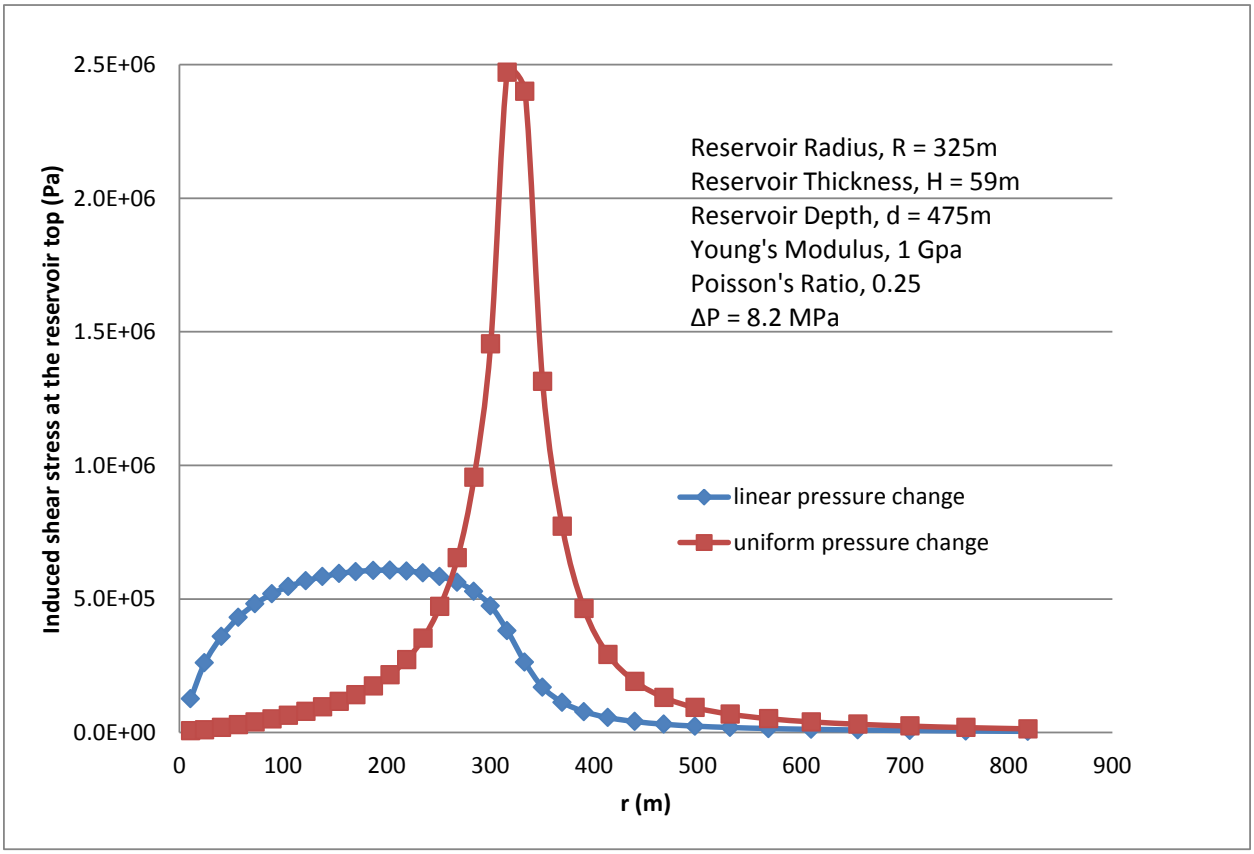

Figure 34. Comparison of induced shear stress for cases with linear and uniform pressure change.

For the same reservoir depth of 1000m with the same reservoir thickness, the induced shear stress is higher when the reservoir radius is smaller, for both uniform pressure change and linear pressure change in the reservoir (see Figure 35). However, for the same reservoir radius, the induced shear stress is higher when the reservoir is thicker, for both uniform pressure change and linear pressure change in the reservoir (see Figure 37).

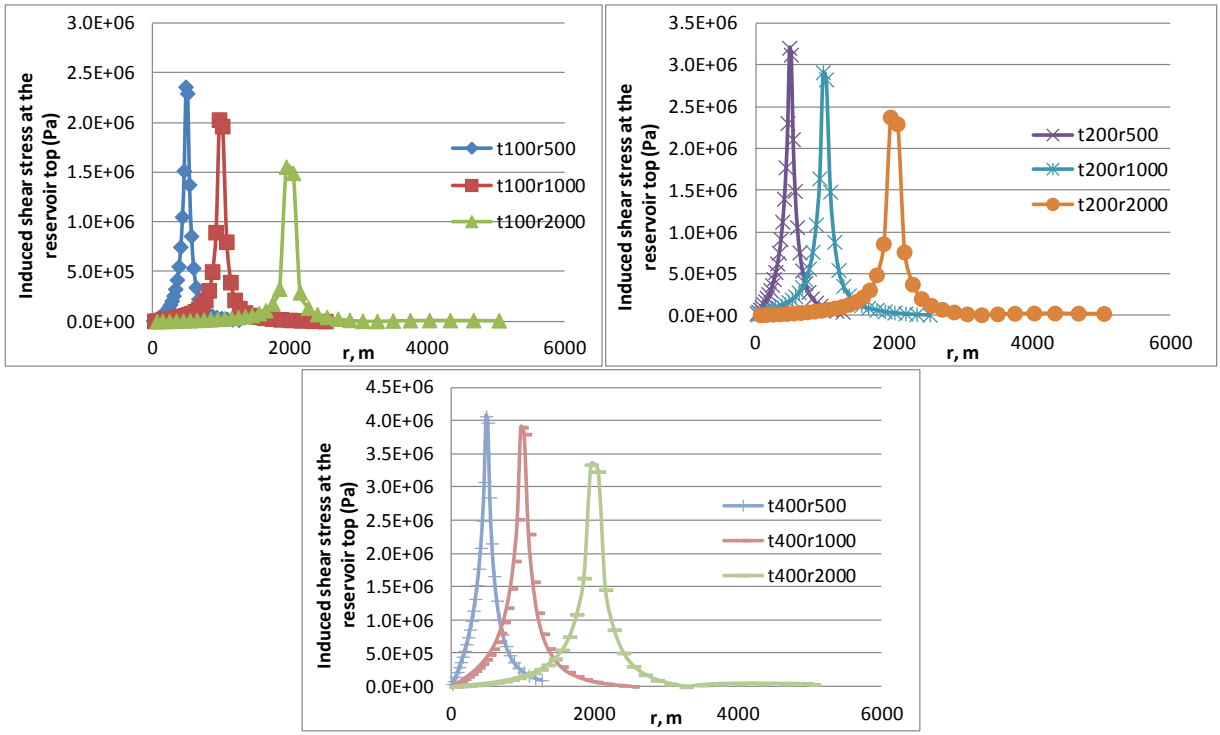

Figure 35. Induced shear stress in the caprock with 100m, 200m, and 300m reservoir thickness (clockwise from upper left) while changing reservoir radius from 500m to 2000m under uniform pressure change.

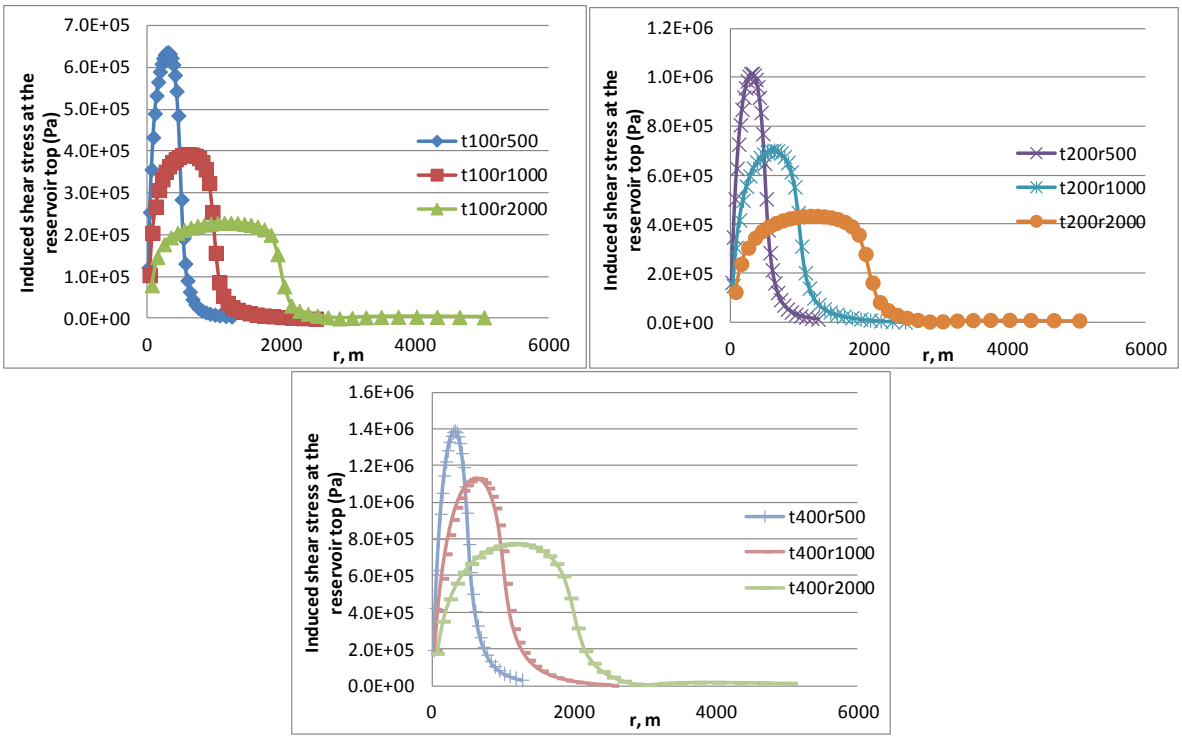

Figure 36. Induced shear stress in the caprock with 100m, 200m, and 300m reservoir thickness (clockwise from upper left) while changing reservoir radius from 500m to 2000m under linear pressure change.

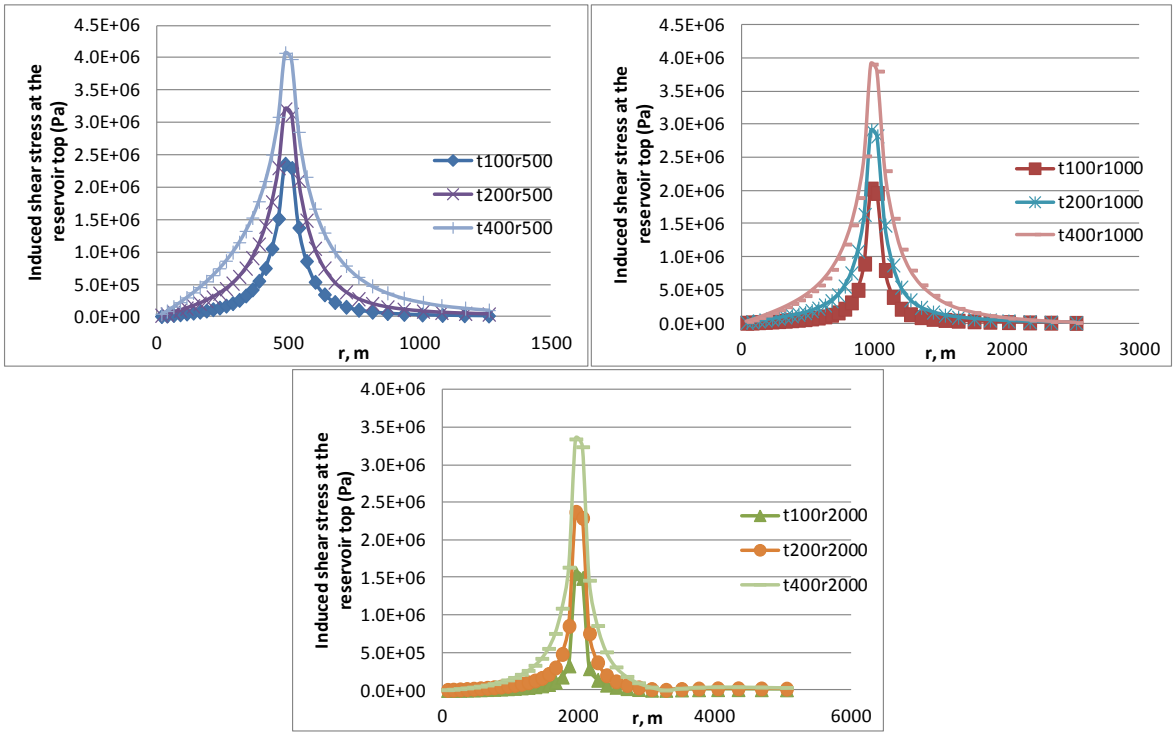

Figure 37. Induced shear stress in the caprock with 500m, 1000m, and 2000m reservoir radius (clockwise from upper left) while changing reservoir thickness from 100m to 400m under uniform pressure change.

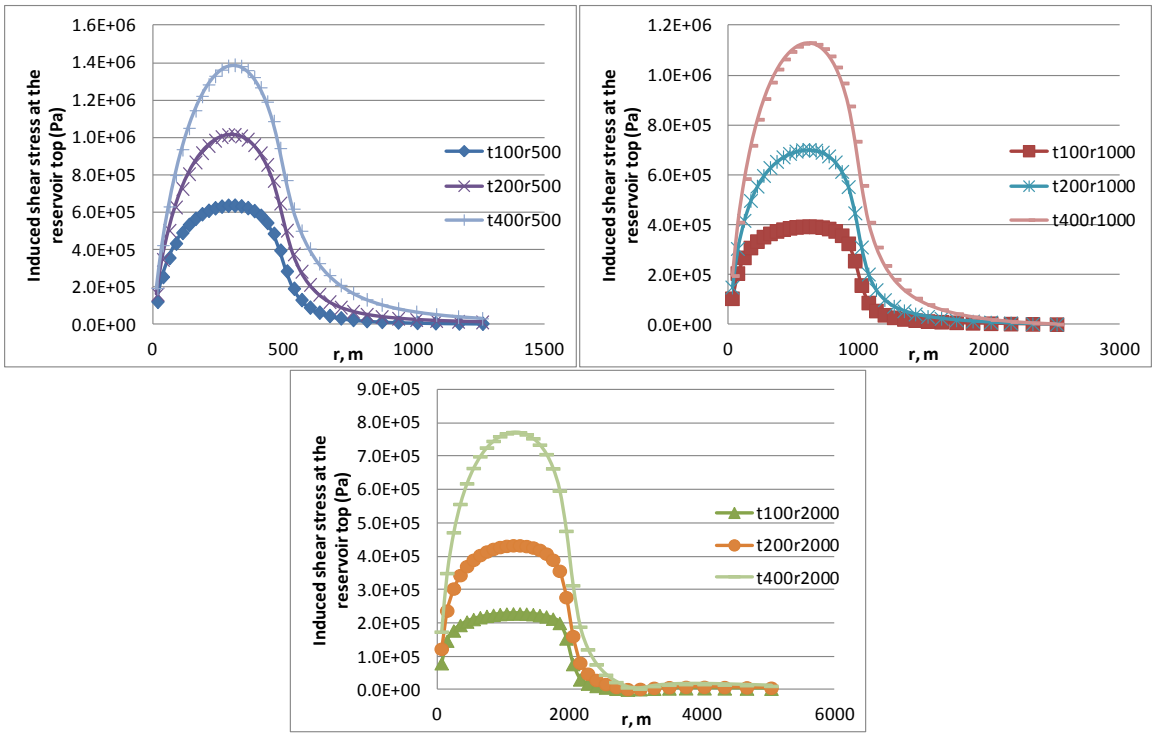

Figure 38. Induced shear stress in the caprock with 500m, 1000m, and 2000m reservoir radius (clockwise from upper left) while changing reservoir thickness from 100m to 400m under linear pressure change.

Finally, when retaining the same reservoir shape, with 100m thickness and 500m radius, the induced shear stress in the caprock is higher the shallower the reservoir; however, for deep reservoirs, the induced shear stress is almost the same when the depth is equal to or larger than the reservoir radius (see Figure 39).

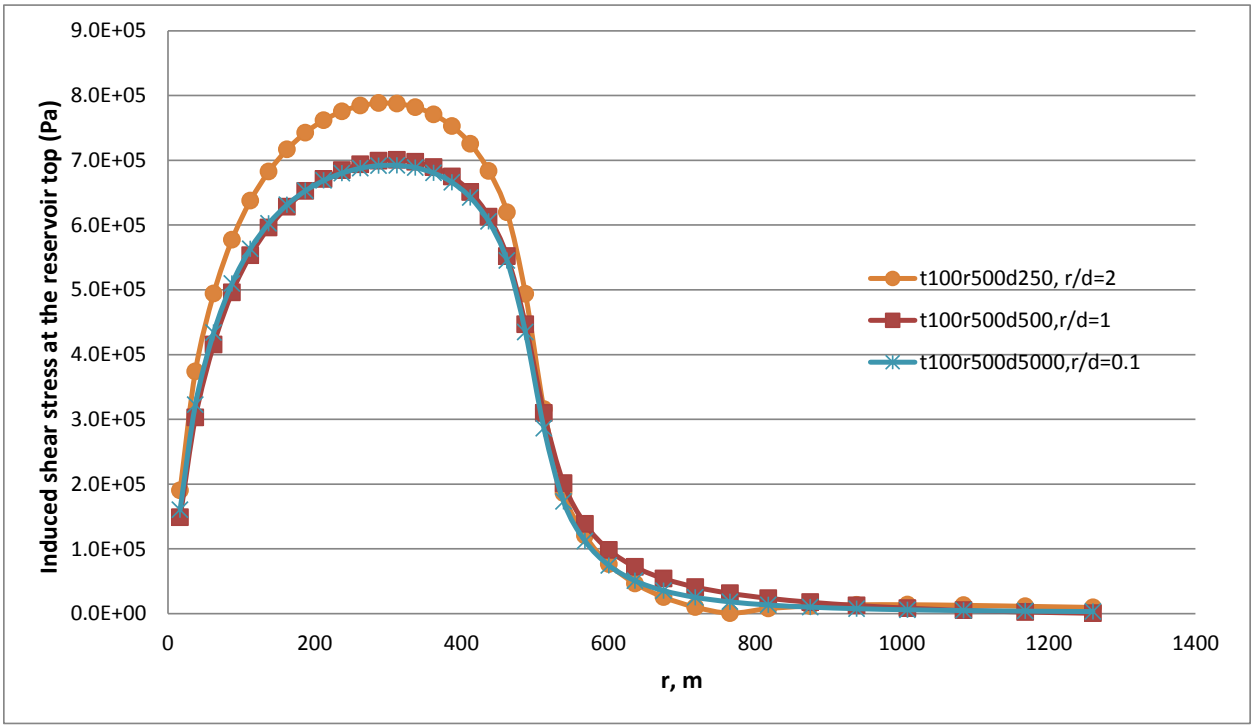

Figure 39. Induced shear stress in the caprock for the same reservoir shape, while changing the reservoir depth, with linear pressure change in the reservoir.

5 Advanced Transport and Geomechanical Simulation for a Range of Typical Geologic Settings and Operating Conditions

A general workflow developed and applied by GeoMechanics to evaluate injection (or production) effects, including induced stresses, possible fault activation or bedding plane slip, subsurface and surface deformation, and well damage risks, is presented in Figure 40. The first step is to establish a 3D geologic model for the area, based on well log data, seismic data, and drilling data. The next step in the characterization process is to develop integrated fluid flow and geomechanical models to simulate CO_2 injection and migration, and to simulate the stresses and displacements induced by injection related pressure and temperature changes.

In summary, first a 3D static geologic model (or models) is established consistent with available seismic, log, and drilling data. Based on this 3D geometry and grid structure, a fluid flow and geomechanical model are also established. In general the fluid flow models cover a smaller volume space than either the geology model or the geomechanical model, as the latter two must extend to the surface and beyond the lateral extent of the reservoir. For this particular project we used RockWorks16 for the static geologic models, TOUGH2 for the fluid and heat flow simulation, and FLAC3D for the geomechanical simulation.

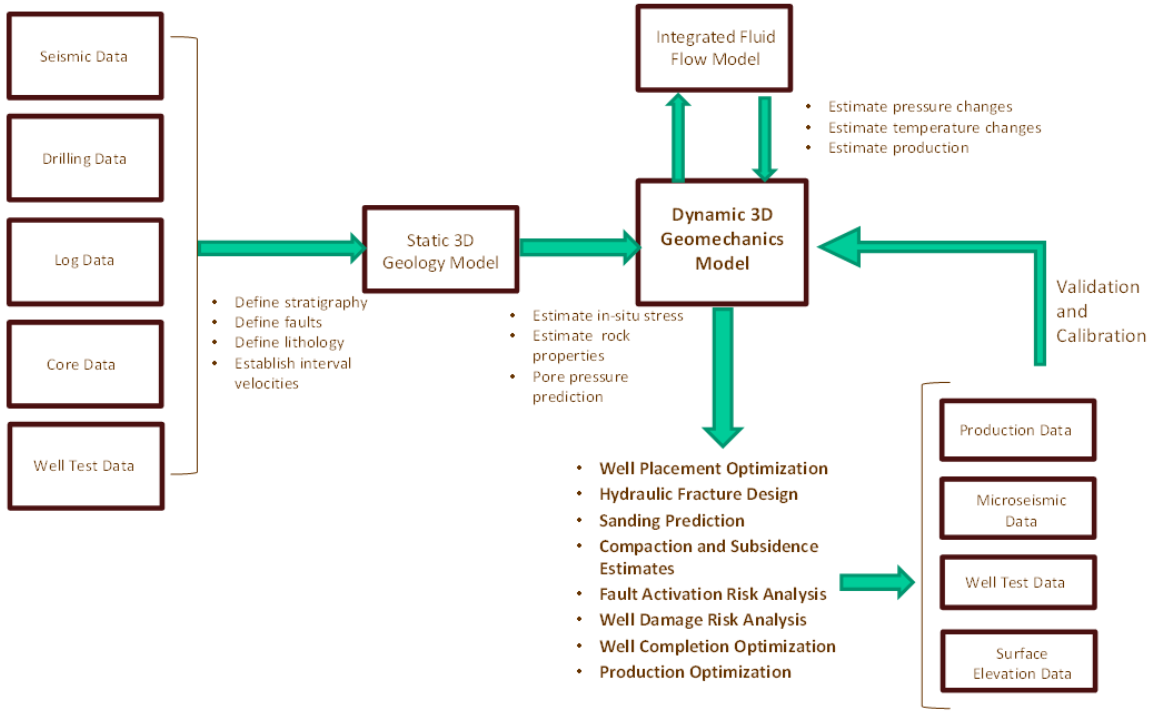

Figure 40. Generalized workflow for assembly and application of integrated geology, fluid flow, and geomechanical modeling

To illustrate the process and sample application, during the course of this project we created detailed geologic models for three large-scale geologic sequestration sites, encompassing a range of geologic settings. Modelling was completed for the Kevin Dome area in Montana, the Wilmington Graben area offshore Los Angeles, and the Louden oil and gas field in Illinois. The Kevin Dome is a relatively low risk operation, the Wilmington

Graben is a relatively higher risk operation, and the Louden oil and gas field somewhere in between (as will be described later in this report).

Initial static geologic models for each site were developed from stratigraphic and lithologic information collected from maps and wells located throughout the fields. The completed geologic models of each of these three sites were used as input for three-dimensional coupled transport flow and geomechanical models to investigate and describe caprock behavior, for a range of CO_2 injection conditions.

Pressure and temperature distributions were simulated using the TOUGH2 family of codes from Lawrence Berkeley National Labs. These codes have been developed to simulate multi-phase, multi-component fluid and heat flow in porous and fractured media. Pressure and temperature results from the TOUGH2 simulations were then used as input into three-dimensional geomechanical models to evaluate induced deformations and stresses within the reservoir and overlying caprock. The geomechanical simulation tool used was FLAC3D, with enhanced constitutive behavior functions developed by Geomechanics Technologies to model formation deformation, faulting, and bedding plane slip. To manage areas with uncertain geology, several geologic scenarios were simulated to determine the horizontal and vertical extent of the CO_2 plume after 30 years of injection. We developed and applied this combined and coupled fluid and temperature flow simulation and geomechanical simulation technique over a range of operating conditions (single and multiple injection wells at varying rates and temperature).

5.1 Kevin Dome, Montana

The Kevin Dome is located in Northern Montana. The area is being studied and characterized for large scale CO_2 sequestration by the Big Sky Carbon Sequestration Partnership (see www.bigskyCO_2.org for latest updates). The proposed sequestration site contains a low-sloping anticline structure composed of carbonate and detrital rocks. Studies are underway by the Big Sky Partnership to characterize injection into the Duperow formation, a zone of high porosity dolomite located at a depth of 1250 m (4100 ft).

For the GeoMechanics Technologies caprock integrity study, however, we were requested by US DOE to perform geomechanical analysis and risk analysis completely independent of the partnership efforts. We therefore collected and analyzed well log data and geologic data from Montana State public records in order to develop combined geologic, fluid flow, and geomechanical models for the area. Figure 41 presents a map view of the project area, with contours elevation of the Duperow Formation, and showing the areal extent of our geologic, fluid flow, and geomechanical model boundaries.

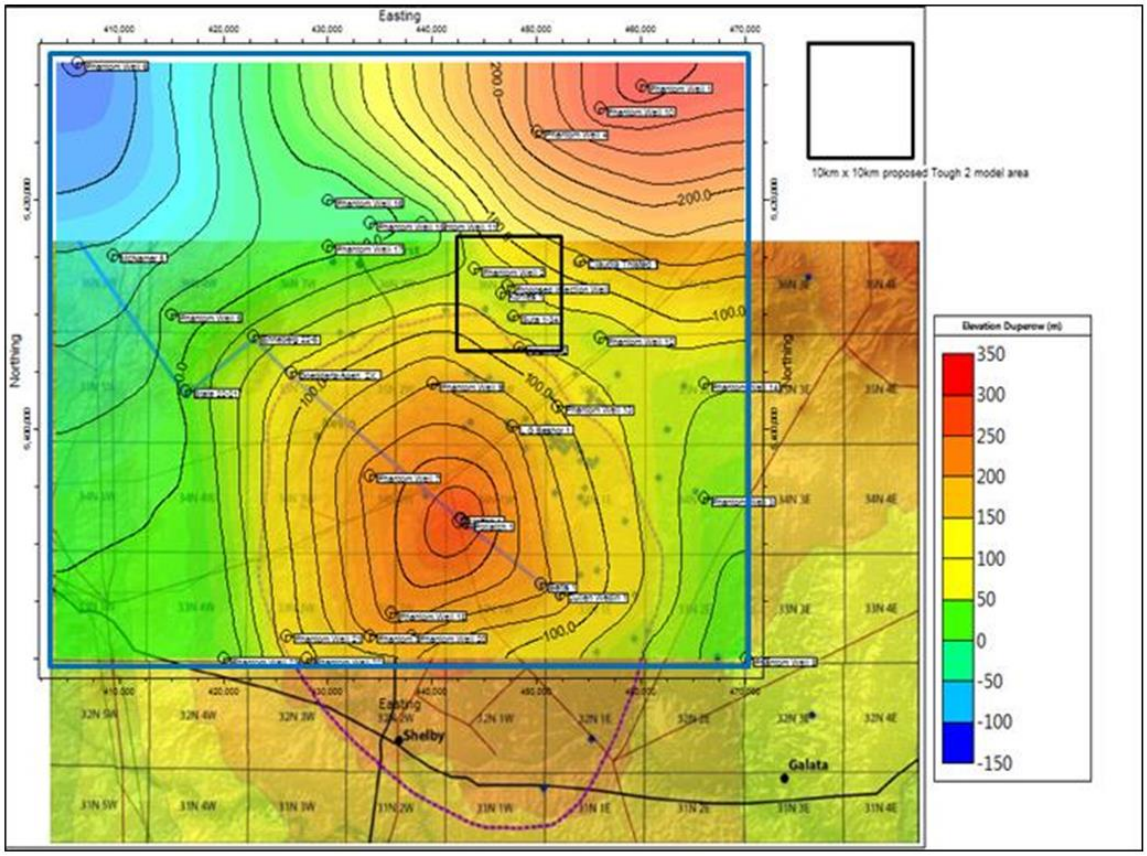

Figure 41. Kevin Dome map. Blue box marks perimeter of the geologic model domain. Black box indicates location of the 10km X 10km combined fluid flow and geomechanical model domains

5.1.1 Geologic Model

First, a 3D stratigraphic and lithology model was constructed for the area (see Figure 42 below) based on well log marker data and available maps. This was constructed using RockWorks16 software. Well control is available but somewhat limited in this area (see available wells in white boxes of Figure 43). While there is a great deal of hydrocarbon production in this region, it is generally limited to shallower formations. Only a few wells penetrate into the proposed, deeper injection formation. Figure 43 shows a cross section through the stratigraphic model centered on the proposed injection well. Digital sonic and density logs for wells State 22-21 and Potlatch O & R 1 were obtained and analyzed for rock mechanical properties.

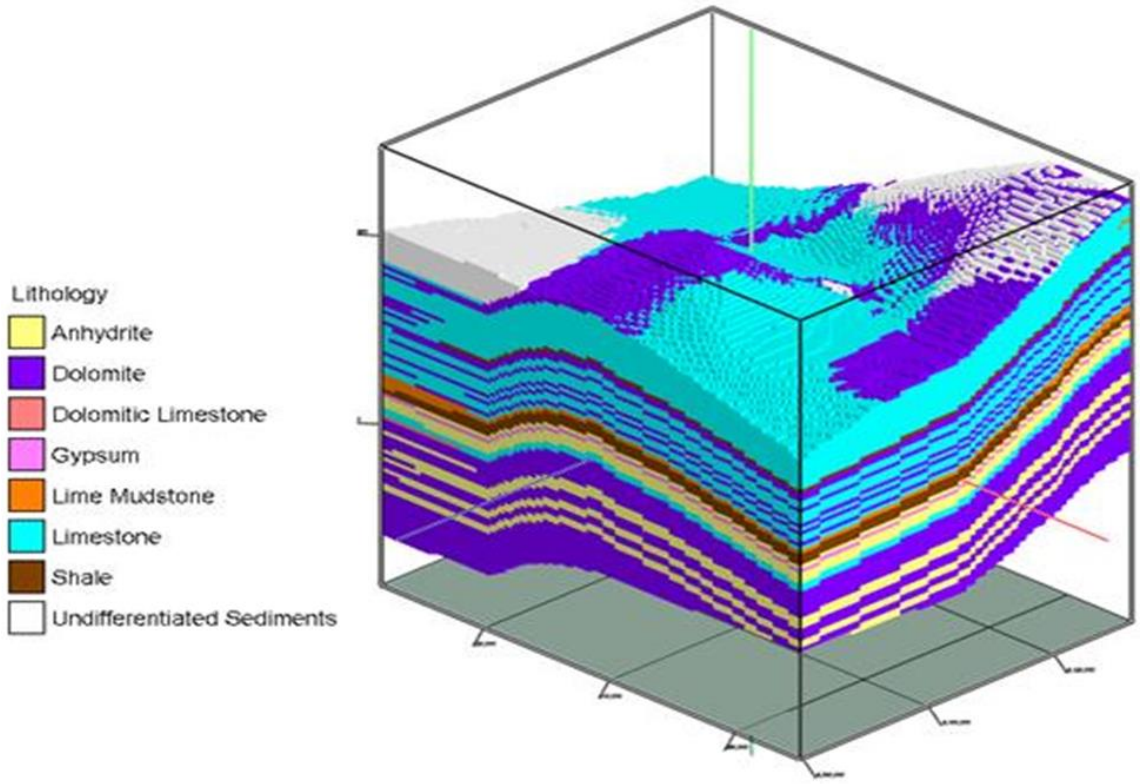

Figure 42. Lithology model developed by GeoMechanics for the Kevin Dome CO_2 injection analysis

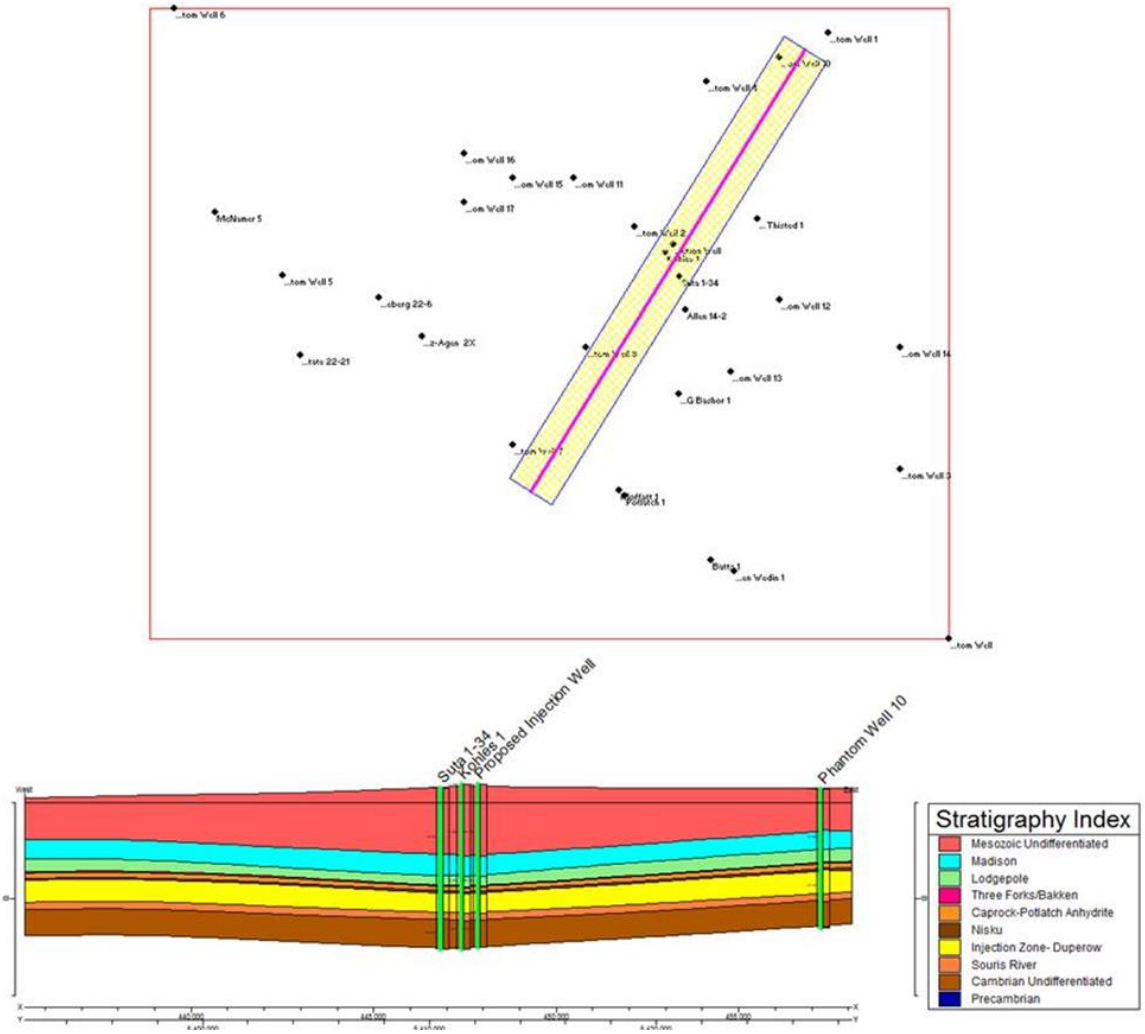

Figure 43. Cross section through stratigraphy model centered on proposed injection well

5.1.2 Fluid Flow Model

After establishing a 3D geology model, the next step in the process is to develop a 3D fluid flow model. For this step we developed a TOUGH2 fluid migration model using the PetraSim graphical user interface. The model established (see Figure 41 and Figure 42) is 10km X 10km in the lateral dimension and 1400m in the vertical direction, spanning a depth interval from -231.72 to 1174.8 m, and centered on the proposed injection well. The injection interval is between -75 m & -95 m (note: negative sign indicates below sea level), which is 1250-1270 m below ground level. The mesh is finer around the well and in the injection interval; totaling 56,129 elements. The stratigraphy and lithology data from the RockWorks16 geologic model were input to the TOUGH2 model.

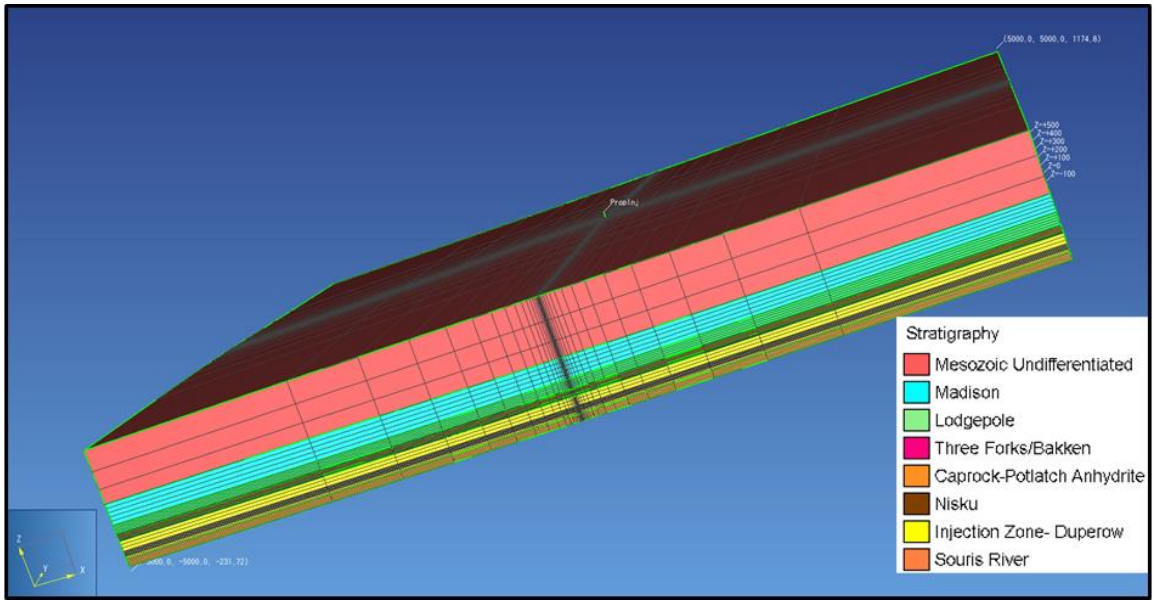

Figure 44. Fluid flow model mesh for Kevin Dome

The density (kg/m^3), effective porosity (%), and three-dimensional permeability (mD) of each material were estimated from literature values. We gathered relative permeability and capillary pressure curves based on similar lithologies and in-situ conditions found near the Kevin Dome area. After we compared the formation depth, pore pressure, temperature, permeability and porosity properties typical for the Kevin Dome area, we chose the Muskeg Anhydrate, Wabamun Carbonate (low K and high K, respectively), and Calmar Shale as our reference formations for determining the relative permeability and capillary pressure curves by using Van Genuchten-Mualem function (Bennion & Bachu 2005 and Bachu & Bennion 2008).

Initial temperature and pressure conditions were set consistent with well log data from this area. The surface temperature is set to 15.56 C (60 F), with a 0.0145 C/m (0.8 F/100ft) temperature gradient. The surface pressure is set to 1.01325E5 Pa (14.7 psi), with a 1.0857 Pa/m (0.48 psi/ft) pressure gradient. The side boundaries are set with constant pressure (initial gradient). We used the ECO_2N module for supercritical CO_2 injection simulation, and simulated isothermal conditions for up to 50 years of constant injection pressure 1.62E7 Pa (2350 psi). This is about 17% higher than the initial pressure. About 15.4 million tons of CO_2 are injected over 50 years (0.308 million tons per year).

Figure 45 presents a top view of the resulting CO_2 plume migration after 50 years of injection. CO_2 flow is well contained vertically beneath the caprock, and extends about 2000 m laterally away from the wellbore. Figure 46 shows the pressure contour in NE-SW and NW-SE directions, centered on the injection well, at the end of 50 years injection. Figure 47 shows the pressure profiles at $\text{time} = 0$ and $\text{time} = 50$ years on a horizontal section through the injection zone, centered at the injection wellbore. The pressure increase at the injection well is about 2.5 MPa (360 psi). This pressure change profile is subsequently used as input to the geomechanical model, in order to estimate induced stresses and deformations.

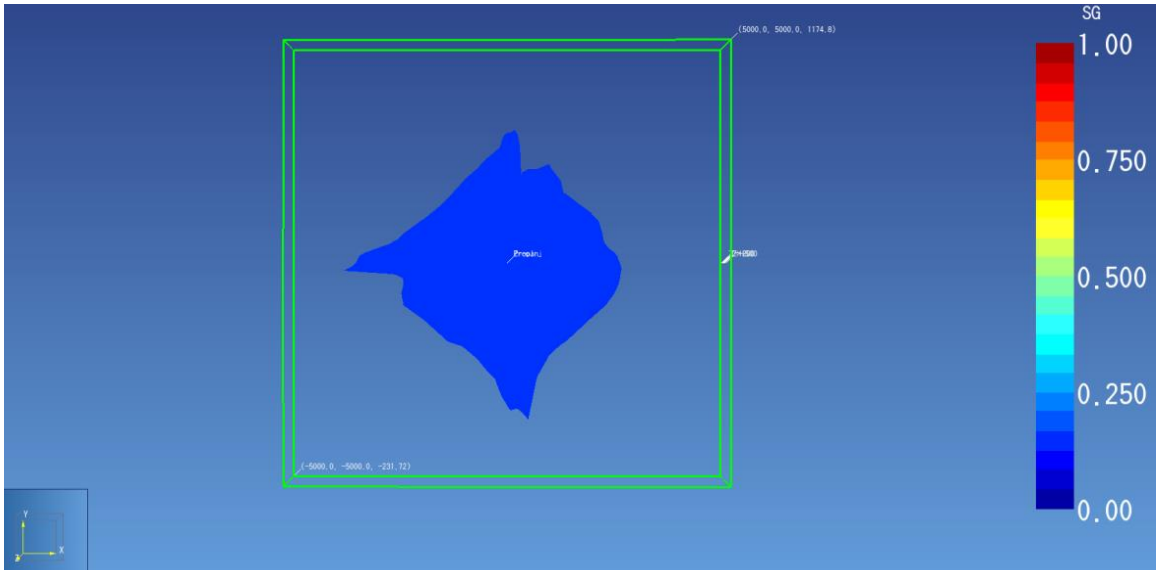

Figure 45. CO_2 supercritical gas plume after 50 years of injection – top view

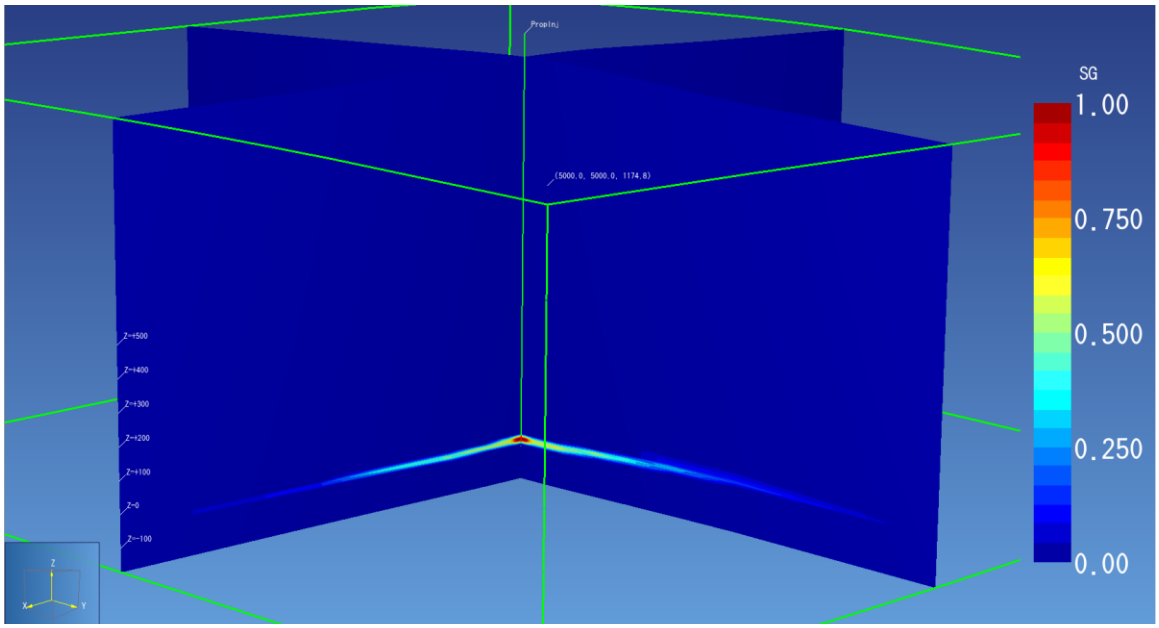

Figure 46. Supercritical CO_2 saturation contour centered on injection well, in NE-SW and NW-SE directions after 50 years of injection

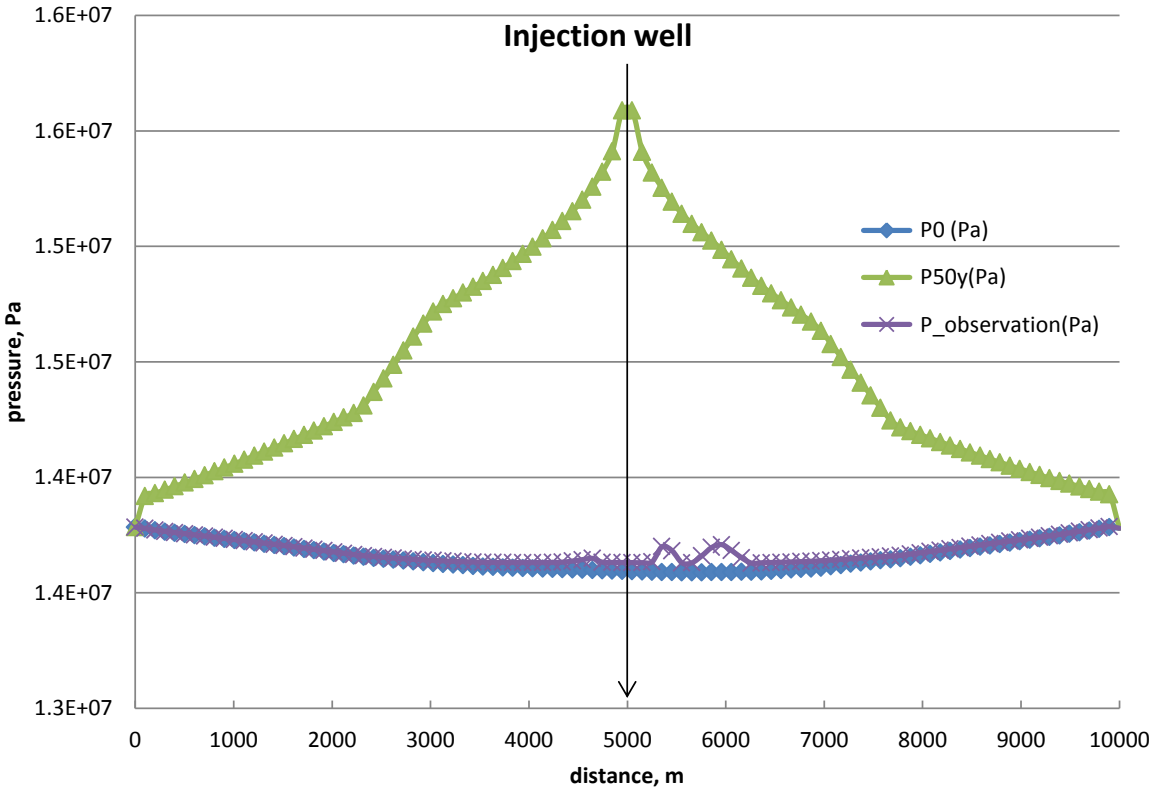

Figure 47. Pressure profile in the injection zone, centered on the injection well, in NE-SW direction

5.1.3 Geomechanical Model

We next developed a 3D geomechanical model for Kevin Dome, mapping grid information and data from the geology and fluid flow models. The dimensions of the geomechanics model are 10,000m x 10,000m in the lateral direction, and about 2500 m in the vertical direction, extending from the surface about 1175m above sea level to 1345 m below sea level, and centered on the injection wellbore. The model has a total of 144,000 elements, with a finer mesh near the injection well and in the Duperow injection formation (Figure 48).

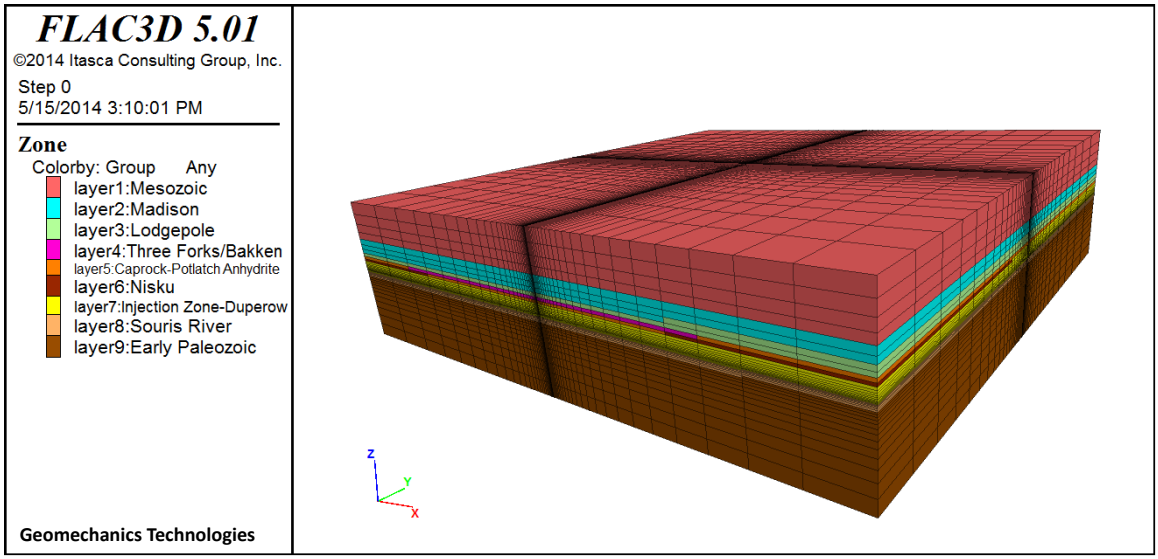

Figure 48. 3D geomechanics model established for Kevin Dome

The mechanical properties of each formation were estimated from log data, as no laboratory core test data are available. We applied roller boundary conditions on all surfaces except the top surface, which is free to move in both vertical and lateral directions. We then simulated the induced stress and displacement during 50 years of injection, by applying pressure changes from the fluid flow simulation to the geomechanics model. The resulting surface deformations are presented in Figure 49. The maximum displacement is above the injection well, with a maximum uplift of about 5 mm. This is relatively minor, primarily due to the low pressure increase and relatively stiff material properties.

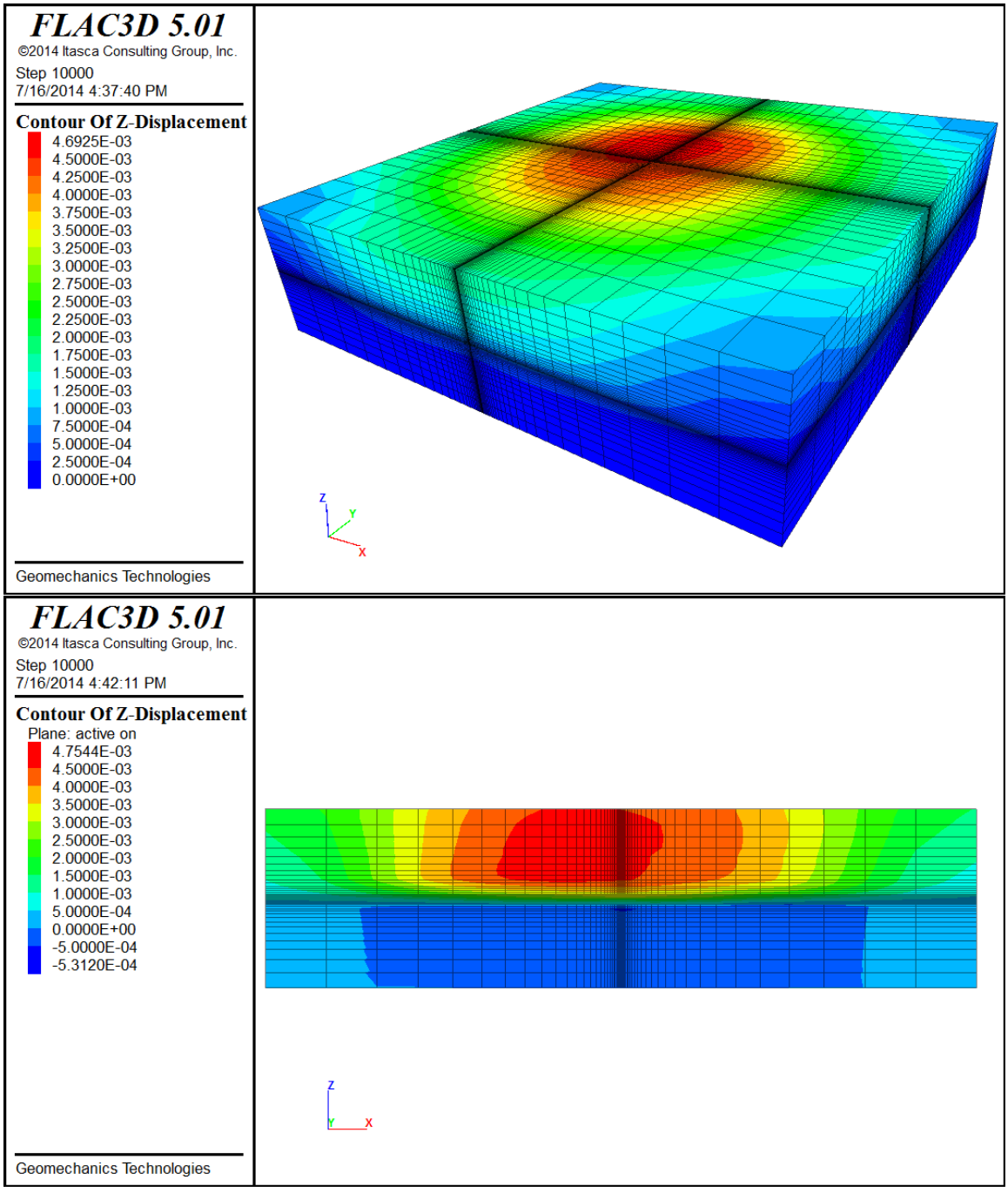

Figure 49. Vertical displacement: 3D view (top) and cross section (below), after 50 years of injection (meters)

We present in Figure 50 cross section views of the induced horizontal stresses. Compressive stresses are induced within the injection interval (zone of increased pressure), while tensile stresses are induced above and below the injection zone. The maximum induced horizontal compressive stress is about 1.4 MPa (about 200 psi). The stress changes induced by injection operations in this case are relatively small compared to in-situ

stresses and compared to estimated shear strength properties for the matrix material and bedding planes. Given these low values, there is no significant risk for caprock fracturing or fault activation.

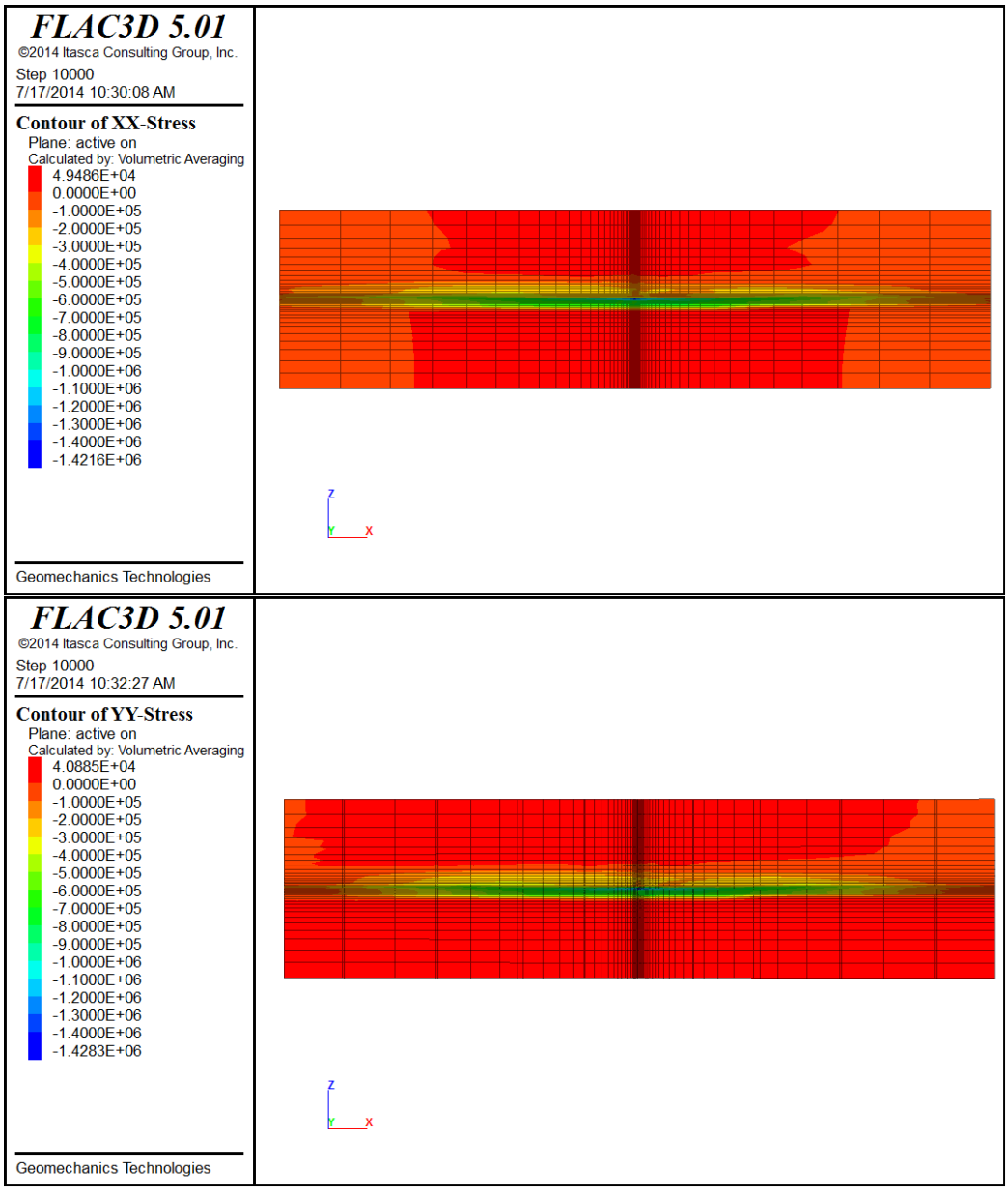

Figure 50. Plot contours of induced horizontal stresses after 50 years of injection, including E-W (top) and N-S (lower) normal stress (Pa)

Figure 51 shows the induced horizontal shear stresses on N-S and E-W sections. These are quite low, with maximum magnitude only on the order of 3.0E+4 Pa.

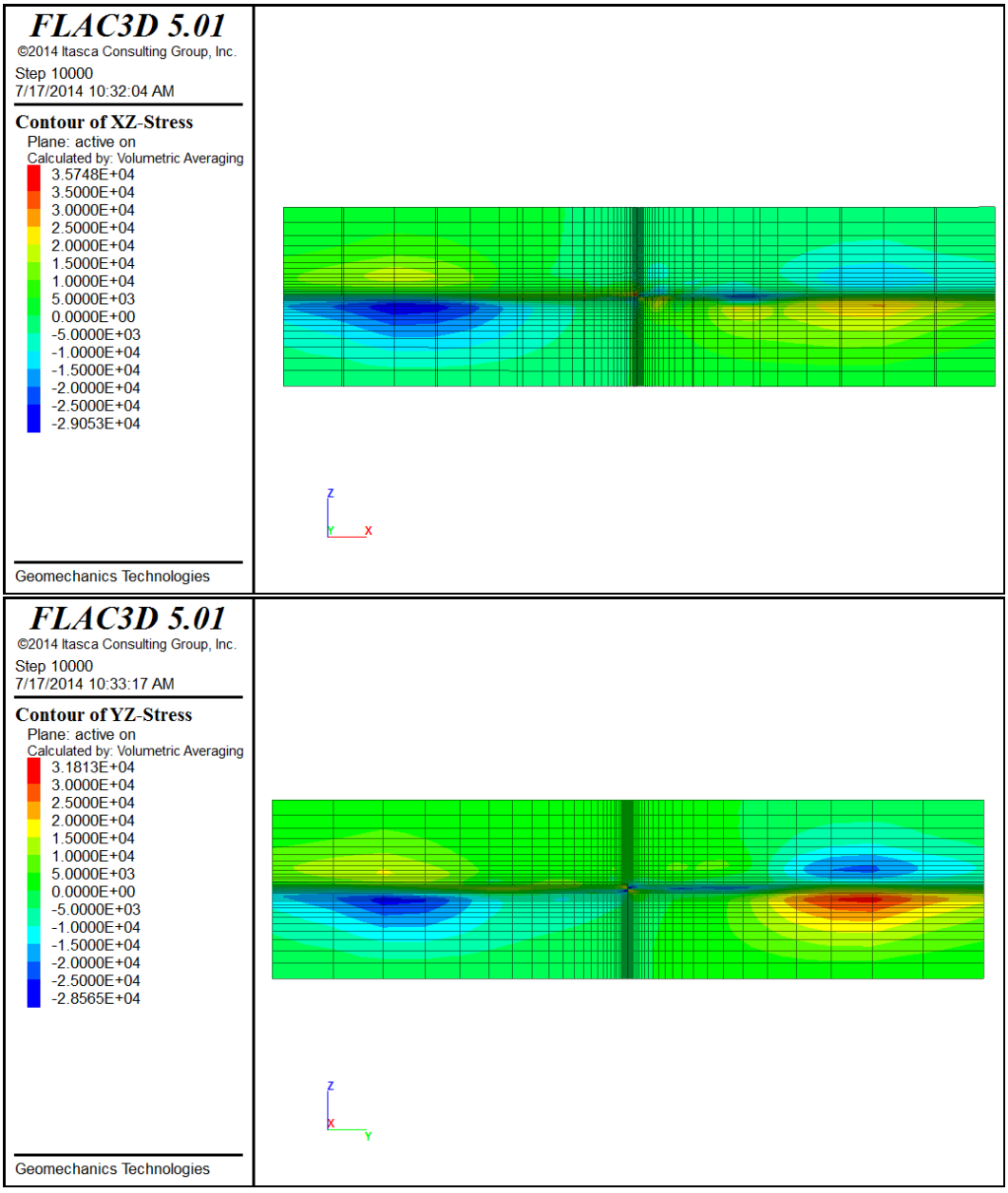

Figure 51. Plot contours of induced horizontal shear stresses after 50 years of injection, displayed on E-W (top) and N-S (lower) sections (Pa)

5.2 Wilmington Graben, Offshore Los Angeles, California

The Wilmington Graben is located offshore Los Angeles, California (Figure 52). The area is being studied and characterized for large scale CO_2 sequestration by GeoMechanics Technologies under DOE contract FE0001922. That effort is more fully described in a companion paper "Characterization of Pliocene and Miocene formations in the Wilmington Graben, Offshore Los Angeles, for large scale geologic storage of CO_2" (see also www.socalcarb.org). The graben is situated between the Palos Verdes fault to the west and the Thums-

Huntington Beach fault to the east. The geologic setting is characterized by turbidite deposits composed of graded sequences of sand, silt, and shale.

Figure 52. Wilmington Graben location, power plants, and refineries within the Los Angeles geologic basin

Pliocene and Miocene sediments in the Los Angeles Basin are massive interbedded sand and shale sequences known to provide excellent and secure traps for oil and gas. The area contains several billion-barrel oil and gas fields, including the giant Wilmington Field in Long Beach (more than two billion barrels produced to date). These formations have been used by Southern California Gas Company for large-scale underground storage of natural gas at half a dozen locations throughout the Los Angeles basin for more than fifty years, demonstrating both the storage potential and security of these formations for CO_2 sequestration.

5.2.1 Geologic Model

The initial geologic characterization effort included assembly and analysis of log data from a dozen existing wells located within both State and Federal waters, and combination of this information into a common database. Several key geologic horizons markers were identified at each well location. Lithology versus depth was also identified for each well, separated into four categories for sand, shale, sand-shale interbed, and silt. To further characterize the area and extend the geologic horizon beyond the discrete well locations in 3D, 3D seismic data available for a portion of the Wilmington Graben was re-processed and analyzed. An additional 175km of 2D marine seismic data was collected in a "data gap" area, using ship borne seismic arrays provided by Cal State Long Beach.

Finally, two new wells were drilled by GeoMechanics Technologies in the north Graben area to establish additional formation characterization data in both the Pliocene and Miocene intervals. Core samples were taken in each well, and measurements made of porosity, permeability, and rock mechanical properties.

Given the key stratigraphic horizons established from seismic data, and lithology versus depth determined from log data, inter-well interpolation was applied to create both stratigraphic and lithology models for the entire 3D volume comprising the Wilmington Graben. The 3D lithology model and an associated fence diagram are provided in Figure 53 and Figure 54.

The offshore Wilmington Graben lies within a turbidite depositional environment. Lithology is known to vary both vertically and laterally. A simple interpolation between wells can sometimes create an overly simplified lithologic model. Seismic horizon data can inform the geologist of general stratigraphic trends, but cannot completely resolve the uncertainty in lateral variation of lithology. To account for such variation and uncertainty, therefore, we considered multiple geologic interpretations of the available data with varying ratios of sand and shale. We developed and considered several alternative lithology distributions, each of which honor the general stratigraphic trend and the specific lithology distribution at each well. These include a baseline geologic model, a high shale geologic model, and low shale geologic model, each of which were considered in subsequent fluid flow simulations.

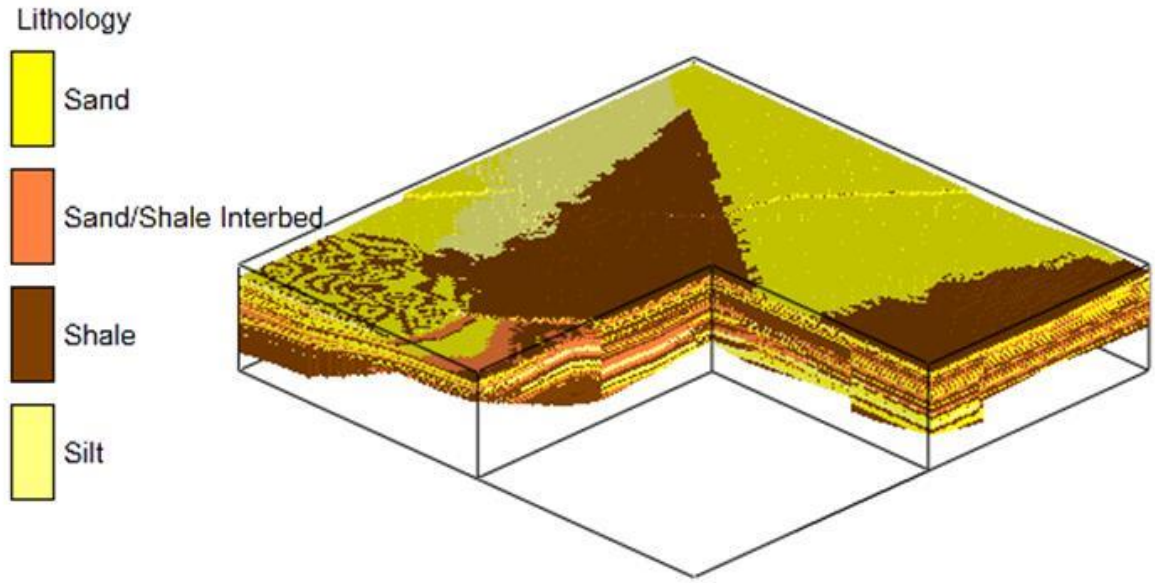

Figure 53: 3D lithology model with cut-away view

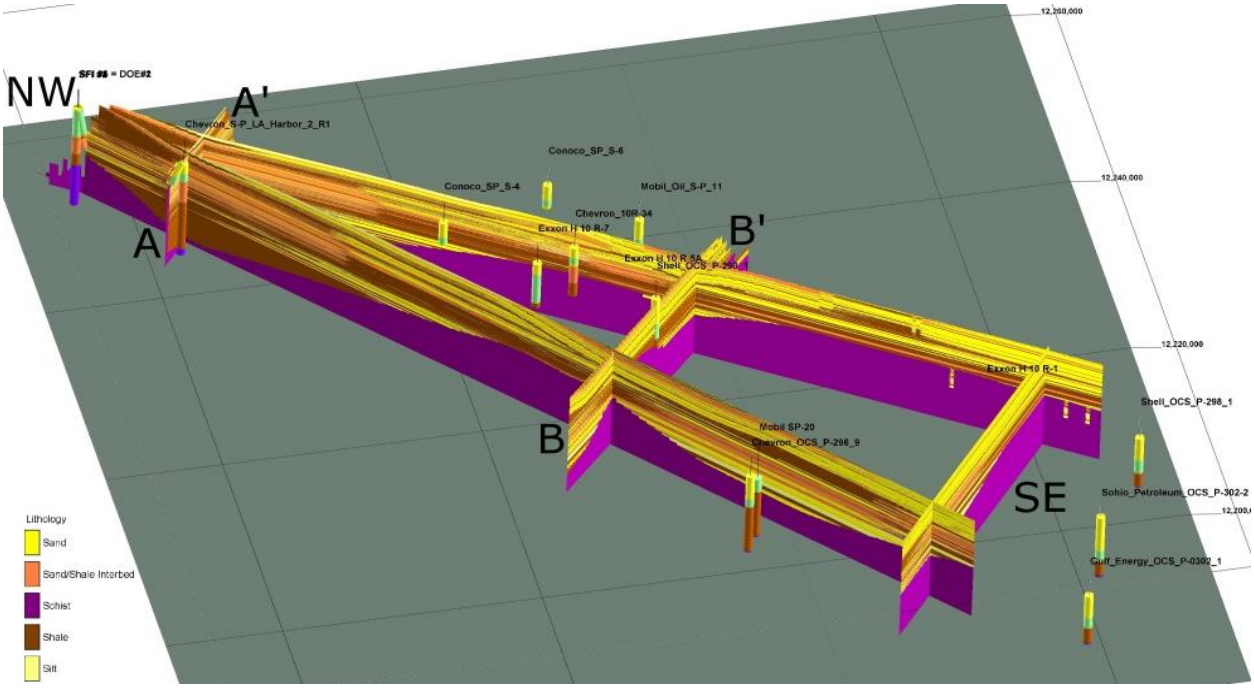

Figure 54. Geologic fence diagram for the Wilmington Graben with lithology interpolated between known wells

5.2.2 Fluid Flow Model

Two areas in the middle and in the northwest of the graben were chosen for fluid flow and geomechanical modelling, as indicated in Figure 55. We present herein results for the middle graben area.

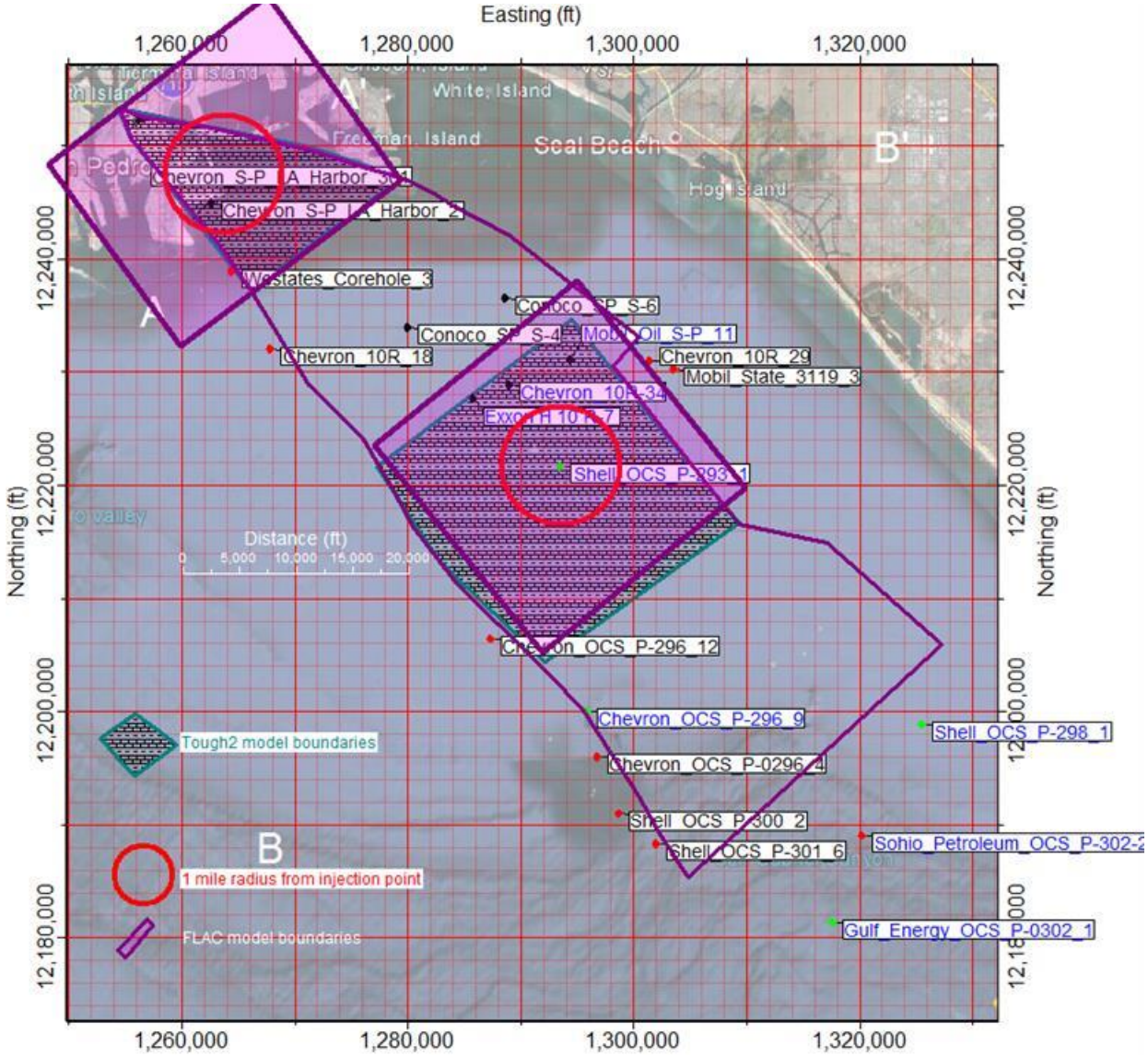

Figure 55. Integrated fluid flow models (shown in hatched area) and geomechanical models (shown in purple overlays)

The conceptual fluid flow model was created by mapping the geology from the RockWorks16 model into a TOUGH2 flow model (Figure 56). The full conceptual model is shown in Figure 57. As the model is bounded on the SW and NE by the Palos Verdes and Thums Huntington Beach faults, respectively (which are known to be sealing), these boundaries were set with no-flow conditions. The NW and SE boundaries of the model were defined as constant pressure conditions (depth dependent).

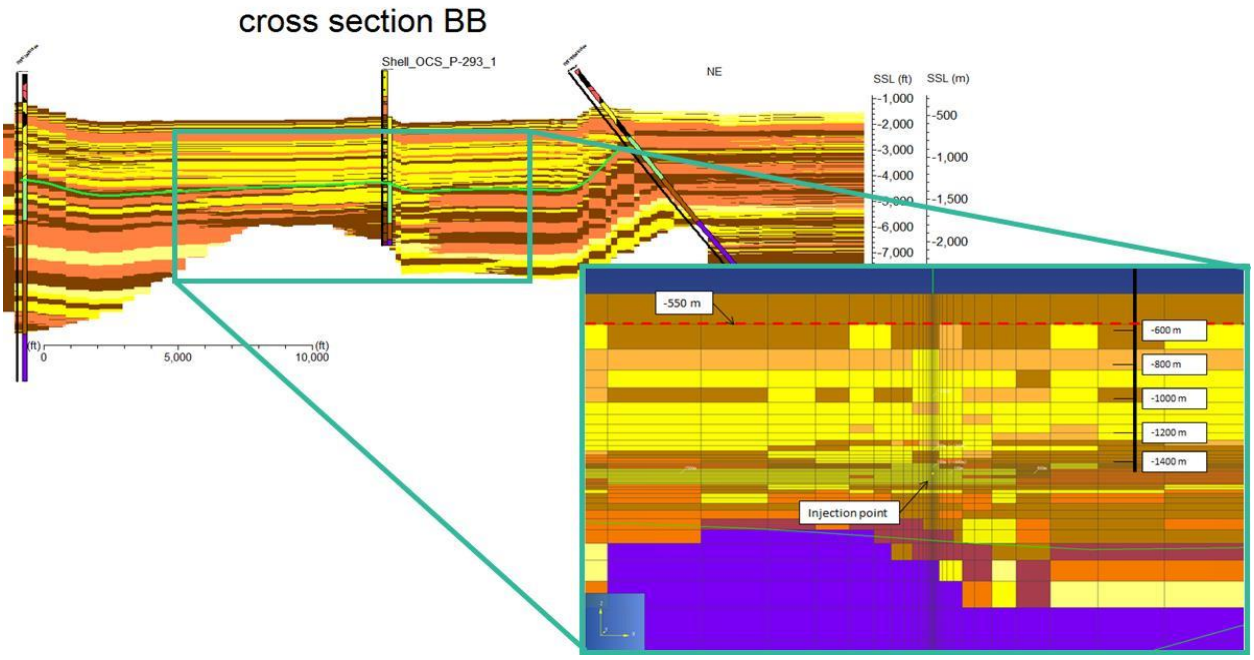

Figure 56. Mapping of lithology from RockWorks16 model to TOUGH2 model

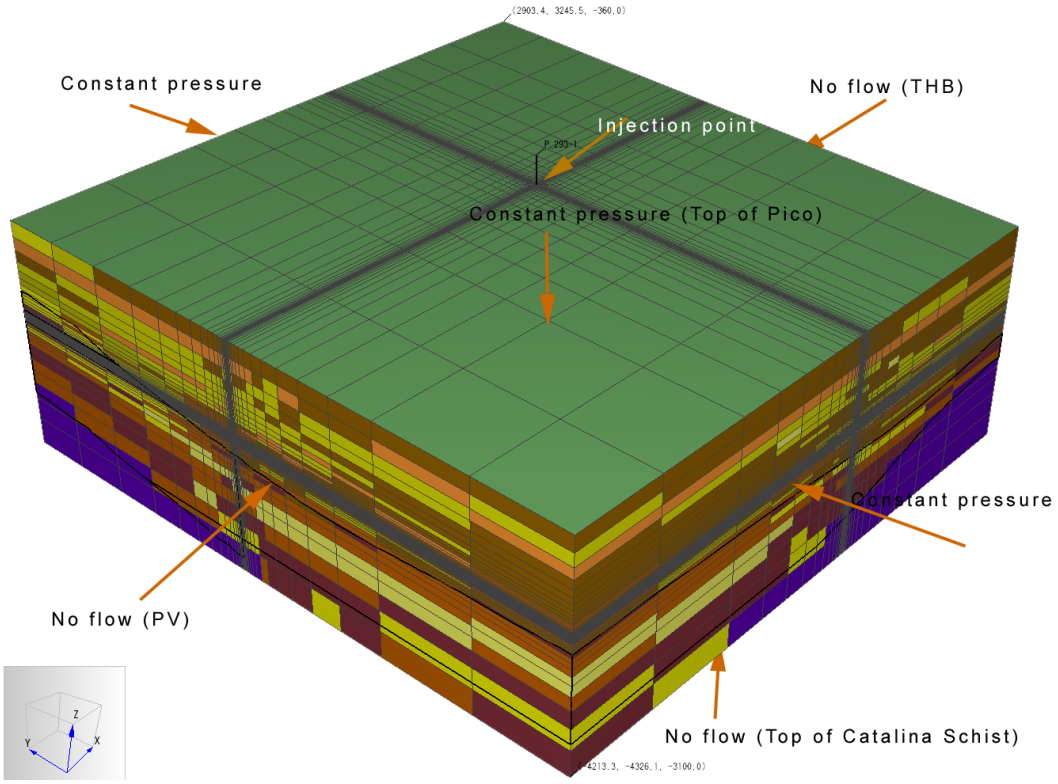

Figure 57. 3D flow model for mid graben area

We simulated thirty years of injection at about 1 million metric tons per year into a sand interval approximately 50m thick. The injection was followed by fifty years of monitoring. The simulation results for the geologic baseline model indicate that after 30 years of injection, the CO_2 plume migrated and extended to a distance of about 1,000m (3,280ft) in the horizontal direction and 450m (1,500ft) in the vertical direction, indicated in Figure 58 and Figure 59.

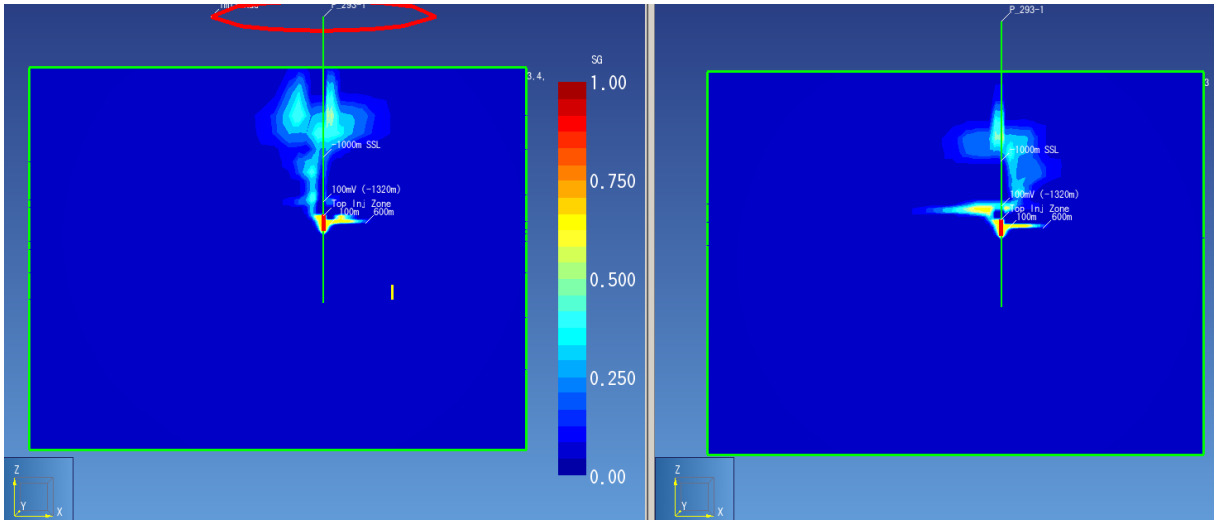

Figure 58. CO_2 migration in baseline model (left) and high shale model (right), both after 30 years of injection; SW-NE cross sections

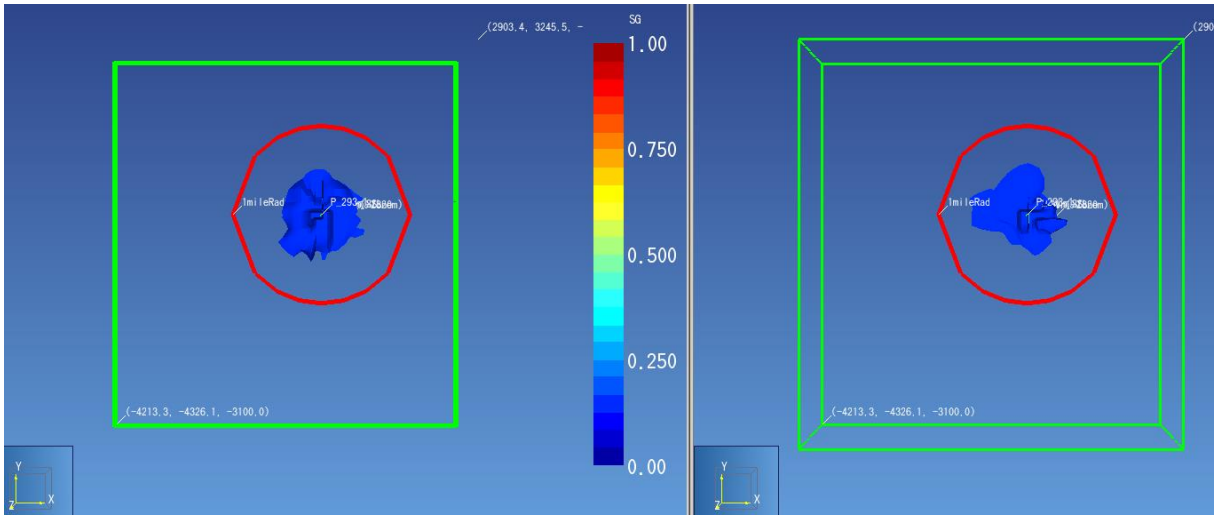

Figure 59. CO_2 migration in baseline model (left) and high shale model (right); both after 30 years of injection; top view

5.2.3 Geomechanical Model

A geomechanical model was also assembled for the central graben area. The purpose was to assess stress changes induced by injection operations, fracturing risks, fault activation risks, and surface deformations. Figure 60 and Figure 61 present illustrations of the geomechanical model for the central graben area. The dimensions of this model are about 8500 m in the lateral directions and 2950m in the vertical direction, starting at the seafloor. The injection wellbore is located at the center of the model. The geomechanical model has a total of 35100 elements, with finer mesh across injection well and the Repetto injection formation. We apply roller boundary conditions on all surfaces except the top surface, which is free to move in both vertical and lateral directions.

Mechanical properties for varying layers were determined with sonic logs calibrated with triaxial rock mechanics testing on core samples. The Palos Verdes and THUMS Huntington Beach faults serve as the no-flow side boundaries of the model, consistent with the fluid flow model. The model is initiated with gravitational loading and initial stresses determined from step-rate testing and borehole breakout analysis. Initial pressure and temperature as a function of depth were also determined for the area. The loading of the model is input via the change in pressure and temperature determined from the fluid flow simulation (i.e. a one-way coupling process). Note that to first approximation, material dilation or compression is related to the change in pressure times compressibility and to the change in temperature times thermal expansion. Increased pressure acts to expand the formation rock, while decreased temperature acts to contract the rock. The surrounding materials resist this expansion and/or contraction, resulting in stresses being induced both within the interval experiencing pressure and temperature change and within the surrounding formation material.

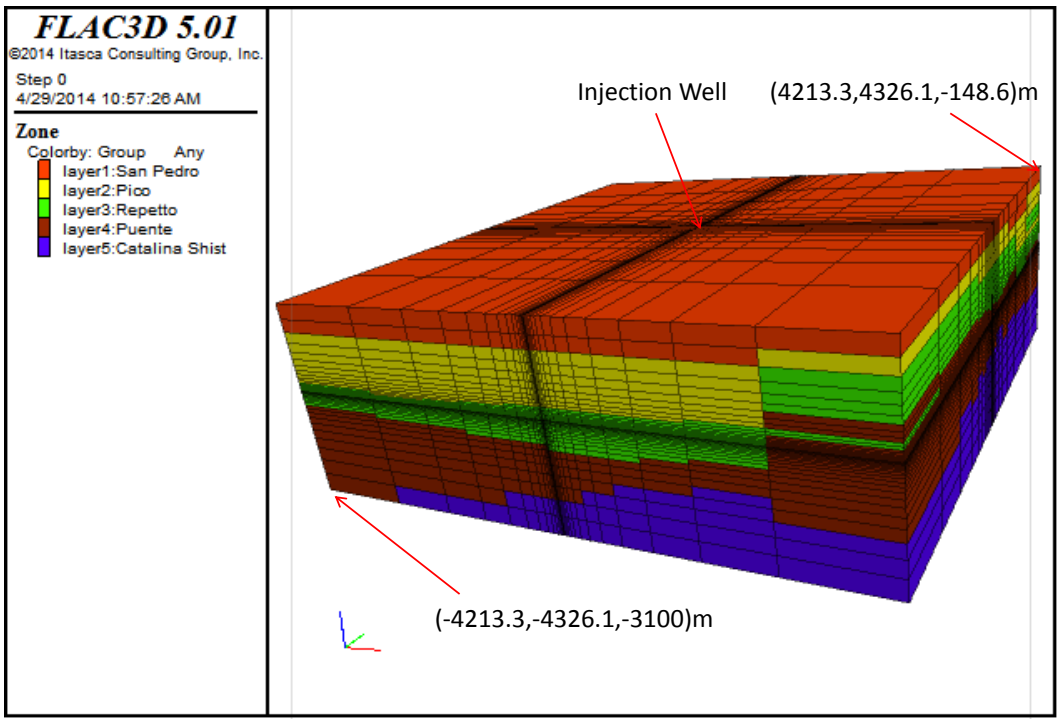

Figure 60. 3D geomechanical model for the central Wilmington area

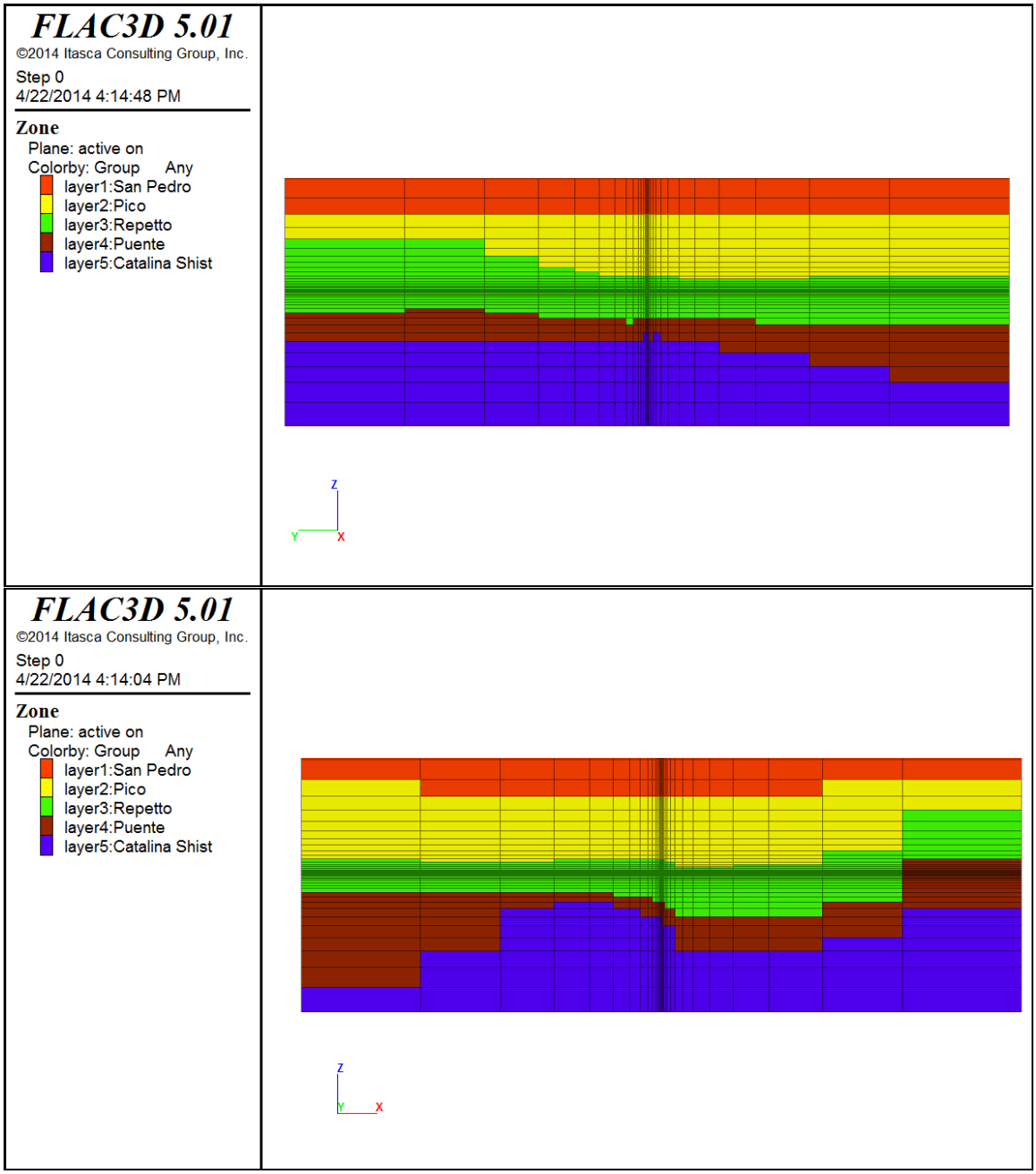

Figure 61. Geomechanics model cross sections centered on the proposed injection wellbore; NW-SE (top) and NE-SW(bottom) directions

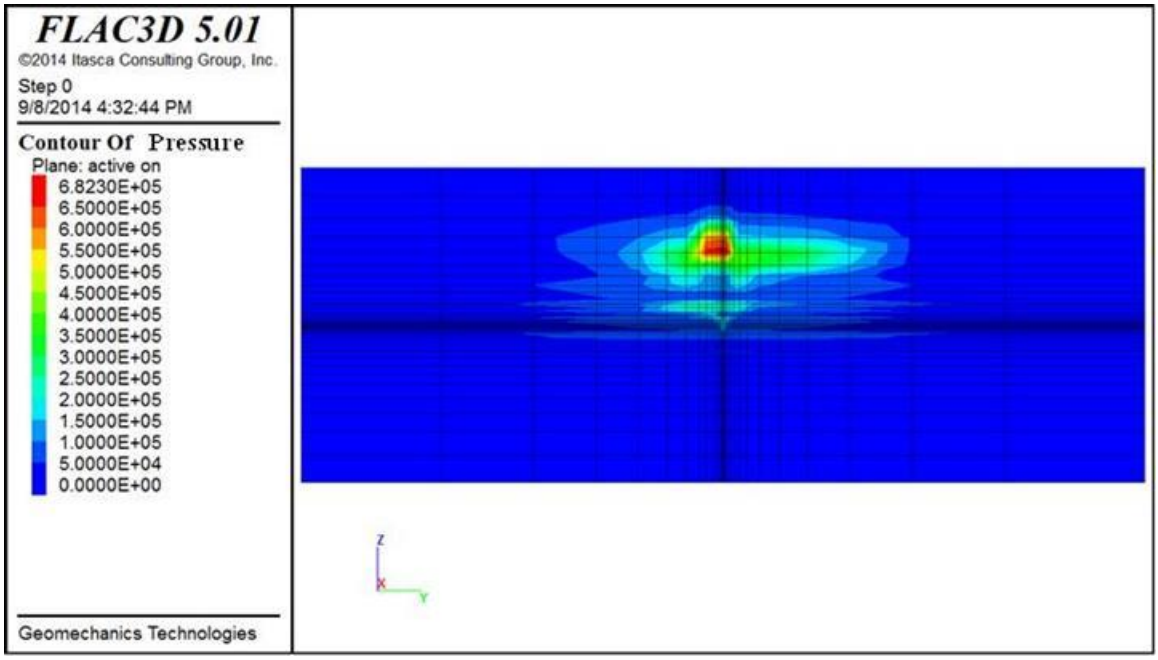

Figure 62 presents the change in pressure after 30 years of injection determined from the fluid flow model and applied as loading to the geomechanical model. Pressure changes are relatively minor, less than 1 MPa throughout the region of CO_2 migration, and concentrated in the area above the injection interval.

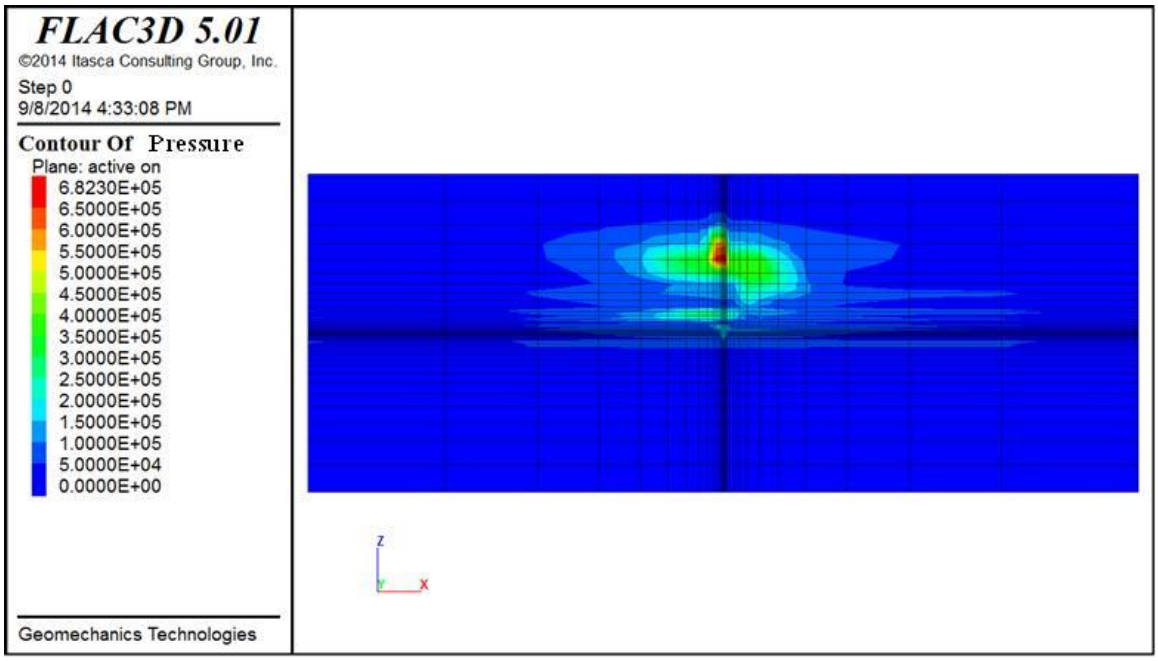

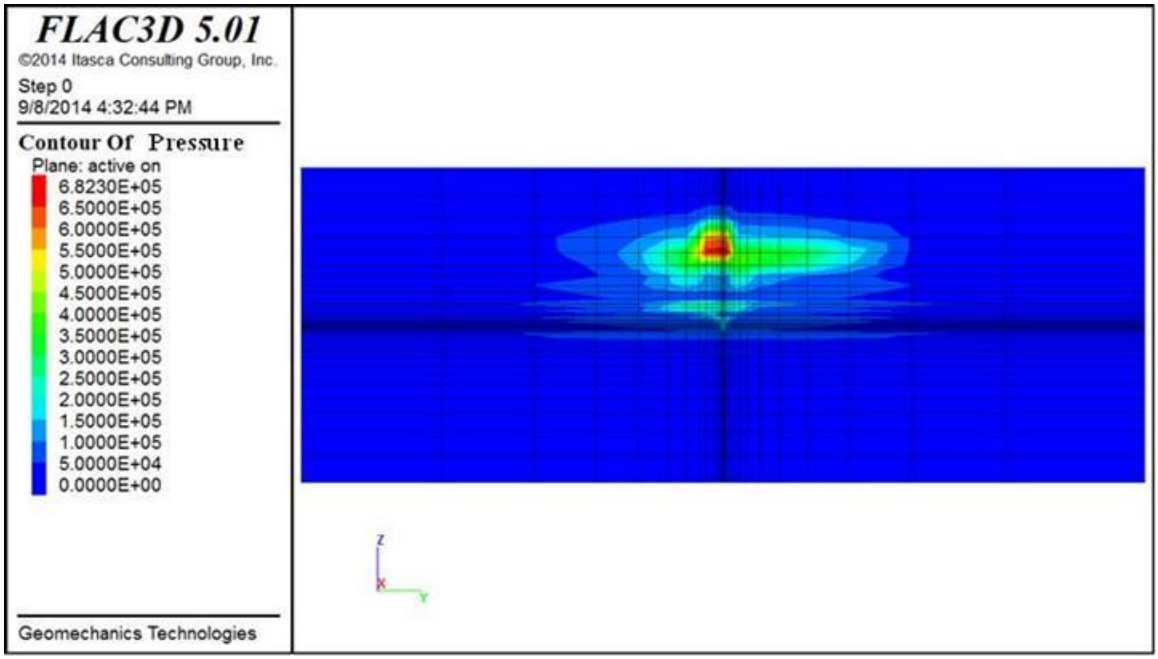

Figure 62. Pressure change after 30 years of injection determined from fluid flow model and input into geomechanical model (Pa); NE-SW (top) & NW-SE (bottom)

Figure 63 illustrates the horizontal stresses induced by such pressure change. Compressive stresses are induced within the pressurized areas and tensile stresses are induced above and below. These induced tensile stresses, however, are significantly below in-situ compressive stresses for the area, so risk for caprock fracturing are very low.

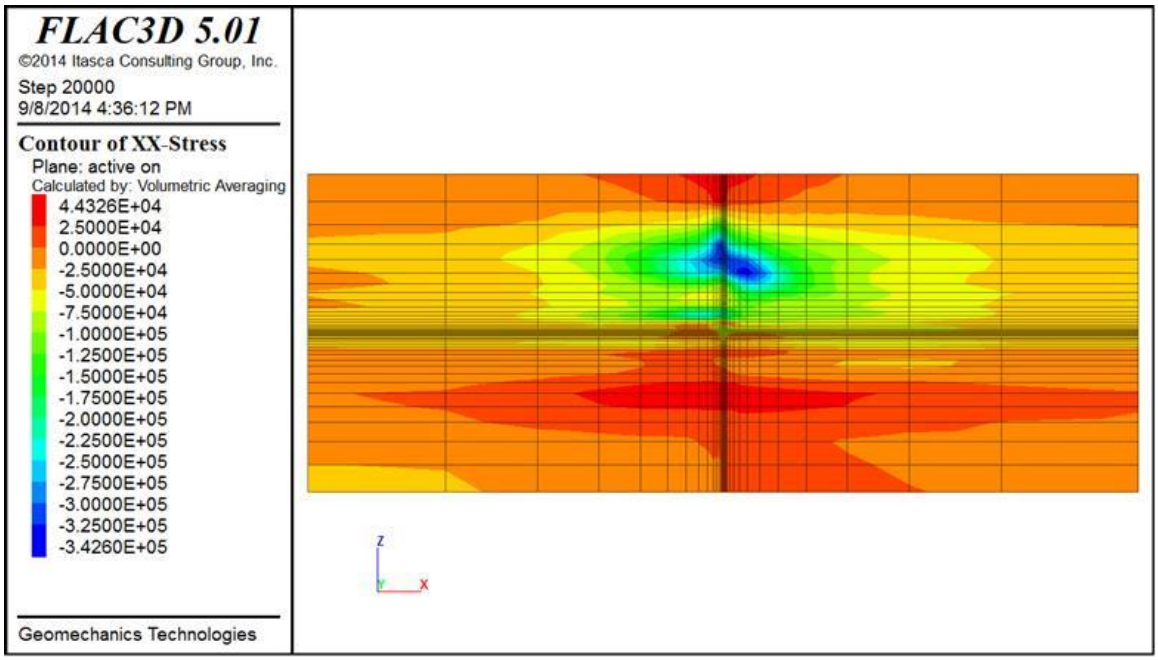

Figure 63. Resulting induced horizontal XX stress change in NE-SW direction (Pa)

Figure 64 shows the induced XZ stress across injection well in NE-SW direction, and the maximum compression and tension stresses are about 3.3E4 Pa and 5.8E4 Pa respectively. Figure 65 shows the induced ZZ stress across injection well in NE-SW direction, and the compression and tension stresses are located above and below the injection point, and the maximum of tension is about 3.5E4 Pa, and the maximum of compression is about 3.1E5 Pa.

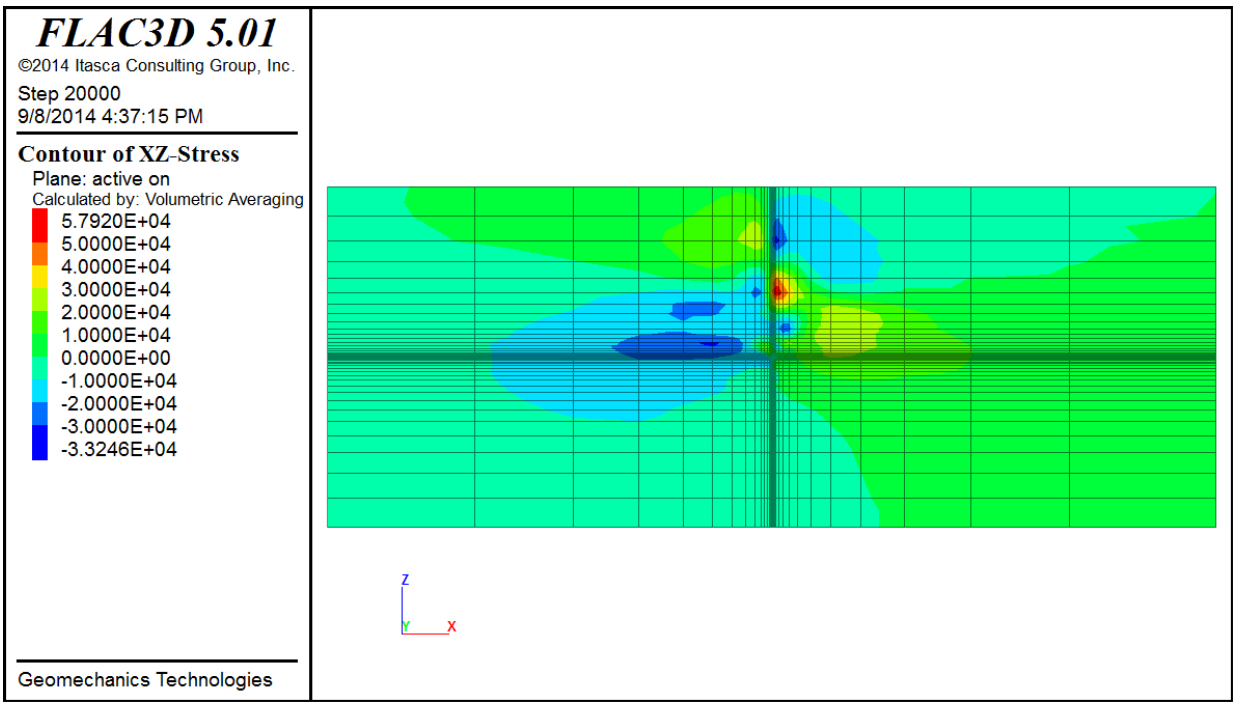

Figure 64. Induced XZ stress in NE-SW direction (Pa)

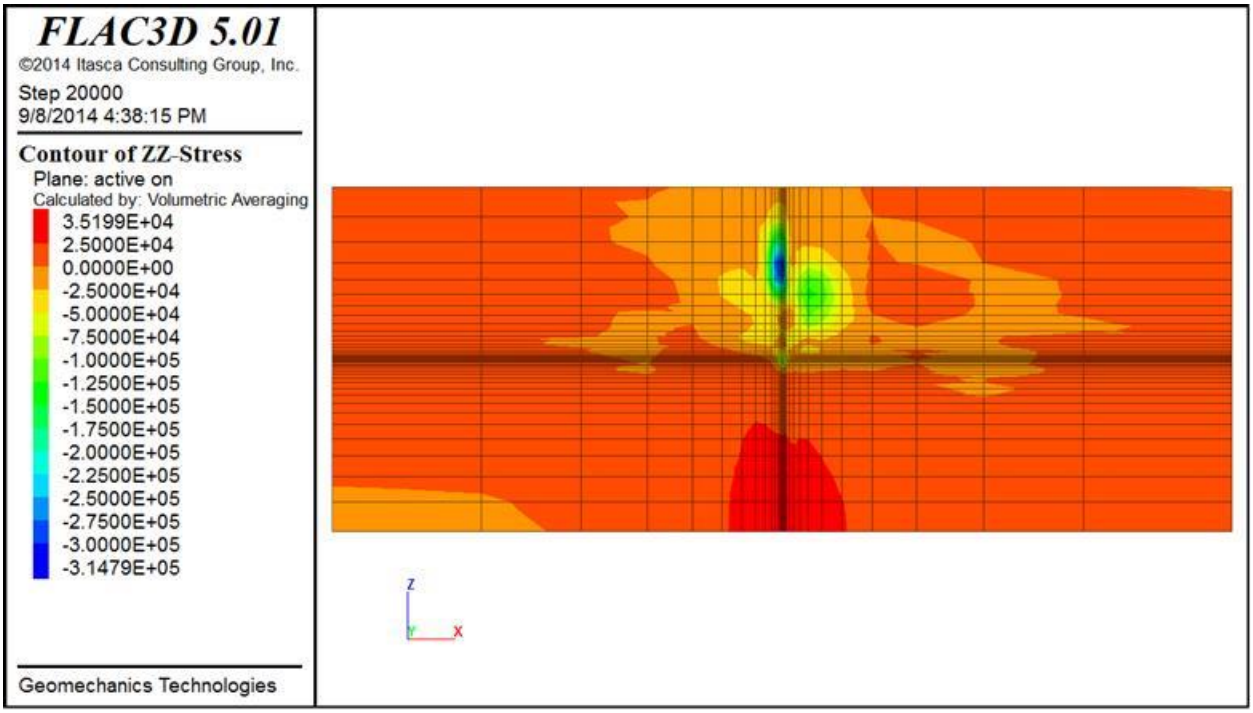

Figure 65. Induced ZZ stress in NE-SW direction (Pa)

Figure 66 shows the induced Z-displacement in 3D and 2D views. There is uplift surrounding the injection well, maximum of 9cm.

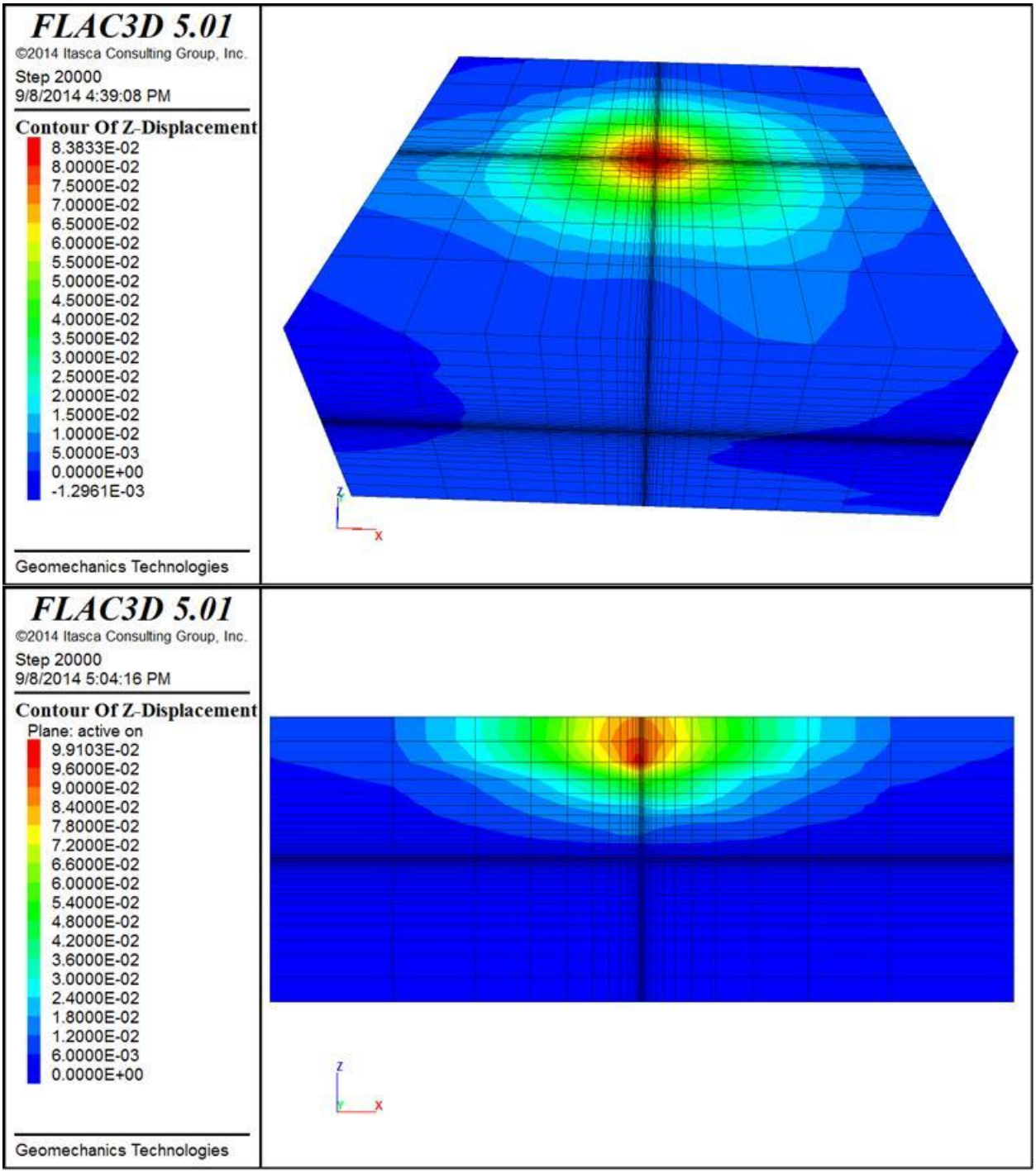

Figure 66. Induced Z displacement, 3D view (top) and NE-SW profile (bottom) (m)

5.3 Loudon, Central Illinois

The Louden natural gas storage field is located in central Illinois and geologically within the Illinois Basin (Figure 67). The Loudon Field is a depleted oil field that was converted to gas storage in 1969 by The Natural Gas Pipeline Company of America (NGPL).

In 1992, PETCO Petroleum Corporation acquired the Loudon Field mineral rights for the strata above the caprock of the gas storage operations. PETCO began producing natural gas from the shallow Carper sands. After June 16, 2000, stored gas from the deeper Grand Tower formation was found in the gas produced by PETCO from the shallower Carper Sand. PETCO suspected and contended that this was trespass caused by NGPL overpressuring the Grand Tower reservoir. Storage gas had collected in the Cedar Valley limestone, the formation originally designated as the primary "caprock." It was further conjectured that cyclic pressurization of both the Grand Tower and Cedar Valley formations induced new fractures and/or re-activated existing fractures in the overlaying New Albany Shale, which is observed to be fractured and gas bearing in other parts of the Illinois Basin.

Figure 67. Loudon field in central Illinois, and the Illinois Basin

5.3.1 Geologic Model

The field is an asymmetrical NE-SW anticline 14 miles long by 4 miles wide (Figure 68), containing a primary caprock composed of the Cedar Valley shale and limestone and a secondary caprock composed of the New Albany shale. The storage reservoir is the Devonian Grand Tower Formation.

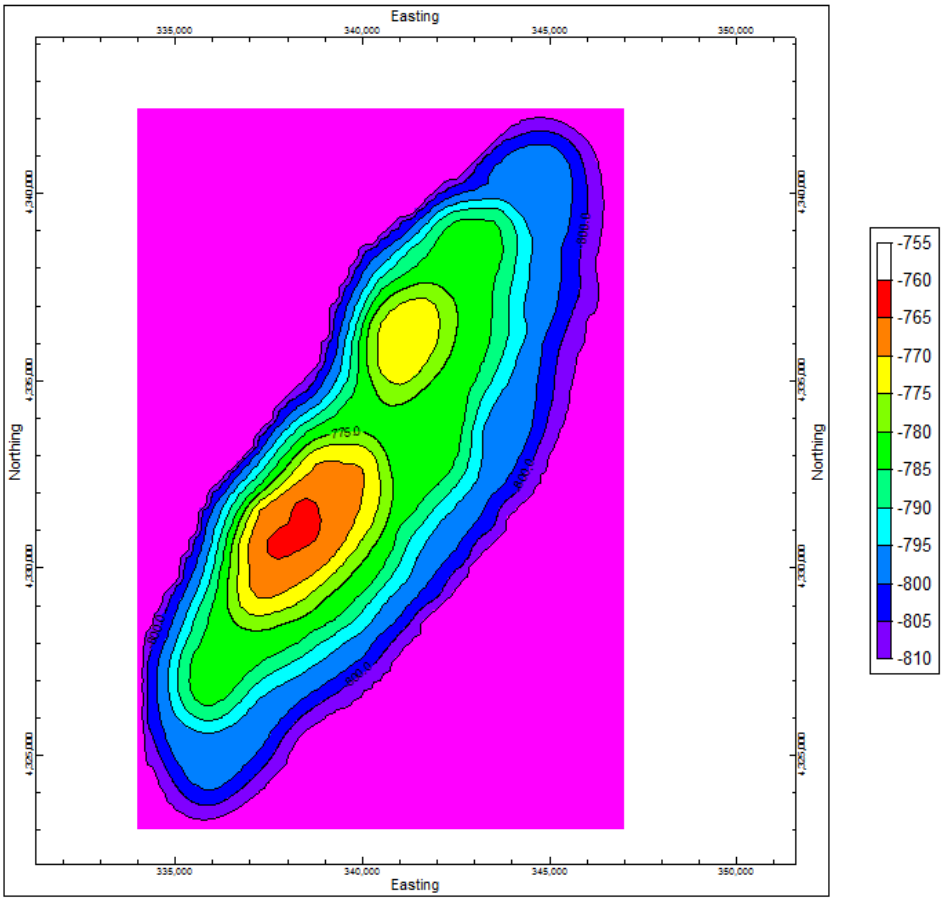

Figure 68. Digitized structure map of the Grand Tower Formation; contour depths are in meters below subsea

The approximate depth of the injection zone is 920-940 m below ground level. The completed lithology model for the entire geologic area is presented below in Figure 69. Fluid flow modelling requires high resolution, so in order to reduce the number of unnecessary cells and thus minimize run-time, a smaller subsection near the point of injection has been clipped from the larger model. To reduce the number of cells in the vertical direction, all cells above the Osage/Borden formation have been excluded from the smaller model. See Figure 70 for the smaller model submitted for fluid flow modelling.

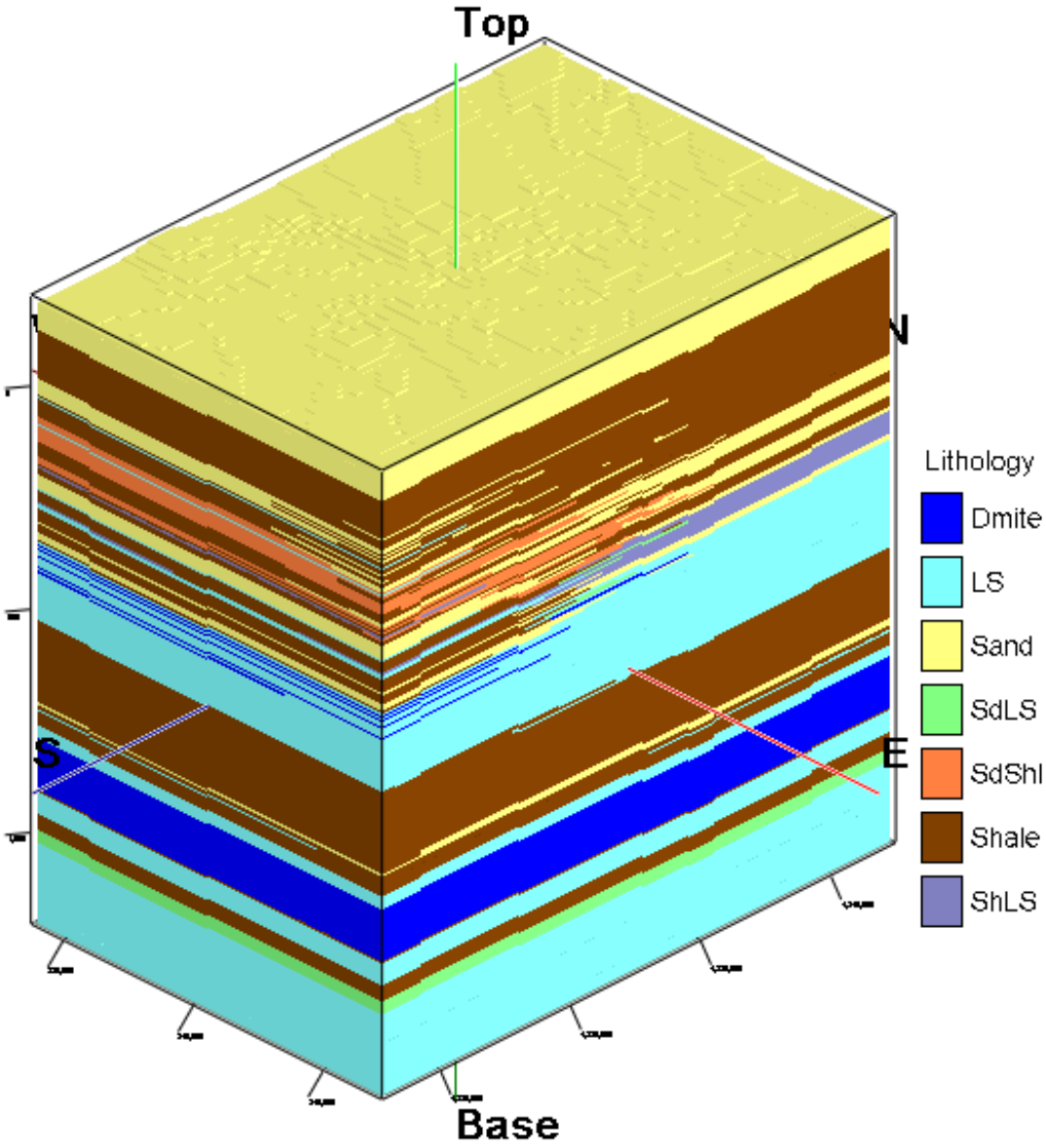

Figure 69. Completed lithology model for the geologic model domain

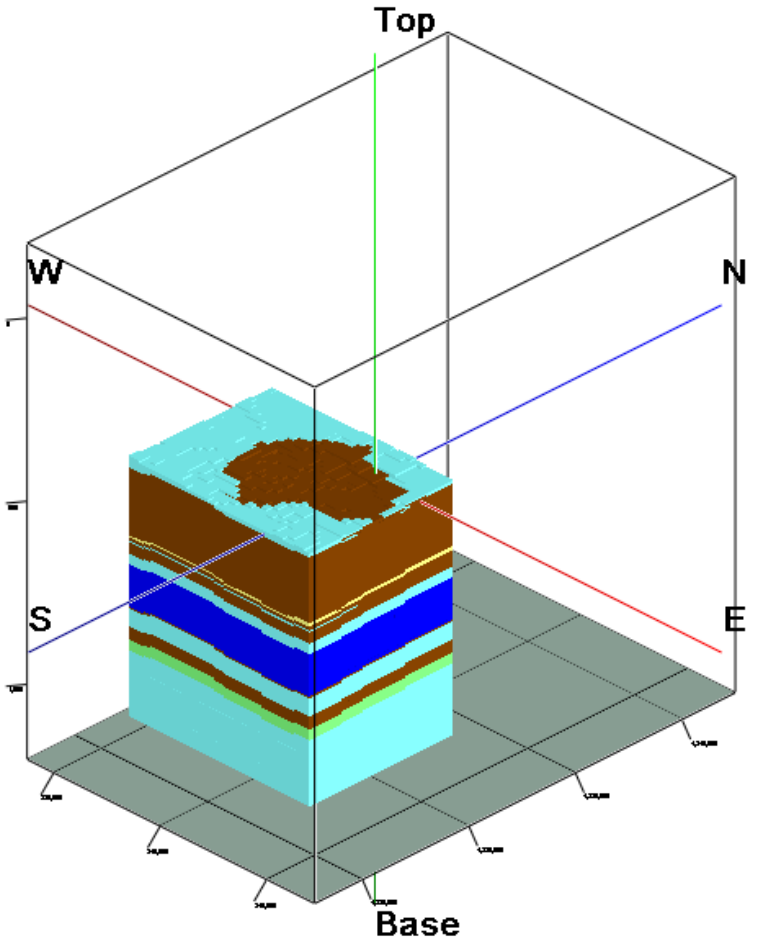

Figure 70. Smaller lithology model submitted for TOUGH2 fluid migration modelling (same lithology key as in Figure 69)

5.3.2 Fluid Flow Model

5.3.2.1 Model Description

A rectangular model was chosen to cover the entire injection zone in the formation. The complete geologic model covers the extent of the Louden field with an area of 13,000 m x 19,193 m (9 x12.5 miles). However, a smaller area surrounding the southern dome structure was used for fluid modelling. This model is 6500 m (-3788.58 m to 2711.42 m) by 8250 m (-3282.13 m to 4967.87 m), and ranges vertically from -350 m to -1200 m (all below sea level), see Figure 71. The Lydia Weaber 5D well located northwest of the center of the Loudon field has been chosen as the injection well site since it is closest to the center of the field and has the best available lithological data. The CO_2 injection well coordinates were translated into a local coordinate system, and the well placed at local coordinate (0,0). The presumed injection interval is between -754~ -774m below sea level in the Grand Tower Formation, which is about 920 m below ground surface, and 410 to 430 m from the top of the model. The mesh is finer near the well and in the injection interval, with a total of 89,920 elements. Figure 72 gives a more detailed cross sectional view of the injection zone dolomite, centered on the injection well.

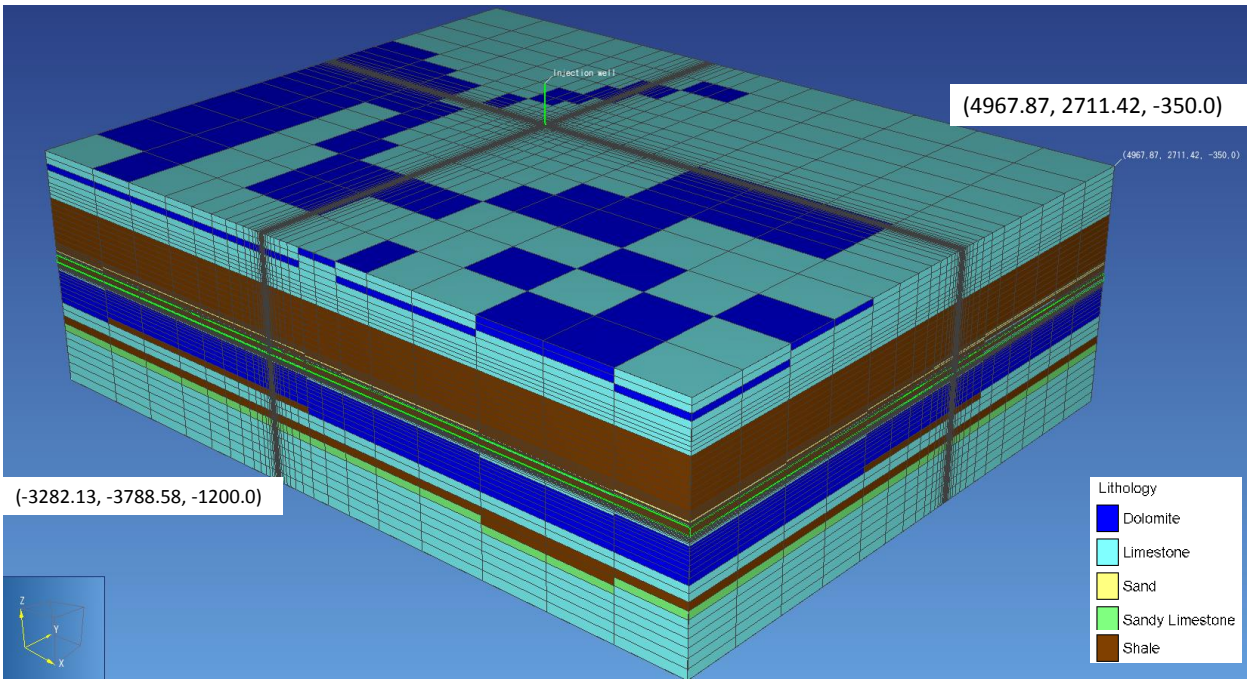

Figure 71. TOUGH2 mesh for Louden (3xVE)

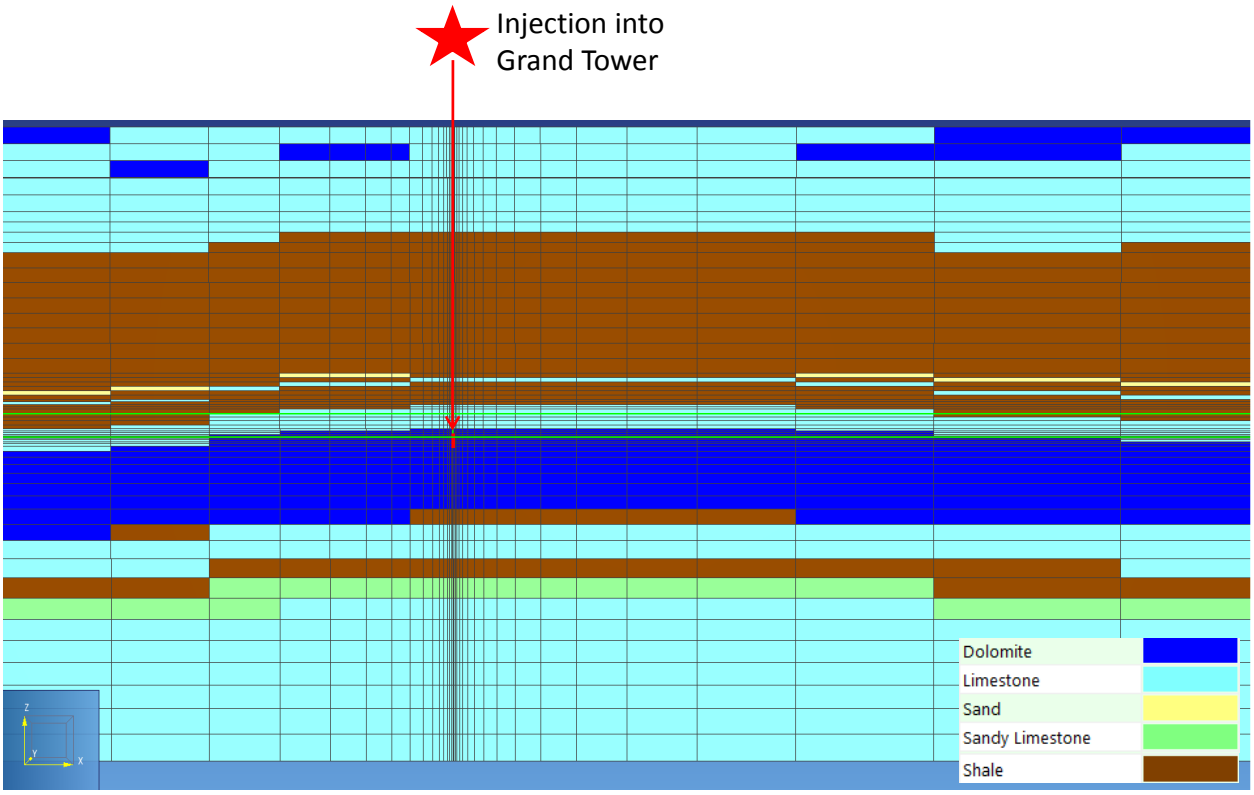

Figure 72. Cross-section plane through injection well (3xVE)

5.3.2.2 Initial Conditions

Initial pressure: the surface pressure is air pressure (1.01E5 Pa or 14.7 psi), with 9727 Pa/m (0.43 psi/ft) pressure gradient. The pressure is about 9.48E6 Pa (1374 psi) in the injection Grand Tower zone.

Initial temperature: the surface temperature is 15.56 Celsius (60 Fahrenheit), with a 0.006 ^{o}C/m (0.33 ^{o}F/100ft) temperature gradient. The temperature is about 21.4 ^{o}C (70.5 ^{o}F) in the injection Grand Tower zone.

Boundary condition: Assume Constant-Pressure-Boundary condition in a thin layer around the model, see Figure 73.

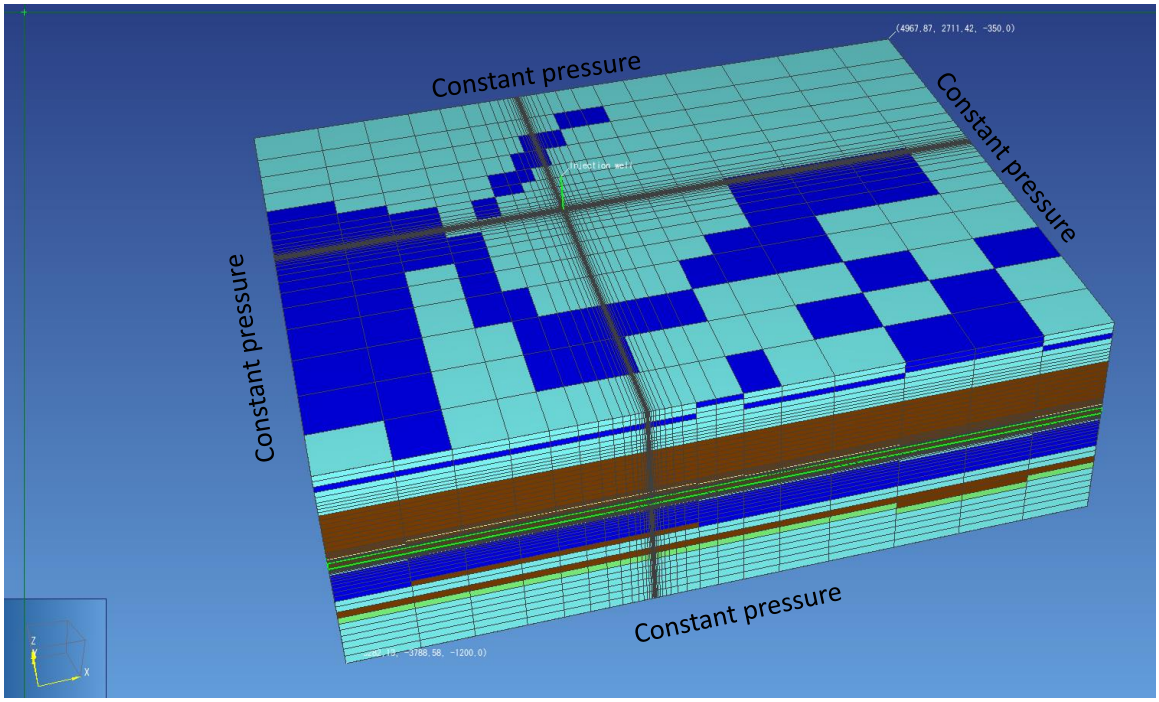

Figure 73. Constant-Pressure-Boundary Condition (3xVE)

5.3.2.3 Material Properties

Table 8 shows the material properties input for the fluid flow model.

Table 8 Input material properties for TOUGH2 model

Material name	density [kg/m³]	effective porosity [-]	x permeability [m²]	y permeability [m²]	z permeability [m²]	wet heat conductivity [W/mC]	specific heat [J/kg-C]	pore compressibility [1/Pa]
Dolomite	2500	0.16	9.86923E-14	9.86923E-14	9.86923E-15	2	1000	2.9E-11
Limestone	2270	0.16	9.86923E-14	9.86923E-14	9.86923E-15	2	1000	2.83E-11
Sand	2531	0.16	9.86923E-14	9.86923E-14	9.86923E-15	2	1000	2.64E-11
Sandy Limestone	2400	0.16	9.86923E-14	9.86923E-14	9.86923E-15	2	1000	2.74E-11
Shale	2514	0.001	9.86923E-17	9.86923E-17	9.86923E-18	2	1000	6.97E-11

	rel. Permeability				capillary pressure				
	vanGenuchten				vanGenuchten				
Material name	λ	S_{lr}	S_{ls}	S_{gr}	λ	S_{lr}	$1/P_0$ (1/Pa)	P_{max}(Pa)	S_{ls}
Dolomite	0.9	0.35	1	0.05	0.9	0.35	8.39E-08	10000	1
Limestone	1.1	0.5	1	0.16	1.1	0.5	8.39E-08	1000000	1
Sand	0.67	0.2	1	0.05	0.67	0.15	0.0004	10000000	1
Sandy Limestone	0.67	0.2	1	0.05	0.67	0.15	0.0004	10000000	1
Shale	0.64	0.36	0.98	0.001	0.64	0.36	8.16E-08	72800000	0.98

5.3.2.4 Results

We chose the ECO_2N module for the supercritical CO_2 injection simulation, and ran the isothermal case up to 50 years at a constant injection pressure 9.95E6 Pa (1443.7 psi, which is about 5% higher than the initial pressure). 11.4 million tons CO_2 are injected after 50 years (0.228 million tons per year). Figure 74 shows the plan view of CO_2 plume after 50 years injection.

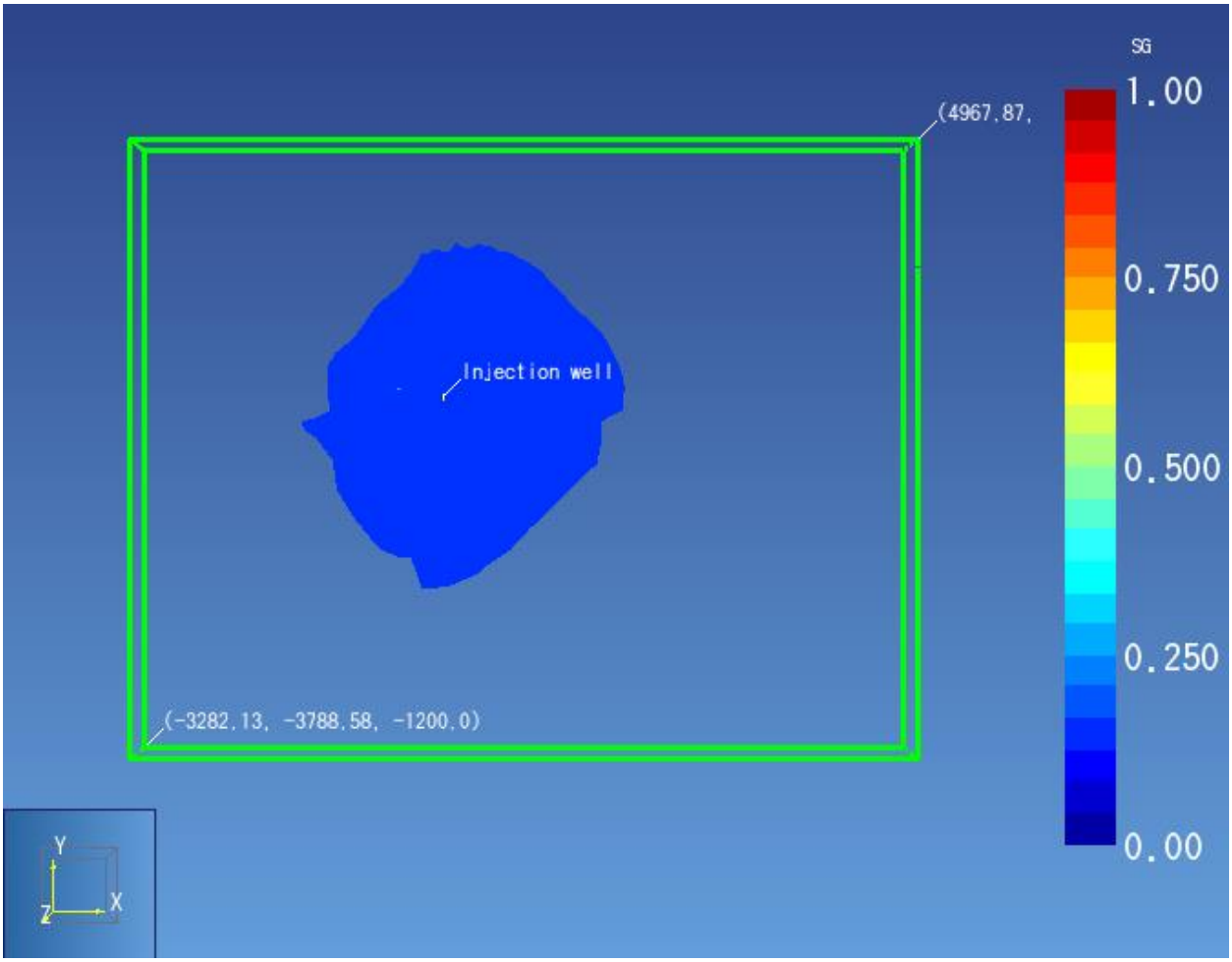

Figure 74. CO_2 gaseous plume after 50 years of injection – plan view

Figure 75 shows the pressure contour in N-S and E-W directions, centered on the injection well, at the beginning and end of the simulation. The pressure range is 5.55E6 Pa to1.36E7 Pa.

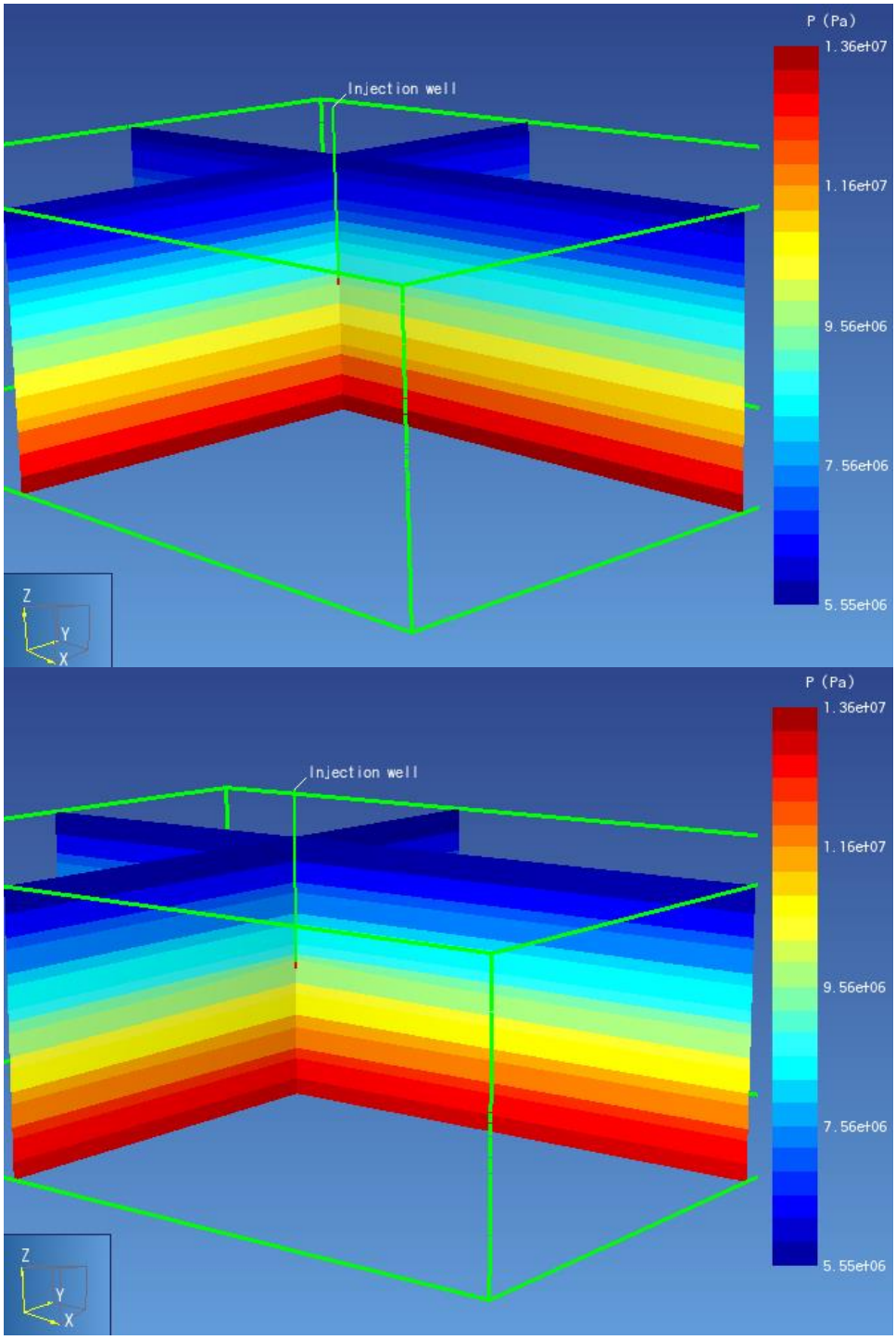

Figure 75. Pressure distribution contour, centered on injection well, in N-S and E-W directions, before injection (top) and after 50 years of injection (bottom) (3xVE)

Figure 76 shows the corresponding supercritical CO_2 saturation changes.

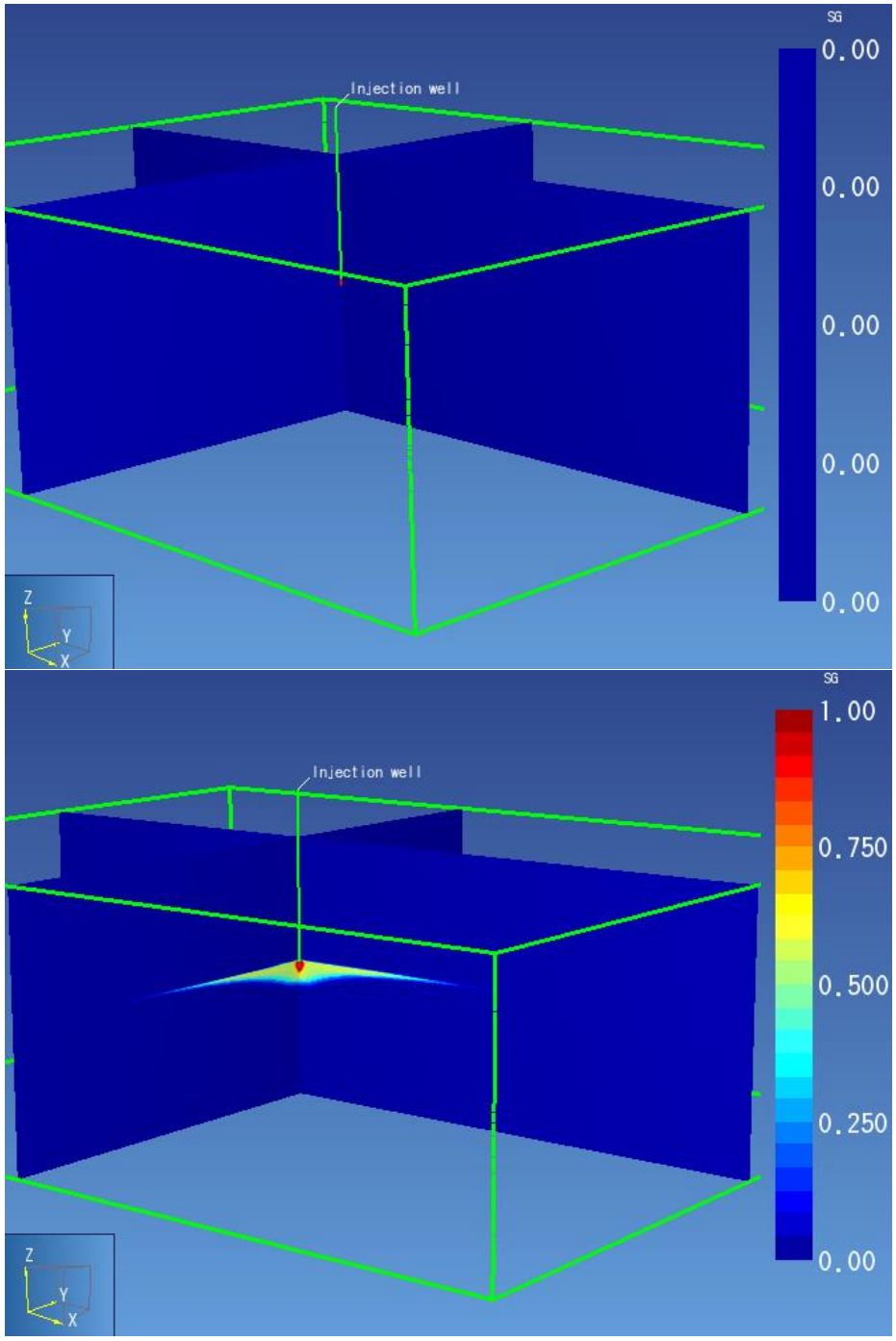

Figure 76. Supercritical CO_2 saturation contour, centered on injection well in N-S and E-W direction, before injection (top) and after 50 years of injection (bottom) (3xVE)

Figure 77 is an enlarged view of Figure 76, E-W direction, after 50 years of injection.

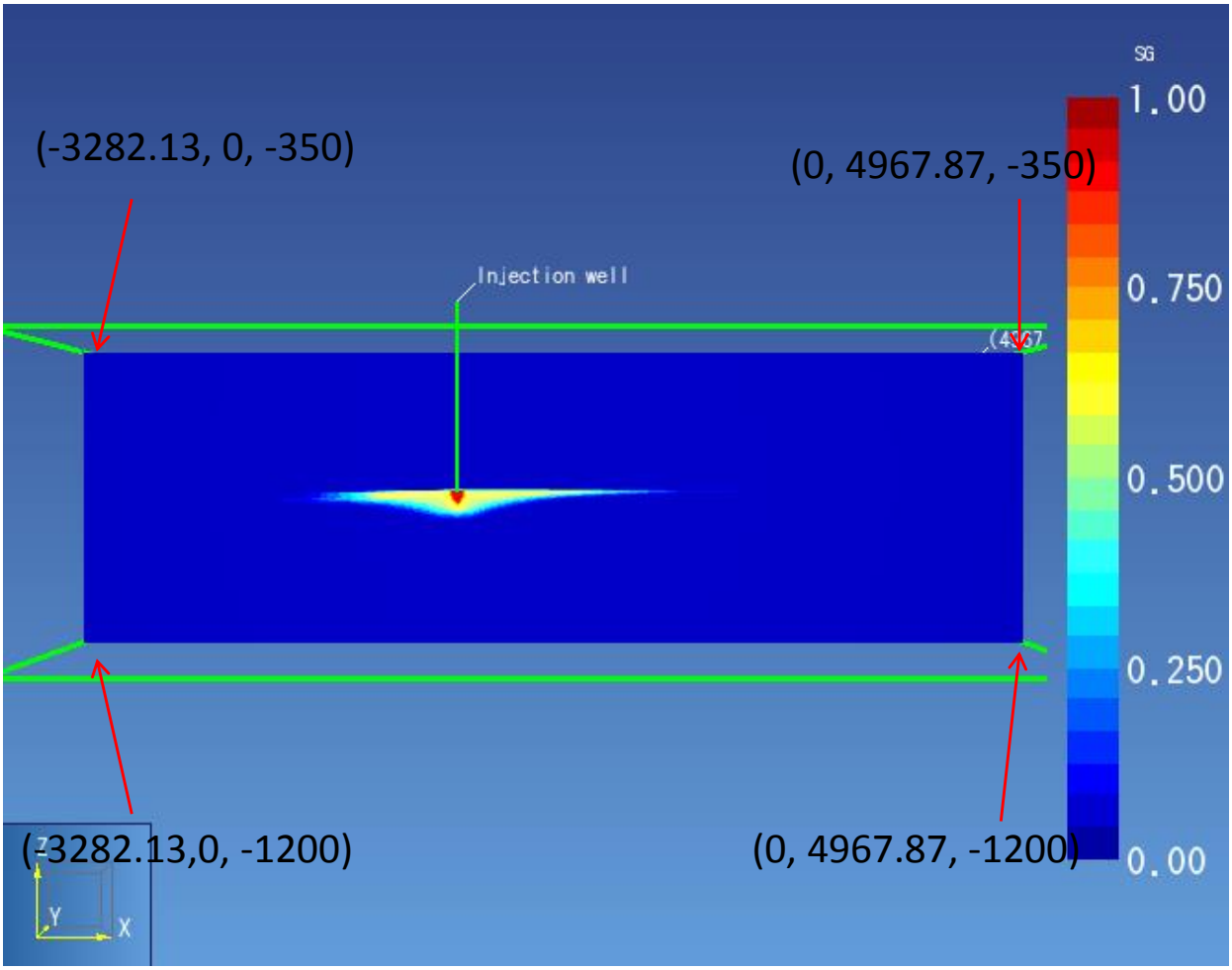

Figure 77. Enlarged view of supercritical CO_2 saturation (Figure 76, above) in E-W direction (3xVE)

5.3.2.5 Observation Phase

We ran the model for another 50 years without injection, after the 50 years of injection, to monitor the pressure and supercritical CO_2 migration. Figure 78 shows the supercritical CO_2 saturation and Figure 79 the contour plot of pressure distribution in N-S and E-W directions, both after the 50-year observation phase.

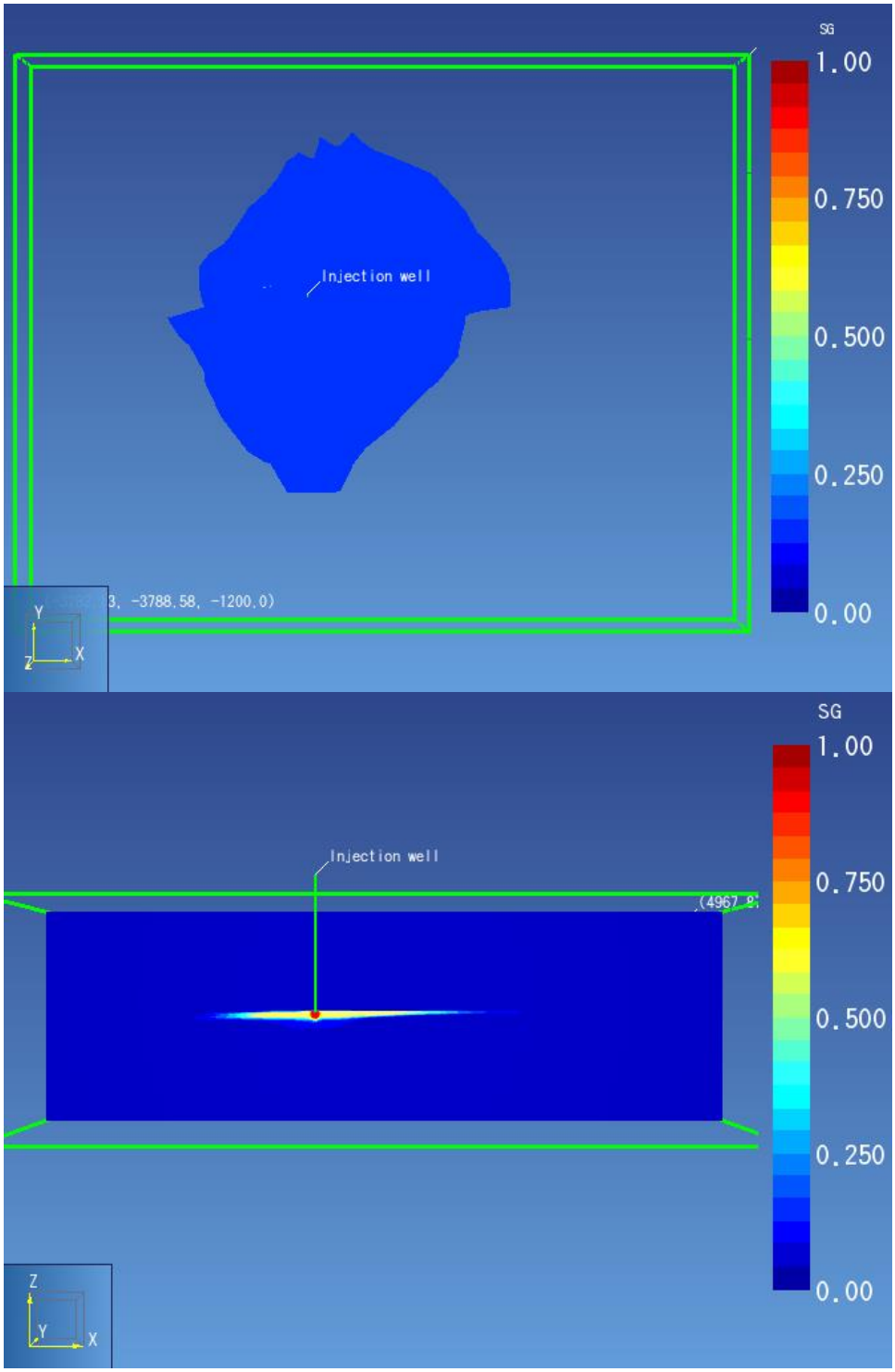

Figure 78. Supercritical CO_2 saturation, plan view (top) and E-W cross section (bottom, 3xVE), after observation phase

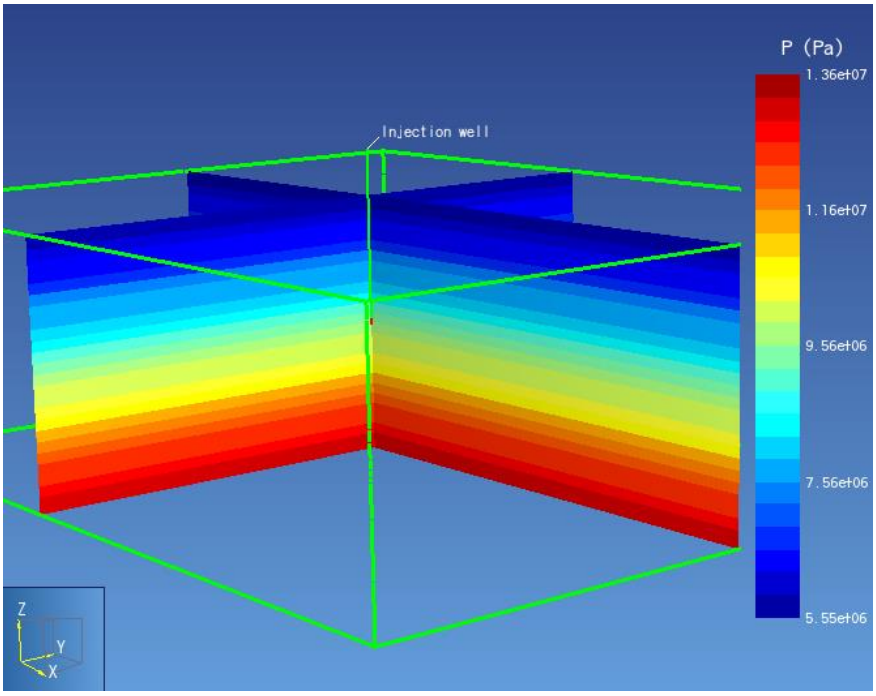

Figure 79. Pressure distribution contour, centered on injection well, in N-S and E-W direction (3xVE), after observation phase

Figure 80 and Figure 81 show pressure profiles at time $t = 0,\ t = 50\ years$, and after the 50-year observation phase, in the injection zone and along injection wellbore, respectively.

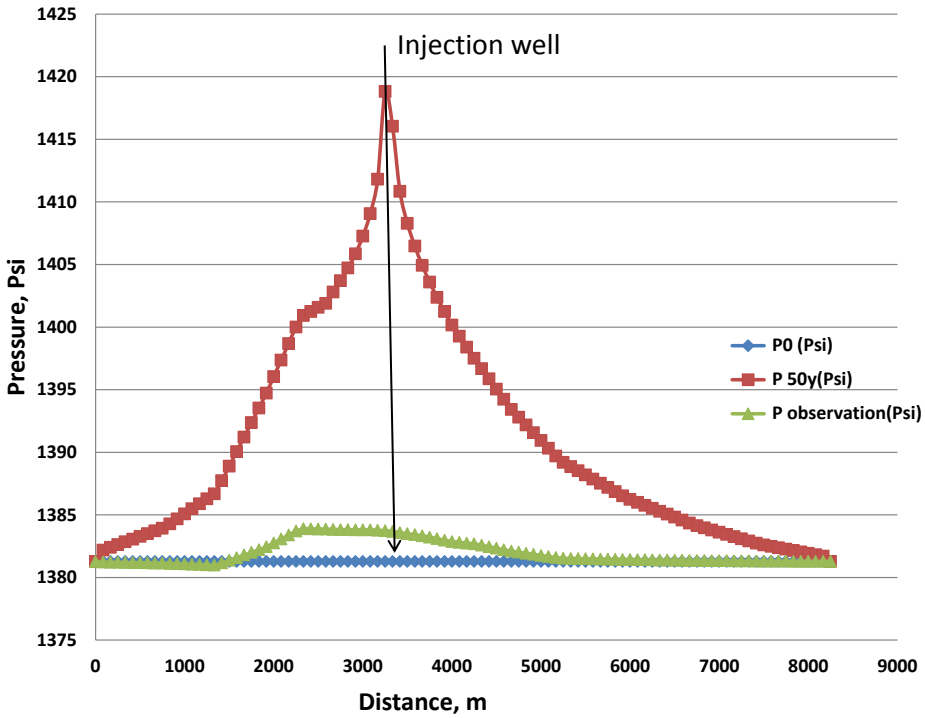

Figure 80. Pressure profile in the injection zone, centered on injection well, E-W direction

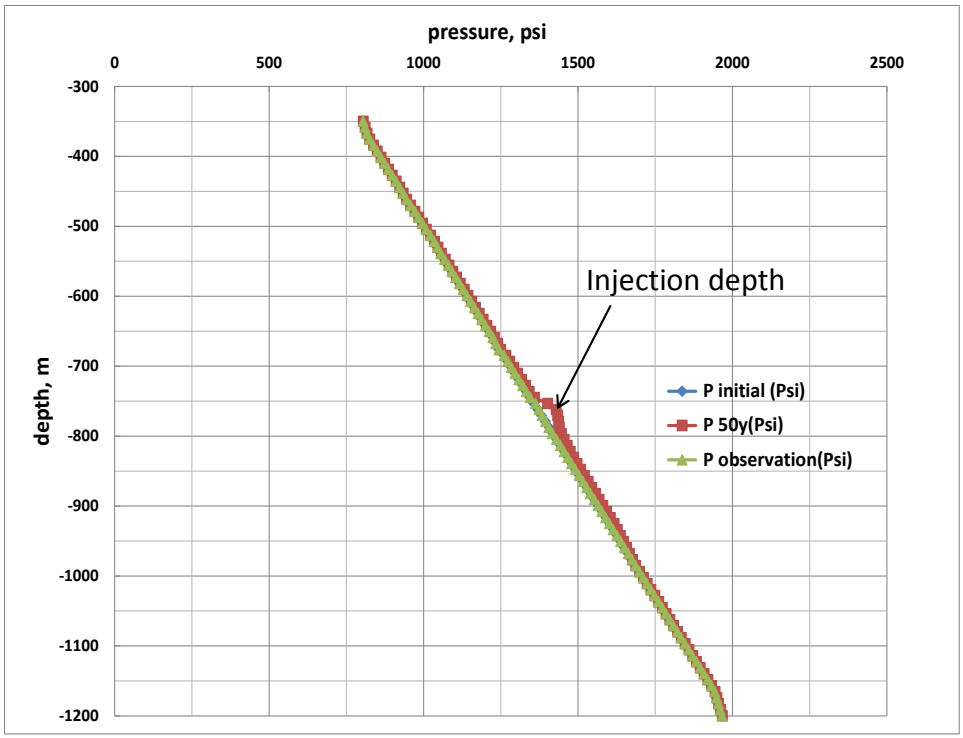

Figure 81. Pressure profile along the injection well

5.3.3 Geomechanical Model

5.3.3.1 Model Description

We created a 3D geomechanical model for Loudon, consistent with the latest geologic and TOUGH2 fluid flow models, with dimensions of 20,000m in both lateral directions (-10,000m to 10,000m) and about 1,900m in the vertical direction (from 180m above sea level to 1,720m below sea level). The injection wellbore is located at the center of the model. The model has a total of 256,000 elements, with a fining mesh near the injection well and in the Grand Tower injection formation. Figure 82 below shows the 3D geomechanical model, and Figure 83 shows the model, centered on the injection wellbore, along N-S and E-W cross sections.

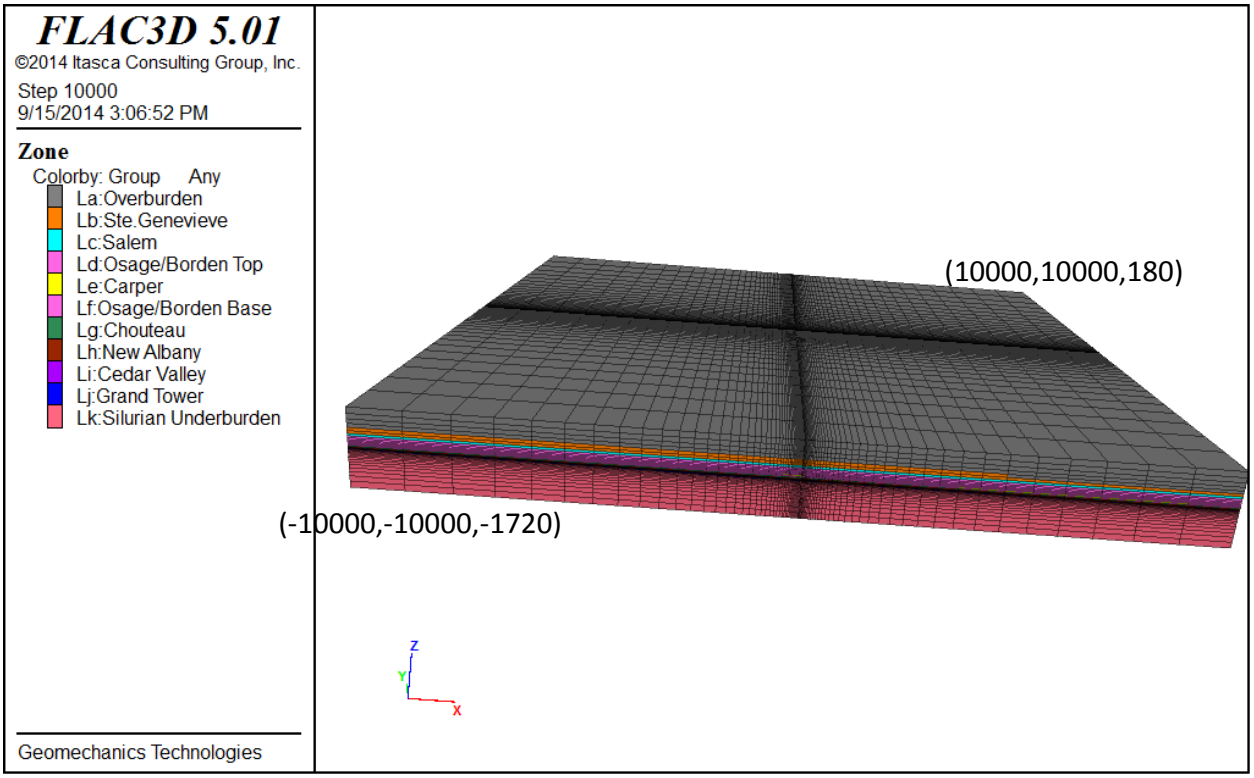

Figure 82. 3D Loudon geomechanics model with FLAC3D software

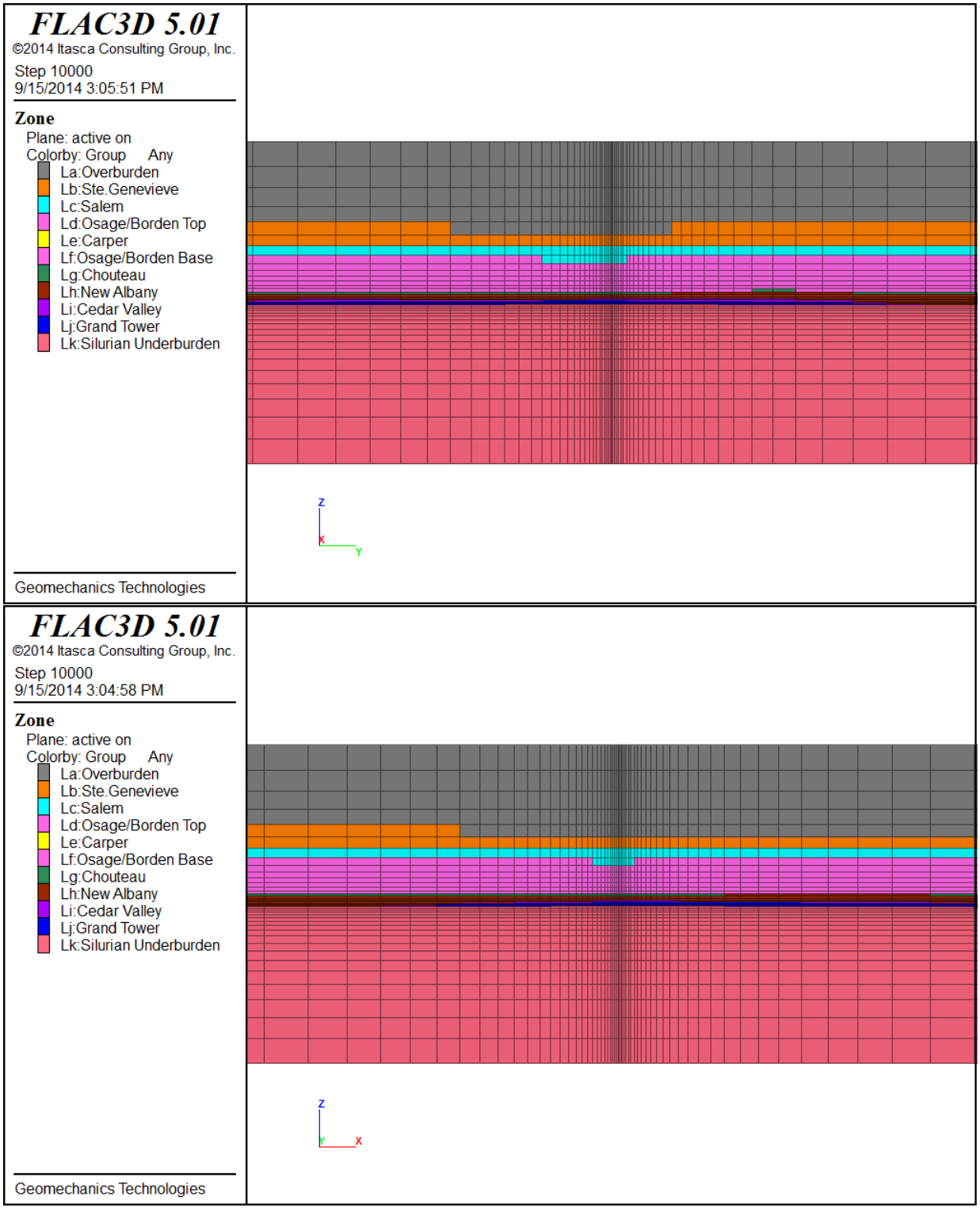

Figure 83. Geomechanics model, centered on injection wellbore, in N-S (top) and E-W (bottom) cross sections

5.3.3.2 Material Properties

Table Input material properties for FLAC3D model

Formation Layers	Ave. Vel (ft/sec)	Ave. Density (g/cc)	poisson's ratio	E (psi)	K (psi)	G (psi)	K(Pa)	G(Pa)	Cm(1/Pa)
Overburden	16975.47	2.265	0.2	7.91E+05	4.40E+05	3.30E+05	3031499628	2.27E+09	1.65E-10
Ste. Genevieve	18329.94	2.381	0.2	9.70E+05	5.39E+05	4.04E+05	3716966356	2.79E+09	1.35E-10
Salem	18175.9	2.065	0.2	8.27E+05	4.60E+05	3.45E+05	3169028201	2.38E+09	1.58E-10
Borden Siltstone	17662.35	2.430	0.2	9.19E+05	5.11E+05	3.83E+05	3521802561	2.64E+09	1.42E-10
Carper	17941.07	2.531	0.2	9.88E+05	5.49E+05	4.12E+05	3784263977	2.84E+09	1.32E-10
Chouteau	17961.82	2.514	0.2	9.84E+05	5.47E+05	4.10E+05	3768668579	2.83E+09	1.33E-10
New Albany	11109.7	2.502	0.2	3.75E+05	2.08E+05	1.56E+05	1434811035	1.08E+09	3.48E-10
Cedar Valley			0.2	9.90E+05	5.50E+05	4.13E+05	3792118000	2.84E+09	1.32E-10
Grand Tower			0.2	9.00E+05	5.00E+05	3.75E+05	3447380000	2.59E+09	1.45E-10
Underburden			0.2	9.60E+05	5.33E+05	4.00E+05	3677205333	2.76E+09	1.36E-10

5.3.3.3 Boundary Condition

We apply roller boundary conditions on all surfaces except the top surface, which is free to move in both vertical and lateral directions (Figure 84).

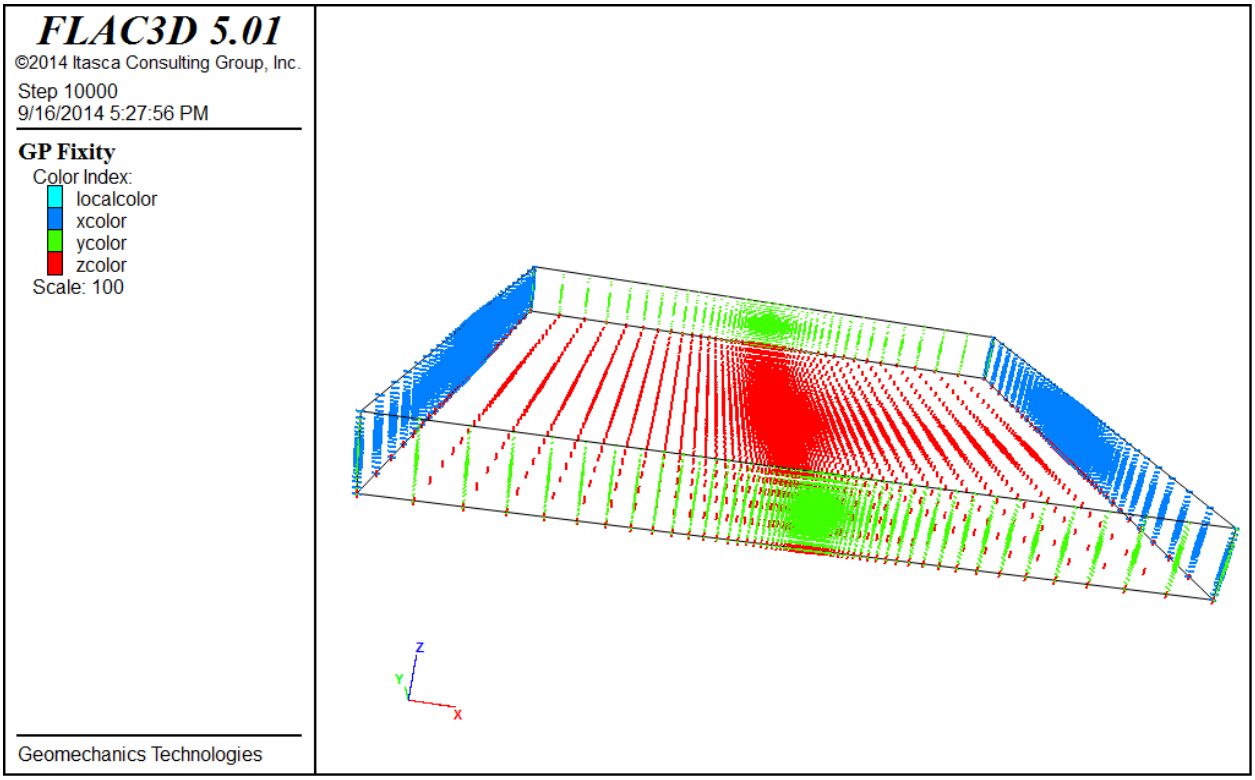

Figure 84. Roller boundary conditions in x, y directions and at the bottom of model

5.3.3.4 Results

We calculated the induced stresses and vertical displacement after 50 years of injection by applying pressure data from the fluid flow simulation above to this geomechanical model. Figure 85 shows the pressure changes after 50 years of injection.

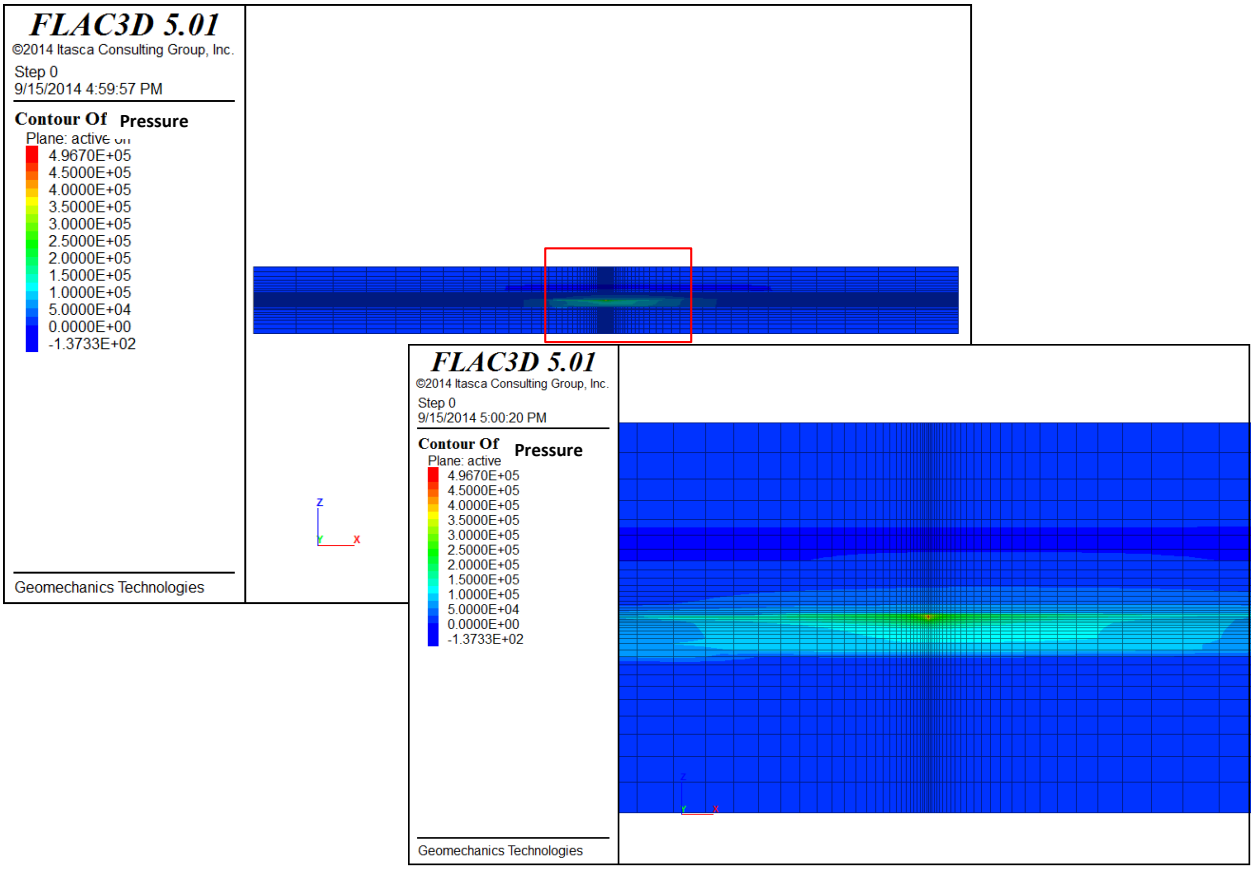

Figure 85. Pressure change contour after 50 years injection, centered on injection well in E-W cross section (Pa)

Figure 86 shows the induced displacements in the z-direction. The maximum displacement, near the injection wellbore, is about 5.7 mm.

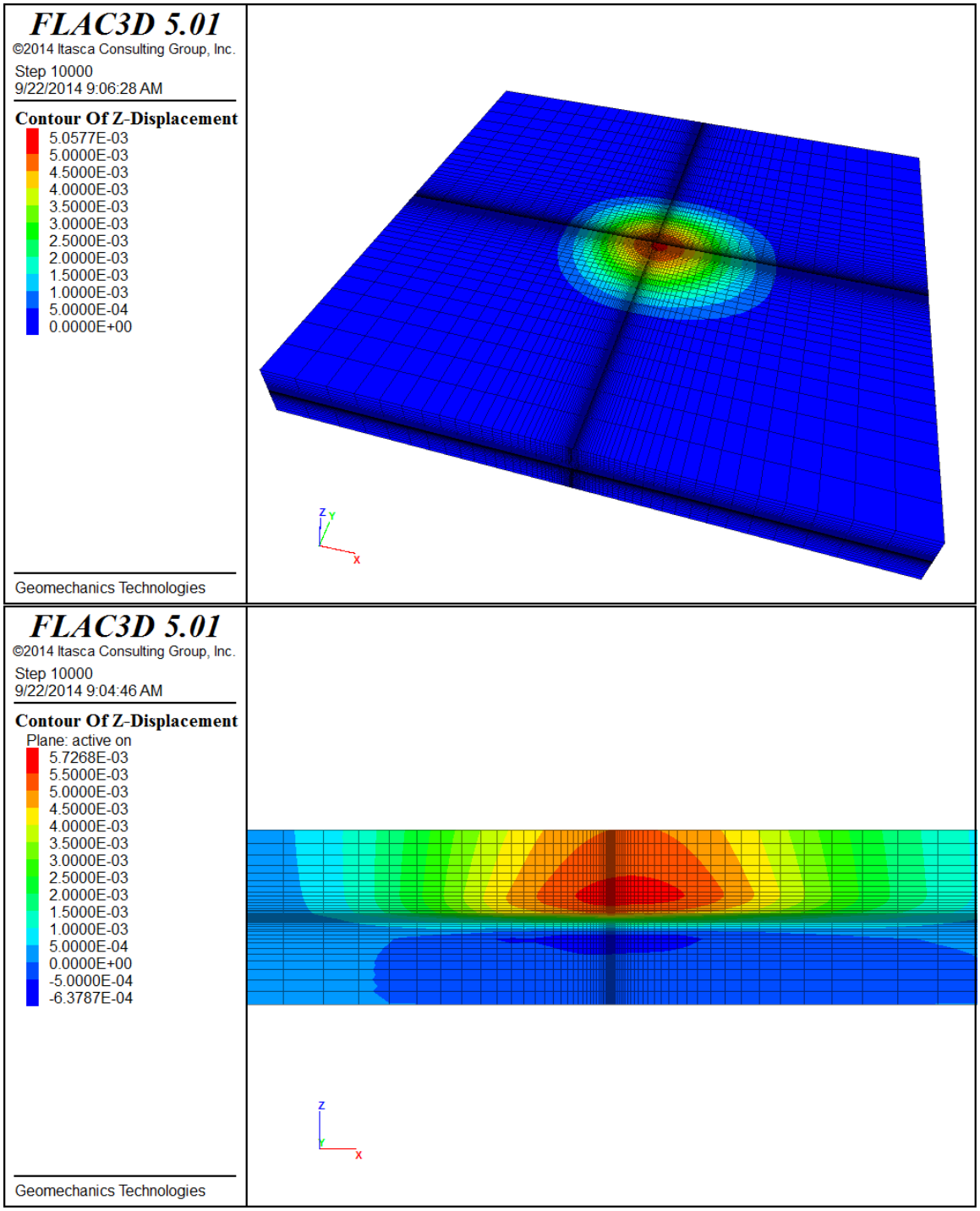

Figure 86. Induced Z-displacement, 3D view (top) and E-W cross section (bottom) (m)

Figure 87 shows the induced XX- and ZZ-stress plot contours, centered on the injection well. There are compaction stresses around the injection well, in the injection zone. The maximum horizontal compaction stress is about 3.5 $\times 10^5$ Pa, and the maximum vertical compaction stress is about 9.5 $\times 10^4$ Pa.

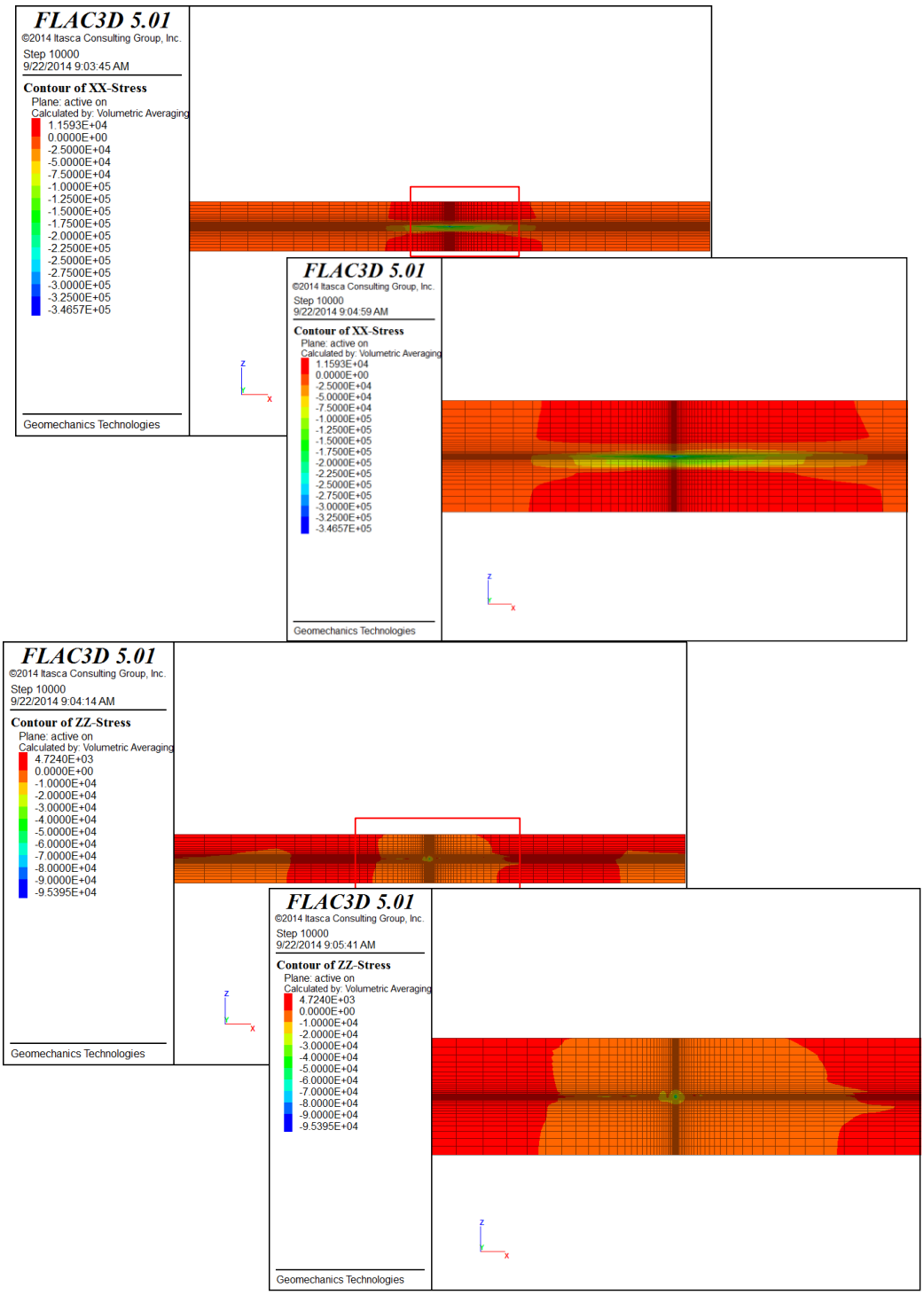

Figure 87. Induced horizontal XX-stress (top) and ZZ-stress (bottom) on E-W cross section (Pa)

Figure 88 shows the induced shear stresses on the E-W cross section. This XZ-stress is about 1.1×10^4 Pa.

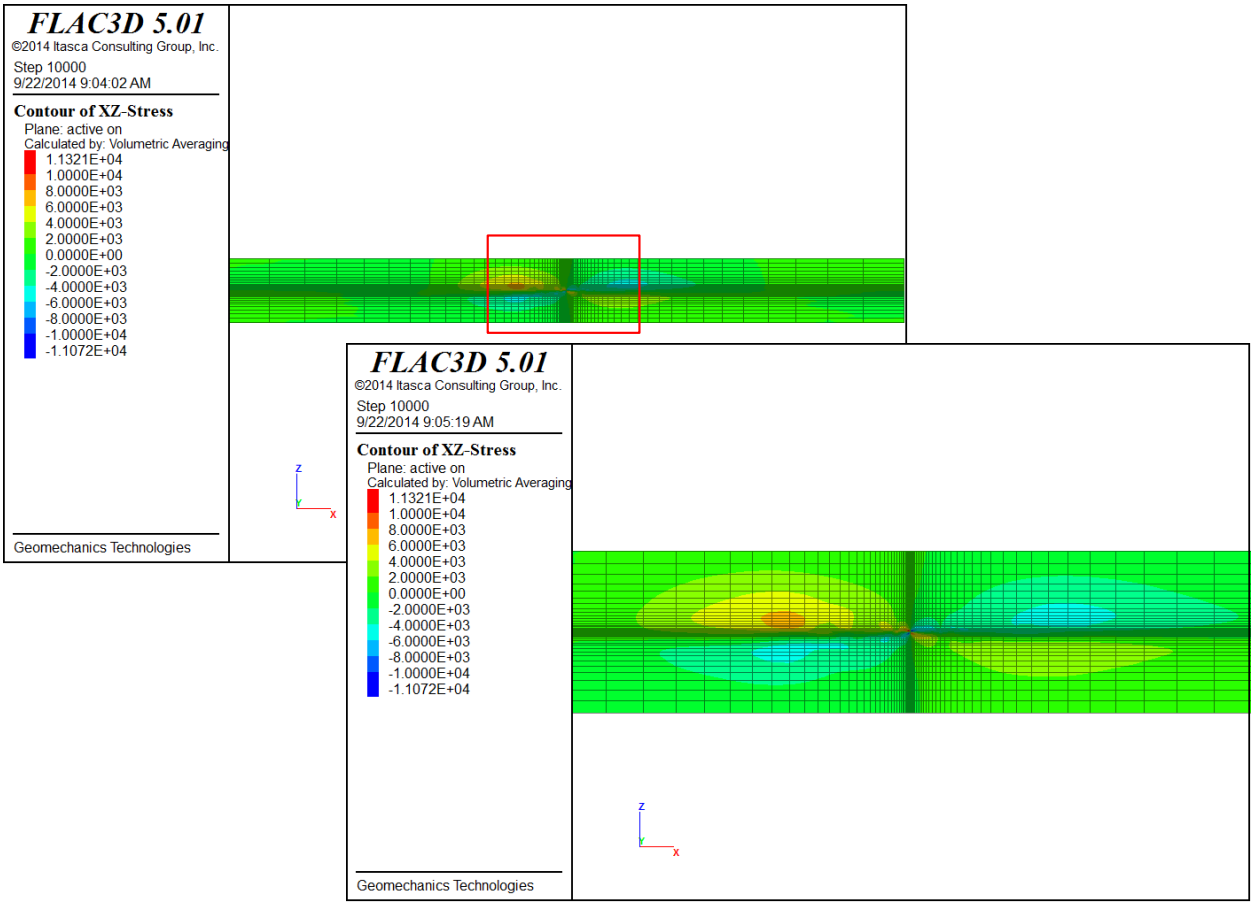

Figure 88. Induced horizontal XZ-stress on E-W cross section (Pa)

6 Development and Application of Quantitative Risk and Decision Analysis Tools for Caprock Integrity

We have developed a Quantitative Risk & Decision Analysis Tool (QRDAT) for caprock integrity evaluation, with the aim of assessing the potential for leakage during CO_2 injection. For this purpose we have established a set of parameters (risk factors) that influence the likelihood of caprock failure. We established order of magnitude value ranges for each parameter, which, when applied to particular geologic and operational settings, enable quantification of risk and offer a means by which to compare potential and active storage sites.

We consider three primary leakage mechanisms. These are tensile fracturing of the caprock, fault activation, and well damage. The set of risk factors can be divided into three main groups:

1. Mechanical state of the storage system, which includes stresses, pressures and faults;
2. Caprock and storage zone system, including reservoir and caprock geometry and properties; and
3. Operations, which include the status of the wells and injection practices.

6.1 Mechanical State Factors

6.1.1 Desired maximum formation pressure/effective minimum horizontal stress

The higher this ratio, the higher the risk for caprock failure. This number is a measure on how close the pressure in the formation is to the failure pressure, as fracturing occurs when the minimum horizontal stress is exceeded by the pressure in the reservoir.

6.1.2 Desired maximum formation pressure/discovery pressure

This ratio is a measure of the pressure increase in the reservoir. The higher this ratio, the larger the pressure increase in the caprock-storage zone system. The magnitude of pressure increase controls the potential for tensile and shear failure in the caprock and so poses risks for CO_2 containment.

6.1.3 Maximum formation pressure/formation depth

Higher formation pressure increases the risk for caprock failure. This value, however, needs be normalized to the formation depth to take into account the fact that high pressures are less influential with increasing depth due to countervailing pressure increases from increasing overburden load. The higher this ratio, the higher the risk for integrity loss.

6.1.4 Stress regime

Simple stabilization relations imply that a compressional stress regime will have the highest risk for reactivation during CO_2 injection, as CO_2 pressure increase will have a destabilizing effect on thrust faults, whereas it has stabilizing effect on normal faults (Figure 89). This only refers to the normal stresses induced by pressure increase. It does not refer to possible direct migration of fluid into the fault zone, which can destabilize either type of fault by reducing the normal effective stress acting to keep the fault from slipping.

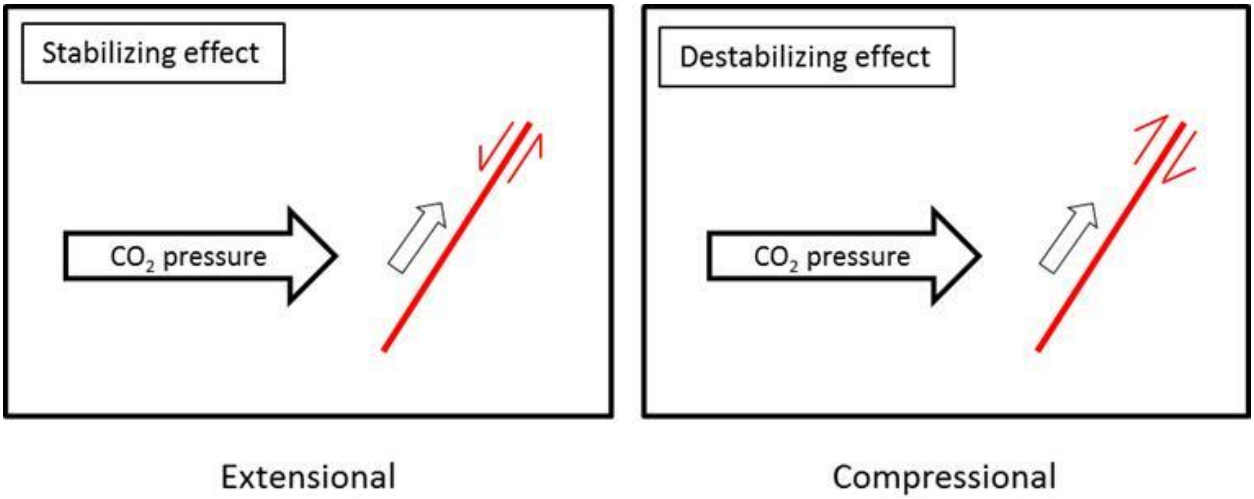

Figure 89. Induced horizontal stresses due to injection tend to stabilize normal faults and destabilize reverse faults

6.1.5 Stress ratio

The stress ratio is defined as σ_3/σ_1. Modelling studies for extensional stress regimes have shown that lower stress ratios lead to larger absolute fault slip magnitudes (Mazzoldi et al. 2012 & Rutqvist et al. 2013). In general, stress ratios are on the order of 0.5-0.7. Lower stress ratios lead to greater fault reactivation risks due to enhanced arching of the resulting normal stress. This causes a larger normal than shear stress ratio and so a greater chance of fault activation.

6.1.6 Fault boundaries

Faults can be activated by supercritical CO_2 encroachment. Stable faults are in equilibrium with the stresses acting on the fault plane. An increase in fluid pressure due to pressurized CO_2 entering the fault plane decreases the effective normal stress on this fault plane. When the fault plane approaches critical stress needed to initiate fault movement, this pore pressure increase may activate the fault. There is consensus that faults may act as flow paths, at least shortly post-failure (Sibson 2013). The presence of one or more close faults that extend far into the caprock increases the risk of caprock integrity loss. Additionally, Orlic et al. (2011) have demonstrated that stress concentrates on fault planes at interfaces between different lithologies, as exist between reservoirs and caprocks. Therefore, fault reactivation may be more likely at the caprock-reservoir interface, increasing this location's sensitivity to integrity loss.

6.1.7 Natural seismicity

High natural seismicity clearly poses a risk for caprock integrity loss. In regions with strong natural seismicity, the presence of pre-existing faults and fracture networks can be expected, which offer potential conduits for fluid migration, and generally reduce caprock integrity.

6.2 Caprock-Storage Zone System Factors

6.2.1 Storage zone lateral extent/depth and caprock lateral extent/thickness

These parameters assess the lateral continuity of both the reservoir and caprock by normalizing it to a fixed value (formation depth and caprock thickness, respectively). Clearly, the more extensive a formation is in the

lateral direction, the smaller the chance that CO_2 will reach a spill point and migrate upwards. Therefore, high ratio values for these parameters indicate low failure likelihood.

6.2.2 Storage zone thickness/depth

High values for this ratio correspond to a relatively thick reservoir at relatively shallow depth, indicating large volumes of CO_2 stored close to the surface. This combination has a major implication if failure in the caprock occurs; the release of a large amount of CO_2 without far to migrate upwards to reach the surface. Thus high ratio values here correspond to high risk.

6.2.3 Caprock strength

A stronger caprock has a lower risk for caprock integrity loss, due to a lower risk for both tensile fracturing and the onset of new faults in the caprock. A fracture develops only when the compressive strength in a rock is overcome, so the higher the unconfined compressive strength the lower the risk for the development of fracture networks. Note that a stronger caprock may lead to higher pressure build-up, which may lead to overburden and surface heave (e.g., In Salah (Rutqvist et al. 2010)). Bending of the caprock during uplift may lead to the development of shear stresses at the top of the caprock (Vilarrassa et al. 2011), but no cases of caprock failure due to surface heave have been reported thus far.

6.2.4 Caprock permeability

Relatively permeable caprocks may lead to loss of CO_2 containment, simply because CO_2 can migrate through them under the influence of strong buoyancy forces. This can occur for caprocks with permeabilities as low as $k > 10^{-18}$ m^2 (Zhou et al. 2008). The permeability of the caprock mainly influences the potential pressure build-up in the caprock and so too the development of fractures. The lower the permeability of the caprock, the less fluid penetration can occur and the less pressure can build up, and, thus, a lower failure risk pertains.

6.2.5 Caprock dip

Caprock dip mainly influences the migration of CO_2 within the reservoir. Due to high buoyancy of the CO_2, the supercritical fluid will tend to move upward in the reservoir until structurally trapped. The greater the caprock dip, the further the CO_2 migrates upwards, with the risk of reaching a spill point or discontinuity in the caprock also increasing. Doughty (2010) demonstrates that dipping caprock-storage zone systems lead to preferred CO_2 migration in the up-dip direction. The greater the dip, and its extent, the more quickly, and further, the CO_2 may migrate laterally. Sub-horizontal reservoirs below anticlinal caprock structures, however, form structural traps and therefore securely contain CO_2.

6.2.6 Caprock thickness

As would be expected, thicker caprocks are lower risk for integrity loss, simply because fracture networks and faults can develop further into the caprock without fully transgressing it. For example, at In Salah a fracture network reaches 100-200 m into the caprock (Verdon et al. 2013), but since the caprock package is up to 950 m thick, this has no effect on the security of storage.

6.2.7 Caprock heterogeneity

Caprock heterogeneity increases the risk for integrity and containment loss for various reasons. First, in case of lateral heterogeneity (e.g. in turbidite settings), CO_2 may reach discontinuities in the caprock, which may allow upward migration. In very heterogeneous caprocks, connected fluid pathways to higher strata may be present. Second, heterogeneity of lithology within the caprock may lead to stress concentrations, as has already been discussed with respect to fault boundaries, rendering these interfaces prone to tensile and shear failure.

6.2.8 Number of sealing strata

The number of individual sealing strata within the general caprock package influences the integrity of the system simply by forming a baffled system of multiple storage locations with multiple caprocks which act as buffers if the primary seal below them fails. Rutqvist et al. (2008) assessed the risk for caprock failure in multilayered systems. Assessing stress developments in a storage system with three caprocks, of which the lower two have failed, they concluded that ensuing upward migration of CO_2 creates the highest shear and tensional failure risk at the interface of the shallowest storage zone and intact caprock. Thus existence of multiple caprocks is not a guarantee for CO_2 containment; however, in general the risk for integrity loss decreases with an increasing number of caprocks above the primary intended seal.

6.3 Operations Risk Factors

6.3.1 Well density and number of uncased wells/total number of wells

The number of wells already drilled through the caprock clearly increases the risk of CO_2 migration. The greater the number of wells fully penetrating the caprock and into the storage zone, the greater the number of potential leakage pathways present. Gasda et al. (2004) illustrate seven pathways by which CO_2 can leak through previously completed, but now plugged and abandoned wellbores.

6.3.2 Number of uncased wells/total number of wells

The risk of leakage is even greater for uncased wells. Best CO_2 practices currently dictate that new well casings are to be designed to stay intact for timescales on the order of thousands of years. The biggest risk overall for safe CO_2 storage is posed by old abandoned wells, residing mainly in depleted hydrocarbon reservoirs, which were not designed for secure storage for timescales of this magnitude (Orlic 2009).

6.3.3 Temperature difference between injected CO_2 and storage zone

Temperature induced stresses are proportional to the change in temperature times the material coefficient of thermal expansion. Excessive cooling causes tensile fractures, which can act as a migration pathway. The greater the difference between initial formation pressure and the injected fluid, the greater the tensile stress perturbation.

6.4 Methodology

For each of the risk factors, we established three orders of magnitude risk value ranges corresponding to low, moderate, and high risk. For example, for the first mechanical state risk factor discussed above, the ratio of desired maximum formation pressure to effective minimum horizontal stress, values of 0.5 and below are considered low risk, between 0.5 and .075 moderate risk, and anything higher than 0.75 is considered high risk. Low risk conditions are assigned a risk score of 1. Moderate risk conditions are assigned a risk score of 10. And high risk conditions are assigned a risk score of 100. The purpose for using order of magnitude risk scores is to develop general ranking criteria that are not overly influenced by any one individual factor, many of which are necessarily subjective in nature.

Risk factor scores are assigned to each of the leakage mechanisms (tensile fracture, fault activation, and well damage). If a risk factor does *not* influence a particular leakage mechanism, it is scored as 1 no matter its value. For example, our caprock-storage zone risk factor of caprock permeability clearly has an effect on tensile failure of the caprock, thus a high value for caprock permeability receives a higher risk score. But caprock

permeability has no effect on the failure of wellbores or the breeching of older wellbores, so a highly permeable caprock does not influence the well damage mechanism.

We have included 19 factors in QRDAT and three leakage mechanism for each. Thus each storage site, or potential storage site, receives 57 factor scores. Total risk is the sum of all factor scores, allowing comparison between alternative sites. For each risk factor we have set up ranges that we associated with high, moderate or low leakage potential.

Table 9 shows the ranges for separate risk factors.

Table 9 Risk factor value ranges in current QRDAT version

Risk factor	Risk factor value ranges		
	High risk	**Moderate risk**	**Low risk**
Lateral extension of the storage zone/formation depth	<25	25-100	>100
Storage zone thickness/storage zone depth	> 0.5	0.1-0.5	< 0.1
Stress regime	Compressional	Transform	Extensional
Caprock strength	Weak	Moderate	Strong
Caprock thickness	≤ 3 m	3-30 m	≥ 30 m
Fault boundaries	Multiple	One	None
Natural seismicity	High	Moderate	Low
Number of caprocks	No	One	Multiple
Maximum formation pressure/formation depth	≥ 0.75	0.625-0.75	≤ 0.625
Desired maximum formation pressure/discovery pressure	≥ 1.5	1.25-1.5	≤ 1.25
Well density	> 15	5-15	< 5
Number of uncased wells/total number of wells	> 0.6	0.2-0.6	< 0.2
Temperature difference between the injected CO_2 and the ambient storage zone temperature	≥ 60 ◦C	30-60 ◦C	≤ 30 ◦C
Caprock heterogeneity	Significant	Moderate	Strong
Caprock permeability	> 10^{-15} m^2	10^{-18}-10^{-15} m^2	< 10^{-18} m^2
Caprock lateral extend/storage zone thickness	<25	25-100	>100
Caprock dip	≥ 8°	2°-8°	≤ 2°
Minimum horizontal stress/vertical stress (stress ratio)	<0.55	0.55-0.65	>0.65

MECHANICAL STATE						
	tens frac		fault reac		well fail	
1. STRESS						
Max P/min princ stress						
a. ≥ 0,75	0	100	0	100	0	100
b. 0,5-0,75	1	10	1	10	1	10
c. ≤ 0,5	0	1	0	1	0	1
Stress regime						
a. Compressional	1	100	1	100	1	100
b. Transform	0	10	0	10	0	10
c. Extensional	0	1	0	1	0	1
Shmin/Sv						
a. < 0.55	0	1	0	100	0	100
b. 0.55-0.65	0	1	0	10	0	10
c. > 0.65	1	1	1	1	1	1
2. PRESSURE						
Desired Max P/Discovery P						
a. ≥ 1.5	0	100	0	100	0	100
b. 1.25-1.5	0	10	0	10	0	10
c. ≤ 1.25	1	1	1	1	1	1
Max P/formation depth						
a. ≥ 0.75	0	100	0	100	0	100
b. 0.625-0.75	0	10	0	10	0	10
c. ≤ 0.625	1	1	1	1	1	1
3. FAULTS						
Fault boundaries						
a. Multiple bounding faults	1	1	1	100	1	100
b. One bounding fault	0	1	0	10	0	10
c. None	0	1	0	1	0	1
Natural seismicity						
a. High	1	100	1	100	1	100
b. Moderate	0	10	0	10	0	10
c. Low	0	1	0	1	0	1

Figure 90. Mechanical state risk factors and ranges included in risk assessment tool

CAPROCK-STORAGE ZONE SYSTEM						
	tens frac		fault reac		well fail	
4. STORAGE ZONE SPECIFIC						
Lateral extent/storage zone depth						
a. <25	1	100	1	100	1	100
b. 25-100	0	10	0	10	0	10
c. >100	0	1	0	1	0	1
Storage zone thickness/storage zone depth						
a. > 0.5	0	100	0	100	0	1
b. 0.1-0.5	0	10	0	10	0	1
c. < 0.1	1	1	1	1	1	1
5. CAPROCK SPECIFIC						
Caprock heterogeneity						
a. Significant	1	100	1	100	1	1
b. Moderate	0	10	0	10	0	1
c. Low	0	1	0	1	0	1
Caprock strength						
a. Weak	0	100	0	100	0	100
b. Moderate	1	10	1	10	1	10
c. Strong	0	1	0	1	0	1
Caprock thickness						
a. ≤ 3m	0	100	0	100	0	1
b. 3-30 m	1	10	1	10	1	1
c. ≥ 30 m	0	1	0	1	0	1
Caprock lateral extent/caprock thickness						
a. <25	1	100	1	100	1	100
b. 25-100	0	10	0	10	0	10
c. >100	0	1	0	1	0	1
Caprock permeability						
a. k > 1E-15 m2	0	100	0	1	0	1
b. 1E-18 m2 ≤ k ≤ 1E-15 m2	1	10	1	1	1	1
c. k < 1E-18 m2	0	1	0	1	0	1
Number of caprocks						
a. Single	0	100	0	100	0	100
b. Double	0	10	0	10	0	10
c. Multiple	1	1	1	1	1	1
Caprock dip						
a. γ ≥ 8°	1	1	1	100	1	1
b. 2°≤γ≤8°	0	1	0	10	0	1
c. γ ≤ 2°	0	1	0	1	0	1

Figure 91. Caprock and storage zone risk factors and ranges included in risk assessment tool

OPERATIONS						
	tens frac		fault reac		well fail	
6. OPERATIONS						
Well density						
a. > 15 km-2	0	1	0	1	0	100
b. 5-15 km-2	0	1	0	1	0	10
c. < 5 km-2	1	1	1	1	1	1
No. of uncased wells/total no. of wells						
a. > 0.6	0	1	0	1	0	100
b. 0.2-0.6	0	1	0	1	0	10
c. < 0.2	1	1	1	1	1	1
ΔT between CO2 and storage zone						
a. ≥ 60 °C	0	100	0	100	0	1
b. 30 °C - 60 °C	1	10	1	10	1	1
c. ≤ 30 °C	0	1	0	1	0	1

Figure 92. Operating parameters risk factors and ranges included in risk assessment tool

6.5 Sample Application to Five Storage Projects

We have applied the risk assessment to evaluate five CO_2 injection and potential injection sites. The first three are potential CO_2 sites under consideration, including the Kevin Dome site (Figure 93), the Louden site (Figure 94), and the Wilmington graben (Figure 95). Two others are actual large scale CO_2 injection sites, including Sleipner in the North Sea (Figure 96) and In Salah in North Africa (Figure 97). The resulting total risk scores are presented in Figure 98.

6.5.1 Kevin Dome

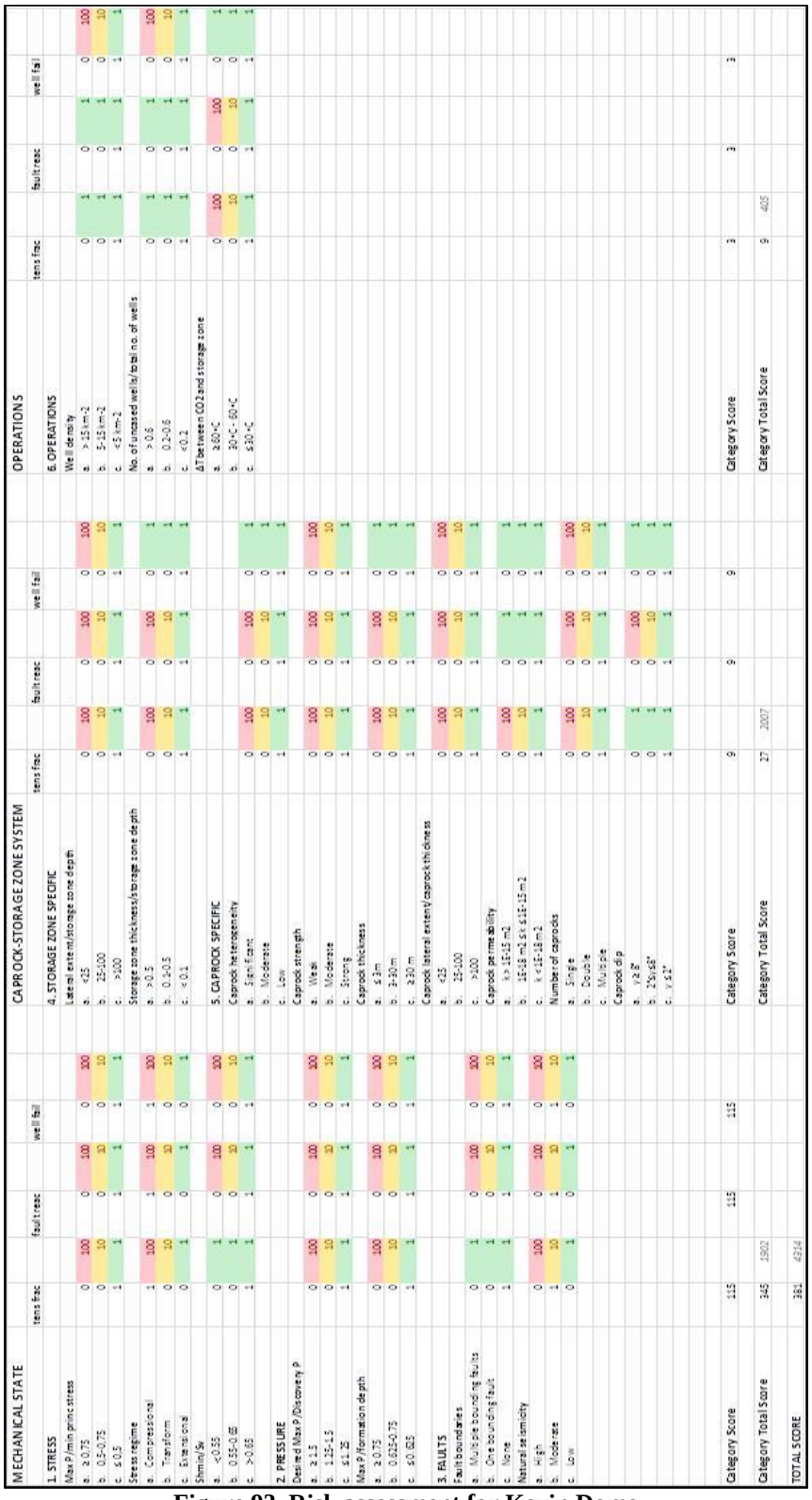

MECHANICAL STATE	tens frac	fault reac	well fail	CAPROCK-STORAGE ZONE SYSTEM	tens frac	fault reac	well fail	OPERATIONS	tens frac	fault reac	well fail
1. STRESS				4. STORAGE ZONE SPECIFIC				6. OPERATIONS			
Max P/min principal stress				Lateral extent/storage zone depth				Well density			
a. ≥ 0.75	0 100	0 100	0 100	a. <25	0 100	0 100	0 100	a. > 15 km-2	0 1	0 1	0 100
b. 0.5-0.75	0 10	0 10	0 10	b. 25-100	0 10	0 10	0 10	b. 5-15 km-2	0 1	0 1	0 10
c. ≤ 0.5	1 1	1 1	1 1	c. >100	1 1	1 1	1 1	c. <5 km-2	1 1	1 1	1 1
Stress regime				Storage zone thickness/storage zone depth				No. of unplugged wells/total no. of wells			
a. Compressional	1 100	1 100	1 100	a. >0.5	0 100	0 100	0 100	a. >0.6	0 1	0 1	0 100
b. Transform	0 10	0 10	0 10	b. 0.2-0.5	0 10	0 10	0 10	b. 0.2-0.6	0 1	0 1	0 10
c. Extensional	0 1	0 1	0 1	c. <0.2	1 1	1 1	1 1	c. <0.2	1 1	1 1	1 1
Shmin/Sv								ΔT between CO2 and storage zone			
a. <0.55	0 1	0 100	0 100	5. CAPROCK SPECIFIC				a. ≥60+C	0 100	0 100	0 1
b. 0.55-0.65	0 1	0 10	0 10	Caprock heterogeneity				b. 30+C - 60+C	0 10	0 10	0 1
c. >0.65	1 1	1 1	1 1	a. Significant	0 100	0 100	0 1	c. ≤30 +C	1 1	1 1	1 1
2. PRESSURE				b. Moderate	0 10	0 10	0 1				
Desired Max P/Discovery P				c. Low	1 1	1 1	1 1				
a. ≥ 1.5	0 100	0 100	0 100	Caprock strength							
b. 1.15-1.5	0 10	0 10	0 10	a. Weak	0 100	0 100	0 100				
c. ≤ 1.15	1 1	1 1	1 1	b. Moderate	0 10	0 10	0 10				
Max P/formation depth				c. Strong	1 1	1 1	1 1				
a. ≥ 0.75	0 100	0 100	0 100	Caprock thickness							
b. 0.625-0.75	0 10	0 10	0 10	a. ≤ 3m	0 100	0 100	0 1				
c. ≤ 0.625	1 1	1 1	1 1	b. 3-30 m	0 10	0 10	0 1				
				c. ≥ 30 m	1 1	1 1	1 1				
3. FAULTS				Caprock lateral extent/caprock thickness							
Fault boundaries				a. <25	0 100	0 100	0 100				
a. Multiple bounding faults	0 1	0 100	0 100	b. 25-100	0 10	0 10	0 10				
b. One bounding fault	0 1	0 10	0 10	c. >100	1 1	1 1	1 1				
c. None	1 1	1 1	1 1	Caprock permeability							
Natural seismicity				a. k > 1E-15 m2	0 100	0 100	0 1				
a. High	0 100	0 100	0 100	b. 1E-18 m2 ≤ k ≤ 1E-15 m2	0 10	0 10	0 1				
b. Moderate	1 10	1 10	1 10	c. k < 1E-18 m2	1 1	1 1	1 1				
c. Low	0 1	0 1	0 1	Number of caprocks							
				a. Single	0 100	0 100	0 100				
				b. Double	0 10	0 10	0 10				
				c. Multiple	1 1	1 1	1 1				
				Caprock dip							
				a. > 2 °	0 1	0 100	0 1				
				b. 2 to 45°	0 1	0 10	0 1				
				c. < 2 °	1 1	1 1	1 1				
Category Score	115	115	115	Category Score	9	9	9	Category Score	3	3	3
Category Total Score	345 1902			Category Total Score	27 2007			Category Total Score	9 405		
TOTAL SCORE	381 4214										

Figure 93. Risk assessment for Kevin Dome

6.5.2 Louden

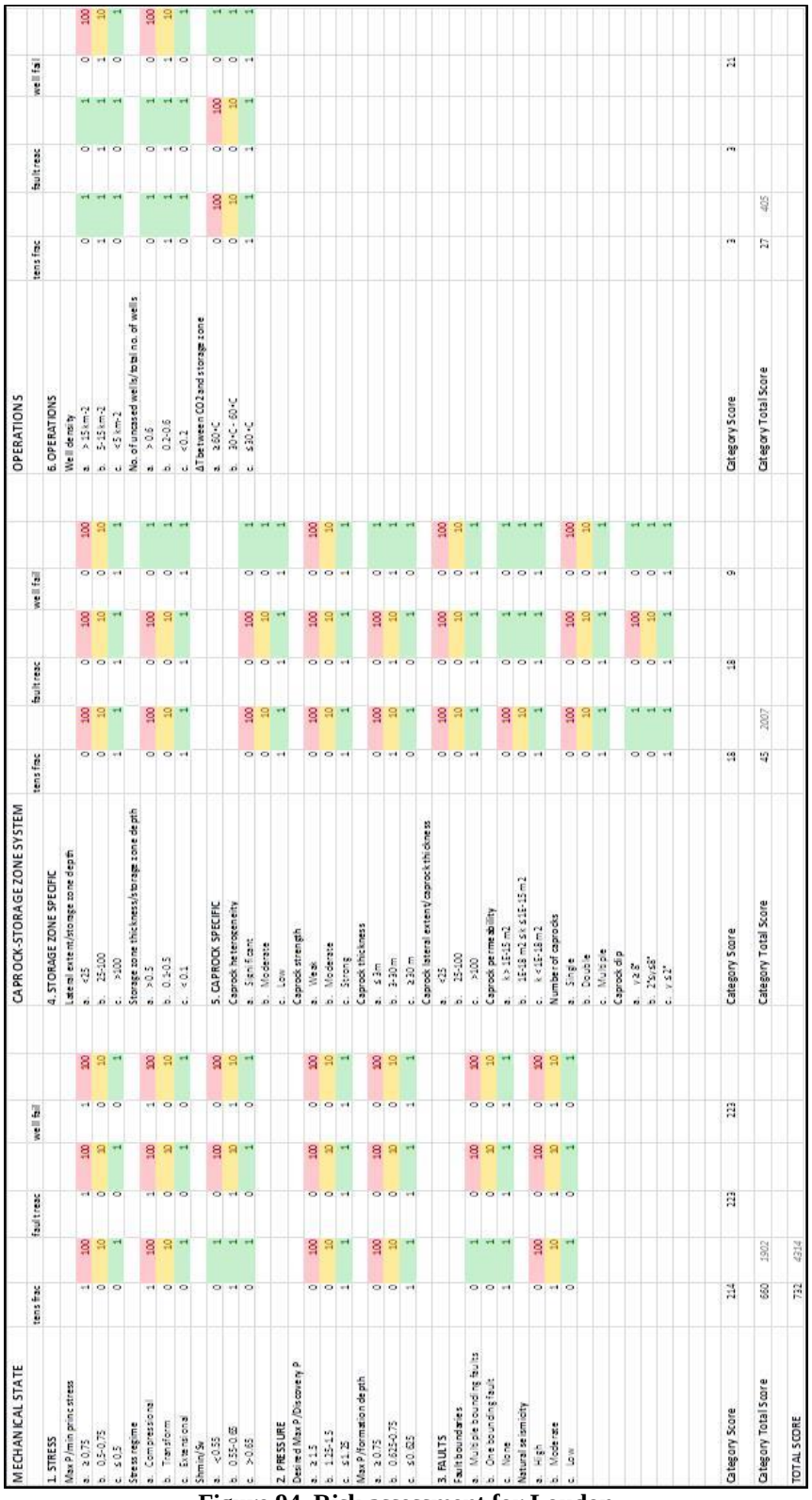

MECHANICAL STATE	tens frac	fault reac	well fail	CAPROCK-STORAGE ZONE SYSTEM	tens frac	fault reac	well fail	OPERATIONS	tens frac	fault reac	well fail
1. STRESS				4. STORAGE ZONE SPECIFIC				6. OPERATIONS			
Max P/min principal stress				Lateral extent/storage zone depth				Well density			
a. ≥ 0.75	1	100	1 100	a. <25	0	100	0 100	a. > 15 km-2	0	1 0	1 0 100
b. 0.5-0.75	0	10	0 10	b. 25-100	0	10	0 10	b. 5-15 km-2	1	1 1	1 1 10
c. ≤ 0.5	0	1	0 1	c. >100	1	1	1 1	c. <5 km-2	0	1 0	1 0 1
Stress regime				Storage zone thickness/storage zone depth				No. of unplugged wells/total no. of wells			
a. Compressional	1	100	1 100	a. >0.5	0	100	0 100	a. >0.6	0	1 0	1 0 100
b. Transform	0	10	0 10	b. 0.2-0.5	0	10	0 10	b. 0.2-0.6	1	1 1	1 1 10
c. Extensional	0	1	0 1	c. <0.2	1	1	1 1	c. <0.2	0	1 0	1 0 1
Shmin/Sv								ΔT between CO2 and storage zone			
a. <0.55	0	1	0 100	5. CAPROCK SPECIFIC				a. ≥60 oC	0	100 0	100 0 1
b. 0.55-0.65	1	1	1 10	Caprock heterogeneity				b. 30 oC - 60 oC	0	10 0	10 0 1
c. >0.65	0	1	0 1	a. Significant	0	100	0 100	c. ≤30 oC	1	1 1	1 1 1
2. PRESSURE				b. Moderate	0	10	0 10				
Desired Max P/Discovery P				c. Low	1	1	1 1				
a. ≥ 1.5	0	100	0 100	Caprock strength							
b. 1.15-1.5	0	10	0 10	a. Weak	0	100	0 100				
c. ≤ 1.15	1	1	1 1	b. Moderate	0	10	0 10				
Max P/formation depth				c. Strong	1	1	1 1				
a. ≥ 0.75	0	100	0 100	Caprock thickness							
b. 0.625-0.75	0	10	0 10	a. ≤ 3m	0	100	0 100				
c. ≤ 0.625	1	1	1 1	b. 3-30 m	1	10	1 10				
				c. ≥ 30 m	0	1	0 1				
				Caprock lateral extent/caprock thickness							
3. FAULTS				a. <25	0	100	0 100				
Fault boundaries				b. 25-100	0	10	0 10				
a. Multiple bounding faults	0	1	0 100	c. >100	1	1	1 1				
b. One bounding fault	0	1	0 10	Caprock permeability							
c. None	1	1	1 1	a. k > 1E-15 m2	0	100	0 1				
Natural seismicity				b. 1E-18 m2 ≤ k ≤ 1E-15 m2	0	10	0 1				
a. High	0	100	0 100	c. k < 1E-18 m2	1	1	1 1				
b. Moderate	1	10	1 10	Number of caprocks							
c. Low	0	1	0 1	a. Single	0	100	0 100				
				b. Double	0	10	0 10				
				c. Multiple	1	1	1 1				
				Caprock dip							
				a. > 8°	0	1	0 100	0 1			
				b. 2%-8°	0	1	0 10	0 1			
				c. < 2°	1	1	1 1	1 1			
Category Score	214	223	223	Category Score	18	18	9	Category Score	3	3	21
Category Total Score	660	1902		Category Total Score	45	2007		Category Total Score	27	405	
TOTAL SCORE	732	4214									

Figure 94. Risk assessment for Loudon

6.5.3 Wilmington Graben

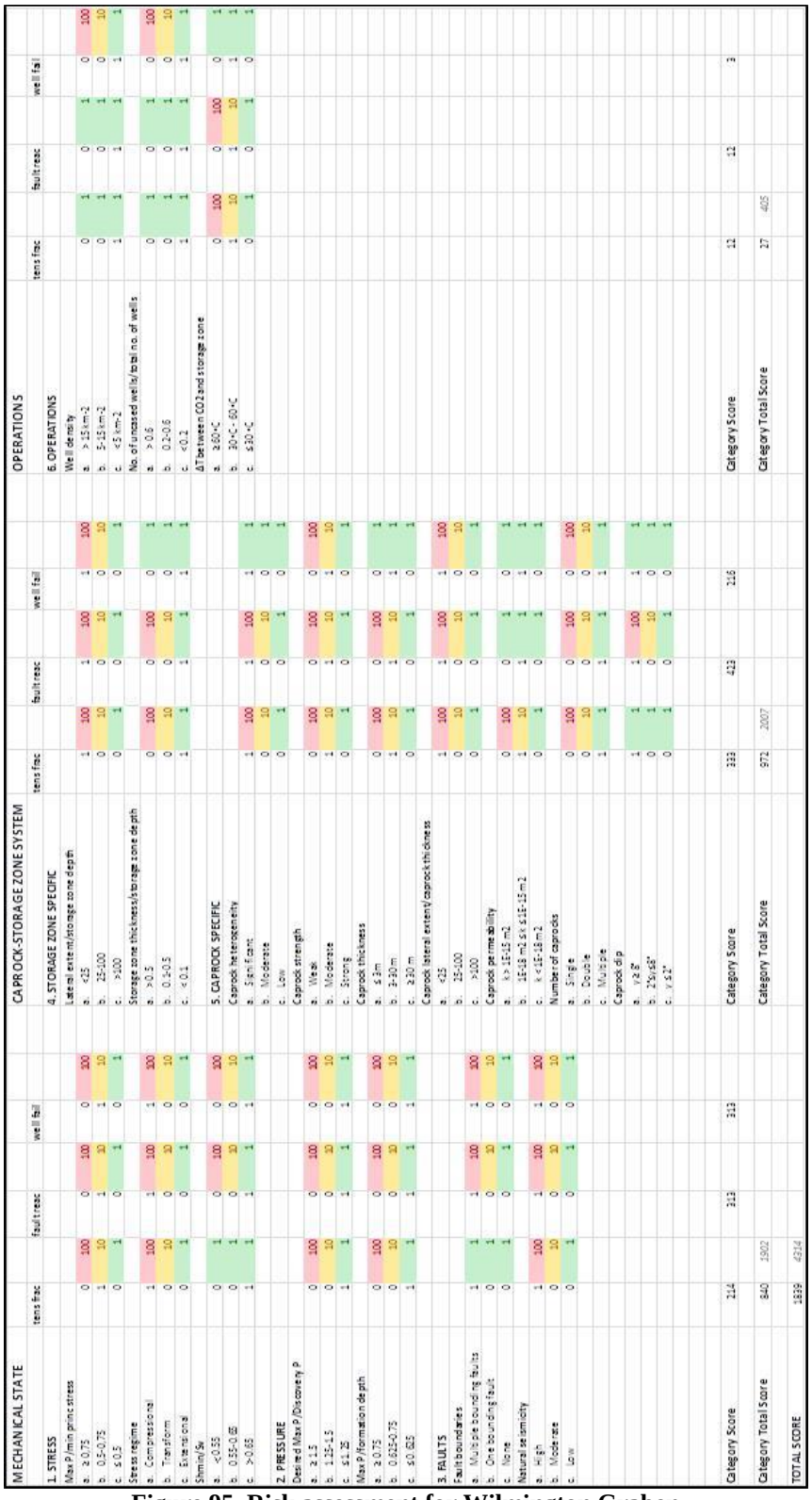

MECHANICAL STATE	tens frac	fault reac	well fail	CAPROCK-STORAGE ZONE SYSTEM	tens frac	fault reac	well fail	OPERATIONS	tens frac	fault reac	well fail
1. STRESS				4. STORAGE ZONE SPECIFIC				6. OPERATIONS			
Max P/min principal stress				Lateral extent/storage zone depth				Well density			
a. ≥ 0.75	0	100	0 100	a. <25	1	100	1 100	a. > 15 km-2	0	1	0
b. 0.5-0.75	1	10	1 10	b. 25-100	0	10	0 10	b. 5-15 km-2	0	1	0
c. ≤ 0.5	0	1	0 1	c. >100	0	1	0 1	c. <5 km-2	1	1	1
Stress regime				Storage zone thickness/storage zone depth				No. of unplugged wells/total no. of wells			
a. Compressional	1	100	1 100	a. >0.5	0	100	0 100	a. >0.6	0	1	0
b. Transform	0	10	0 10	b. 0.2-0.5	0	10	0 10	b. 0.2-0.6	0	1	0
c. Extensional	0	1	0 1	c. <0.2	1	1	1 1	c. <0.2	1	1	1
Shmin/SH				5. CAPROCK SPECIFIC				ΔT between CO2 and storage zone			
a. <0.55	0	1	0 100	Caprock strength				a. ≥60-C	0	100	0
b. 0.55-0.65	0	1	0 10	Caprock heterogeneity				b. 30-C - 60-C	1	10	1
c. >0.65	1	1	1 1	a. Significant	1	100	1 100	c. ≤30 -C	0	1	0
2. PRESSURE				b. Moderate	0	10	0 10				
Desired Max P/Discovery P				c. Low	0	1	0 1				
a. ≥ 1.5	0	100	0 100	Caprock strength							
b. 1.15-1.5	0	10	0 10	a. Weak	0	100	0 100				
c. ≤ 1.15	1	1	1 1	b. Moderate	1	10	1 10				
Max P/formation depth				c. Strong	0	1	0 1				
a. ≥ 0.75	0	100	0 100	Caprock thickness							
b. 0.625-0.75	0	10	0 10	a. ≤ 3m	0	100	0 100				
c. ≤ 0.625	1	1	1 1	b. 3-30 m	1	10	1 10				
				c. ≥ 30 m	0	1	0 1				
				Caprock lateral extent/caprock thickness							
3. FAULTS				a. <25	1	100	1 100				
Fault boundaries				b. 25-100	0	10	0 10				
a. Multiple bounding faults	1	1	1 100	c. >100	0	1	0 1				
b. One bounding fault	0	1	0 10	Caprock permeability							
c. None	0	1	0 1	a. k> 1E-15 m2	0	100	0 100				
Natural seismicity				b. 1E-18 m2 ≤ k ≤ 1E-15 m2	1	10	1 10				
a. High	1	100	1 100	c. k < 1E-18 m2	0	1	0 1				
b. Moderate	0	10	0 10	Number of caprocks							
c. Low	0	1	0 1	a. Single	0	100	0 100				
				b. Double	0	10	0 10				
				c. Multiple	1	1	1 1				
				Caprock dip							
				a. > 2 °	1	1	1 100				
				b. 2 to 0°	0	1	0 10				
				c. < 2 °	0	1	0 1				
Category Score	214	313	313	Category Score	333	413	216	Category Score	11	12	3
Category Total Score	840	1902		Category Total Score	972	2007		Category Total Score	27	405	
TOTAL SCORE	1839	4214									

Figure 95. Risk assessment for Wilmington Graben

6.5.4 Sleipner

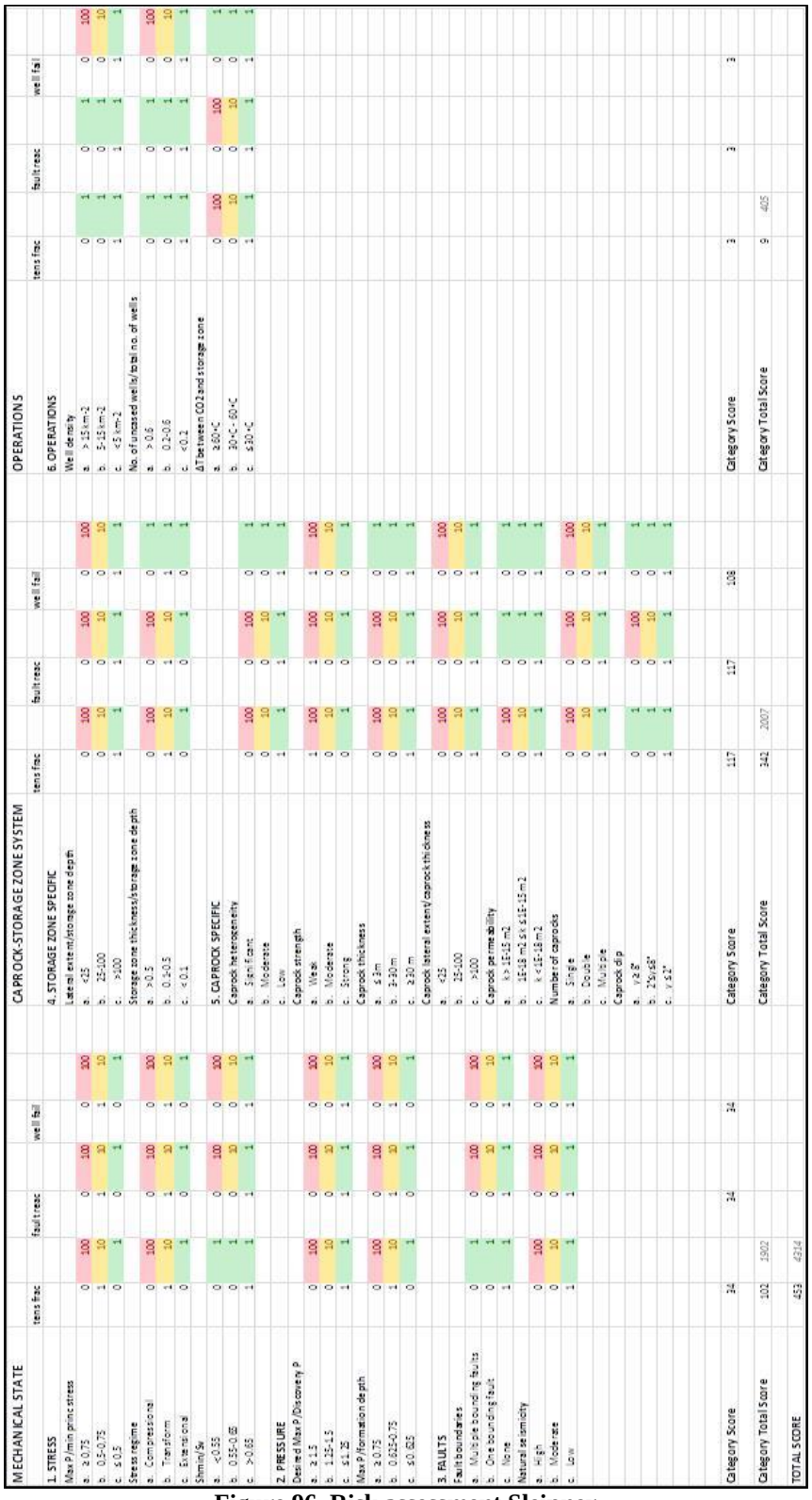

MECHANICAL STATE	tens frac	fault reac	well fail	CAPROCK-STORAGE ZONE SYSTEM	tens frac	fault reac	well fail	OPERATIONS	tens frac	fault reac	well fail
1. STRESS				4. STORAGE ZONE SPECIFIC				6. OPERATIONS			
Max P/min principal stress				Lateral extent/storage zone depth				Well density			
a. ≥ 0.75	0	100	0 100	a. <25	0 100	0 100	0 100	a. > 15 km-2	0	1 0	1 0 100
b. 0.5-0.75	1	10	1 10	b. 25-100	0 10	0 10	0 10	b. 5-15 km-2	0	1 0	1 0 10
c. ≤ 0.5	0	1	0 1	c. >100	1 1	1 1	1 1	c. <5 km-2	1	1 1	1 1 1
Stress regime				Storage zone thickness/storage zone depth				No. of unsealed wells/total no. of wells			
a. Compressional	0	100	0 100	a. >0.5	0 100	0 100	0 100	a. >0.6	0	1 0	1 0 100
b. Transform	1	10	1 10	b. 0.2-0.5	1 10	1 10	1 10	b. 0.2-0.6	0	1 0	1 0 10
c. Extensional	0	1	0 1	c. < 0.2	0 1	1 1	0 1	c. <0.2	1	1 1	1 1 1
Shmin/Sv								ΔT between CO2 and storage zone			
a. <0.55	0	1	0 100	5. CAPROCK SPECIFIC				a. ≥60+C	0	100 0	0 1
b. 0.55-0.65	0	1	0 10	Caprock heterogeneity				b. 30+C - 60+C	0	10 0	0 1
c. >0.65	1	1	1 1	a. Significant	0 100	0 100	0 100 1	c. ≤30 +C	1	1 1	1 1 1
2. PRESSURE				b. Moderate	0 10	0 10	0 10 1				
Desired Max P/Discovery P				c. Low	1 1	1 1	1 1				
a. ≥ 1.5	0	100	0 100	Caprock strength							
b. 1.15-1.5	0	10	0 10	a. Weak	1 100	1 100	1 100 1				
c. ≤ 1.15	1	1	1 1	b. Moderate	0 10	0 10	0 10 1				
Max P/formation depth				c. Strong	0 1	0 1	0 1				
a. ≥ 0.75	0	100	0 100	Caprock thickness							
b. 0.625-0.75	1	10	1 10	a. ≤ 3m	0 100	0 100	0 100 1				
c. ≤ 0.625	0	1	0 1	b. 3-30 m	0 10	0 10	0 10 1				
				c. ≥ 30 m	1 1	1 1	1 1 1				
3. FAULTS				Caprock lateral extent/caprock thickness							
Fault boundaries				a. <25	0 100	0 100	0 100 1				
a. Multiple bounding faults	0	1	0 100	b. 25-100	0 10	0 10	0 10 1				
b. One bounding fault	0	1	0 10	c. >100	1 1	1 1	1 1 1				
c. None	1	1	1 1	Caprock permeability							
Natural seismicity				a. k > 1E-15 m2	0 100	0 100	0 1 1				
a. High	0	100	0 100	b. 1E-18 m2 ≤ k ≤ 1E-15 m2	0 10	0 10	0 1 1				
b. Moderate	0	10	0 10	c. k < 1E-18 m2	1 1	1 1	1 1 1				
c. Low	1	1	1 1	Number of caprocks							
				a. Single	0 100	0 100	0 100				
				b. Double	0 10	0 10	0 10				
				c. Multiple	1 1	1 1	1 1				
				Caprock dip							
				a. > 2 °	0 1	0 100	0 1				
				b. 2 to 5°	0 1	0 10	0 1				
				c. < 5°	1 1	1 1	1 1				
Category Score	34	34	34	Category Score	117	117	108	Category Score	3	3	3
Category Total Score	102	1902		Category Total Score	342	2007		Category Total Score	9	405	
TOTAL SCORE	453	4314									

Figure 96. Risk assessment Sleipner

6.5.5 In Salah

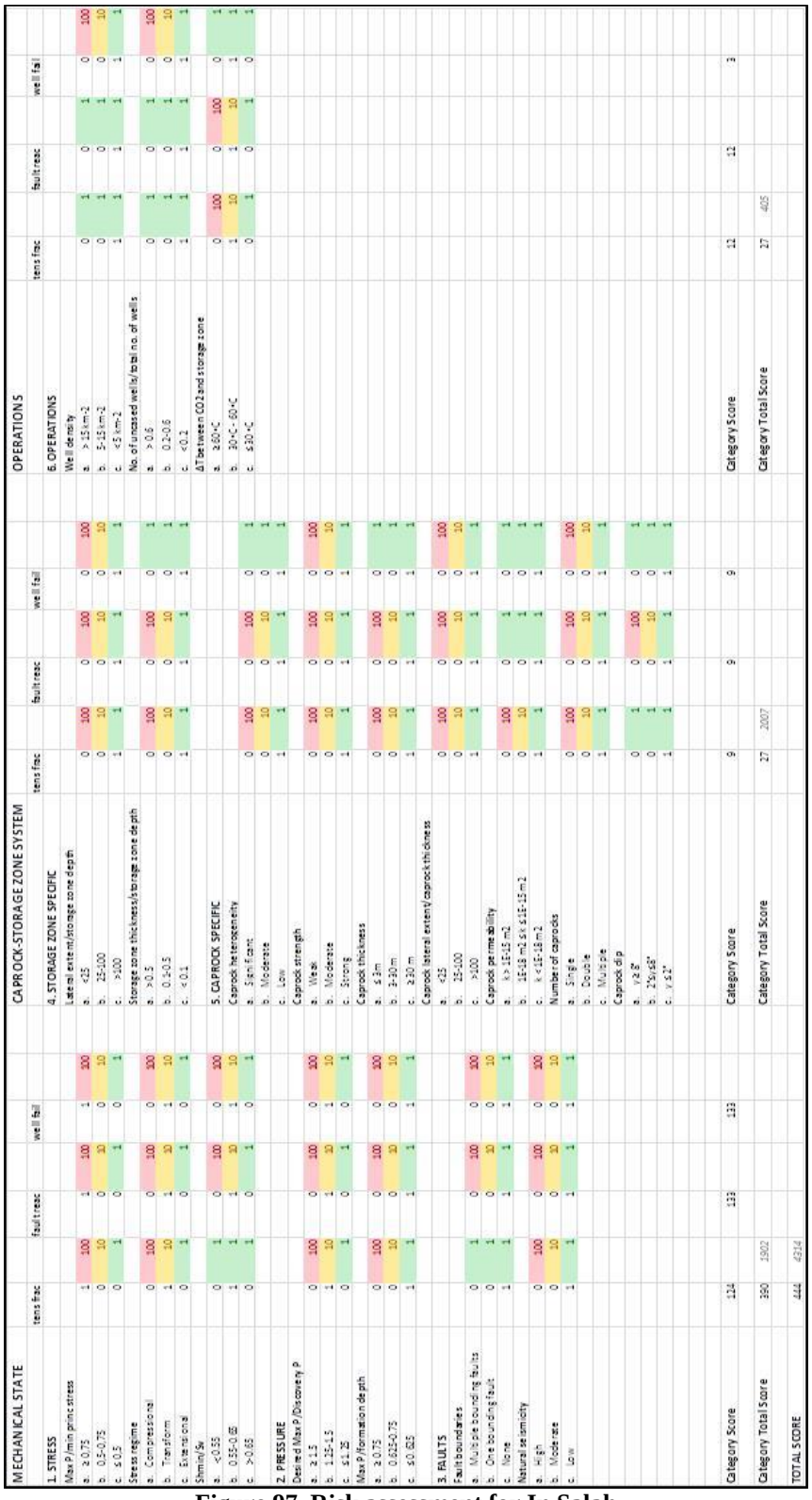

MECHANICAL STATE	tens frac	fault reac	well fail	CAPROCK-STORAGE ZONE SYSTEM	tens frac	fault reac	well fail	OPERATIONS	tens frac	fault reac	well fail
1. STRESS				4. STORAGE ZONE SPECIFIC				6. OPERATIONS			
Max P/min principal stress				Lateral extent/storage zone depth				Well density			
a. ≥ 0.75	1 100	1 100	1 100	a. <25	0 100	0 100	0 100	a. > 15 km-2	0	1 0	1 0
b. 0.5-0.75	0 10	0 10	0 10	b. 25-100	0 10	0 10	0 10	b. 5-15 km-2	0	1 0	1 0
c. ≤ 0.5	0 1	0 1	0 1	c. >100	1 1	1 1	1 1	c. <5 km-2	1	1 1	1 1
Stress regime				Storage zone thickness/storage zone depth				No. of unplugged wells/total no. of wells			
a. Compressional	0 100	0 100	0 100	a. >0.5	0 100	0 100	0 100	a. >0.6	0	1 0	1 0
b. Transform	1 10	1 10	1 10	b. 0.2-0.5	0 10	0 10	0 10	b. 0.2-0.6	0	1 0	1 0
c. Extensional	0 1	0 1	0 1	c. < 0.1	1 1	1 1	1 1	c. <0.2	1	1 1	1 1
Shmin/Sv								ΔT between CO2 and storage zone			
a. <0.55	0 1	0 100	0 100	5. CAPROCK SPECIFIC				a. ≥60+C	0	100 0	1 1
b. 0.55-0.65	1 1	1 10	1 10	Caprock heterogeneity				b. 30+C - 60+C	1	10 1	1 1
c. >0.65	0 1	0 1	0 1	a. Significant	0 100	0 100	0 100	c. ≤30 +C	0	1 0	1 1
2. PRESSURE				b. Moderate	0 10	0 10	0 10				
Desired Max P/Discovery P				c. Low	1 1	1 1	1 1				
a. ≥ 1.5	0 100	0 100	0 100	Caprock strength							
b. 1.15-1.5	1 10	1 10	1 10	a. Weak	0 100	0 100	0 100				
c. ≤ 1.25	0 1	0 1	0 1	b. Moderate	0 10	0 10	0 10				
Max P/formation depth				c. Strong	1 1	1 1	1 1				
a. ≥ 0.75	0 100	0 100	0 100	Caprock thickness							
b. 0.625-0.75	0 10	0 10	0 10	a. ≤ 3m	0 100	0 100	0 100				
c. ≤ 0.625	1 1	1 1	1 1	b. 3-30 m	0 10	0 10	0 10				
				c. ≥ 30 m	1 1	1 1	1 1				
3. FAULTS				Caprock lateral extent/caprock thickness							
Fault boundaries				a. <25	0 100	0 100	0 100				
a. Multiple bounding faults	0 1	0 100	0 100	b. 25-100	0 10	0 10	0 10				
b. One bounding fault	0 1	0 10	0 10	c. >100	1 1	1 1	1 1				
c. None	1 1	1 1	1 1	Caprock permeability							
Natural seismicity				a. k> 1E-15 m2	0 100	0 100	0 100				
a. High	0 100	0 100	0 100	b. 1E-18 m2 ≤ k ≤ 1E-15 m2	0 10	0 10	0 10				
b. Moderate	0 10	0 10	0 10	c. k < 1E-18 m2	1 1	1 1	1 1				
c. Low	1 1	1 1	1 1	Number of caprocks							
				a. Single	0 100	0 100	0 100				
				b. Double	0 10	0 10	0 10				
				c. Multiple	1 1	1 1	1 1				
				Caprock dip							
				a. > 2 °	0 1	0 100	0 1				
				b. 2 to 5°	0 1	0 10	0 1				
				c. < 5°	1 1	1 1	1 1				
Category Score	124	133	133	Category Score	9	9	9	Category Score	11	12	3
Category Total Score	180 1902			Category Total Score	27 2007			Category Total Score	17 405		
TOTAL SCORE	444 4214										

Figure 97. Risk assessment for In Salah

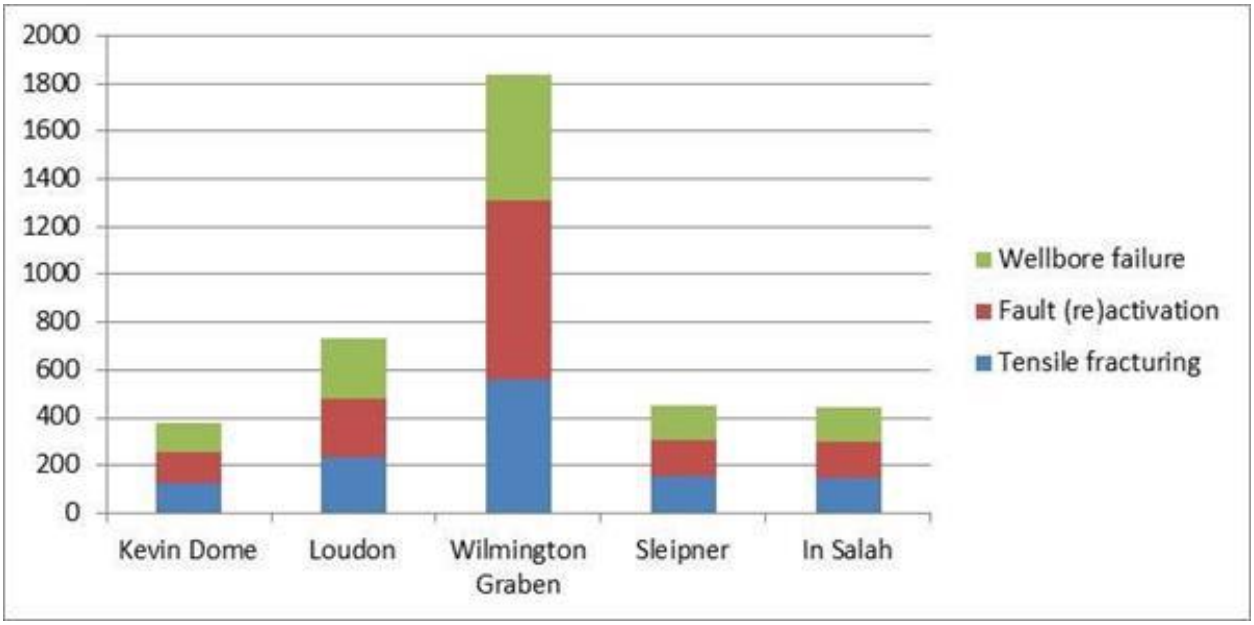

Figure 98. Total QRDAT risk scores for five CO_2 potential and actual injection sites

Table 10 shows the risk scores for the five locations, including the category scores for the three leakage mechanisms: mechanical state, caprock-reservoir system and operations. The likelihood scores for each site may then be converted to absolute order-of-magnitude probability. An example is provided in

Table 11, and is applied and shown in Figure 99. The resulting order-of-magnitude probability showed that both the Loudon and Wilmington Graben have a relatively high 10^{-1} risk values, while the other three site examples have relatively moderate 10^{-2} risk values. Note that these leakage risk ranges are generally consistent with the historical observations of leakage risk in the natural gas storage industry, as discussed earlier in this paper. Also note that of the two actual operating examples, In Salah experienced out of zone fracture concerns and has been shut-in.

Table 10 Estimated Site Risk Scores

Category	Range of risk scores	Kevin Dome	Loudon Field	Wilmington Graben	Sleipner	In Salah
Mechanical State	21-1902	345	660	840	102	390
Caprock-Reservoir System	27-2007	27	45	972	342	27
Operations	9-405	9	27	27	9	27
TOTAL	57-4314	381	732	1839	453	444

Table 11 Relative Risk Scores and Order-of-Magnitude Probabilities

Relative Ranking Score Value	Loss Event Probability Order-of-Magnitude Value
greater than 500	10^{-1}
301 – 500	10^{-2}
201 – 300	10^{-3}
101 – 200	10^{-4}
Less than 100	10^{-5}

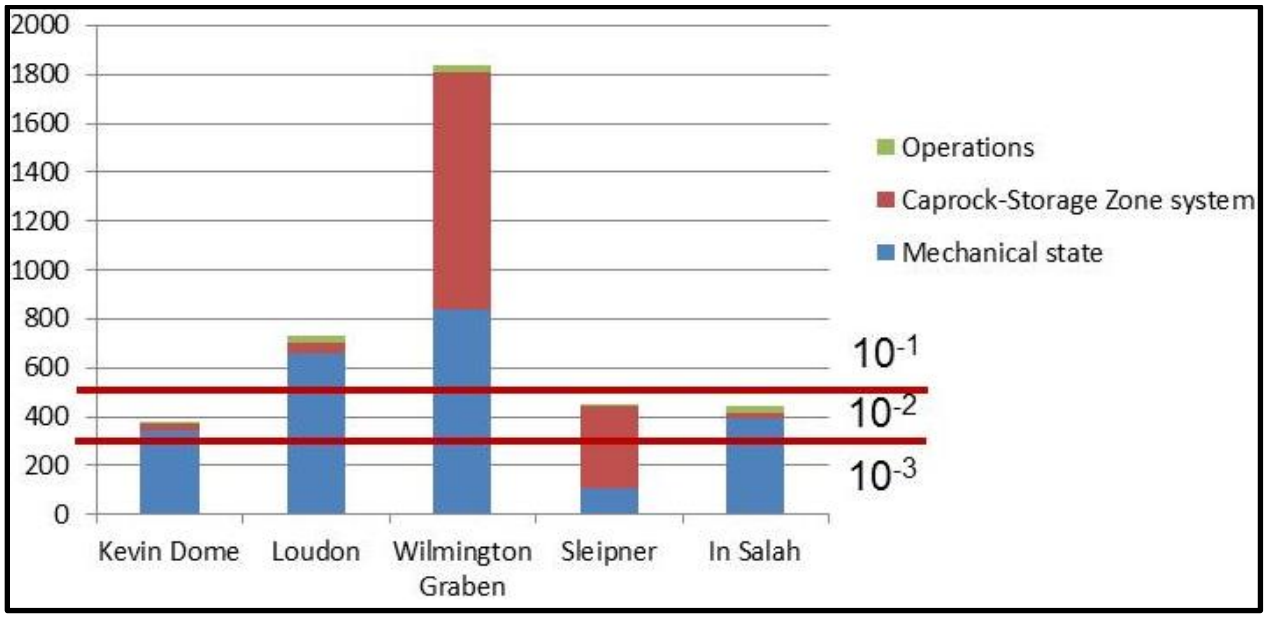

Figure 99. Relative risk scores and the contribution of the three main groups of risk scores to the relative risk ranking

7 Develop Recommendations and Guidelines for Caprock Characterization and CO_2 Injection Operating Practices

7.1 Recommendations for Characterization

Characterization is the set of all activities that contribute to the construction of a 3D geologic model for an area proposed for CO_2 injection operations. These activities and this model will be used to determine if a site is suitable and, if so, under what operating constraints.

7.1.1 Review Literature & Data

7.1.1.1 Existing well logs & files

Available well logs and files for previously drilled boreholes in the area of interest should be located, copied if possible, and reviewed. These data provide both valuable geologic information for characterization and help in evaluating the risk of CO_2 release via these boreholes.

Often these logs and files will have, at the very least, stratigraphic information for the geologic model, but usually lithologic information as well, which can be correlated between wellbores to determine lateral consistency and extent of the caprock and reservoir. Depending on the logs available, other properties may also be interpreted and included in the geologic model.

Each well file should have information concerning its completion and abandonment, which can be interpreted for building a picture of the wellbore as it is in its current state. This picture can be evaluated to determine the degree of risk this particular wellbore poses for the escape of CO_2 from the designated reservoir. In addition, all of the wellbores taken together will be evaluated for the risk their sheer numbers and concentration pose.

7.1.1.2 Well core samples

Available core samples from the wells previously drilled in the area of interest should be accessed and reviewed, particularly those from the proposed caprock and reservoir formations. These may provide information about important formation properties not found in the well logs and files, e.g., porosity, permeability, micro-fracturing.

7.1.1.3 Seismic data

Seismic data for the area of interest may be more difficult to locate and access than logs, files, and core samples, as most of it is produced in exploration efforts by industry and remains proprietary. For most areas, however, some of these data, usually basic in nature, are available through academic and industry publications, and can provide valuable information for supplementing and verifying the geologic information gleaned from well logs, files, and cores.

7.1.1.4 Other published data for compiling the regional and local geology

Often there are already articles published in academic and industry journals concerning the geology of an area of interest. If not for the specific local geology of a particular site being evaluated, regional geologic descriptions encompassing the area of interest can usually be found. Previous studies may provide valuable information about stratigraphy, lithology, and specific rock properties, as well as the consistency of these properties over lateral extent, and the presence of structural features, such as folds and faults. Like seismic data, this information supplements and verifies geologic information gleaned from well bore data, perhaps aiding in the interpretation of observations not previously understood.

7.1.2 3D Seismic

The first step in generating new data is the acquisition of additional high-resolution 3D seismic data of the local area of interest. Such focused high-resolution data reveal local particularities in stratigraphy, lithology, and structure, thus refining interpolations and extrapolations from previously collected data, and providing guidance in selecting the best points of injection. Regarding, for example, particularized local structures, earlier production/injection processes to exploit hydrocarbon reservoirs may have created fractures unseen at lower resolutions. These fractures could be sealed in time by precipitation of newly formed minerals, but could also be re-opened as a consequence of new changes in stresses during injection and storage of CO_2 (Jimenez and Chalaturnyk 2003).

7.1.3 Drill Exploratory Wells

Particularly for saline reservoirs in areas where oil and gas have not been found and deep wells do not already exist to provide structural and lithologic information, exploratory wells will be necessary. Direct observations at wellbore scale both corroborate and/or correct geologic interpretations of previously collected data at varying scales and provide important rock properties that may not have already been well-documented.

7.1.3.1 Suites of electric logs

Electric logs provide a wealth of petrophysical and rock mechanical properties necessary for the geologic model. First, several log measurements allow for the interpretation of lithology which provides vertical location information within the greater stratigraphic and lithologic contexts. Thus the targeted reservoir and caprock formations can be specifically identified. In addition, acoustic logs and density measurements provide several rock mechanic properties necessary for evaluating the strength of the caprock, e.g., Poisson's ratio and Young Modulus.

7.1.3.2 Well core samples

Rock properties can be directly measured in a lab to correct previous interpretations and/or to more precisely correlate the exploratory well's stratigraphy and lithology with others in the area for which data has already been collected. Particularly, the porosity, permeability, and fluid saturation of target reservoir formations and their caprocks can be directly measured and recorded in the geologic model for future calculations of, for example, injectable capacity.

7.1.3.3 Injection testing

If possible to implement, injection testing will provide direct measurement of several geomechanical and petrophysical properties crucial for evaluating a formation's suitability for CO_2 injection. For example, step-rate, buildup, and fall-off tests can determine formation pressure, fracture pressure, and near and far-field formation permeability.

7.1.4 Develop 3D Geologic Model

A geologic model forms the basis for risk analysis and numerical simulation. It depicts the reservoir formation, the confining zone and the lithologies of the rocks overlying the confining zones. The model shows the thickness of the various lithologies, and their structure, and contains information on the relevant petrophysical and geomechanical properties of the rocks and contained fluids. In sum, the geologic model serves as a database for all of the data collected during the characterization phase and will be a resource for siting and operational decisions.

- Integrate existing and new well log data with existing and new seismic data
- Ascertain lithology, porosity, permeability and other rock properties from well logs
- Populate grid with lithology and other property estimates
- Visualizations
    - Lithologic and stratigraphic cross sections
    - Structure contour maps
    - Isopach maps
    - 3D Model

7.2 Recommendations for Siting

7.2.1 Surface Conditions

7.2.1.1 Industrial setting

Preferably industrial or rural setting. Preferably not residential or commercial.

7.2.1.2 Near source(s)

The nearer the injection project is located to industrial sources of CO_2, e.g., fossil fuel burning power plants and refineries, the lower the cost of transport.

7.2.1.3 Pipeline access

Best is access to already existing pipelines that are suitable for transporting CO_2. But at the very least, injection operations need to be located such that there is the possibility of constructing pipeline between them and their sources of CO_2.

7.2.2 Wellbore Concentration

Clearly, areas with a high concentration of abandoned wellbores that penetrate through the caprock present a *prima facie* greater risk. If to be considered at all, greater scrutiny of the projected CO_2 plume migration is required. The likelihood of the plume intersecting leaky wellbores is a function of the plume size and wellbore spatial density. Numerical simulations are used to predict the movement or behavior of CO_2 once it is injected into the subsurface, and can eliminate or validate a site accordingly.

7.2.3 Caprock-Storage Zone System

7.2.3.1 Faulted caprock

The absence of faults cross-cutting the caprock is preferred.

7.2.3.2 Seismicity

In case faults are present, regions with low natural seismicity are desired.

7.2.3.3 Multiple caprocks

A storage location with multiple caprocks is preferred, as it there are several possible collection zones in case failure of the primary seal occurs.

7.2.3.4 Caprock thickness

The thicker the caprock sequence the better, as the likelihood of an intact seal increases with caprock thickness and it is less likely to degrade sufficiently for storage failure over time with repeated pressure and stress cycling.

7.2.3.5 Caprock structure

Dipping caprocks are only desirable in case they form a closed aniticlinal or periclinal structure. Otherwise (sub)horizontal caprocks are preferred to monoclinal structures to avoid CO_2 spilling.

7.2.3.6 Other caprock features

Homogeneous, impermeable, and strong caprocks are preferred.

7.2.3.7 Lateral continuity of caprock and storage zone

The more lateral continuity of both, the better.

7.2.3.8 Storage zone depth

Deep storage zones are preferred over shallow storage zones for two reasons: the distance for CO_2 to migrate towards the surface is greater in case a loss event takes place and confining pressures are higher at depth.

7.2.3.9 Storage zone temperature

Cold reservoirs are preferred over hot reservoirs, as they are at lower risk for thermally-induced stressing.

7.3 Recommendations for Operating Practices

The structure and properties of the subsurface are inherently heterogeneous and variable at many scales. Because of practical concerns, it is unlikely that sufficient data will be available to "validate" or test models of trapping mechanisms and associated failure modes with complete certainty. For example, the number of wells that could provide calibration data, including log and rock data, is generally limited, especially at saline formation sites. Numerical simulations should be used to develop a better understanding of this heterogeneity when data is not available. Numerical simulations are also used to inform geologic CO_2 storage project design, operations and closure. (DOE, 2013a)

7.3.1 Develop 3D Geomechanical Model

7.3.1.1 Estimate in situ stresses

Estimate in situ stress based on borehole breakouts and step-rate fracture data. The maximum injection pressure can be predicted by determining the in-situ stress profile.

7.3.1.2 Estimate material properties

Estimate mechanical stiffness and strength properties (log and core analysis).

7.3.1.3 Determine operationally induced stresses, bedding plane slip, and fault activation risk

Estimate stress variations and stresses induced by CO_2 injection operations, including bedding plane slip and fault activation risks.

7.3.2 Develop CO_2 Injection & Migration Model

- Evaluate CO_2 injectivity and long-term migration:
  - taking into account measured properties (permeability, pressures, temperatures, salinity), and
  - applying the model to evaluate CO_2 injectivity and long-term migration.
- Simulate various injection scenarios
- Interpret pressure and saturation changes *vs* time

7.3.3 Injection Rates & Pressures

In order to prevent fracturing, the maximum injection pressure should always be kept below the level at which the caprock may shear (fracture pressure determined by injection testing and geomechanical model). The risk of leakage through fracturing is low as long as the storage pressure does not exceed the initial reservoir pressure.

However, there is a certain level of overpressure, at which CO_2 can be safely contained. This "safety factor" depends on the stress state of the caprock, which depends on depth, pore pressure, rock properties and sedimentary and tectonic histories. The maximum injection pressure can be predicted by determining the in-situ stress profile (Damen et al. 2006).

7.4 Other Recommendations & Guidelines

Currently there is no standardized method or set of methods for evaluating risk and/or uncertainty for CO_2 sequestration projects. Application or adaptation of advanced industrial quantitative risk assessment methods seems premature at this point because of a lack of specific data. The development of frameworks and qualitative methods looks most applicable for current projects (Condor et al. 2011). Over the past decade a host of risk assessment tools have been developed (Appendix 1: Other Risk Assessment Tools (DOE, 2013a)) relying on a dozen methods (Appendix 2: Other Risk Assessment Methods (Condor et al. 2011)).

Our focus has been mainly on evaluating and reducing risk of potential CO_2 loss because of insufficient caprock integrity. A more comprehensive risk analysis would also explore the adverse impacts from unplanned CO_2 migration out of the confining zone and the potential for adverse impacts from other project-related operational and financial events. These include public safety and health, environmental (ecosystem) safety, greenhouse gas (GHG) emissions to the atmosphere, damage to natural resources (e.g., water and hydrocarbons), and financial loss for investors or insurers (DOE, 2013a).

8 Conclusion

As part of GeoMechanics Technologies' DOE-funded project, *Development of Improved Caprock Integrity and Risk Assessment Techniques*, we have completed a multi-phase geomechanical caprock integrity study to advance the understanding of caprock integrity issues associated with large scale CO_2 injection. First, from our detailed review, analysis, and description of historical leakage events related to caprock integrity within the natural gas storage industry, we conclude that risks for gas leakage events are generally higher than previously estimated and published, and are in the range of 10^{-2} to 10^{-1}. Second, coupled transport flow and geomechanical simulations of three large-scale geologic sequestration sites were completed to analyze their potential of caprock failure due to geomechanical damage. Induced stresses in each of the fields investigated are not sufficient to raise concerns regarding caprock fracturing or fault activation. Third, we have developed and documented a quantitative risk and decision analysis tool to assess caprock integrity risks. Application to five study sites indicates that the Kevin Dome site presents the least risk for CO_2 injection, while the Wilmington Graben site presents the highest risk.

9 References

Agyarko, L.B. and Mansoori, G.A. (2013) A review of non-renewable energy options in Illinois. J of Oil, Gas and Coal Technology 6(3):288–347.

Augustiniak, A. *Knoblauch – die Gischichte eines Dorfes, das immer mehr in Vergessenheit gerät*. World Wide Web Address: <http://www.heimatverein-ketzin.de/knoblauch4.htm>

Bachu S, Bennion B. Effects of in situ conditions on relative permeability characteristics of CO_2-brine system. Environ Geol 2008; 54(8):1707-1722

Bennion B, Bachu S. Relative permeability characteristics for supercritical CO_2 displacing water in a variety of potential sequestration zones in the Western Canada Sedimentary Basin. Paper SPE 95547 presented at the SPE Annual Technical Conference and Exhibition, Dallas, 9-12 October 2005. DOI: 10.2118/95547-MS.

Benson SM. Lessons learned from natural and industrial analogues for storage of carbon dioxide in deep geologic formations. LBNL #51170, technical report for BP-DOE CRADA under contract DE-AC03-76F00098; 2002.

BENSON, S. & HEPPLE, R. 2005. Chapter 28: Prospects for early detection and options for remediation of leakage from CO_2 storage projects. In: THOMAS, D. C. & BENSON, S. M. (eds) Carbon Dioxide Capture for Storage in Deep Geologic Formations, Volume 2. Elsevier Limited, 1189–1203.

Bergmann, P., Yang, C., Lüth, S., Juhlin, C., Cosma, C. (2011) *Time-lapse processing of 2D seismic profiles with testing of static correction methods at the* CO_2 *injection site Ketzin (Germany)*. Journal of Applied Physics, 75 (11), pp. 124-139.

Big Sky Carbon Sequestration Partnership, acquired via personal communication.

Bruno, M.S.; DeWolf, G.; Foh, S. (2000), Geomechanical Analysis and Decision Analysis for Delta Pressure Operations in Gas Storage Reservoir, Presented at the American Gas Association Operations Conference, Denver, CO, May7-9

Bruno, M.S., Dusseault, M.B., Balaa, T.T., Barrera, J.A., Geomechanical Analysis of Pressure Limits For Gas Storage Reservoirs, Paper USA-328-5, presented at the North American Rock Mechanics Symposium, *NARMS '98*, June 3-5, 1998.

Burton EA, Myhre R, Myer L, Birkinshaw K. Geologic carbon sequestration strategies for California, The Assembly Bill 1925 Report to the California Legislature. California Energy Commission, Systems Office. CEC-500-2007-100-SD; 2007.

BUSCHBACH, T. C. & BOND, D. C. 1974. Underground Storage of Natural Gas in Illinois — 1973. Illinois Petroleum 101, Illinois State Geological Survey, Department of Registration and Education, Urbana, Illinois.

California Division of Oil and Gas (DOGGR), 1992, California Oil and Gas Fields, Volume II: Southern, Central Coastal and Offshore California; Sacramento, California Department of Conservation, Division of Oil, Gas and Geothermal Resources.

CO_2SINK.org. *Technical information – Monitoring: Geology of the Ketzin anticline*. World Wide Web Address: <http://www.CO_2sink.org/techinfo/geology1.htm>

Condor, J., Unatrakarn, D., Wilson, M., & Asghari, K. (2011). A comparative analysis of risk assessment methodologies for the geologic storage of carbon dioxide. *Energy Procedia*, *4*, 4036-4043.

Damen, K., Faaij, A., & Turkenburg, W. (2006). Health, safety and environmental risks of underground CO_2 storage–overview of mechanisms and current knowledge. *Climatic Change*, *74*(1-3), 289-318.

Det Norske Veritas (DNV), 2010, CO_2*QUALSTORE: Workbook with examples of applications*. DNV Report No. 2010-0254. Hovik, Norway: Det Norske Veritas AS. Accessed 3/11/2013. World Wide Web Address: http://www.dnv.com/binaries/CO_2QUALSTORE_Workbook_tcm4-436659.pdf

Doughty C. Investigation of CO_2 plume behavior for a large-scale pilot test of geologic carbon storage in a saline formation. Transport in porous media 2010, 82(1), 49-76.

DOE, 2013a, Risk analysis and simulation for geologic storage of CO_2: U.S. Department of Energy, National Energy Technology Laboratory, available at: http://www.netl.doe.gov/research/coal/carbon-storage/carbon-storage-infrastructure/best-practices.

EIA. 2006. U.S. Underground natural gas storage developments: 1998:2005. Energy Information Administration, Office of Oil and Gas, October 2006. World Wide Web Address: http://www.eia.doe.gov/pub/oil_gas/natural_gas/feature_articles/2006/ngstorage/ngstorage.pdf

EIA. 2013a. Lower 48 States Natural Gas Working Underground Storage. Energy Information Administration. Accessed 3/11/2013. World Wide Web Address: www.eia.gov/dnav/ng/hist/nw_epg0_sao_r48_bcfw.htm

EIA. 2013b. U.S. Underground Natural Gas Storage Capacity. Energy Information Administration. Accessed 3/11/2013. World Wide Web Address: http://www.eia.gov/dnav/ng/ng_stor_cap_dcu_nus_m.htm

Evans, D.J. and West, J.M. An appraisal of underground gas storage technologies and incidents, for the development of risk assessment methodology. HSE Research Report RR605. Norwich, UK: Crown, 2008.

Evans DJ. A review of underground fuel storage events and putting risk into perspective with other areas of the energy supply chain. Geol Soc Spec Publ 2009;313:173–216.

FÆRSETH, R.B. 2006. Shale smear along large faults: continuity of smear and the fault seal capacity. *Journal Geological Society, London*, 163, 741-751.

Förster, A., Norden, B., Zinck-Jørgensen, K., Frykman, P., Kulenkampff, J., Spangenberg, E., Erzinger, J., Zimmer, M., Kopp, J., Borm, G., Juhlin, C., Cosma, C., Hurter, S. (2006) Baseline characterization of the CO_2SINK geological storage site at Ketzin, Germany. Environmental Geosciences, V. 13, No. 3 (September 2006), pp. 145-161.

Gas Storage Europe (GSE), 2012, *Storage map*.

Gasda SE, Bachu S, Celia MA. Spatial characterization of the location of potentially leaky wells penetrating a deep saline aquifer in a mature sedimentary basin. Environ Geol 2004; 46(6-7), 707-720.

Geertsma, J. (1973), *Land Subsidence above Compacting Oil and Gas Reservoirs*, J. Pet. Tech.*25*, 734–744.

Gor, G.Y., Stone, H.A., Prevost, J.H. (2012) Fracture propagation driven by fluid outflow from a low-permeability reservoir, *Journal of the Mechanics and Physics of Solids* http://arxiv.org/pdf/1203.4543

GUREVICH, A. E., ENDRES, B., ROBERTSON, J. O. & CHILINGAR, G. V. 1993. Gas migration for oil and gas fields and associated hazards. Journal of Petroleum Science and Engineering, 9, 223–238.

Intergovernmental Panel on Climate Change (IPCC). Carbon dioxide capture and storage: summary for policymakers and technical summary. ISBN 92-9169-119-4; 2005.

International Energy Agency Greenhouse Gas R&D Programme (IEAGHG) (2009) Natural and industrial analogues for geological storage of carbon dioxide. IEA Greenhouse Gas R&D Programme, Cheltenham, UK.

Jimenez, J. and Chalaturnyk, R. J.: 2003, 'Are disused oil and gas reservoirs safe for the geological storage of CO_2?' in Gale, J. and Kaya, Y. (eds), *Sixth International Conference on Greenhouse Gas Control Technologies*, Kyoto, vol. I, Pergamon, Amsterdam, pp. 471–476.

Juhlin , C., Cosma , C., Förster, A., Giese, R., Juhojuntti, N., Kazemeini, H., Norden, B., Zink-Jørgensen, K. (2006) *Baseline 3D seismic imaging for the* CO_2*SINK project in the Ketzin area, Germany*. Proceedings 8th Greenhouse Gas Technology Conference, Trondheim, Norway

Katz DL. Containment of gas in storage fields, in SPE Reprint Series 1999; No. 50, 28-33.

Katz, D.L. and K.H. Coats, *Underground Storage of Fluids*, Urich's Books, Ann Arbor, MI, 1968.

Keeley, D. Failure rates for underground gas storage: significance for land use planning assessments. HSE Research Report RR671. Norwich, UK: Crown, 2008.

Khilyuk, L.F., Chilingar, G.V., Endres, B., and Robertson, Jr., J.O. *Gas Migration: Events Preceding Earthquakes*. Houston: Gulf Publishing, 2000.

Lewicki JL, Birkholzer J, Tsang C. Natural and industrial analogues for leakage of CO_2 from storage reservoirs: identification of features, events, and processes and lessons learned. Environ Geol 2006; Vol. 52, Nos. 3, p, *457-467.*

Mazzoldi A, Rinaldi AP, Borgia A, Rutqvist J. Induced seismicity within geological carbon sequestration projects: maximum earthquake magnitude and leakage potential from undetected faults. International Journal of Greenhouse Gas Control 2012; 10, 434-442.

Miyazaki B, Well integrity: an overlooked source of risk and liability for underground natural gas storage. Lessons learned from incidents in the USA, *Geological Society, London, Special Publications*, 2009;313:163–72.

Myer, L. CCS safety and analogues. International seminar on perspectives for near term CCS deployment and capacity building for emerging economies. Porto Alegre, Brazil, October 17–19, 2007. Accessed 3/11/2013. World Wide Web Address: http://www.cslforum.org/documents/9_CCSSafetyAnaloguesMyerOct182007.pdf

NaturalGas.org, 2011. *Storage of natural gas*. Web. 3 April 2013. < http://www.naturalgas.org/naturalgas/storage.asp >

Nygaard, R. "Geomechanical simulation of CO_2 leakage and cap rock remediation," DOE/EPA Collaborative Review - Tracking Geologically - Sequestered CO_2: Monitoring, Verification, & Accounting (MVA), Simulation, and Risk Assessment, March 23-24, 2010. Pittsburgh. Web. 2 August 2012. < http://www.netl.doe.gov/publications/proceedings/10/doe-epa/Nygaard.pdf>

Orlic, B. (2009). Some geomechanical aspects of geological CO_2 sequestration. KSCE Journal of Civil Engineering 2009; 13(4), 225-232.

Orlic B, ter Heege J, Wassing BBT. Assessing the short-term and long-term integrity of top seals in feasibility studies of geological CO_2 storage. In 45th US Rock Mechanics/Geomechanics Symposium. American Rock Mechanics Association; January 2011.

Perry KF. Natural gas storage industry experience and technology: potential application to CO_2 geological storage. In Benson SM, editor. Carbon dioxide capture for storage in deep geologic formations - results from the CO_2 Capture Project, v. 2: Geologic storage of carbon dioxide with monitoring and verification, London: Elsevier; 2005, p. 815-825.

PETCO Petroleum Corporation and Bergman Petroleum Corporation v. Natural Gas Pipeline Company Of America (PETCO/BPC v NGPL), CP66-141 (U.S. District Court, S.D. Illinois, April 20-21, 2004).

PETCO Petroleum Corporation and Bergman Petroleum Corporation v. Natural Gas Pipeline Company of America (PETCO/BPC v NGPL), No. 03-cv-4086-JPG, Doc 124 (U.S. District Court, S.D. Illinois, May 10, 2011a).

PETCO Petroleum Corporation and Bergman Petroleum Corporation v. Natural Gas Pipeline Company Of America (PETCO/BPC v NGPL), Doc. 132 (U.S. District Court, S.D. Illinois, June 3, 2011b).

Rutqvist J. The geomechanics of CO_2 storage in deep sedimentary formations. International Journal of Geotechnical and Geological Engineering (in press) doi:10.1007/s10706-011-9491-0 (2012).

Rutqvist J, Birkholzer JT, Tsang CF. Coupled reservoir–geomechanical analysis of the potential for tensile and shear failure associated with CO_2 injection in multilayered reservoir–caprock systems. International Journal of Rock Mechanics and Mining Sciences 2008; 45(2), 132-143.

Rutqvist J, Rinaldi A P, Cappa F, Moridis G J. Modelling of fault reactivation and induced seismicity during hydraulic fracturing of shale-gas reservoirs. Journal of Petroleum Science and Engineering 2013; 107, 31-44.

Rutqvist J, Vasco DW, Myer L. Coupled reservoir-geomechanical analysis of CO_2 injection and ground deformations at In Salah, Algeria. International Journal of Greenhouse Gas Control 2010; 4(2), 225-230.

Schilling, F.R. (2007) *Ketzin –a Pilot Project for* CO_2 *Storage: Characterization, Monitoring, and Injection Technologies*. Presentation at 2007 International G8 Workshop on Clean Coal Technology, Leipzig.

Sen, B. (1950) Note on the stresses produced by nuclei of thermo-elastic strain in a semi-infinite elastic solid. *Quart. appl. Math., 8.*

Sibson RH. Stress switching in subduction forearcs: Implications for overpressure containment and strength cycling on megathrusts. Tectonophysics 2013; 600, 142-152.

Southern California Earthquake Data Center (SCEC), 2013, Significant earthquakes and faults. Accessed April 20, 2013. World Wide Web Address: <http://www.data.scec.org/significant/losangeles.html>

US Energy Information Administration (EIAa). Lower 48 States Natural Gas Working Underground Storage. Accessed 3/11/2013. World Wide Web Address: www.eia.gov/dnav/ng/hist/nw_epg0_sao_r48_bcfw.htm

US Energy Information Administration (EIAb). U.S. Underground Natural Gas Storage Capacity. Accessed 3/11/2013. World Wide Web Address: http://www.eia.gov/dnav/ng/ng_stor_cap_dcu_nus_m.htm

US Energy Information Administration (EIAc). U.S. Underground natural gas storage developments: 1998:2005. Office of Oil and Gas, October 2006. Accessed 3/11/2013. World Wide Web Address: http://www.eia.doe.gov/pub/oil_gas/natural_gas/feature_articles/2006/ngstorage/ngstorage.pdf

Verdon JP, Kendall JM, Stork AL, Chadwick RA, White DJ, Bissell RC. Comparison of geomechanical deformation induced by megatonne-scale CO_2 storage at Sleipner, Weyburn, and In Salah. Proceedings of the National Academy of Sciences 2013; 110(30), E2762-E2771.

Vilarrasa V, Olivella S, Carrera J. Geomechanical stability of the caprock during CO_2 sequestration in deep saline aquifers. Energy Procedia 2011; 4, 5306-5313.

Watson S., Metcalfe R. and Bond, A. Scoping calculations for releases from potential UK UNGS facilities. HSE Research Report RR606. Norwich, UK: Crown, 2008.

Yordkayhun, S., Ivanova, A., Giese, R., Juhlin, C., Cosma, C. (2009) *Comparison of surface seismic sources at the* CO_2*SINK site, Ketzin, Germany*. Geophysical Prospecting, 57, 125-139, doi: 10.1111/j.1365-2478.2008.00737.x

Zhou Q, Birkholzer JT, Tsang CF, Rutqvist J. A method for quick assessment of CO_2 storage capacity in closed and semi-closed saline formations. International Journal of Greenhouse Gas Control 2008; 2(4), 626-639.

10 Appendices

10.1 Appendix 1: Other Risk Assessment Tools (DOE, 2013a)

Tool	Organization/ Personnel	Goal/ Description	Projects Used/ Conceptual examples	Risks Considered	Methodology family	Impact Categories	Sub-models/ Processes/ Components Considered	Inputs	Workflow	Outputs	Computational /Visualization Tools Used	Reference
Quintessa FEP database	Quintessa	Addresses features, events and processes (FEPs) of the system relevant to long-term safety and performance. Documents the decision-making process	Weyburn, In Salah	FEPs cover technical, operational and programmatic risks	Qualitative, FEP-screened by experts	Includes HSE, casualties, water, air impacts	~200 FEPs grouped into 8 categories	Expert inputs on various FEP categories	Experts participate in workshops to identify and, aggregate FEPs to provide scenarios. A base case scenario (also termed "normal" or "expected evolution" scenario) is defined and alternative "what if?" scenarios for comparison. The FEP database is used either to guide selection of FEPs in the workshop or (more usually) to audit the scenarios produced from "project-specific" FEPs identified in the workshop.	Identifies scenarios to be addressed in system-level models to ensure long-term safety & performance Can be used as an audit tool to evaluate such system models	Quintessa FEP database	Quintessa website Savage et al., 2004
TNO Risk Assessment Methodology	TNO	Demonstrate long-term safety performance of underground CO_2 storage		Technical, Programmatic	Expert-elicited probability and consequence matrices	Include human casualties, environmental risks, groundwater contamination	TNO FEP database & process-level simulations	Site characterization, well characterization, expert inputs on FEPs	1. Assessment basis defined 2. Critical FEPs are grouped into scenarios 3. Experts estimate range and identify probability distribution functions (pdfs) for the parameters of each scenario 4. Monte Carlo (MC) procedure is performed for thousands of input data sets	PDFs of CO_2 plume characteristics from the Monte Carlo procedure (impacted areas, concentrations, fluxes) can be used to calculate impacts (casualties, environmental risks, USDW contamination, etc.)	SIMED II	TNO, Wildenborg et al., 2004
CO_2QUALSTORE guideline	Det Norske Veritas (DNV)	Life-cycle risk-based approach to site selection and qualification Common protocol for *third parties and regulators* to assess safety and reliability of GS Structured basis for decision making	Developed as a part of the Joint Industry Partnership (JIP)	GS life-cycle risks	Qualitative/ Semi-quantitative with "panel" inputs	Multiple categories	Site Screening, Assessment, Selection, Design, Construction, Operation, Closure (transfer-of-responsibility)	Screening, characterization reports, injection and operation plan, storage performance forecast, impact assessment, contingency plans, MVA plans	Structured hazard & safeguard identification --------- Risk ranking in a "workshop" with the risk matrix approach Risk assessment follows the ALARP (as low as reasonably practicable) principle --------- Transparent documentation of the iterative risk assessment process	Iterative risk analysis is used to update various operational plans and provide basis for project qualification and regulatory compliance	NA	pages 65-75 of the DNV CO_2QUALSTORE guideline
Carbon Storage Scenario Identification Framework (CASSIF)	TNO	Storage Performance Assessment Both multiple-site screening and single-site certification possible		Technical (containment, effectiveness)	Qualitative, scenario-based	Well, Confining Zone, Fault leakage	Chemical, Mechanical	Expert inputs to FEPQuest, FEPMan 40 questions on basin geometry, reservoir parameters, etc. TNO facilitates *Workshop*	FEPQuest: Expert inputs used to highlight FEPs and identify knowledge gaps --------- FEPMan: Grouping and pre-selection of FEPs --------- Workshop: Select Risk Factors, Create Scenarios using mindmapping tools	Consensus on a set of FEP-based scenarios about site-specific risk factors	SQL-based FEP database, VUE for visualizing FEP interactions	Yavuz, F. et al., 2009

Tool	Organization/ Personnel	Goal/ Description	Projects Used/ Conceptual examples	Risks Considered	Methodology family	Impact Categories	Sub-models/ Processes/ Components Considered	Inputs	Workflow	Outputs	Computational /Visualization Tools Used	Reference
Risk Identification and Strategy using Quantitative Evaluation (RISQUE)	URS	Semi-quantitative technique to estimate both the probability and impact of a set of risk events for multiple projects/ injection sites	Weyburn, CO_2CRC: Otway, Gorgon, BP: In Salah	Technical, Community	Semi-quantitative, expert-elicited probability and consequence matrices	Reservoir Performance Project Viability Community Impacts	Containment, Effectiveness Community safety, amenity & environment	Key Performance Indicators (KPIs) for various impacts Site information Project duration, CO_2 quantity, etc.	Key Performance Indicators (KPIs) used to define baseline to assess impacts to various receptors --- Expert panel identifies risk events, probabilities, costs and potential consequence outcomes. --- Consequence information used in a simple spreadsheet model with Monte Carlo simulations to generate outputs over a range of confidence limits.	Overall- and impact-wise cost-benefit risk profiles for multiple projects --- Ranking of each project against KPIs --- A plot indicating where each project falls in the "containment risk index - effectiveness risk index" space	Monte Carlo simulations via Oracle Crystal Ball add-on for MS Excel	Bowden, A. & Rigg, A., 2005; Bowden, A. & Rigg, A., 2004
Screening and Ranking Framework (SRF)	C. M. Oldenburg	Independent assessment of containment/ dispersion potential through numerical evaluation of various attribute properties *(multi-attribute utility analysis)* --- Multi-site evaluation to identify site with the least HSE risk	Ventura oil field, Rio Vista gas field	Technical and Community (Health, Safety and Environmental (HSE))	Qualitative, expert-elicited probabilities	Health, Safety and Environment	Primary/Secondary Confinement Attenuation Potential --- 1. Long-term potential for primary containment of CO_2 2. Secondary containment potential if 1 fails 3. Attenuation potential if 2 fails	Primary/ secondary/shallow confining zone properties, depths, Injection zone attributes, Information on existing wells, hydrology, faults and topography	Experts assess importance of each property, and assign certainties Spreadsheet uses inputs to generate average assessment and certainties	Overall score for each impact category, average certainty --- Graph of average attribute assessment vs. average certainty	MS Excel-based	Oldenburg, C.M., 2006
Certification Framework (CF)	C. M. Oldenburg, S. Bryant, J.-P. Nicot - CCP	Certification of a single site, given adequate characterization data Containment & effectiveness risk only	Kimberlina site, southern San Joaquin valley	Technical (containment, effectiveness)	Quantitative, system-level model, probabilities partly calculated using fuzzy logic	CO_2, brine leakage via wells and faults into "compartments"; emission credits & atmosphere, near-surface, health & safety, USDWs and HC/mineral resources	CF Submodels: 1. Injection zone simulation 2. Fault encounter probability 3. Fault connectivity probability 4. Wellbore flow and fault leakage 5. Dense phase atmospheric dispersion	Site characterization, fault population statistics, injection zone, injection rate, time frame, existing wells and faults, limits on CO_2/brine concentrations/ fluxes in each compartment, thresholds on leakage risks	Impacts: modeling & simulation of proxy concentrations or fluxes --- $P_{source\text{-}conduit}$ * $P_{conduit\text{-}compartment}$ = $P_{source\text{-}compartment}$ --- CO_2 plume location, size, pressure signal calculated via reservoir simulations or pre-computed simulations --- Reservoir simulation results fed to conduit model to calculate flux/concentration of CO_2/brine.	Severity of impact = degree to which flux/ concentration exceeds the limit for a given compartment Risk = (Impact * $P_{source\text{-}compartment}$) --- CO_2/brine leakage risk </=/> provided threshold --- Injection plan or site characterization modified to decrease risk	TOUGH2, CMG-GEM	Oldenburg, C.M., 2009

Tool	Organization/ Personnel	Goal/ Description	Projects Used/ Conceptual examples	Risks Considered	Methodology Family	Impact Categories	Sub-models/ Processes/ Components Considered	Inputs	Workflow	Outputs	Computational /Visualization Tools Used	Reference
Vulnerability Evaluation Framework (VEF)	U.S. EPA	Identify conditions leading to increased/ decreased susceptibility to adverse impacts from GS. --- Not used for measuring the severity of an outcome, performance assessment or to specify data requirements		Technical (containment, effectiveness, contamination), Community (human health and welfare) Economic	Qualitative	Impacts to human health, atmosphere, ecosystems, USDW, surface waters, and the geosphere	Evaluation Flowcharts 1. Confinement system 2. Injection zone 3. CO_2 stream 4. GS footprint delineation 5. Human health and welfare, atmosphere, ecological factors, GW / surface water, CO_2 spatial area, pressure spatial area 6. Wells 7. Faults	Information on GCS system and geologic attributes of the injection and confining zones : (capillary entry pressures, permeability, travel time, plume lateral extent, wells, faults/ fracture zones, geochemical processes, geomechanical processes, tectonic activity, injectivity, physical capacity)	Spatial area around the injection site in which impacts are evaluated is defined --- Input information used in a series of evaluation flowcharts to determine if high/low vulnerability exists for a particular scenario	High/low vulnerability for a particular situation Means to manage the vulnerability indicated VEF can be used to prioritize monitoring and mitigation efforts focused on geologic features and overlying receptors	N.A.	U.S. EPA, 2008
Performance Assessment (PA)	Quintessa	1. Evaluate effectiveness of the system or sub-system relative to some criteria of interest to particular stakeholders. --- 2. Allows integration of quantitative, qualitative site information, numerical models, and value judgments by experts in a decision-support framework. --- 3. Evidence Support Logic (ESL) and the PA framework can also be used for iterative planning	In Salah, Shell (ESL aspects)	FEPs cover technical, operational and programmatic risks, as required by the context of the assessment	Evidence-support (3-valued) logic (ESL) Distinguishes cases of poor-quality data from uncertain data	Can be implemented so as to consider any impact categories of interest to stakeholders. The decision-support tool based on ESL can be used to analyze decisions and determine implications of information / uncertainties on impacts of concern	1. Online FEP database 2. QPAC-CO_2: modular, general-purpose simulation code 3. TESLA, a decision-support tool which implements ESL and allows development of a hierarchical, logical hypothesis model to provide common structure for all the evidence for/against/ uncertainty corresponding to a root-level hypothesis	Expert definition of a context for the PA Site-specific FEPs Expert evaluation of FEPs Expert definition of performance-relevant hypotheses Expert judgments of evidence for / against each hypothesis mapped on to a numerical scale of 0 to 1 representing evidence for and against (judgments can be based on a wide range of information, including outputs from numerical models)	Define context for the PA FEP analysis and scenario development of a decision tree (also termed a "hypothesis model" using TESLA. Analysis of scenarios or aspects of scenarios using numerical modeling tools, including QPAC-CO_2 Identification of various sources of evidence that corroborate/falsify various sub-hypotheses in the decision tree (including outputs from numerical models) Propagation of evidence through the decision tree to assess the dependability of the root hypothesis	Ratio plots of evidence for/against vs. uncertainty for the overall hypothesis indicate a measure of confidence (ex: for/ against significant chances of leakage from the injection zone) --- Hypotheses where the evidence is uncertain can be re-evaluated at a later stage with new data, including monitoring data	TESLA QPAC-CO_2 Quintessa FEP database	Metcalfe et al., 2009, TESLA User Guide

Tool	Organization/ Personnel	Goal/ Description	Projects Used/ Conceptual examples	Risks Considered	Methodology family	Impact Categories	Sub-models/ Processes/ Components Considered	Inputs	Workflow	Outputs	Computational /Visualization Tools Used	Reference
Carbon WorkFlow	Schlumberger Carbon Services	Evaluate risks associated with FEPs against project values on a likelihood-severity scale. Establish basis for allocating resources for risk reduction, and provide structure to document and track risk reductions.	WESTCARB Kimberlina Project, CA SCS PurGen Project, NJ Cemex CCS Project, TX Aquistore Project, SK	All Technical and Programmatic risks (project-specific) to project goals and values	Semi-quantitative; FEPs ranked through expert elicitation using a risk matrix approach	Categories designed to suit the project: e.g. HSE, Financial, Technical (Injectivity, Capacity, Containment), Research, Industry stewardship / social acceptance.	1. Risk = Severity (S)*Likelihood (L), each evaluated on categorical scales. 2. Values assigned through working-group consensus, and/or from aggregated "votes" in plenary session. 3. Participants' skill self-evaluation applied as expertise qualification. 4. Workshops structured to promote information sharing and calibration, yet to minimize heuristic pitfalls.	1. List of 50-80 pre-screened FEPs from sources including Quintessa. 2. Aggregate experience of 20-30 internal and external experts. 3. Presentations on project knowns, unknowns, plans, and risks. 4. Mined-data inputs (under development).	1. Invited experts rank FEPs by project risk. 2. Small panel generates key scenarios from higher-ranked FEPs. 3. Broader group provides Risk Response Actions (RIRAs) for scenarios. 4. Risk manager creates executable Risk Response Action Groups (RIRAGs). 5. RIRAGs are assigned to individuals for completion, documentation, and periodic risk-reduction review.	1. List of FEPs ranked by associated risk. 2. List of relevant Scenarios ranked by associated risk. 3. List of Risk Response Actions to be assigned within a project management structure. 4. Format for risk tracking and periodic review.	1. Spreadsheet graphics. 2. Live displays of "votes" and data during workshops.	Hnottavange-Telleen, K., Krapac, I. & Vivalda, C., 2009 --- Hnottavange-Telleen, K., 2010
Oxand Performance & Risk (P&R™) Methodology	Oxand, Schlumberger	Quantify CO_2 leakage through a well for well integrity performance- and risk-assessment Provide initial risk-assessment and mitigation plans to regulators	Ongoing: PCOR	CO_2 leaks/ flow through wellbores	Quantitative Risk matrix evaluation: semi-quantitative	Public acceptance, Financial, Technological, HSE, USDW impacts	• Well leakage: Darcy two-phase flow • Chemical reactions: Cement degradation, carbonation, casing corrosion Likely does not simulate CO_2 injection and plume movement through the target formation to the wellbore	Site characterization, well characterization, cement properties, probability distributions of uncertain parameters	• Risk scenario identification Stochastic simulations to evaluate CO_2 flow along well • Identify targets impacted due to CO_2 leakage • Evaluate risk scenarios from simulation data using a risk matrix • Risks are compared against acceptance limits • Basis for mitigation actions	CO_2 leakage rate; Identification of leakage pathway, Targets impacted identified Risk probability	SIMEO™-STOR	Meyer, V. et al., 2009

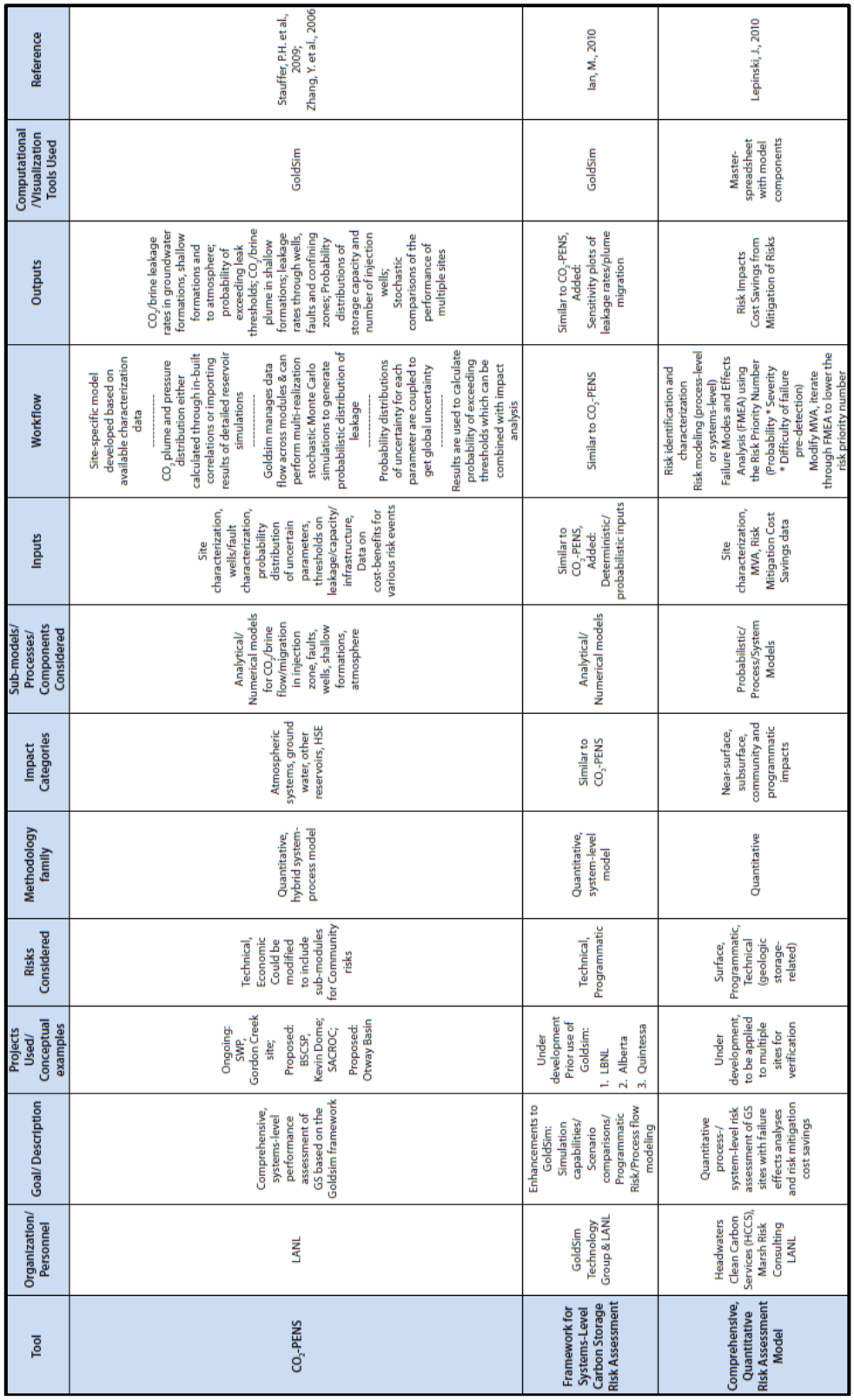

Tool	Organization/ Personnel	Goal/Description	Projects Used/ Conceptual examples	Risks Considered	Methodology family	Impact Categories	Sub-models/ Processes/ Components Considered	Inputs	Workflow	Outputs	Computational /Visualization Tools Used	Reference
CO_2-PENS	LANL	Comprehensive, systems-level performance assessment of GS based on the Goldsim framework	Ongoing: SWP, Gordon Creek site; Proposed: BSCSP, Kevin Dome; SACROC; Proposed: Otway Basin	Technical, Economic Could be modified to include sub-modules for Community risks	Quantitative, hybrid system-process model	Atmospheric systems, ground water, other reservoirs, HSE	Analytical/ Numerical models for CO_2/brine flow/migration in injection zone, faults, wells, shallow formations, atmosphere	Site characterization, wells/fault characterization, probability distribution of uncertain parameters, thresholds on leakage/capacity/ infrastructure, Data on cost-benefits for various risk events	Site-specific model developed based on available characterization data --- CO_2 plume and pressure distribution either calculated through in-built correlations or importing results of detailed reservoir simulations --- Goldsim manages data flow across modules & can perform multi-realization stochastic Monte Carlo simulations to generate probabilistic distribution of leakage --- Probability distributions of uncertainty for each parameter are coupled to get global uncertainty --- Results are used to calculate probability of exceeding thresholds which can be combined with impact analysis	CO_2/brine leakage rates in groundwater formations, shallow formations and to atmosphere; probability of exceeding leak thresholds; CO_2/brine plume in shallow formations; leakage rates through wells, faults and confining zones; Probability distributions of storage capacity and number of injection wells; Stochastic comparisons of the performance of multiple sites	GoldSim	Stauffer, P.H. et al., 2009; Zhang, Y. et al., 2006
Framework for Systems-Level Carbon Storage Risk Assessment	GoldSim Technology Group & LANL	Enhancements to GoldSim: Simulation capabilities/ Scenario comparisons/ Programmatic Risk/Process flow modeling	Under development Prior use of Goldsim: 1. LBNL 2. Alberta 3. Quintessa	Technical, Programmatic	Quantitative, system-level model	Similar to CO_2-PENS	Analytical/ Numerical models	Similar to CO_2-PENS, Added: Deterministic/ probabilistic inputs	Similar to CO_2-PENS	Similar to CO_2-PENS, Added: Sensitivity plots of leakage rates/plume migration	GoldSim	Ian, M., 2010
Comprehensive, Quantitative Risk Assessment Model	Headwaters Clean Carbon Services (HCCS), Marsh Risk Consulting LANL	Quantitative process-/ system-level risk assessment of GS sites with failure effects analyses and risk mitigation cost savings	Under development, to be applied to multiple sites for verification	Surface, Programmatic, Technical (geologic storage-related)	Quantitative	Near-surface, subsurface, community and programmatic impacts	Probabilistic/ Process/System Models	Site characterization, MVA, Risk Mitigation Cost Savings data	Risk identification and characterization Risk modeling (process-level or systems-level) Failure Modes and Effects Analysis (FMEA) using the Risk Priority Number (Probability * Severity * Difficulty of failure pre-detection) Modify MVA, iterate through FMEA to lower the risk priority number	Risk Impacts Cost Savings from Mitigation of Risks	Master-spreadsheet with model components	Lepinski, J., 2010

10.2 Appendix 2: Other Risk Assessment Methods (Condor et al. 2011)

Method	Goal	Data needed	Industrial application	Application for GSC
DRA	Analytical point estimate calculations	Numerical and qualitative expert estimation for scenario development and model development	Safety engineering (sensitivity analysis)	Initial risk assessment. No uncertainty estimations
PRA	Predict the probability of safety failures of complex systems	Numerical qualitative expert estimation for scenario development, model development quantifying PDFs	Safety engineering	Detailed risk assessment. Uncertainty estimation
FEP	Scenario development	Qualitative expert estimation for scenario development	Scenario analysis	Screening and Site selection
VEF	Conceptual framework for regulators and technical experts	Qualitative expert estimation to identify which areas should be in-depth studied	Hazard identification and potential consequences	Framework for site selection and regulator guidance
SWIFT	Elaborate hypothesis	Qualitative expert estimation to identify hazards	Hazard identification in engineering	Hazard and consequence mapping
MCA / MAUT	Evaluation of alternatives in multiple objective	Qualitative and numerical expert estimation for data input utility	Decision making	Framework for screening and site selection
RISQUE	Systemic process with participation of expert panels	Qualitative and numerical expert estimation in event-tree approach	Hazard identification and potential consequences	Hazard and consequence mapping
CFA / SRF	Estimation of risk based on probabilities of occurrence in individual features	Qualitative and quantitative estimation of risk and uncertainty	Development of simple probabilistic models	Managing risks in GSC sites
MOSAR	Identifying and preventing risks	Qualitative and quantitative data for a well-known system	Risk reduction in complex systems	Systematic risk analysis for well-known sites
ESL	Identification of uncertainties in decisions	Qualitative and quantitative understanding of uncertainties	Reduction of uncertainties in well-known systems	Detailed PRA and dealing with uncertainties
P&R	Risk mapping in wellbores under the criteria of degradation scenarios	Qualitative and quantitative data for wellbores	Risk evaluation under the concept of ALARP	Long-term well integrity
SMA	Estimation of risk based on probabilities.	Quantitative estimation of risk and PDFs	Development of complex models in well-known systems	PRA for the whole CCS chain